Analysis of the molecular function of kazrin in endosomal trafficking

Adrian Baumann

UNIVERSITAT DE BARCELONA

FACULTAT DE FARMÀCIA I CIÈNCIES DE L'ALIMENTACIÓ

PROGRAMA DE DOCTORAT EN BIOMEDICINA

Analysis of the molecular function of kazrin in endosomal trafficking

Institut de Biologia Molecular de Barcelona (IBMB-CSIC)

Doctorando Adrian Baumann

Directora de la tesis Maria Isabel Geli Fernandez

Tutor de la tesis Albert Tauler Girona

Adrian Baumann, 2018

Resumen

La endocitosis es esencial para la célula eucariota. Permite a las células modificar rápidamente los complejos implicados en señalización y los transportadores de nutrientes e iones expuestos en la superficie celular, y es además esencial para mantener la homeostasis de proteínas de membrana y de lípidos y para distribuir el material intracelular. Por tanto, el tráfico endocítico puede regular la capacidad de la célula para detectar cambios en su microambiente y reaccionar ante ellos.

Esta Tesis se centra en el estudio de la kazrina C, una proteína humana originalmente identificada en un cribado genético destinado a aislar cDNAs cuya sobreexpresión inhibía la endocitosis dependiente de clatrina (EMC), una de las vías de internalización endocítica mejor caracterizadas. Experimentos preliminares demostraron que la kazrina C era capaz de interaccionar con la maquinaria endocítica asociada a clatrina y que la depleción de la kazrina aceleraba la EMC y el reciclaje de la transferrina (Tfn), impidiendo sin embargo su transporte a los endosomas de reciclaje localizados perinuclearmente. Por otro lado experimentos basados en la immunofluorescencia indicaron que la kazrina C se localizaba en los endosomas tempranos donde se clasifica el material para su reciclado o degradación (Endosomas de clasificación), junto con la GTPasa rab4, la subunidad γ-adaptina del adaptador de clatrina AP-1 y EHD3.

El trabajo aquí presentado confirma los efectos de la depleción de la kazrina sobre el tráfico de de la Tfn, utilizando una aproximación diferente para minimizar su expresión celular y ratifica mediante fraccionamiento subcelular el reclutamiento de la kazrina en endosomas tempranos. En consistencia con estas observaciones, demostramos también que en células transfectadas de manera transitoria, GFP-kazrina forma microdominios sobre endosomas marcados con YFP-rab4 en células vivas. Además, este trabajo aporta evidencias sólidas que demuestran una interacción directa de la Kazrina C con el dominio N-terminal de la clatrina y con su adaptador AP-1, que junto con Rab4b, y al igual que la kazrina, son necesarios para el transporte entre los endosomas de clasificación y los de reciclaje. Finalmente demostramos en este trabajo que la kazrina colocaliza con la actina endosomal y que interacciona directamente con el complejo Arp2/3 y su activador endosomal WASH y que tanto la depleción como la sobreexpresión de kazrina aumentan considerablemente la cantidad de actina polimerizada sobre estos orgánulos. Los datos son coherentes con un modelo según el cual la kazrina actuaría como un inhibidor citosólico de WASH, que sin embargo, una vez activado en las membranas endosomales podría inducir la polimerización de actina dependiente de WASH y del complejo Arp2/3 sobre dominios enriquecidos en clatrina.

Tomados en su conjunto, nuestros resultados sugieren un papel de la kazrina en la encrucijada de reciclaje en los endosomas de clasificación, favoreciendo el transporte hacia los endosomas perinucleares de reciclaje e inhibiendo la via corta de reciclaje desde los endosomas de clasificación a la membrana plasmática. A nivel molecular, los datos sugieren que la kazrina podría controlar el balance de la polimerización de actina inducida por WASH, inhibiendo la misma sobre los microdominios ricos en retrómero, implicados en la vía corta de reciclaje a membrana plasmática, y promoviéndola en subdominios asociados a clatrina, implicados en el transporte a los endosomas perinucleares.

Abstract

Endocytosis and endosomal trafficking are of central meaning in all eukaryotic cells. It enables cells to rapidly modify their surface exposure of signalling complexes, nutrient and ion transporters, to maintain the homeostasis of lipids and proteins, to distribute internalized material within the cell, and to initiate and maintain cell motility, among others. Hence, the endocytic uptake and transport processes can regulate the capacity of the cell to sample and react to with their environment.

This thesis focused on the study of kazrin C, a human protein originally identified in our group, whose overexpression interferes with clathrin-mediated endocytosis (CME), one of the best studied endocytic pathways. Preliminary experiments demonstrated that kazrin C interacts with the clathrin-associated machinery from rat brain extracts. Further, that data indicated that depletion of kazrin accelerates CME and recycling of the widely used endocytic marker transferrin (Tfn), whereas it impairs arrival of internalized Tfn to the perinuclear endosomal recycling compartment (ERC). Last, initial experiments suggested that kazrin might localized to sorting endosomes (SE), together with rab4, γ-adaptin and EHD3.

The work presented here confirmed the previously observed effects in Tfn uptake and endocytic trafficking upon kazrin depletion. Further, subcellular fractionation experiments biochemically reinforced the view that a fraction of kazrin is localized to endosomal compartments. Consistently also, transfected GFP-kazrin could be seen forming subdomains on YFP-rab4 positive endosomes in living cells. Further, we provide biochemical evidence indicating that kazrin C directly interacts with clathrin and the clathrin adaptor AP-1, which together with rab4b, have been implicated in the transport between the sorting and recycling endosomes, similar to kazrin. Finally, we found that kazrin co-localize with endosomal actin and that it directly interacts with the Arp2/3 complex and WASH, the main the activator of the Arp2/3 complex on endosomal membranes. Both, depletion and overexpression of kazrin resulted in accumulation of endosomal actin. The data suggest that kazrin might inhibit cytosolic WASH, but upon activation, it might induce WASH-dependent actin polymerization on AP-1 and clathrin-enriched endosomal subdomains, promoting the formation or fission of transport intermediates between the sorting and recycling compartments.

Altogether, the results indicated a role for kazrin at the sorting endosomal recycling trafficking crossroad, favouring transport towards the ERC together with clathrin and AP-1, versus the short loop recycling path to the plasma membrane. At the molecular level, the data suggest kazrin might control the balance of WASH-induced actin polymerization on either retromer or clathrin-enriched endosomal subdomains.

Agradecimentos / Acknowledgements

Special thanks to Maribel for all the help and guidance during the years; to my lab mates for the support and constant supply of cookies; to all other lovely colleagues; to Elena Rebollo for many intensive and exciting hours at the microscope, amazing experimental design and an incredible semi-automatic macro for analysis of actin on endosomes – an impossible task accomplished; of course to my parents, to my friends being there for me, HELGA, and everyone else I simply forgot to mention.

Index

Abbreviatons

AD	Alzheimer disease
aa	amino acid
AP	amyloid precursor protein
Aβ	amyloid β peptide
BACE1	β-site amyloid precursor protein cleaving enzyme 1
β2-AR	beta2-adrenergic receptor
CCP	clathrin-coated pit
CCV	clathrin-coated vesicle
CE	cornified envelope
CHC	clathrin heavy chain
CHC TD	clathrin heavy chain terminal domain
CHCR	clathrin heavy chain repeat
CD-MPR	cation-independent mannose-6-phosphate receptor
CI-MPR	cation-dependent mannose-6-phosphate receptor
CLC	clathrin light chain
CLEM	correlative light and electron microscopy
CLIC	clathrin-independent carriers
CME	clathrin mediated endocytosis
CP	cytoplasma
CRC	cargo recognition complex
EE	early endosomes
EEA1	early endosome antigen 1
EGF	epidermal growth factor
EM	electron microscopy
ER	endoplasmatic reticulum
ERC	endocytic recycling compartment
ESCRT	endosomal sorting complexes required for transport
FACS	fluorescence activated cell sorting
GEEC	GPI-AP enriched early endosomal compartments
GPCR	G-protein coupled receptors
ILV	intraluminal vesicle
LDL	low-density lipoprotein
LDLR	low-density lipoprotein receptor
LE	late endosomes
LOAD	late-onset Alzheimer disease
MHC class I	major histocompatibility complex (MHC) class I
MT	microtubule
MTOC	microtubule-organizing center
MVB	multi vesicular bodies
PtdIns(3)K	phosphatidylinositol 3-kinase
PtdIns	phosphoinositide
PtdInsPxs	phosphoinositide mono and polyphosphate
PM	plasma membrane

QIEM	quantitative immuno-electron microscopy
RE	recycling endosomes
RTK	receptor tyrosine kinase
SE	sorting endosome
siRNA	small interfering RNA
SNX	sorting nexin
STxB	Shiga toxin B-subunit
TfnR	transferrin
TfnR	transferrin receptor
TGN	trans golgi network
TIRF microscopy	total internal reflection fluorescence microscopy
TREM	time-resolved electron microscopy
WLS	Wnt signalling receptor Wntless

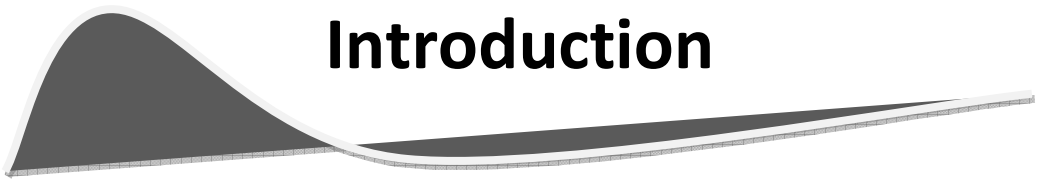

Introduction

1 Introduction

Kazrin C, the focus of this thesis, was originally identified as a human protein that when overexpressed interferes with clathrin–mediated endocytosis (CME) (Schmelzl and Geli 2002). Subsequent studies indicated that this protein is recruited to the plasma membrane (PM) and the sorting endosomes (SE) and it might play a role controlling endocytic transport. During the course of this thesis, we provide evidence indicating that kazrin C directly interacts with clathrin and clathrin adaptors as well as WASH and the Arp2/3 complex and that it controls actin polymerization on endosomal membranes. The introduction will therefore discuss the general molecular mechanisms of endocytic membrane traffic with extended sections on the structure and functions of clathrin and actin along the endocytic pathway and beyond.

1.1 Endocytosis

Endocytosis is the process whereby eukaryotic cells internalize parts of their PM together with extracellular material to form vesicular or tubular transport intermediates that detach form the cell surface and travel into the cytosol (Fig. 1). Endocytosed material can then be delivered through the endosomal system to the degradative compartment, the lysosome, can be recycled back to the PM or can be transported to the Golgi apparatus, where it will gain access to the secretory pathway (Mukherjee, Ghosh et al. 1997, Di Fiore and von Zastrow 2014).

Even though equitable samples of the extracellular media and PM components are taken up during endocytosis, cargo destined for internalization can be selectively packed in endocytic vesicles. Endocytic cargo can in turn be differentially labelled as such in response to intracellular, environmental and developmental influences, which can in addition modulate the formation or internalization of endocytic transport intermediates themselves. Thereby, endocytosis serves as a fast mechanism to modify in a regulated manner the surface exposure of signalling complexes, cell-cell and cell-matrix junctions, nutrient and ion transporters or damaged proteins. Hence, endocytosis plays essential roles not only in nutrient uptake and processing (Antonescu, McGraw et al. 2014), but also in the homeostasis of PM lipids and proteins (Apaja, Xu et al. 2010, Kumari, Mg et al. 2010), in the response to stress (Watanabe and Boucrot 2017), the propagation and localization of signalling (Di Fiore and von Zastrow 2014), the establishment off cell polarity (Lecuit and Pilot 2003, Scita and Di Fiore 2010), the control of cell cycle progression and cell division (Albertson, Riggs et al. 2005, Scita and Di Fiore 2010), the initiation and maintenance of cell motility (Lecuit and Pilot 2003), the generation of morphogen gradients during development (Fischer, Eun et al. 2006) or the re-programming of cells under pathological or physiological conditions (Scita and Di Fiore 2010). In addition, endocytosis fulfils very specialized physiological tasks in multicellular organisms, including the regeneration of synaptic vesicles to assure the transduction of signals among neurons (Cremona and De Camilli 1997), or the presentation of antigens and the defence against pathogens by macrophages and other cell types of the immune system (Trombetta and Mellman 2005). In this context, it is not surprising that malfunction of endocytosis at different levels is associated with a growing number of human diseases including cancer and neurological disorders (De Matteis and Luini 2011). Further, within the biomedical framework, understanding how the endocytic pathways work is of interest to deliver drugs to particular cellular compartments and it can be intervened to prevent host invasion by a number of pathogens (Gruenberg and van der Goot 2006).

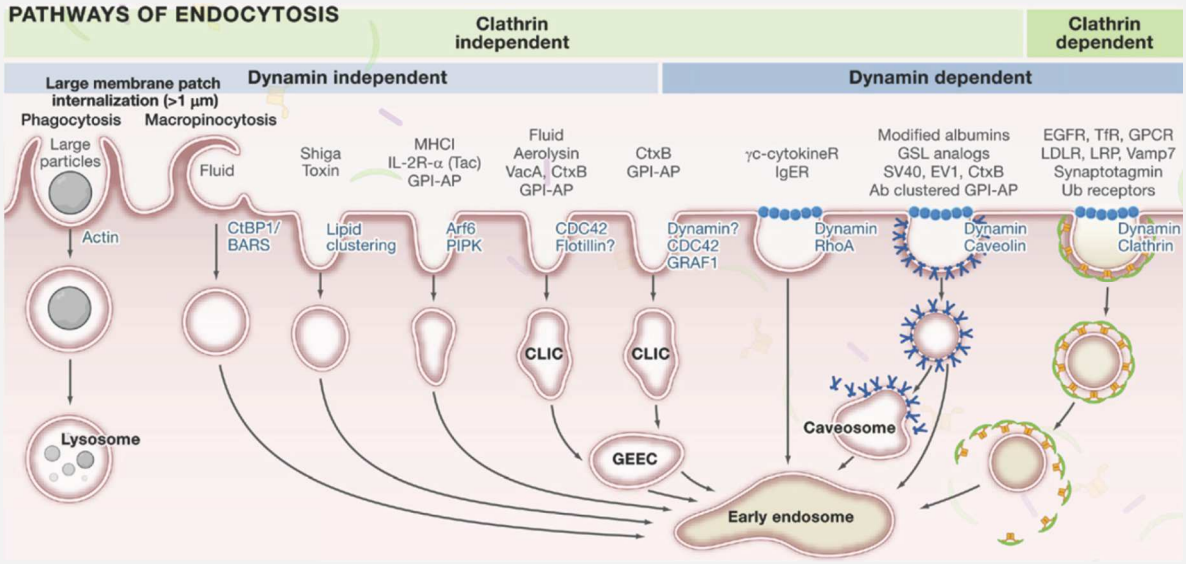

Figure 1. Overview of Endocytic Mechanisms.
Schematic representation of the cellular endocytic pathways classified by the morphology and size of invaginations, the machinery implicated in their biogenesis or the types of cargo. For further details see text in chapter 1.1. Obtained from (Wieffer, Maritzen et al. 2009).

Several endocytic pathways work in parallel in most cell types (Fig. 1). In higher eukaryotes, they can be classified by the morphology and size of the membrane invaginations, the machinery implicated in their biogenesis or the types of cargo internalized. The macroscale endocytic processes include **phagocytosis** (size of the primary transport intermediates being 1 to many µm), induced upon external stimuli by for example bacteria cell-surface contact, and **micropinocytosis** (size of the primary transport intermediates being 0.2 – 10 µm), which can be seen as a form of cell drinking that is induced by growth factors like epidermal growth factor (EGF) (Kumari, Mg et al. 2010). The microscale endocytic processes (size of the primary transport intermediates being 50 – 200 nm) include, as the best characterized, **clathrin and caveolae-mediated endocytosis** (Kumari, Mg et al. 2010). Both implicate the assembly of proteinaceous coats at the inner surface of the PM, which drive membrane invagination and produce pits in the range of 120 to 200 nm of diameter, and the activity of the GTPase dynamin to drive vesicle fission. Well characterized cargoes for CME are for example the transferrin (TfnR) or the LDL receptors (LDLR), as well as most Receptor Tyrosine Kinases (RTKs) and G-Protein Coupled Receptors (GPCRs). Caveolae is thought to mediate uptake of albumin or the autocrine motility factor, among others (del Pozo, Balasubramanian et al. 2005). Other less well-characterized pathways for microscale endocytosis include the **CLIC/GEEC pathway** controlled by the small GTPases Cdc42 and Arf1, responsible for the internalization of GPI-anchored proteins via tubular transport intermediates, or the **flotilin-dependent pathway**, which resembles in many aspects caveolin-mediated endocytosis (Kumari, Mg et al. 2010). Another clathrin and dynamin-independent **endocytic pathway associated with the small GTPase Arf6** and responsible for the internalization of the MHCI, β-integrin and interleukin-2-α has been proposed, which has not been morphologically characterized yet (Fig. 1) (Naslavsky, Weigert et al. 2003, Naslavsky, Weigert et al. 2004).

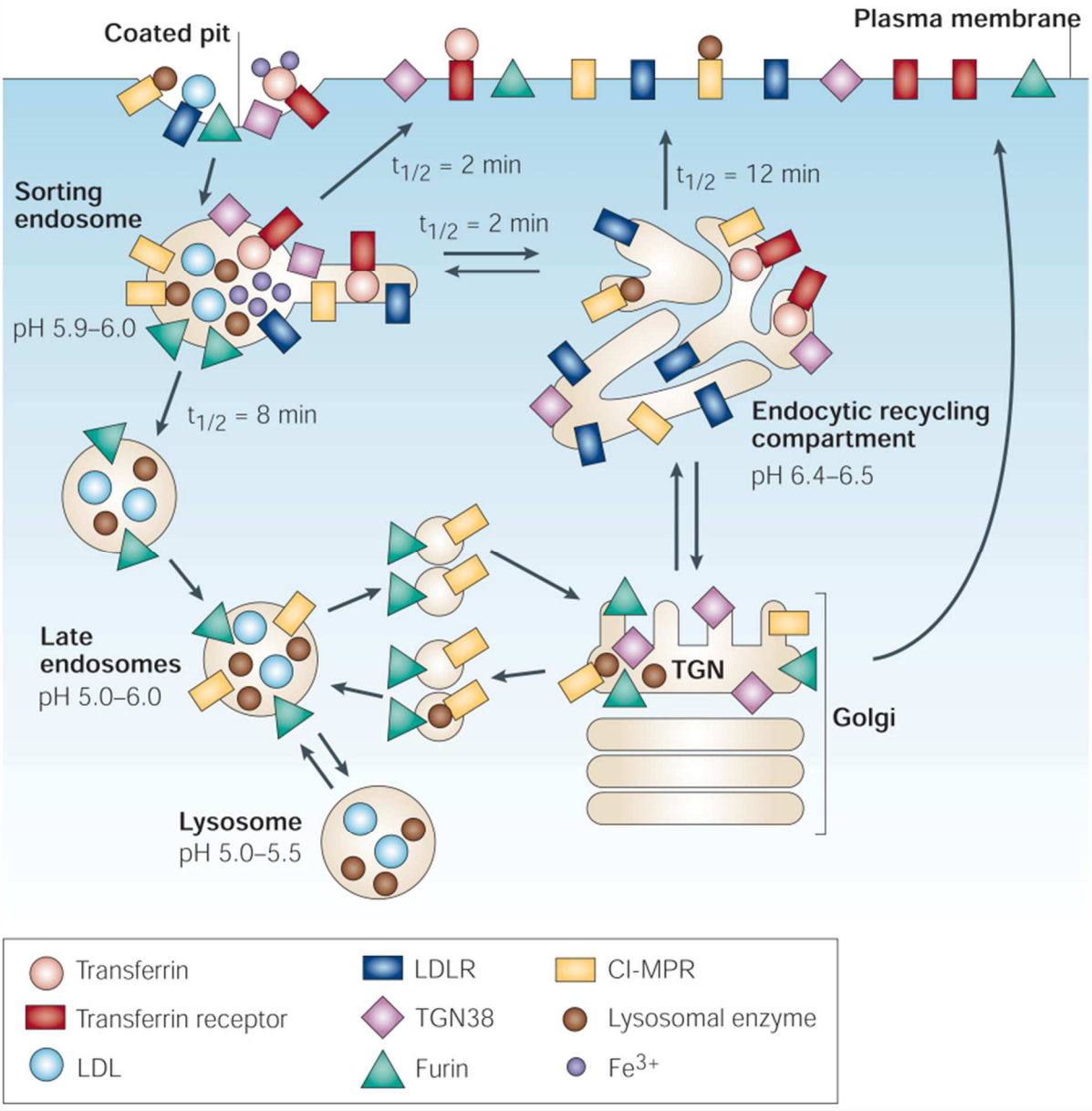

Figure 2. Endocytic Pathways.
The model shows the post-endocytic itineraries of several molecules. The TfnR binds its ligand, diferric transferrin (Tfn); LDLR binds low-density lipoprotein (LDL); and the cation-independent mannose-6-phosphate receptor (CI-MPR) binds lysosomal enzymes. All of these membrane proteins concentrate into clathrin-coated pits, and their initial delivery site is the SEs. Most membrane proteins rapidly exit the SE and they are either returned directly to the PM or they are transported to the endocytic recycling compartment (ERC). Furin is retained in the SE as the compartment begins to mature into a late endosome (LE), and furin is delivered to the Golgi from LE. From the ERC, essentially all of the LDLRs and TfnR recycle to the PM. Tfn, unlike most other ligands (for example, LDL), is not released from its receptor in the acidic environment of the SE. The two irons (Fe 3+) are released from Tfn at the acidic pH and transported into the cytoplasm, but iron-free Tfn remains bound to its receptor until it is returned to the PM. At the neutral extracellular pH, iron-free Tfn is released from the TfnR. About 80% of the internalized TGN38 and CI-MPR also return to the PM, and the rest is delivered to the TGN. The CI-MPR can go from the TGN to LE, where any ligand that is still bound can dissociate as a result of exposure to low pH. From the LE, furin and free CI-MPR can move to the TGN, and molecules in the TGN can be delivered back to the PM. The $t_{1/2}$ values are approximate and cell-type dependent. Obtained from (Maxfield and McGraw 2004).

Upon internalisation, endosomal vesicles fuse with each other and with existing **early endosomes** (EEs), also called **sorting endosomes** (SEs) (Fig. 2). EEs are peripherally located tubular networks, where internalized cargo can be sorted to different destinations. SEs only accept incoming material

for about 5 - 10 minutes until they start to translocate along microtubules (MT) into the cell, generally towards the Microtubule-Organizing Center (MTOC), and mature (Maxfield and McGraw 2004). Membrane proteins recycling back to the PM or targeted to the Golgi are packed in tubular transport intermediates that will fuse with the target membranes. Recycling to the PM can be effected directly from the SEs or even earlier (van der Sluijs, Hull et al. 1992, Choudhury, Sharma et al. 2004), or involve an intermediate transport step to the **endosomal recycling compartment** (ERC) (Maxfield and McGraw 2004). On the contrary, membrane proteins destined for degradation are usually labelled with ubiquitin and packed in **intraluminal vesicles** (ILVs) that bud from the limiting membranes of the endosomes into their lumen. As the SE matures, it accumulates ILVs, becomes more acidic and acquires hydrolases. As a result, **multivesicular bodies** (MVBs), also called **late endosomes** (LEs), are formed, which will either fuse with pre-existing lysosomes or acquire their own properties (Maxfield and McGraw 2004, Huotari and Helenius 2011). In the **lysosome**, internalized material and pathogens, as well as defective or disused proteins, are broken down into their single components, which then can be reused by the synthetic machineries to build up new molecules (Fig. 2) (Maxfield and McGraw 2004, Huotari and Helenius 2011).

The endosomal system accomplishes a broad range of cellular functions. In somatic cells, it operates together as a dynamic whole, divided into two spatiotemporally distinct fractions - a relatively immobile perinuclear pool of vesicles and tubules localized around the MTOC and a highly dynamic endosome population in the periphery of the cell (Watts 2012, Di Fiore and von Zastrow 2014, Neefjes, Jongsma et al. 2017). The actual architecture supports the functional attributes of the system. Once the vesicular transport intermediate with the material taken up from the extracellular space fuse with the EE, the EEs travel towards the perinuclear cloud, where they mature into or fuse with proteolytic late compartments (Huotari and Helenius 2011, Bright, Davis et al. 2016, Jongsma, Berlin et al. 2016). In this way, efficient and tight regulation of the system is ensured by setting cargo acquisition and processing apart.

Increasing evidence indicates that the **endosomal network** is much more than an intermediate outstation in the pathway for degradation. Elements of the recycling system are required for the proper assembly and maintenance of apical membrane specializations including **primary cilia** and **apical microvilli**, and they administrate many aspects of **junctional protein maintenance** as well as **apical and basolateral identity** in polarized cells (Wang, Brown et al. 2000, Lecuit and Pilot 2003, Scita and Di Fiore 2010, Goldenring 2015). Endosomes can also be active **signalling platforms**, which can be transported to specific cellular regions along long distances, such as neuronal axons (Marlin and Li 2015, Eichel and von Zastrow 2018). Thereby, endocytosis not only controls the time window and intensity of signalling by targeting engaged receptors for degradation as originally though, but it can also define its geometrical distribution within the cell and the particular output (Stenmark 2009, Scita and Di Fiore 2010). Special interest has attracted the study of **APPL1 signalling endosomes** in the last years. APPL1 is an adaptor protein localized to a subset of very early EEs, which subsequently mature to the *bona fide* SEs (Palfy, Remenyi et al. 2012). APPL1 positive endosomes are transiently formed upon stimulation of certain RTKs and accumulate subsets of signalling modules such as Akt and GSK3β (Schenck, Goto-Silva et al. 2008, Diggins and Webb 2017). Thus, sequestration of receptors in this compartment defines the signalling output (Varsano, Taupin et al. 2012, Banach-Orlowska, Szymanska et al. 2015).

Lysosomes constitute the last stage along the endocytic transport. They are spherical vacuoles containing hydrolytic enzymes, which can break down many kinds of biomolecules. Its luminal pH is

within the 4.5 – 5.0 range, optimal for hydrolytic enzymes. The lysosomes not only act as the waste disposal system of material taken up by the endocytic pathway, but also dispose unwanted material from the cytoplasm and intracellular organelles through autophagy (Luzio, Pryor et al. 2007). Mutations in the genes encoding for lysosomal hydrolytic enzymes are responsible for more than 30 different human genetic disorders, which are collectively known as lysosomal storage diseases (Boustany 2013). These diseases result from an accumulation of specific substrates, due to the inability to break them down, and they are related to several neurodegenerative disorders, cancer, cardiovascular, and ageing-related diseases. In addition, and similar to the endosomal system, evidence has accumulated during the last decades demonstrating that lysosomes are much more than disposal organelles. Besides degradation of polymers, the lysosome is involved in secretion, PM repair, cell signalling, and energy metabolism, and can give rise to specialized organelles such as the **melanosomes**, **lytic granules**, **lung lamellar bodies** or **platelet dense granules** (Luzio, Pryor et al. 2007).

1.1.1 Molecular Mechanisms Involved in Endocytic Protein Traffic

Many aspects of protein and lipid trafficking among the endocytic organelles are still far from being understood, but mechanisms executing such transport can mainly be ascribed to three general models that also apply to other cellular trafficking corridors such as the secretory pathways:

1) Non vesicular transport, executed by shuffling proteins, mainly associated to the transport of lipids.

2) Transport using vesicular and tubular intermediates that emanate from donor membranes and fuse with acceptor organelles.

3) Maturation or interconversion of organelles, usually coupled with their transport along the actin and tubulin networks.

Non vesicular transport is not directly the focus of this thesis and therefore, it will not be further discussed. Excellent reviews on the subject can be found in (Lev 2010, Saheki and De Camilli 2017). The **formation of transport intermediates** normally involves the assembly of proteinaceous coats on the cytosolic leaflet of the organelle limiting membrane or the PM. Such coats, as those composed of clathrin and clathrin adaptors, caveolin and cavin, retromer or retriever and sorting nexins, recruit cargo and impose curvature on the lipid bilayer. Assembly of coats with intrinsic curvature, insertion of amphipathic helices, molecular crowding, modification of lipids or the mechanochemical forces generated by actin polymerization or molecular motors, have been invoked to participate in membrane remodelling during the formation of transport intermediates (Farsad and De Camilli 2003, Simunovic, Bassereau et al. 2018). Often, a distinct machinery such as the members of the dynamin family is required to drive final scission of the transport intermediate from the donor membrane (Ramachandran 2011, Campelo and Malhotra 2012). Upon uncoating and **transport along the actin and/or tubulin networks**, the vesicle or tubule limiting membrane fuses with the donor compartment, via a mechanism that involves tethering complexes and SNARES, which ensures the specificity of the donor/acceptor exchange (Kummel and Ungermann 2014). **Tethering** seems to be a prerequisite for most membrane fusion events associated with membrane traffic within the cell. Molecular tethers are either long coiled-coil dimers or monomers, or multisubunit complexes that

link opposing membranes destined to fusion over distances of 25 nm and which engage SNARES. Following tethering, a trans-SNARE complex will form, which overcomes the energy barrier preventing lipid bilayer merging. In this complex, an approximately 16-turn helix of one SNARE wraps around similar helices on three other SNAREs to form a parallel four-helix bundle called a SNAREpin, which is essential for membrane fusion. The centre of the four-helix bundle contains an ionic layer comprising an arginine (R) and three glutamine (Q) residues, each contributed by a different R-SNARE and 3 Qa-, Qb- and Qc-SNAREs, respectively (Malsam, Kreye et al. 2008, Kummel and Ungermann 2014, Witkos and Lowe 2017). Transport via the generation of transport intermediates along the endocytic pathway is well established between the PM and the EE and between the endosomes and the PM or the Golgi apparatus (Fig. 3).

Compartment **maturation** involves the progressive conversion of one organelle into another. The process implicates the exchange of identity markers such as specific tethering complexes and SNARES, which definethe cargo that will be accepted by the limiting membrane. Maturation is often accompanied by the transport of the compartment along cytoskeleton tracks toward the MTOC or the cell periphery, the acquisition or extraction of material via the fusion or budding of transport intermediates, the biochemical biosynthesis and turnover of lipids, in particular, phosphoinositides, and the exchange of small GTPases (Huotari and Helenius 2011). The maturation model is currently well accepted for the transport between the sorting and the late endosomes and it probably also applies, at least to a certain extent, to the recycling pathway through the ERC (see Fig. 6) (Huotari and Helenius 2011, Scott, Vacca et al. 2014).

One of the key regulators of most membrane transport steps within the cell are the **small GTPases** of the **rab and arf families**. The rab protein family of regulatory G proteins has more than 60 members (Maxfield and McGraw 2004, Stenmark 2009), whereas the arf family, including also arf-like (arl) proteins and Sar1, comprises about 30 members (Donaldson and Jackson 2011). Rabs and arfs orchestrate a complex interplay between multiple GTPases, effector proteins, tethering factors, protein and lipid kinases and phosphatases, as well as motor proteins, which ensure the directionality of membrane traffic and the identity of organelles. Trafficking steps controlled by small GTPases include the recruitment of coats, membrane deformation and cargo loading, the control of coat disassembly, vesicle and organelle motility, and finally, the homotypic or heterotypic membrane fusion (Stenmark 2009). Further, their GTPase cycle can monitor the conversion of membrane subdomains with distinct properties essentially contributing to organelle maturation (Fig. 3 and 4).

The rab and arf family members show a very distinct and specific membrane localization pattern throughout the cell and they represent one building-block to maintain the integrity of the cellular organelles or organelle subdomains therein, indispensable for their functionality. Thus rab5 is recruited on forming vesicles at the PM and decorates APPL1 and sorting endosomes. Rab4 labels membrane subdomains on EEs often adjacent to, but not overlapping with, the rab5 subdomains. Rab11, rab8 and arf6 are enriched in ERCs, and rab7 and rab9 are identity landmarks of LEs and lysosomes (Fig. 4) (Stenmark 2009).

Small rab and arf GTPases exist in an active GTP-bound state, which hooks the effector, and an inactive GDP-bound state. Their activation, inhibition or the guanine nucleotide exchange is facilitated by an extensive number of regulatory proteins, working hand in hand to synchronize the chains of events meshed together. Exchange of GDP to GTP is catalysed by guanine nucleotide exchange factors (GEFs). Conversion from the active to the inactive form occurs through GTP

hydrolysis. This event is not only driven by the intrinsic GTPase activity of the rab proteins but it is also catalysed by GTPase-activating proteins (GAPs) (Stenmark 2009). Rab GDP dissociation inhibitors (GDIs) stabilize the inactive state but, even more important, work as a chaperon to actively modify rab GTPases in the cytosol, mediate their delivery to particular destinations and recycle them back to the cytosol (Fig. 4A) (Matsui, Kikuchi et al. 1990, Ullrich, Stenmark et al. 1993, Soldati, Shapiro et al. 1994, Ullrich, Horiuchi et al. 1994). Several domains enriched in particular GTPases can coexist on the membrane of an endosomal compartment without actually overlapping (Fig. 4C). Some rab effectors contain binding sites for two or more different GTPases, thereby acting as molecular connectors (de Renzis, Sonnichsen et al. 2002).

As for the small regulatory GTPases, the particular **phosphoinositide mono- and polyphosphate** ($PtdInsP_xs$) composition of the membranes limiting the compartments also defines their identity. Thus, PtdIns(4)P is enriched in the Golgi and the ERC, $PtdIns(4,5)P_2$ is mainly present at the PM, whereas PtdIns(3)P labels early SEs and $PtdIns(3,5)P_2$ decorates LEs and lysosomes (Fig. 8A) (Haucke 2005, Wallroth and Haucke 2018). Many endocytic proteins bear lipid binding domains such as the FYVE, PH, PX, BAR, ENTH, ANTH, PROPPIN and GRAM domains that specifically recognize certain phosphoinositide mono- or polyphosphates (Lemmon 2008). Particular $PtdInsP_xs$ species are synthesized or turn over locally by the action of PtdIns and $PtdInsP_xs$ kinases and $PtdInsP_xs$ phosphatases, which are often controlled by the activity of small GTPases (Jean and Kiger 2012). In turn, rab and arf effectors often bear $PtdInsP_xs$ binding domains, which synergizes with their GTPase binding sites, imposing a double code that ensures organelle and subdomain identity (Vicinanza et al, 2008). Thus, for instance, APPL1 is recruited to endosomes by $PtdIns(4,5)P_2$ and rab5, whereas the tethering factor EEA1 recognizes rab5 and PtdIns(3)P on more mature SE (Diggins and Webb 2017). Thereby, small regulatory GTPases and $PtdInsP_xs$ cooperate to regulate endocytic coat assembly, endosomal maturation, the formation of ILVs or homo- and heterotypic fusion (Fig. 4B) (Huotari and Helenius 2011).

The particular transport processes along the endocytic compartments will be discussed in detail within the following sections.

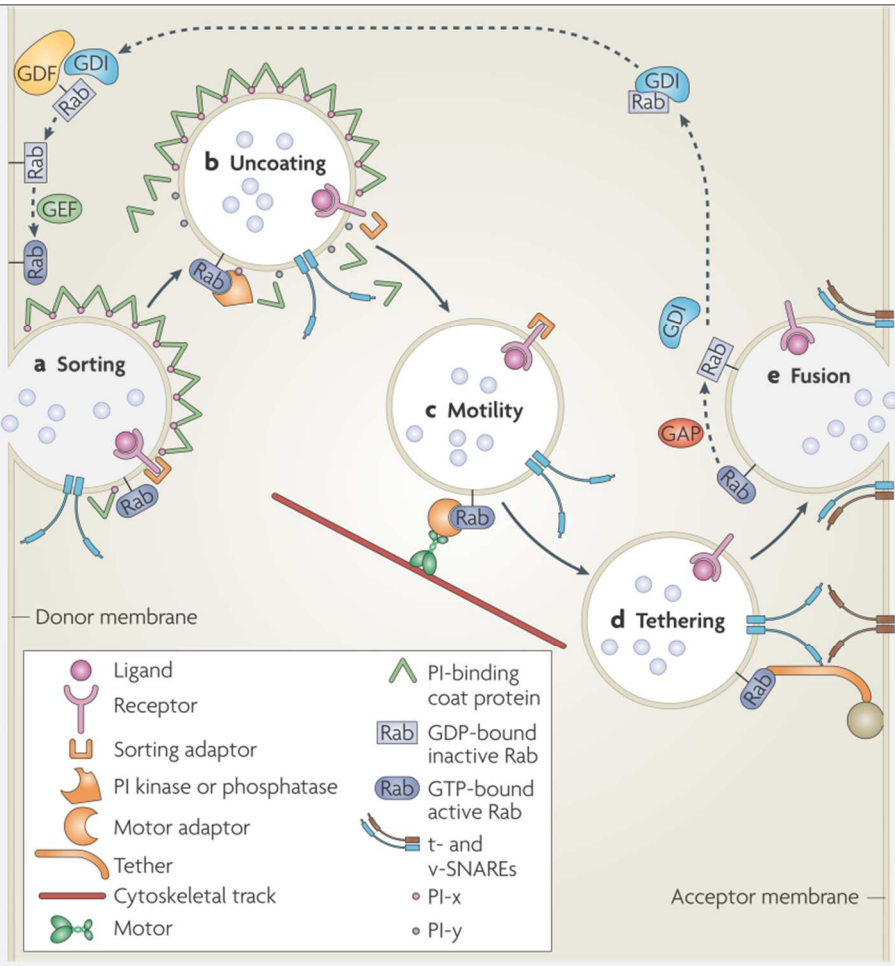

Figure 3. Vesicle Trafficking and Rab GTPases.
Distinct membrane trafficking steps that can be controlled by a rab GTPase and its effectors (indicated in orange). **a**) An active GTP-bound rab can activate a sorting adaptor to sort a receptor into a budding vesicle. **b**) Through recruitment of phosphoinositide (PI) kinases or phosphatases, the PI composition of a transport vesicle might be altered (the conversion of PI-x into PI-y) and thereby cause uncoating through the dissociation of PI-binding coat proteins. **c**) Rab GTPases can mediate vesicle transport along actin filaments or microtubules (collectively referred to as cytoskeletal tracts) by recruiting motor adaptors or by binding directly to motors (not shown). **d**) Rab GTPases can mediate vesicle tethering by recruiting rod-shaped tethering factors that interact with molecules in the acceptor membrane. Such factors might interact with SNAREs and their regulators to activate SNARE complex formation, which results in membrane fusion. **e**) Following membrane fusion and exocytosis, the rab GTPase is converted to its inactive GDP-bound form through hydrolysis of GTP, which is stimulated by a GTPase-activating protein (GAP). Targeting of the rab–GDP dissociation inhibitor (GDI) complex back to the donor membrane is mediated by interaction with a membrane-bound GDI displacement factor (GDF). Conversion of the GDP-bound rab into the GTP-bound form is catalysed by a guanine nucleotide exchange factor (GEF). For further details see text in chapter 1.1.1. Obtained from (Stenmark 2009).

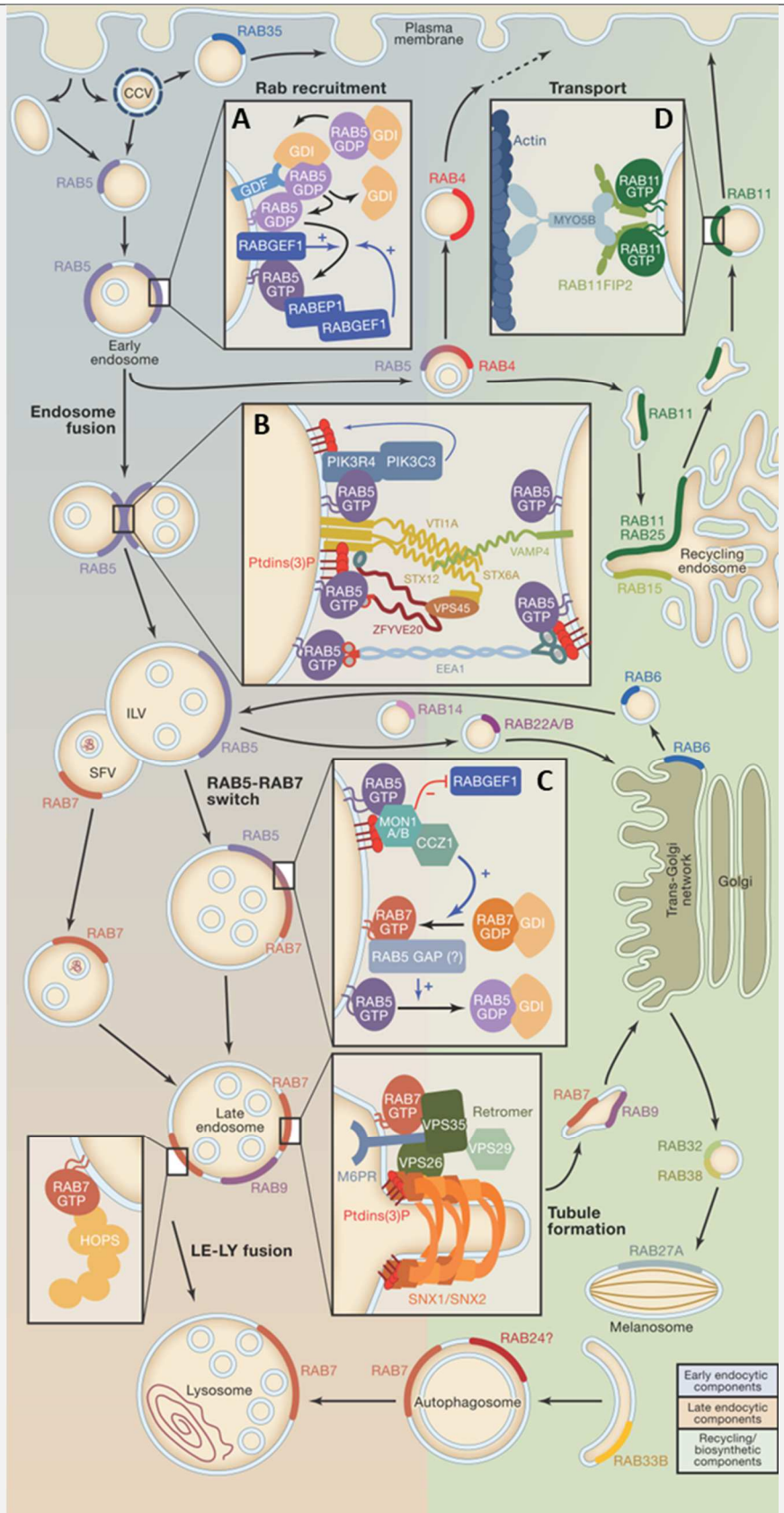

Figure 4. Mammalian Rab GTPases in Endocytic Trafficking.
A. For further details see text in chapter 1.1.1. **B.** For further details see text in chapter 1.1.1. **C.** For further details see text in chapter 1.1.1 and 1.1.1.2. **D.** For further details see text in chapter 1.2.2.3. Obtained from (Galvez, Gilleron et al. 2012).

1.1.1.1 Clathrin-mediated Transport from the PM to SEs

As discussed before, endocytic uptake from the PM can use a variety of molecular machineries which generate morphologically distinct transport intermediates in charge of transporting different cargo. Since this thesis focuses in part on CME, formation and turnover of clathrin-coated vesicles (CCVs) will be discussed further. Excellent reviews on the clathrin independent endocytic pathways can be found in (Ferreira and Boucrot 2018).

The endocytic pathway involving the assembly of a clathrin coat at the inner surface of the PM has been subject of countless studies during the last decades and became the best characterized coat-dependent budding process *in vivo* and *in vitro* (Kirchhausen 2000). More than 60 evolutionarily conserved proteins have been involved in CME but the actual mechanism driving membrane deformation still remains controversial (Kaksonen and Roux 2018). Several molecular mechanisms have been invoked to drive membrane deformation and vesicle fission for CME, including the assembly of clathrin cages with inherent curvature, attached to lipids and cargo (Kirchhausen 2000), the activity of ENTH and BAR domains inducing membrane curvature (Itoh and De Camilli 2006), molecular crowding (Stachowiak, Schmid et al. 2012), Arp2/3-dependent actin polymerization (Schafer 2002), the mechanochemical activity of dynamins (Praefcke and McMahon 2004) or myosins (Krendel, Osterweil et al. 2007), actin polymerization (Idrissi and Geli 2014) and the biogenesis, turn over and translocation of certain lipid species (Haucke 2005).

The machinery and stepwise progress of CME at the cortex is for the most part conserved from yeast to mammals (Kaksonen and Roux 2018), even though the relative implication of the different bending and fission machineries varies. Basically, AP-2 and clathrin play central roles in membrane bending in metazoan, whereas actin and myosin-I have a much more essential role in yeast (Kaksonen and Roux 2018). The requirement for actin in CME in mammalian cells seems to depend on the membrane tension, the cell type and the membrane subdomain (Galletta, Mooren et al. 2010). Likewise, dynamin is essential for vesicle fission in mammals, whereas other redundant mechanisms can efficiently detach endocytic vesicles from the PM in yeast.

A comprehensive sequence of events occurring during the formation of a CCV at the PM was first defined in yeast and subsequently in mammalian cells, using live cell fluorescence imaging of endocytic protein pairs tagged with different GFP variants (Taylor, Perrais et al. 2011, Kukulski, Schorb et al. 2012). Once the early components of the endocytic machinery including clathrin and the muniscin BAR-containing proteins FCHO1 and -2 are assembled, recruitment of cargo adaptors such as the epsins, AP-2 or AP180, presumably loaded with cargo, progressively follows (Idrissi and Geli 2014). Concentration of cargo adaptors seems to be key to promote stabilization and maturation of the clathrin coat and bending of the lipid bilayer (Idrissi and Geli 2014). Even though, clathrin was originally thought to directly assemble in a curved conformation, imposing bending to the attached membrane, accumulating evidence now shows that the clathrin coat first assembles in a flat configuration and only subsequently bends (Idrissi, Blasco et al. 2012, Kukulski, Schorb et al. 2012, Skruzny, Brach et al. 2012, Avinoam, Schorb et al. 2015). What triggers initial assembly of clathrin coats is still not understood. The local biogenesis of PtdIns(4,5)P_2 might be involved in the process, provided that FCHO1 and -2 bear BAR domains that bind PtdIns(4,5)P_2 (Idrissi and Geli 2014). However, experimental evidence indicates that PtdIns(4,5)P_2 has a more important role promoting the stabilization of clathrin cages by inducing a conformational change in the clathrin adaptors that promotes simultaneous clathrin and cargo binding (Skruzny, Desfosses et al. 2015, Garcia-Alai,

Heidemann et al. 2018) or in engaging the endocytic coat to actin (Kaksonen, Toret et al. 2005). **Clathrin and clathrin adaptors** stay at the cell cortex for about 1 - 2 minutes, followed by the recruitment of **type I and type VI myosins** and a burst of **N-WASP and Arp2/3-**dependent actin polymerization, which has been implicated in the stabilization of the membrane curvature in yeast and in the fission of endocytic vesicles, both in yeast and mammalian cells (Boettner, Chi et al. 2011, Taylor, Perrais et al. 2011, Weinberg and Drubin 2012). Shortly after or concomitant with the initiation of the actin burst, proteins involved in scission, such as **dynamin,** and BAR-domain containing proteins, such as **SNX9 or endophilins**, are recruited to the endocytic sites. Again, even though the GTP-dependent fission of endocytic vesicles by dynamin is well documented *in vivo* and *in vitro,* the details on the molecular mechanism driving scission still need to be worked out and it might implicate *in vivo* the generation of membrane tension by the actin machinery, the local biosynthesis of poly-unsaturated lipids or the activity of BAR and ENTH domains (Renard, Johannes et al. 2018). The newly formed vesicle then travels into the cytosol, probably pushed by an actin tail (Kaksonen, Toret et al. 2005, Galletta, Chuang et al. 2008, Kukulski, Schorb et al. 2012, Skruzny, Brach et al. 2012), quickly uncoats and finally fuses with other newly formed endocytic vesicles or pre-formed endosomes (Fig. 5) (Taylor, Perrais et al. 2011, Idrissi and Geli 2014)(Taylor, Perrais et al. 2011).

During vesicle budding from the PM, rab5 in complex with a rab5-GDI is recruited to the clathrin coat and it is required for endocytic uptake (also see chapter 1.2). After budding, **uncoating** of the newly born vesicle is necessary for the forthcoming fusion with other vesicles and endosomal compartments. CCVs keep rab5 attached, which coordinates together with its GEF the coat release via promoting **dephosphorylation of the clathrin adaptor AP-2** and the turnover of PtdIns(4,5)P_2 by phosphatases such as **synaptojanin-1** (Semerdjieva, Shortt et al. 2008). Coat disassembly is also facilitated by **Hsc70 ATPase** (Rapoport, Boll et al. 2008, Xing, Bocking et al. 2010) and the DNAJ-domain containing protein **auxilin** (Lee, Wu et al. 2006, Yim, Sun et al. 2010), which disassemble the clathrin cages, and through protein phosphorylation by members of the **AAK1 and GAK kinase** family and **casein kinase 2**, which disrupt several endocytic complexes (Korolchuk and Banting 2003).

At EEs, rab5 is activated by its GEF rabex-5. Activated rab5-GTP then in turn recruits rabaptin-5, an activator of rabex-5, and the PI-3 kinase Vps34, which generates PtdIns(3)P. PtdIns(3)P and rab5-GTP then synergize to bring several rab5 effectors involved in membrane fusion, which bear FYVE domains, such as the tethering complex EEA1, an elongated coiled-coil dimer, and rabenosyn-5, a protein that directly interacts with the SNARE regulator Vps45 (Simonsen, Lippe et al. 1998, Callaghan, Simonsen et al. 1999, McBride, Rybin et al. 1999, Simonsen, Gaullier et al. 1999, Morrison, Dionne et al. 2008). Thereby, the rab5 activation is amplified by a positive feedback loop that establishes endosome membrane subdomains ready to accept vesicle for fusion (Stenmark, Vitale et al. 1995, Horiuchi, Lippe et al. 1997). Upon tethering, fusion with EEs is mediated by the R-SNARE VAMP4 and the Q-SNAREs syntaxin 13, Vti1A and syntaxin 6.

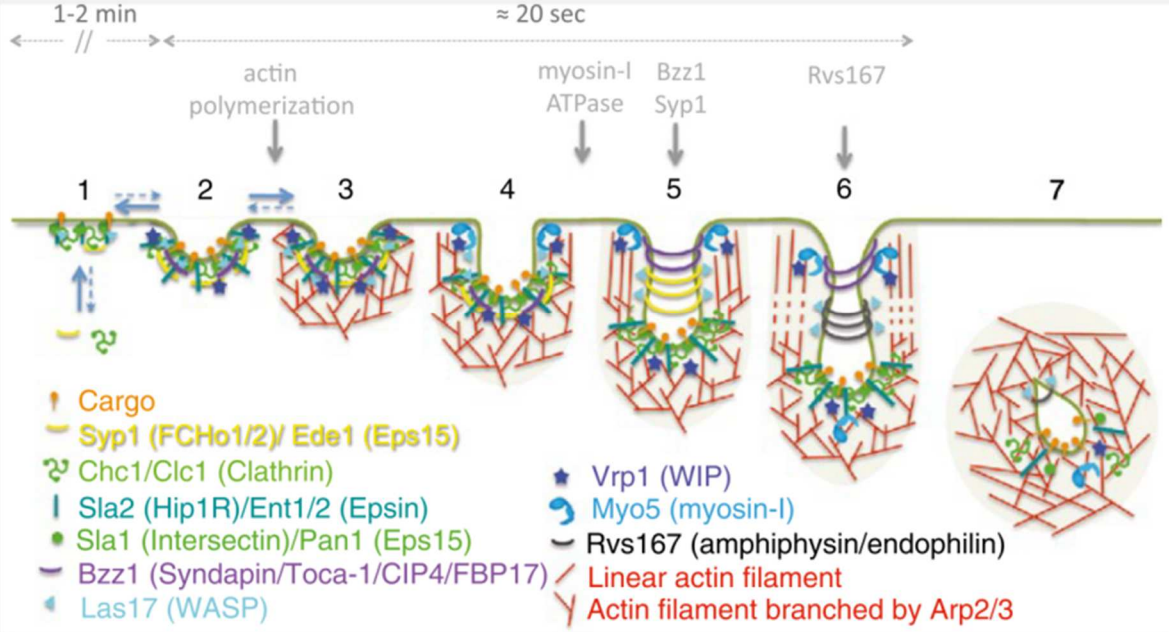

Figure 5. Molecular Model for Sequential Recruitment of Endocytic Protein During CME (in yeast).

Shown are some of the most studied components. Yeast nomenclature and the corresponding mammalian homologues or functional counterparts (between parentheses) are indicated. 1) The early and the coat modules assemble on a flat PM. 2) Membrane invagination and actin polymerization are initiated, most likely in response to a certain threshold of cargo and cargo adaptors. Protein crowding might promote initial membrane curvature. 3) Assembly of an actin cap is initiated. 4) Growth of the branched actin cap promotes the initial elongation of the profile. Concentration of Myo5 (myosin-I)/Vrp1 (WIP) at the base of the emerging bud promotes appearance of barbed ends facing the PM. 5) Biased growth of these filaments will push the actin cap and the linked actin coat inward and promote the directed elongation of the profile. The motor domain of Myo5 (myosin-I) pushes inwards the growing actin filaments attached to the coat causing the elongation and the narrowing of the profile. By sensing the increased membrane curvature or tension of the tubules, Bar proteins move from the tip to the tubular area of the invagination and constrict it. 6) Progressive recruitment of bar proteins might then promote further elongation and/or constriction of the endocytic tubule. Transient depolymerisation of actin at the invagination neck might be required for vesicle scission. The fission reaction probably needs the tubulating activity, segregation of lipid domains, actin polymerization and the mechanochemical activity of dynamin. 7) The released vesicle continues to move into the cell interior. Movement might be powered by the different NPFs that remain associated with the vesicle. The localization of the endocytic proteins around the released vesicle is hypothetical. Gray arrows show the critical requirement of different endocytic machineries at different stages of the process. Equilibrium arrows denote possible reversibility between the indicated stages. Dashed blue arrows point to a possibly less favourable progression. Obtained from (Idrissi and Geli 2014).

1.1.1.2 Maturation of SEs to LEs and Biogenesis of ILVs

The SE has a half-life time of about 8 minutes, during which it continually receives newly endocytosed vesicles from the surface and exports recycling molecules by the fission of tubules (see chapter 1.1.1.5 for recycling) (Maxfield and McGraw 2004). As maturation occurs, SEs travel into the cytosol along microtubule tracks and progressively loose their capacity to fuse with incoming vesicles from the PM (Fig. 6) (Huotari and Helenius 2011).

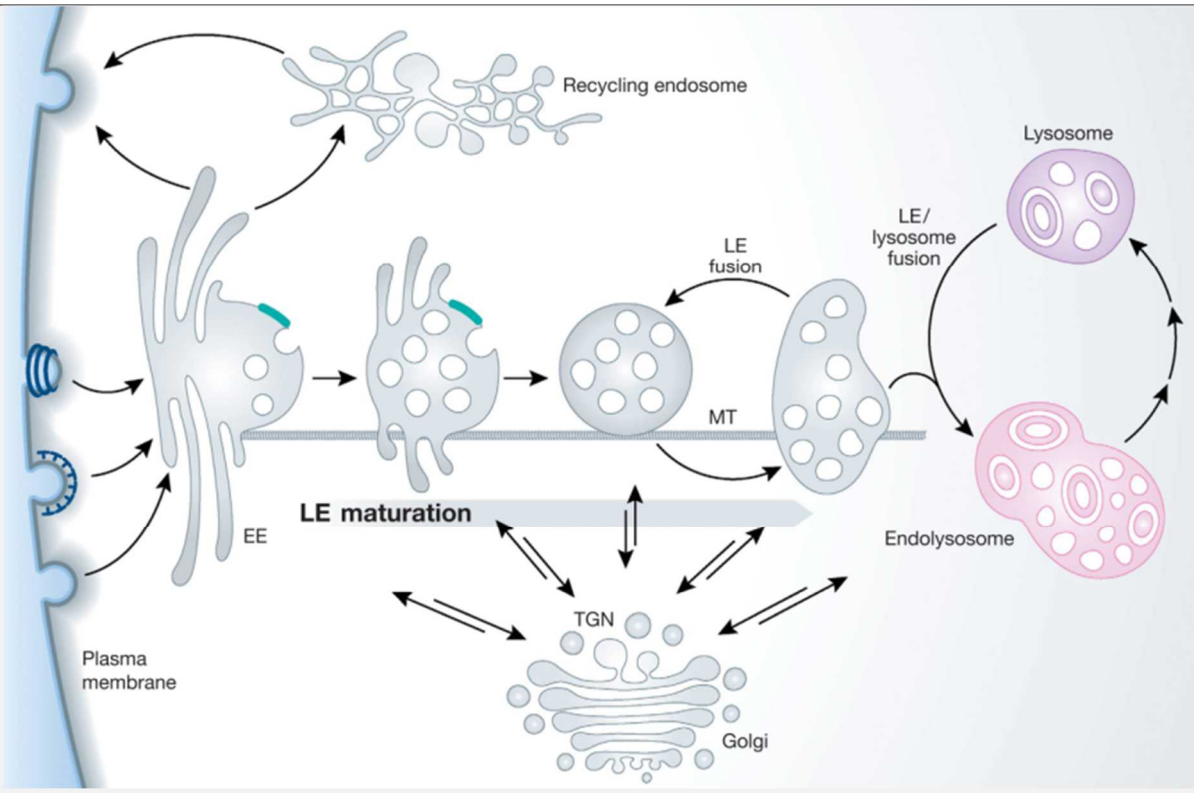

Figure 6. Model of Endosomal Maturation.
The primary endocytic vesicles deliver their contents and their membrane to EEs in the peripheral cytoplasm. After a period of about 8 to 15 min during which the EEs accumulate cargo and support recycling to the PM (directly or via ERC in the perinuclear region), conversion of the EEs to LEs takes place. Thus, as the endosomes are moving towards the perinuclear space along microtubules (MT), the nascent LEs are formed inheriting the vacuolar domains of the EE network. They carry a selected subset of endocytosed cargo from the EE, which they combine en route with newly synthesized lysosomal hydrolases and membrane components from the secretory pathway. They undergo homotypic fusion reactions, grow in size, and acquire more ILVs. Their role as feeder system is to deliver this mixture of endocytic and secretory components to lysosomes. To be able to do it, they continue to undergo a maturation process that prepares them for the encounter with lysosomes. The fusion of an endosome with a lysosome generates a transient hybrid organelle, the endolysosome, in which active degradation takes place. What follows is another maturation process; the endolysosome is converted to a classical dense lysosome, which constitutes a storage organelle for lysosomal hydrolases and membrane components. Obtained from (Huotari and Helenius 2011).

The maturation of EEs to LEs, defined as the organelles with capacity to fuse with lysosomes, occurs as a steady conversion of the organelle properties and composition. During maturation, membrane components such as receptors, transporters and lipids derived from the PM that need to return to their original location, are sorted out from the bulk fraction of the luminal content, containing fluid, soluble nutrients and large particles (Huotari and Helenius 2011), in thin tubules with a high surface/lumen ratio. At least a fraction of these tubules is generated by retromer or retromer related complexes and their associated sorting nexins (SNX) (see chapter 1.1.1.4 and 1.1.1.5). The luminal content will then be delivered to the lysosome once the endosomes acquire the proper fusion machinery. When transmembrane proteins need to be targeted to the lysosome, they are labelled with ubiquitin moieties and packed in ILVs in an ESCRT-dependent manner, which will be conveyed towards the lysosome with the rest of the luminal cargo (Frankel and Audhya 2017).

As already mentioned, the small rab and arf GTPases govern membrane trafficking. At the SE rab5 and its associated effectors occupy a leading position. Conversion to the LE implicates the **replacement of rab5 for rab7** (Rink, Ghigo et al. 2005, Vonderheit and Helenius 2005, Poteryaev,

Datta et al. 2010). How exactly this transition occurs in concert with other molecular changes on the endosomal membranes is slowly starting to emerge and it seems to implicate coordinated positive and negative feedback loops (Fig. 4C).

As the biogenesis of PtdIns(3)P and the activation of rab5 reach a threshold, a negative feedback loop is initiated by the recruitment of the **Mon1/Ccz1 complex,** which shuts down rabex-5 and functions as a rab7 GEF, leading to the disassembly of the rab5 effectors and the recruitment of the rab7 associated machinery in a process that has been called the **'cut off switch' model** (Fig. 7) (Del Conte-Zerial, Brusch et al. 2008). One crucial consequence of the rab5 to rab7 conversion is the exchange of the fusion machinery on the endosomal membrane and thereby, the exchange of the fusogenic specificity. The LEs can no longer fuse with EEs but follow their path towards degradation, acquiring the necessary tethering complexes and SNAREs to fuse with lysosomes. Two tethering complexes define the endosomal identity: the EE CORVET complex and the LE HOPS complex (kleine Balderhaar and Ungermann 2013, Solinger and Spang 2013). **CORVET,** composed by a core of Vps11, Vps18, Vps16 and Vps33, all shared with HOPS, and two specific subunits, Vps3 and Vps4, which interact with rab5. CORVET probably accepts newly formed CCVs coming from the Golgi complex, bearing the GGA1, GGA2 and AP-1 adaptors (Angers and Merz 2011) and drives homotypic fusion of EEs. However, the SNAREs involved in the process have not been worked out. **HOPS** also bears the core subunits but, instead of Vps39 and Vps4, it includes Vps39 and Vps41, which interact with rab7, and mediate binding to LE and lysosomal SNAREs (Solinger and Spang 2013). HOPS governs homotypic and heterotypic fusion of LE with lysosomes and autophagosomes (see next section), as well as the acceptance of the AP-3-dependent transport intermediates from the Golgi (Balderhaar and Ungermann 2013). The Vps39 HOPS subunit also binds to Mon1, which acts as a GEF for rab7, thereby installing a positive feedback loop that stabilizes the rab7 subdomains (Nordmann, Cabrera et al. 2010, Poteryaev, Datta et al. 2010).

As mentioned before, $PtdInsP_x$s also define the identity of endosomal membrane compartments, together with small GTPases. Hence, also their conversion takes a central position during the maturation process (Fig. 8). Whereas the EEs mainly contain **PtdIns(3)P**, LE are **PtdIns(3,5)P_2** dominated (Di Paolo and De Camilli 2006, Hullin-Matsuda, Taguchi et al. 2014). Again, this change is coordinated by the rab switch which defines the $PtdInsP_x$ modifying machinery recruited to endosomes (Di Paolo and De Camilli 2006, Viaud, Mansour et al. 2016). As mentioned before, rab5-GTP recruits the **class III phosphatidylinositol 3-kinase (PtdIns(3)K) VPS34**, the main producer of PtdIns(3)P through direct interaction with its partner, p150. The complex also binds to rab7. Interestingly though, interaction with rab7 is more prominent when rab7 is in its inactive GDP-bound conformation (Schu, Takegawa et al. 1993, Christoforidis, Miaczynska et al. 1999, Murray, Panaretou et al. 2002, Stein, Feng et al. 2003). Therefore, progressive activation of rab7 reduces the interaction of VPS34 on membranes, providing a negative feedback control to PtdIns(3)P synthesis and, as a consequence, to the recruitment of **FYVE domain** containing rab5 effectors (Di Paolo and De Camilli 2006) (Lindmo and Stenmark 2006). PItdIns(3)P is also consumed by its conversion to PtdIns(3,5)P_2. Vps34 in turn forms a complex with the **PItdIns(3)P-5-kinase PIKfyve** in mammals and Fab1 in yeast, which generates PtdIns(3,5)P_2 from PtdIns(3)P. $PtdInsP_x$s conversion is tightly linked to other endosome maturation steps (Huotari and Helenius 2011). Parts of the ESCRT machinery responsible for ILV formation are recruited by both PtdIns(3)P and PtdIns(3,5)P_2 (Katzmann, Stefan et al. 2003, Whitley, Reaves et al. 2003, Teo, Gill et al. 2006). This probably allows ILV formation and cargo sorting to be coordinated with the rab conversion and the rest of the maturation programme (See Fig. 8 and following sections).

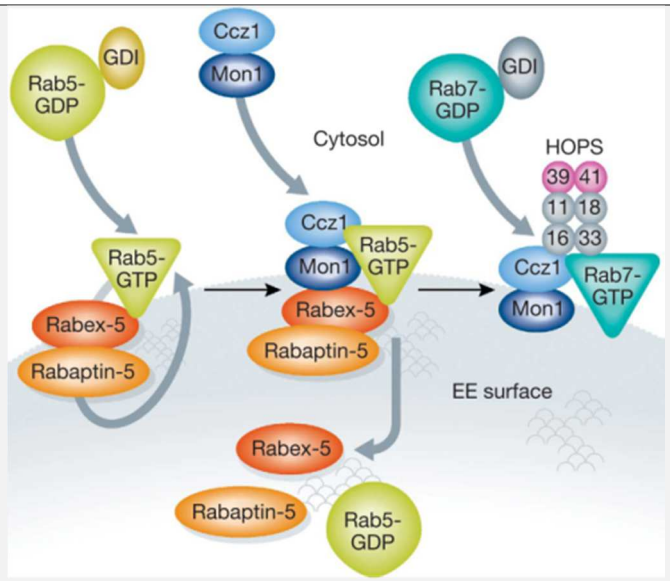

Figure 7. 'Cut off switch' Model.
The rab5/rab7 switch during endosome maturation. Normally, rab5-GDP and rab7-GDP reside in the cytosol bound to its GDI. Rab5 is activated to its GTP-bound and membrane-associated form by the GEF rabex-5 on EE membranes. The rab5 effector rabaptin-5 binds to rabex-5 and promotes the activation of rab5, thus forming a positive feedback loop in which more rab5 molecules are activated and recruited. To initiate the rab switch, Mon1/SAND-1 in complex with Ccz1, binds to rab5, PtdIns(3)P, and rabex-5, causing disassociation of rabex-5 from the membrane. This in turn terminates the feedback loop, resulting in rab5 inactivation and disassociation. The Mon1/SAND-1–Ccz1 complex promotes (directly or indirectly) the recruitment and activation of rab7. Members of the HOPS complex (Vps11, Vps16, Vps18, Vps33, Vps39, and Vps41) are able to bind both, rab7 and the Mon1/SAND-1–Ccz1 complex. The HOPS complex mediates membrane tethering, needed for fusion with other LEs and lysosomes. Obtained from (Huotari and Helenius 2011).

EE to LE maturation also implicates a **switch in cytoplasmic motility** and subcellular localization. The endosomes associate with a set of microtubule-dependent motors that allow them to move over long distances into the perinuclear region of the cell. Rab7 recruits factors such as **RILP** (rab7-interacting lysosomal protein), a protein that connects LEs to **dynein** motors able to move along microtubules towards the MTOC, where the TGN, the ERC and lysosomes are located (Luzio, Pryor et al. 2007, Huotari and Helenius 2011). Cholesterol levels can modulate the RILP mediated engagement of endosomes to dynein via the Oxysterol Related Protein ORP1L (Neefjes, Jongsma et al. 2017).

Apart from changes on the endosomal membrane, **acidification of the luminal pH** has an important impact on the maturation process (Fig. 2). EEs have a pH in the 6.8 – 6.1 range, LEs in the 6.0 – 4.8 range, and in lysosomes, the pH can drop to values around 4.5 (Yamashiro and Maxfield 1987). The low pH provides a better environment for hydrolytic reactions of the hydrolases received from the TGN, but it is also essential for membrane trafficking, for the sorting of cargo and for the inactivation of internalized pathogens (Maxfield and McGraw 2004). The difference in extracellular and EE pH provides the asymmetry needed to allow receptors to release their cargo inside the cell. The difference between endosomal and the final lysosomal pH permits the stepwise accumulation of active hydrolases (Luzio, Pryor et al. 2007) (Xu and Ren 2015). How acidification is coupled to the maturation process is far from being understood. The **large V-ATPase** serves as a transmembrane pore for protons in the endosomal system, which binds and hydrolyses the ATP (Forgac 2007, Marshansky and Futai 2008). Recent evidence indicates that binding of the rab7 effector RILP to the V-ATPase may stabilize the pump and therefore promote acidification (De Luca, Cogli et al. 2014). In

addition, production of PtdIns(3)P might be required for its initial assembly (Huotari and Helenius 2011). On the other hand, since V-ATPases generate a positive inside membrane potential, acidification is also affected by a variety of independent factors such as Na^+/K^+ ATPases and channels for the influx of counter ions and therefore, also changes in lumenal ionic environment occur (Huynh and Grinstein 2007, Jentsch 2007, Marshansky and Futai 2008, Huotari and Helenius 2011).

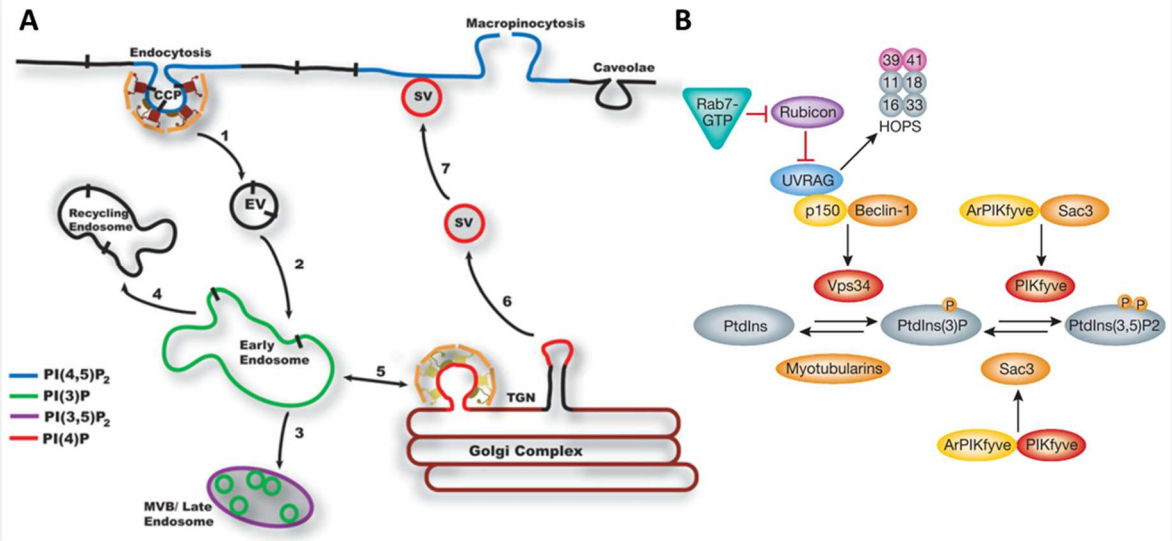

Figure 8. PtdInsPs Regulation of the Endocytic and Exocytic Pathways.
A. PtdIns(4,5)P_2 (blue) is required for the assembly of CCPs as well as for macropinocytosis and for fusion of secretory vesicles and granules (SVs). PtdIns(3)P (green) is present in early endosomes and internal vesicles of the MVB. At the boundary membrane of the MVB, PtdIns(3)P is converted into PtdIns(3,5)P_2 (purple). PtdIns(4)P (red) localizes to the Golgi complex and in particular to the TGN. Endocytic vesicle (EV). Obtained from (Haucke 2005). **B.** On EEs, PtdIns(3)P is synthesized by the kinase VPS34, which forms a core complex together with p150 and Beclin-1. The complex binds on endosomes to UVRAG, which is normally inhibited by a rab7 effector, rubicon. Once activated, rab7 sequesters rubicon from UVRAG, allowing it to activate the HOPS complex. Dephosphorylation of PtdIns(3)P is catalysed by members of the myotubularin family. The kinase responsible for conversion of PtdIns(3)P to PtdIns(3,5)P_2 is PIKfyve (Fab1). It forms an active complex with its activator ArPIKfyve (Vac14p) and the phosphatase Sac3 (Fig4). This complex is required for both the kinase and the phosphatase activities. Obtained from (Huotari and Helenius 2011).

As rab5 exchanges for rab7, PtdIns(3)P is converted to PtdIns(3,5)P_2 and the lumen acidifies. The endosomes gain **lysosomal hydrolases** and membrane proteins in a stepwise manner. These lysosomal components are transported mainly from the TGN. In the TGN, the cytosolic hydrolases need to be coupled to membrane bound receptors for efficient transport in vesicles to the endosomes. Fully processed hydrolases are marked with a mannose 6-phosphate and recognized with high affinity by multifunctional transmembrane receptors such as the CD-MPR (catium-dependent mannose 6-phosphate receptor) and CI-MPR (catium-independent mannose 6-phosphate receptor) (Ghosh, Dahms et al. 2003). The transport of enzymes from the TGN to the endosomes mainly relies on the formation of CCVs that work in concert with **AP-1 and GGA adaptor** proteins for delivery to the EEs, and with **AP-3** for delivery of membrane proteins to the LEs (Park and Guo 2014).

Finally, endosomal maturation is also associated with the **formation of ILVs** that carry the membrane associated ubiquitinated proteins destined for degradation (Huotari and Helenius 2011). Indeed, formation of ILVs seems to be a pre-requisite for transfering material to Lysosomes (Luzio, Pryor et al. 2007). The formation of ILV is dependent on the **ESCRT** (Endosomal Sorting Complexes Required for Transport) **complexes**, which trap ubiquitinated cargo and drive membrane deformation with opposite curvature, as compared to the clathrin and the COPI/II coats (Fig. 9) (Raiborg and Stenmark

2009, Hurley and Hanson 2010, Huotari and Helenius 2011). The ESCRT machinery was originally identified in yeast and is evolutionary conserved. It consists of a subset of 17 proteins, assembled in five different subcomplexes, ESCRT-0 to –III and the Vps4-Vta1 complex (Hurley and Hanson 2010). Some of this subcomplexes are also involved in viral budding from the PM and cytokinesis (Votteler and Sundquist 2013, Scourfield and Martin-Serrano 2017).

ESCRT-0, comprising HRS and Stam, selectively recognizes PtdIns(3)P on the endosomal membranes through the HRS FYVE domain (Raiborg, Bache et al. 2001), and ubiquitinated cargo through several ubiquitin interacting motifs (Katzmann, Babst et al. 2001, Bilodeau, Urbanowski et al. 2002). ESCRT-0 on its own can assemble into larger complexes (Mayers, Fyfe et al. 2011, Takahashi, Mayers et al. 2015), creating subdomains that facilitate the retention of ubiquitinated cargoes (Sachse, Urbe et al. 2002, Raiborg and Stenmark 2009, Norris, Tammineni et al. 2017). ESCRT-0 subdomains may be further stabilized by flat clathrin lattices that are recruited by the C-terminal clathrin binding motif of the ESCRT-0 subunit HRS (Raiborg, Bache et al. 2001, Raiborg, Bache et al. 2002, Sachse, Urbe et al. 2002). However, a universal requirement for clathrin in ILV cargo sorting remains to be demonstrated (Wollert and Hurley 2010). Interestingly, ESCRT-0 has been found to interact with clathrin already in clathrin-coated pits, suggesting that cargoes are sorted rapidly upon cellular internalization (Mayers, Wang et al. 2013).

ESCRT-0 also recruits ESCRT-I and ESCRT-II, which also collect and concentrate ubiquitinated cargo (Stuffers, Brech et al. 2009). The **ESCRT-I complex** is a heterotetramer (1:1:1:1) of Vps23, Vps28, Vps37, and Mvb12. Vps23 contains one ubiquitin E2 variant domain, which is responsible for the binding of ubiquitin and the ESCRT-0 complex. Mvb12 can also bind ubiquitin via its carboxy-terminus. Vps28 is responsible for the interaction of ESCRT-I and ESCRT-II by associating with the GLUE domain (GRAM-Like Ubiquitin-binding in EAP45) of Vps36 through its carboxy-terminal four-helix bundle domain (Teo, Gill et al. 2006, Hurley and Hanson 2010). **ESCRT-II** is a heterotetramer (2:1:1) composed of two Vps25 subunits, one Vps22, and one Vps36 subunit. Vps36 contains a GLUE domain that binds PtdIns(3)P and the ESCRT-I Vps28 subunit. ESCRT-II coordinates assembly of ESCRT-III that drives membrane deformation and vesicle invagination (Hurley and Hanson 2010). The **ESCRT-III** complex contains both essential (Vps20, Snf7, Vps24 and Vps2) and nonessential components (Vps60, Did2, and Ist1) and it is likely the most important of all the ESCRT machinery, since it plays a role in all ESCRT mediated processes (Hurley and Hanson 2010). ESCRT-III forms long filaments that coil around the site of membrane constriction just prior to membrane cleavage (Wollert, Wunder et al. 2009). These filamentous structures function as a ring-like fence that plugs the budding vesicle to prevent cargo proteins from escaping into the cell's cytosol. Vps20 initiates assembly of ESCRT-III by acting as a nucleator of Snf7 polymer assembly (Teis, Saksena et al. 2008). Vps24 then associates with Snf7 to cap the complex and recruit Vps2. Vps2 then brings the AAA-ATPase Vps4 to the complex. Last, the **Vps4-Vta1 complex** induces ESCRT disassembly and cargo de-ubiquitination (Hurley and Hanson 2010). The AAA-ATPase domain of Vps4 hydrolyses ATP to power disassembly of the ESCRT-III complex (Lata, Schoehn et al. 2008, Saksena, Wahlman et al. 2009). Vta1 is thought to act as an activator of Vps4, aiding its assembly and enhancing its AAA-ATPase activity

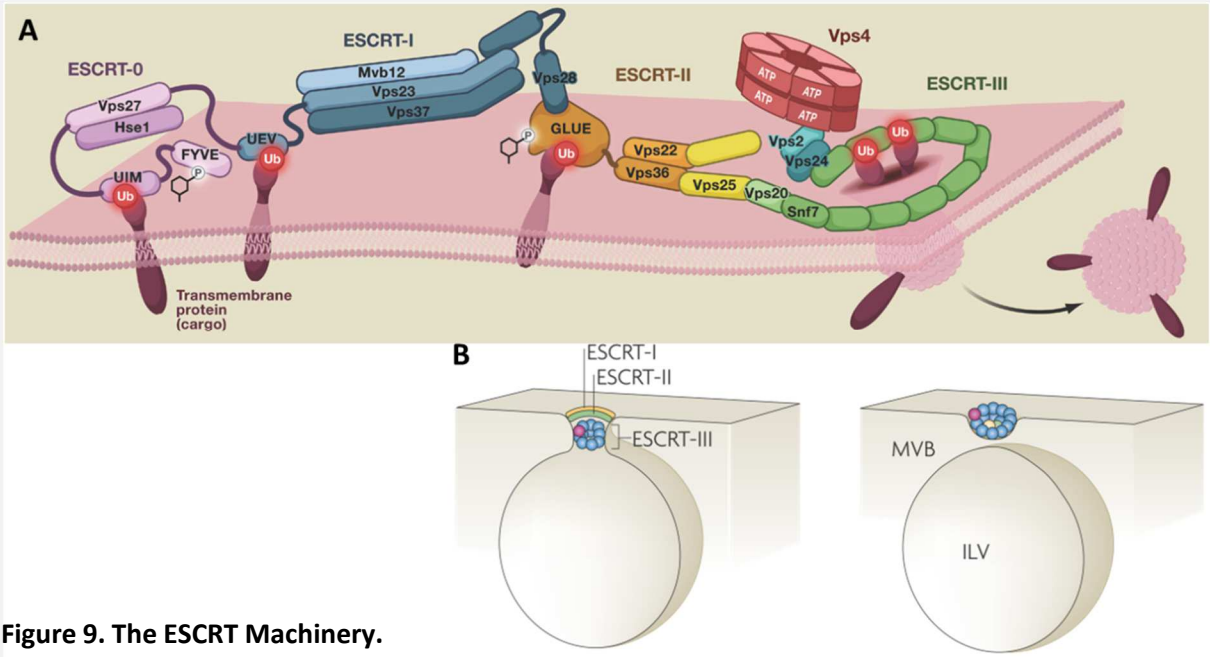

Figure 9. The ESCRT Machinery.

A. The sequential action of ESCRT-0,-I,-II,-III, and the Vps4 complex is required to form MVB vesicles and to sort ubiquitinated membrane proteins into these vesicles. Initiation/Cargo Recognition: ESCRT-0 is a heterodimer consisting of Vps27 and Hse1. ESCRT-0 binds PtdIns(3)P on endosomes via a FVYE domain and ubiquitianted cargo via two UIM domains. ESCRT-0 recruits ESCRT-I and thereby initiates the MVB pathway. Cargo Sorting: 1) ESCRT-I is a heterotetramer consisting of Vps23, Vps28, Vps37, and Mvb12. The UEV domain of Vps23 binds ubiquitinated membrane proteins. Vps28 interacts with the GLUE domain of Vps36 in ESCRT-II. 2) ESCRT-II is a heterotetramer formed of Vps36, Vps22, and two Vps25 molecules. The GLUE domain of Vps36 binds PtdIns(3)P, Vps28, and ubiquitianted membrane proteins. Vps25 interacts with Vps20 of ESCRT-III. Cargo Sequestration/MVB Vesicle Formation: ESCRT-III assembles into a highly ordered filament-like hetero-oligomer. Vps20 nucleates the homo-oligomerization of Snf7 that is capped by Vps24. Vps24 recruits Vps2 and initiates Vps4-dependent ESCRT-III disassembly. ESCRT-III is required for the last steps of MVB sorting, cargo sequestration, and MVB vesicle formation. Disassembly: The AAA-ATPase, Vps4 disassembles ESCRT-III and catalyses the final step of the MVB pathway. The MIT domain of Vps4 interacts directly with the C-terminal region of Vps2 (MIM1) and Vps20 (MIM2). Obtained from (Teis, Saksena et al. 2009). **B**. Integration of budding and scission. After assembling in the bud neck ESCRT-III spiral assembles on the bud-proximal side of ESCRT-II to carry out scission of the intralumenal vesicle (ILV). Obtained from (Hurley and Hanson 2010). For further details see text in chapter 1.1.1.2.

1.1.1.3 Transport from LE to Lysosomes

Internalized material that is not recycled will be delivered to the lysosomes for degradation. The mechanism for transfer of endocytosed material from late endosomes to lysosomes remained controversial for years, with different models proposing: 1) the biogenesis of transport intermediates from LE and their fusion with lysosomes, 2) a “kiss and run” fusion mechanism that will allow transfer of luminal material while preserving the identity of the organelles, 3) progressive maturation of LE to lysosomes by acquisition of hydrolases from the Golgi and acidification of the lumen or, 4) complete heterotypic fusion between LE and lysosomes (Luzio, Pryor et al. 2007). Live-cell imaging currently favours the view that both “kiss and run” and “complete heterotypic” fusion events occur between LEs and lysosomes (Bright, Gratian et al. 2005). The direct and complete fusion of late endosomes with lysosomes would consume both organelles if no recovery process occurred. Therefore, a membrane-retrieval process to remove endosomal membrane proteins and recycle SNAREs is necessary, which probably involves the retromer (Luzio, Pryor et al. 2007). Overall, the lysosome

reformation process could be considered as maturation, being the lysosome defined as the compartment that bears hydrolytic enzymes but not MPRs.

In common with other fusion events in the secretory and endocytic pathways, the fusion of LE and lysosomes requires an initial step of tethering mediated by HOPS, the formation of a trans-SNARE complex, the presence of *N*-ethylmaleimide sensitive factor (NSF), soluble NSF attachment proteins (SNAPs) and the small GTPase rab7 (Luzio, Pryor et al. 2007). Much has been learnt from studies in yeast using an *in vitro* assay that monitor vacuolar fusion (Darsow, Rieder et al. 1997, Fischer von Mollard and Stevens 1999, Wang, Stromhaug et al. 2002, Wang, Stromhaug et al. 2003, Merz and Wickner 2004). In mammals, antibody-mediated blocking in cell-free systems demonstrates that Syntaxin-7, Vti1B and Syntaxin-8 are required both for homotypic LE fusions and heterotypic LE–lysosome fusions. What distinguishes the two fusion events is the R-SNARE, which is VAMP8 for homotypic LE fusion, and VAMP7 in the case of heterotypic fusion of endosomes with lysosomes (Luzio, Parkinson et al. 2009).

1.1.1.4 Retrograde Transport from the Endosomes to the Golgi

As previously mentioned, lysosomal hydrolases need to be coupled to membrane bound receptors for efficient transport from the Golgi to the endosomes. Fully processed hydrolases are marked with a mannose 6-phosphate and recognized with high affinity by multifunctional transmembrane receptors such as the CD-MPR and the CI-MPR. The enzymes separate from the receptors at the acidic pH of the endosomes and the reusable MPR is returned to the TGN several times for another round of enzyme delivery (Maxfield and McGraw 2004). Likewise, v-SNAREs need to be recycled back to their organelle of origin to be packed again in transport intermediates.

Transport from the endosomes to the TGN relays on the activity of **retromer and sorting nexins (SNXs)** (Fig. 10A) (Gallon and Cullen 2015). Retromer was first identified in yeast as a complex required for the retrograde transport of Vps10, the functional homolog of the MPRs (Seaman, McCaffery et al. 1998). The yeast retromer comprises five subunits organized in two subcomplexes: 1) The cargo-selective core subcomplex formed by Vps26, Vps29 and Vps35, and 2) the tubulating SNXs Vps5 and Vps17. The mammalian retromer also functions in retrograde transport of the CI-MPR to the TGN, in complex with the Vps5 and Vps17 counterparts SNX1, SNX2, SNX5, SNX6 and SNX32, respectively, which form a heterodimer (Gallon and Cullen 2015). In mammalian cells, though, the Vps26/ Vps29/Vps35 heterotrimer can work with other non-tubulating SNXs that significantly contribute to cargo selection (Gallon and Cullen 2015). Further, the core subcomplex does not bind so tightly to the SNX dimer in mammalian cells as in yeast cells (Swarbrick, Shaw et al. 2011). Hence, the heterotrimeric Vps26/Vps29/Vps35 retromer subcomplex will be from now on referred to as retromer. Besides the MPR, the classical SNX–BAR–retromer subcomplex also returns the Sortilin-related receptor (SorLA) and SorCS1 (Sortilin-related Vps10 domain containing receptor 1), the iron transporter DMT1 (divalent metal transporter 1) and the Wnt signalling receptor Wntless (WLS) to the TGN (Belenkaya, Wu et al. 2008, Franch-Marro, Wendler et al. 2008, Pan, Baum et al. 2008, Lane, Raines et al. 2010, Tabuchi, Yanatori et al. 2010, Fjorback, Seaman et al. 2012).

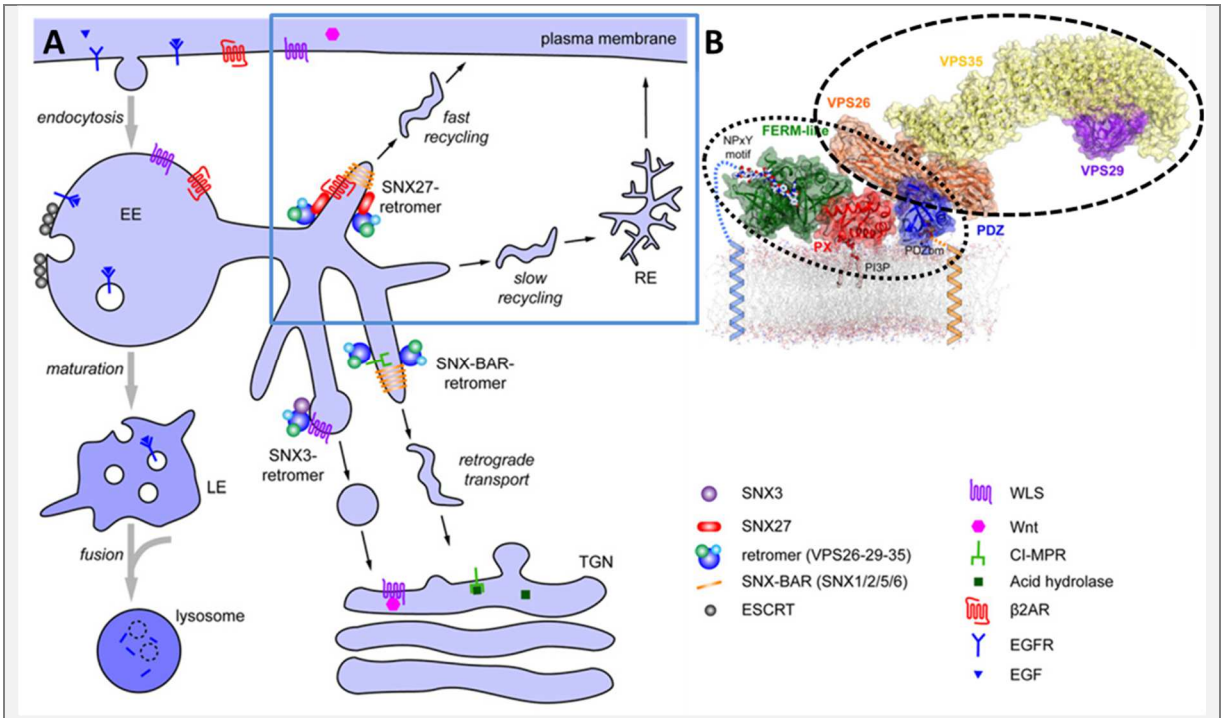

Figure 10. Retromer-mediated Trafficking Pathways.

A. Mammalian retromer mediates at least three distinct export pathways from endosomes. The 'canonical' SNX–BAR–retromer, comprising the core retromer trimer and the SNX–BAR subcomplex, mediates retrograde trafficking of cargo such as CI-MPR from endosomes to the TGN. The SNX3–retromer, comprising the core retromer trimer and SNX3, traffics the WLS receptor from endosomes to the TGN. The SNX27–retromer transports cargo bearing PDZbms from endosomes to the PM. The blue square marks the retrograde transport pathways to the PM. Obtained from (Gallon and Cullen 2015). **B**. Model of the SNX27–retromer complex. SNX27 is marked by a dotted circle. The PDZ domain (blue) and the FERM-like domain (green) of SNX27 bind PDZbm- and NPXY/NXXY-containing transmembrane cargo respectively, whereas the PX domain of SNX27 (red) associates with the endosomal lipid PtdIns(3)P. The three subunits of retromer are marked by a dashed circle. VPS26 (orange) binds the PDZ domain of SNX27, VPS35 (yellow) binds VPS26 and VPS29 (purple) in turn binds VPS35. Obtained from (Gallon and Cullen 2015). For further details see text in chapter 1.1.1.4 and 1.1.1.5.

The VPS26-VPS29-VPS35 trimer is an elongated structure in which VPS26 and VPS29 bind to the N- and C-terminal portions of VPS35 (VPS35N and VPS35C), respectively (Fig. 10B) (Hierro, Rojas et al. 2007). VPS26 has a bilobed β sandwich, arrestin-like fold (Shi, Rojas et al. 2006, Collins, Norwood et al. 2008), but the structural details of its interaction with VPS35N are not known. VPS29, on the other hand, has a phosphoesterase fold (Collins, Skinner et al. 2005, Wang, Guo et al. 2005) that serves as a scaffold for the α-helical solenoid structure of VPS35C (Hierro, Rojas et al. 2007).

The **SNX family** includes 33 members in mammals (Gallon, Clairfeuille et al. 2014). SNXs are characterized by their specific type of PhoX homology (PX) domain, the SNX–PX domain, which binds $PtdInsP_x$s and, most commonly, to PtdIns(3)P (Teasdale and Collins 2012). Since PtdIns(3)P is enriched at the EE, most SNXs are associated with this membrane compartment. The family can be divided into five subfamilies according to their domain organization: the SNX–BAR, SNX–FERM (protein 4.1/Ezrin/Radixin/Moesin), SNX–PX, SNX–PXA–RGS–PXC and SNX–MIT subfamilies (Teasdale and Collins 2012). Vps5 and Vps17 and their mammalian counterparts are members of the SNX–BAR subfamily. In addition to the SNX–PX domain, all SNX–BAR subfamily members bear a C-terminal BAR domain (van Weering, Verkade et al. 2010), which is capable of dimerizing with another BAR domain to form a rigid banana-shaped structure in homo- and hetero-dimers (van Weering, Sessions et al. 2012). BAR domain dimers prefer to associate with curved membranes, thereby sensing curvature

(Zimmerberg and McLaughlin 2004). Furthermore, they can form higher order helical arrays that are capable of tubulating membranes (see Fig. 11) (Frost, Perera et al. 2008).

Retromer tubules destined to the TGN are thought to emanate at the transition point between the rab5 to rab7 conversion (Hierro, Gershlick et al. 2015). The SNX dimer binds to PtdIns(3)P through its PX domain, whereas the Vps26, Vps29 and Vps35 core is recruited by activated rab7-GTPase (Gallon and Cullen 2015). Rab5 does not directly bind to retromer but interfering with its activity prevents recruitment of both subcomplexes, possibly by preventing PtdIns(3)P production and rab7 activation (Rojas, van Vlijmen et al. 2008). Rab7 inhibition in turn, detaches the core subunits but not the SNXs (Rojas, van Vlijmen et al. 2008).

The retromer can also function in the endosome-to-TGN transport in concert with other SNXs, such as the SNX–PX SNX3 (see Fig. 10A). **SNX3** binds to the VPS35 retromer subunit (Harrison, Hung et al. 2014) and it is required for endosome-to-TGN transport of the WLS (Zecca, Basler et al. 1996, Harterink, Port et al. 2011) and the bone morphogenetic (BMP) type 1 receptor (Gallon and Cullen 2015). Recent structural evidence has deciphered the cargo recognition mechanism of the retromer SNX3 complex. The structural data demonstrates that the cargo recognition signal accommodates in a groove formed at the SNX3 and VPS26 contact interface (Lucas, Gershlick et al. 2016).

Besides the retromer complexes, SNXs can act as trafficking coats in the absence of VPS26, VPS29 and VPS35. Thus, the SNX-BAR **SNX4, SNX41 and SNX42**, but not the retromer core, are required for the sorting of the yeast SNARE Snc1 and Atg27 from EE to the TGN (Ma, Burd et al. 2017). Whether another retromer-like complex exists that might assist the function of these SNXs is not known.

The Arp2/3 activator **WASH** is also essentially required for retromer-mediated trafficking (Gomez and Billadeau 2009). WASH is a constitutively active actin nucleating promoting factor (see chapter 1.2.2.2.1.1), which is maintained inactive as part of a 600 kDa complex composed of FAM21, SWIP (strumpellin- and WASH-interacting protein; also known as KIAA1033), strumpellin and CCDC53 (coiled-coil domain-containing protein 53) plus associated F-actin barbed end CP (Fig. 19) (Bear 2009, Derivery, Sousa et al. 2009, Gomez and Billadeau 2009, Campellone and Welch 2010, Jia, Gomez et al. 2010, Rottner, Hanisch et al. 2010, Seaman, Gautreau et al. 2013). Partial depletion of WASH causes accumulation of endosomal tubules (Derivery, Sousa et al. 2009, Gomez and Billadeau 2009), suggesting a participation in the fission of retromer generated tubules. On the other hand, a complete knockout showed enlarged endosomes but no excessive tubulation (Gomez, Gorman et al. 2012), indicating that WASH might also participate in the formation of retromer generated tubules and/or in the organization of endosomal membrane subdomains. The recruitment of the WASH complex happens, at least partially, through an interaction between FAM21 and VPS35 (Harbour, Breusegem et al. 2010). It has been proposed that a single FAM21 molecule might bind multiple retromer complexes on the endosome membrane, perhaps to coordinate the density of retromer and associated cargo with actin subdomain formation or to actively cluster retromer complexes into actin-decorated subdomains (Jia, Gomez et al. 2012).

Retrograde transport to the TGN of the CI-MPR in mammals, and Vps10 in yeast, also requires clathrin and the clathrin adaptor AP-1 (Meyer, Zizioli et al. 2000, Seaman 2005). Depletion of clathrin or retromer completely blocks retrieval of the CI-MPR, indicating that both complexes work in the same pathway. Interestingly, one component of the retromer, SNX1, has been shown to alternatively bind to HRS and the auxilin homolog **RME-8**, a protein that disassembles endosomal clathrin, and which also binds WASH. The depletion of RME-8 or Hsc70 causes an accumulation of clathrin on

endosomes and also disrupts retrograde trafficking of cargo like STxB (Shiga toxin B-subunit), CI-MPR and WLS (Shi, Sun et al. 2009). However, clathrin does not associate with retromer tubules nor is it required for SNX–BAR tubule formation (McGough and Cullen 2013). The emerging picture is that SNX1, HRS, clathrin, actin and RME-8 form a sorting loop that decides whether cargo is send for degradation or is packed in retrograde transport intermediates, with its disassembly required for the formation of the retromer tubules. However, the exact clathrin/retromer functional relation remains to be deciphered.

Finally, a role for the cargo adaptor **TIP47 and rab9** in the clathrin-independent recycling of the MPRs from the LE has been proposed. TIP47 is recruited from the cytosol onto the surface of late endosomes by rab9 GTPase, which enables TIP47 to bind to MPR cytoplasmic domains with enhanced affinity. Of notice is that TIP47 decorated tubules are the only transport intermediates emanating from endosomes that have been reported to fuse with the TGN (Carroll, Hanna et al. 2001, Barbero, Bittova et al. 2002).

Fusion of retromer coated tubules with the TGN has never been reported and therefore, to be precise, the machinery involved in their tethering and fusion has not been described. Nevertheless, one can assume that tethering complexes and SNAREs whose mutation alter retrograde traffic to the endosome, will be indeed the fusion machinery for this transport intermediates. Some of these tethering factors are hetero-oligomeric complexes similar to HOPS or CORVET, whereas others are single elongate polypeptides or homodimers such as Golgin-245 and Golgin-97, which resemble EEA1 (Oka and Krieger 2005, Goud and Gleeson 2010, Lu and Hong 2014). At the TGN, the hetero-oligomeric complexes GARP/VFT (Golgi-associated retrograde transport/Vps fifty three), COG (conserved oligomeric Golgi) and TRAPP-II (transport particle-II), as well as the golgins, have been shown to play roles receiving the retrograde cargo in concert with the small regulatory GTPases rab6 and Arl1 (Chia and Gleeson 2011).

The **GARP**/VFT complex has been best characterized in *S. cerevisiae*, and it comprises four subunits (Vps51, Vps52, Vps53 and Vps54). GARP/VFT is recruited to the TGN through interactions with the rab6 GTPase and the SNARE Tgl1, and it seems to have a general role in the tethering of various retrograde carriers from EE and LE (Bonifacino and Hierro 2011). The **COG** complex comprises eight subunits, COG1–8 whereas the **TRAPP-II** complex includes 10 subunits (Bet3, Bet5, Trs20, Trs23, Trs31, Trs33, Trs65, Trs85, Trs120 and Trs130) (Chia and Gleeson 2011). Although the primary function of COG and TRAPP-II might be intra Golgi and ER to Golgi trafficking, respectively, mutation of their subunits has also been reported to impair retrograde transport of some cargo from endosomes (Bonifacino and Rojas 2006).

The mammalian **Golgin-245 and Golgin-97** and the yeast counterpart Imh1 contain a C-terminal GRIP domain ('golgin-97, RanBP2α, Imh1, p230' domain) that interacts with the Arl1 GTPases, and which is responsible for their recruitment to the TGN. The recruitment of Arl1 to membranes is regulated by another member of this GTPase family, Arl3. Mutations in Imh1, Arl1 or Arl3 cause phenotypes that are consistent with an impairment of trafficking from late endosomes to the TGN in yeast, and with the retrograde transport from early and/or recycling endosomes in mammalian cells (Bonifacino and Rojas 2006).

The assignment of specific **SNAREs** to endosome-to-TGN traffic is still tentative. In *S. cerevisiae*, a complex that is formed by the SNAREs Snc1 or Snc2 (which are themselves cargoes for retrograde transport) and the Tlg1, Tlg2 and Vti1 has been implicated in retrograde transport to the TGN,

presumably from EE (Bonifacino and Rojas 2006). In human cells, two SNARE complexes have been implicated in the transport of Shiga toxin from EE and ERC to the TGN — one is composed of GS15 syntaxin-5, GS28 and YKT6, and the other of VAMP4 (or VAMP3) and syntaxin-16, syntaxin-6 and VTI1a (Bonifacino and Rojas 2006).

1.1.1.5 Retrograde Transport to the PM.

As the SEs lower their pH, many internalized ligands are released form their receptor, which might be transported back to the PM (Mukherjee, Ghosh et al. 1997). Likewise, SNAREs need to be recycled back to the PM. The recycling system to the PM is divided in two different routes, a short circuit emanating from SE, associated to rab4 subdomains, and the longer pathway implicating delivery of material to the recycling endosomes, which is orchestrated by rab11. The short-loop recycling pathway from SE seems to emerge from **rab4**-positive domains at the SE. The published literature though is not clear on the precise role of rab4 in recycling, as expression of dominant-negative rab4 inhibits fast recycling but small interfering RNA-mediated knock down of rab4 increases rapid recycling, perhaps by blocking EE-to-ERC transport (Deneka, Neeft et al. 2003, Yudowski, Puthenveedu et al. 2009). Recent studies using RNA interference and knockout approaches have indicated that **rab35** is an important regulator of rapid recycling (Allaire, Ritter et al. 2006, Kouranti, Sachse et al. 2006, Patino-Lopez, Dong et al. 2008, Sato, Sato et al. 2008).

The cargo sorted from the SE to the PM is concentrated into outgrowing tubules formed by the **retromer** core subunits Vps26, Vps35 and Vps29, and by SNX27 on rab4 positive endosomes (Temkin, Lauffer et al. 2011). Recently, a retromer-like complex called **retriever**, which works in concert with SNX17, has been identified. This complex also works in the retrieval to the PM of cargo distinct from those travelling in retromer tubules (McNally, Faulkner et al. 2017). Thus, SNX27 and retromer are required to transport GPCRs such as the β2AR or the glucose transporter GLUT1, whereas SNX17 and retriever drives recycling of β1α5 integrin (Fig. 12) (Gershlick and Lucas 2017).

SNX17 and SNX27 are SNX–FERM subfamily members that bear a FERM-like domain, located C-terminal, next to the SNX-PX domain (Ghai, Mobli et al. 2011). The FERM-like domain interacts with other proteins by binding of an NPxY motif that acts as a sorting signal (Gallon and Cullen 2015). The domain comprises approximately 300 amino acids divided into three modules (F1-3), where each module has a characteristic structure, and generally mediates interactions of membranes or cytoskeletal elements with cytoplasmic proteins (Chishti, Kim et al. 1998). SNX27 is larger than SNX17 and is the only SNX that contains an extra PDZ (post-synaptic density 95/discs large/zonula occludens) domain, located N-terminal to the SNX–PX domain (Gallon and Cullen 2015). The PDZ domains mediate interactions with other proteins through binding to a short peptide motif termed a PDZ-binding motif (PDZbm) (Fig. 11) (Gallon and Cullen 2015).

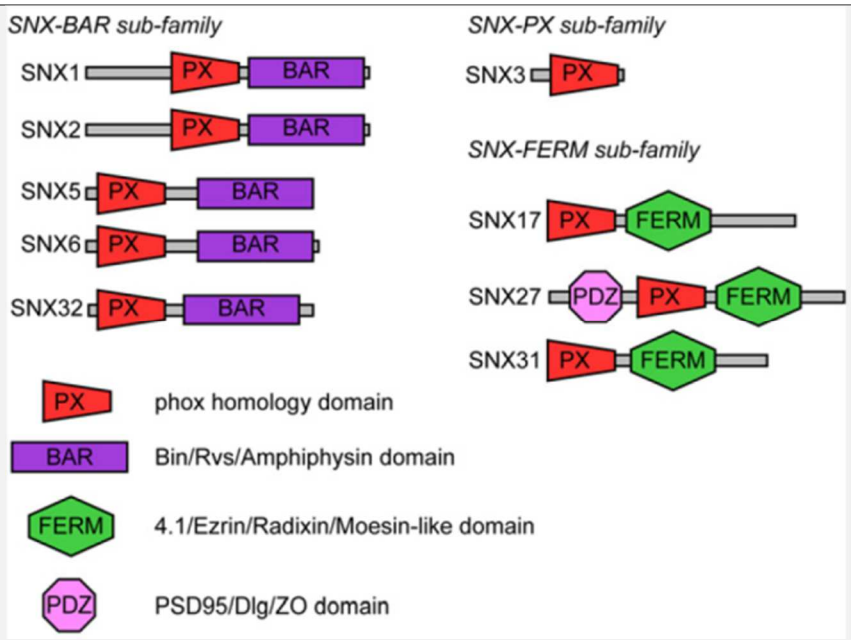

Figure 11. SNXs Associated with Retromer.
Domain architecture of SNXs that associate with retromer, divided into three subfamilies based on their constituent domains. Obtained from (Gallon and Cullen 2015).

The Arp2/3 activator **WASH** is also essentially required for retromer-mediated trafficking to the PM (see chapter 1.2.2.2.1.1), as shown for the β2-AR (Temkin, Lauffer et al. 2011). The recruitment of the WASH complex happens again through an interaction between FAM21 and VPS35 (Harbour, Breusegem et al. 2010). Interaction of the WASH complex with SNX27 probably reinforces the recruitment to regions of endosomes in which retromer-mediated recycling to the PM occurs (Fig. 12) (Steinberg, Gallon et al. 2013).

The **retriever** complex shares homology with the retromer complex but is in charge of distinct cargoes. The retriever complex is also evolutionally conserved in metazoan and it has evolved along with its interaction partners, the WASH and the **CCC complexes** (consisting of CCDC93, CCDC22, COMMD) (McNally, Faulkner et al. 2017). The existence of retriever was hypothesized based on mass spectrometry maps of mammalian interactomes and 3D modelling (Mallam and Marcotte 2017) and shortly after the complex was described biochemically (McNally, Faulkner et al. 2017). Equally to the retromer, retriever is a heterotrimeric complex composed of the VPS29 subunit of the retromer and two other subunits: C16orf62, which displays structural similarity to VPS35, and DSCR3, postulated to be the paralogue of VPS26 (Rabouille 2017). Despite their similarities, the two complexes have a different mode of recruitment to endosomes. In contrast to the retromer, which gets recruited through SNXs and rab7, the retriever gets recruited through the CCC complex and WASH. Additionally, the CCC complex is essential for retriever function, whereas it does not seem to be associated with the retromer (Fig. 12) (Gershlick and Lucas 2017).

It is demonstrated that functional SNX17 is physically linked to the CCC complex and that the C-terminal domain of SNX17 is necessary and sufficient for association with retriever (McNally, Faulkner et al. 2017). The CCC complex itself does not associate with endosomes but interacts with the FAM21 subunit of the WASH complex on endosomes (Phillips-Krawczak, Singla et al. 2015). Accordingly, FAM21 was shown to be recruited to the membrane independent of the retromer and

to be necessary for both endosomal recruitment and cargo sorting of retriever (Gershlick and Lucas 2017).

The retriever complex seems to be the long missing piece explaining a retromer independent PM recycling pathway from the endosomes carrying important cargoes, including the LDLR (Burden, Sun et al. 2004) and LDLR-related protein 1 (LRP1) (Stockinger, Sailler et al. 2002, van Kerkhof, Lee et al. 2005), the endothelial cell adhesion molecule P-selectin (Knauth, Schluter et al. 2005), APP (Lee, Retamal et al. 2008), GLUT1 and β-integrins (Bottcher, Stremmel et al. 2012, Steinberg, Heesom et al. 2012). Mass spectrometry analysis indicates that it could be involved in the transport of around 140 distinct cargoes (McNally, Faulkner et al. 2017).

Also emerging from SE, **GGA3**, **arf6** and **clathrin** have been invoked to carry the Met/hepatocyte growth factor receptor tyrosine kinase to the PM. GGA3 loss abrogates Met recycling from a rab4 endosomal subdomain, resulting in pronounced trafficking of Met toward degradation (Parachoniak, Luo et al. 2011). How this pathway crosstalks, if at all, with the retriever and retromer subdomains has not been investigated in detail.

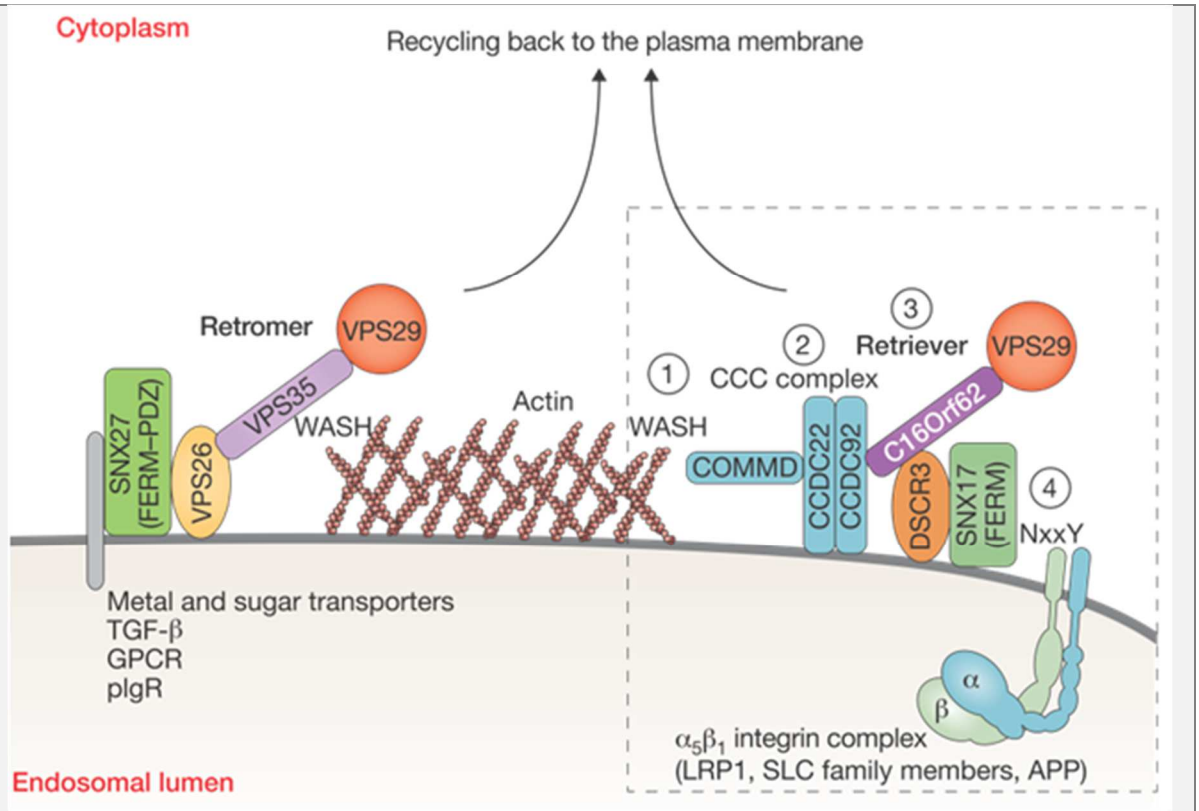

Figure 12. Schematic Models of Retromer and Retriever.
Comparative molecular composition of retromer (left) and retriever (right). Retromer comprises the three subunits VPS29 (red), VPS35 (light violet) and VPS26 (light orange). When retromer binds SNX27, it mediates the recycling of a large number of receptors to the PM in a WASH-dependent manner. Retriever also comprises three subunits, VSP29 (red), C16orf62 (dark violet) and DSCR3 (dark orange). Retriever's recruitment to endosomes (3) depends on the CCC complex (2), which is recruited to the endosomes in a WASH-complex-dependent, retromer-independent manner (1). Once retriever is at the endosomes, it binds SNX17, which itself is bound to the NxxY motif of the cytoplasmic domain of β1-integrin (4). The subunits of retromer and retriever are color-coded to illustrate structural homology. Obtained from (Rabouille 2017).

The long-loop recycling pathway employs an intermediate compartment in transit to the PM: the **rab11-positive recycling endosomes (ERC)**. Recycling endosomes are a dynamic system of tubular

organelles (see Fig. 2) (Maxfield and McGraw 2004), often overlooked in fixed cells (Baetz and Goldenring 2013). The tubules of the ERC usually have diameters around 60 nm and are associated with microtubules. The distribution within the cell varies among different cell types – in some cell types the ERC is mostly condensed perinuclear (e.g. CHO, Cos-7), in others, it shows a more disperse distribution (e.g. MEFs) (Hopkins 1983, Yamashiro, Tycko et al. 1984, McGraw, Dunn et al. 1993, Lin, Gundersen et al. 2002, Goldenring 2015). The ERC can sort cargo to different destinations, including the TGN (Goldenring 2015), but most of it returns to the PM. How material is delivered from SE to ERC is not well understood but it might imply a maturation process similar to that driving SE to LE maturation. In this case though, the **rab5 to rab11 conversion**, which has been reported experimentally by live cell fluorescence imaging (Rink, Ghigo et al. 2005), will dominate, probably accompanied by the turnover of PtdIns(3)P to PtdIns and its subsequent modification to PtdIns(4)P (Ketel, Krauss et al. 2016). How different events along the maturation in the recycling pathway are coupled at the molecular level has only started to emerge. A member of the Eps15 Homology Domain protein family, with tubulating capacity, **EHD3**, binds to the rab5 effector **rabenosyn-5** and to the rab11 target **RAB11FIP2,** and its depletion prevents transport to the ERC, emerging as a putative linker of SE and ERC, which might modulate the conversion (Naslavsky, Rahajeng et al. 2006). On the other hand, recent evidence demonstrates that PM surface delivery of endosomal cargo requires the hydrolysis of PtdIns(3)P by the **phosphatidylinositol 3-phosphatase MTM1** accompanied by **phosphatidylinositol 4-kinase-2α (PI4K2α)-dependent generation of PI(4)P,** and the recruitment of the exocyst tethering complex, in order to enable membrane fusion with the PM (Ketel, Krauss et al. 2016). How these events are coordinated is far from being understood.

Besides the endosomal maturation model proposing the SE to ERC conversion, a role **for AP-1 and clathrin** in the generation of transport intermediates from the SE and the ERC, controlled by the **rab4b** isoform, has also been suggested based on *in vivo* and *in vitro* data (Perrin, Lacas-Gervais et al. 2013). However, AP-1 and clathrin transport intermediates loaded with cargo in transit from EE to ERC, have not been unequivocally identified and hence, it might be that AP-1 and clathrin contribute to EE to ERC maturation by delivering material to or from the TGN.

The ERC represents a long-lived compartment (Maxfield and McGraw 2004). Therefore, formation of transport intermediates is required to deliver material to the PM or the Golgi but the machinery involved is not completely elucidated yet. The genetic screen for endocytosis mutants in *C. elegans* has been instrumental in expanding our understanding of recycling from the ERC (Grant, Zhang et al. 2001). The first endocytosis mutant from the screen, **RME-1,** and its mammalian homologue **EHD1**, are required for the recycling of MHC class I molecules and, in some cells, the TfnR (Balklava, Pant et al. 2007, Grant and Donaldson 2009). In addition, **rab11** plays a pivotal role, which might be assisted by **arf6** for the recycling of cargo associated to sphingolipid and cholesterol-enriched membrane domains (Caplan, Dell'Angelica et al. 2000, Wilcke, Johannes et al. 2000, Lin, Grant et al. 2001). Similar to EHD3, EHD1 also has tubulating activity (Grant and Caplan 2008). In addition, EHD1 can bind to PtdIns(4)P, a property that seems to be important for the association of EHD1 with the tubular profiles of recycling endosomes (Grant and Caplan 2008). On the other hand, **clathrin** and adaptor proteins such as **ACAP1** have been observed on the ERC, and perturbation of clathrin alters recycling of Tfn, GLUT4 and integrins (Stoorvogel, Oorschot et al. 1996, van Dam and Stoorvogel 2002, Li, Peters et al. 2007, Majeed, Vasudevan et al. 2014). Whether the EHD1 and the clathrin machinery crosstalk is not known at the moment.

Rab11-positive recycling transport intermediates are delivered to the cell surface along actin filaments via **myosin V** motors (Welz and Kerkhoff 2017). Activated **rab11** binds to its **RAB-FIP2** effector, which in turn recruits myosin V (Fig. 4D) (Welz and Kerkhoff 2017). The vesicles are tethered to the PM by rab11 binding to the Exocyst component Sec15, which forms a tripartite docking complex (Welz and Kerkhoff 2017). The **exocyst** is an octameric tethering complex (Sec3, Sec5, Sec6, Sec8, Sec10, Sec15, Exo70 and Exo84) that interacts with SNARE complexes and subsequently mediates vesicle fusion and the delivery of cargo proteins to the PM. Not much information is available on the **SNAREs** involved in exocyst-mediated fusion of recycling transport intermediates with the PM. Recent evidence indicates the Q-SNAREs SNAP23 and SNAP25 and the R-SNARE VAMP2 could participate in the long circuit recycling of the TfnR to the PM (Kubo, Kobayashi et al. 2015).

An upcoming question is why cells developed two distinct ways of endosomal recycling back to the PM. The reason may lie in the complexity of the endosomal system itself and the diversity of tasks carried out in a cellular context. An emerging view is that the short recycling circuit will deliver material close to where it was internalized, therefore participating in processes that require the detection of signalling gradients. On the contrary, passing through the ERC will be associated to proteins that need to be delivered to particular cellular locations labelled by the exocyst, including the podosomes, primary cilia, cell-cell and cell-matrix junctions or dendrite branches (Maxfield and McGraw 2004, Jones, Caswell et al. 2006, Grant and Donaldson 2009). The tethering and SNARE machinery involved in the recognition of cargo following the short circuit has not been elucidated yet.

1.2 Clathrin and Actin in the Endocytic Pathway and Beyond

1.2.1 Clathrin

1.2.1.1 Structure and Biochemistry of the Clathrin Triskelions

Clathrin is a protein complex usually assembled as a triskelion, composed of 3 heavy chains (approx. 190 kDa each) and 3 light chains (approx. 27 kDa) (Fig. 13 B). Both chains are present in all eukaryotic organisms analysed so far, showing for the heavy chain a high degree of sequence conservation (Wakeham, Abi-Rached et al. 2005). Clathrin is recruited from the cytosol to different cellular membranes including the PM, those limiting the Golgi-apparatus and the endosomal system. There, it plays key roles in many intracellular membrane trafficking pathways, including receptor-mediated endocytosis at the PM, lysosome biogenesis and endosomal sorting (Brodsky 2012).

Most organisms contain a single copy of the gene encoding for the clathrin heavy and light chains, except for vertebrates, where in most species gene duplication gave rise to two clathrin heavy chains (CHCs) and clathrin light chains (CLCs) (Wakeham, Abi-Rached et al. 2005). Humans express **CHC17 and CHC22**, named after the chromosomes where the corresponding genes are located. The isoforms show 85% similarity at the protein level, but evolved to have distinct biochemical properties, interacting partners and cellular functions (Wakeham, Abi-Rached et al. 2005, Dannhauser, Camus et al. 2017). CHC17 has a functional orthologue in all eukaryotes and it is involved in numerous membrane trafficking pathways. CHC22, on the other hand, mediates a very defined step in retrograde transport from endosomes to the TGN (Dannhauser, Camus et al. 2017). CHC22 is highly

expressed in human skeletal muscle and fat tissues, where it controls transport pathways that influence targeting of the insulin-regulated glucose transporter Glut4. However, the gene encoding CHC22 clathrin is a pseudogene in mice (Wakeham, Abi-Rached et al. 2005) and CHC22 is not expressed, implicating the existence of a different mechanism for trafficking of Glut4 (Vassilopoulos, Esk et al. 2009, Esk, Chen et al. 2010). Additionally, CHC22 has been implicated in neuronal development and it is detected at low levels in other tissues, where it might be involved in trafficking of other specific cargo (Dannhauser, Camus et al. 2017). CHC22 may also play a role in membrane organization, as indicated by its localization on LEs (Esk, Chen et al. 2010). At steady state, most cellular CHC22 is associated with membranes, while CHC17 is about half cytosolic, half membrane-associated. CHC22 cannot substitute for CHC17 in endocytosis, indicating profound differences in the way they function (Brodsky 2012). Interestingly, CHC22 does not seem to interact with the clathrin light chains (Brodsky 2012, Dannhauser, Camus et al. 2017). For simplicity, CHC17 will be referred to as CHC or clathrin from now on, unless CHC22 is explicitly mentioned.

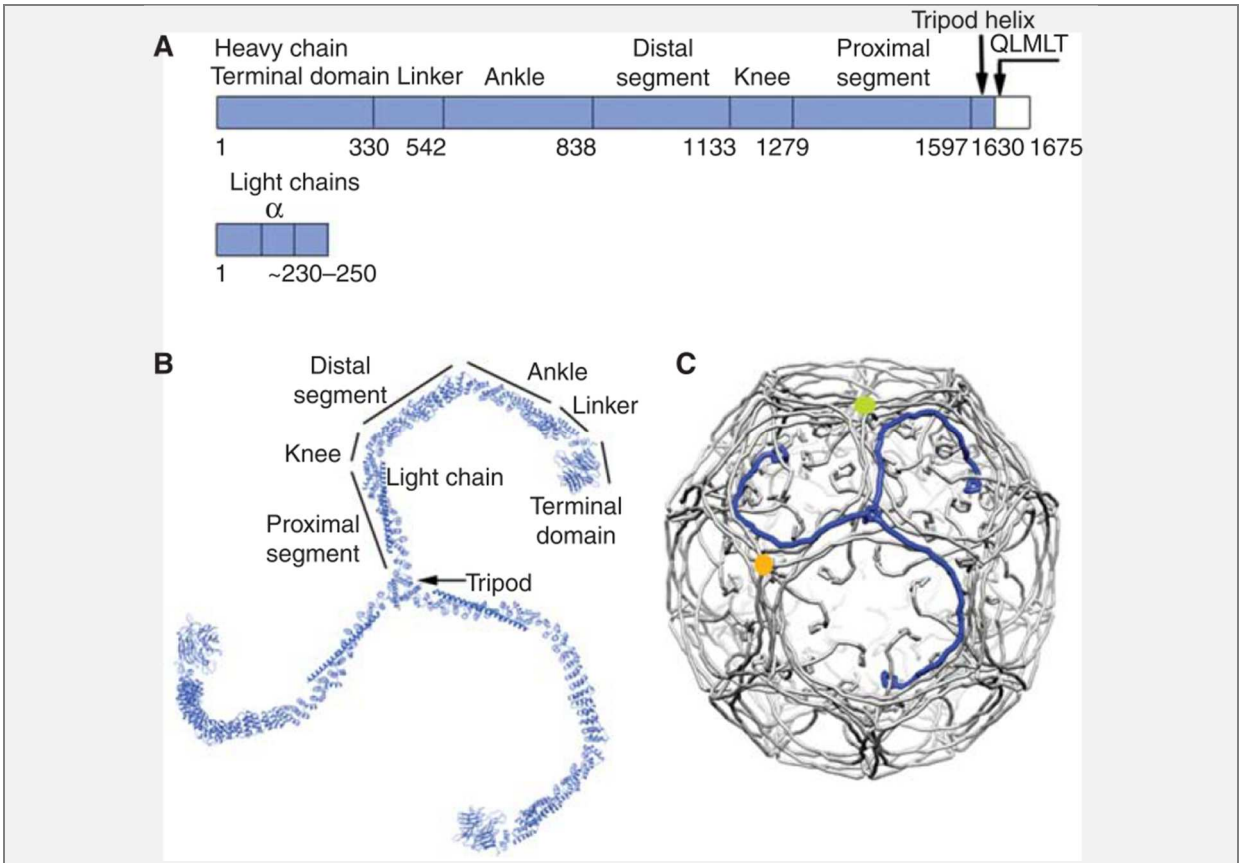

Figure 13. Structure of Clathrin.

A. Organization of the clathrin heavy- and light-chain polypeptides. The name or phase designating various segments appears above the corresponding region of the sequence. Human cells have two light chains (LCa and LCb), each with tissue-specific splice variants, yielding the range of lengths shown. There is no detectable preference of one or the other for association with a heavy chain; the central, α-helical segment, which mediates heavy-chain association, is almost completely conserved in all light-chain forms. A second heavy-chain gene in human cells encodes a paralog found in muscle and fat tissue that is involved in intracellular traffic, but not in endocytosis- It does not bind light chains. **B.** Full a-carbon (Ca) representation of a clathrin triskelion, viewed along its threefold axis as if from the outside of a coat. The various segments of the heavy chain are labelled, and the central a-helical region of the light chain on each leg is also shown. **C.** Packing of triskelions in a clathrin coat. The structure shown is that of a "D6 barrel," one of the simplest and smallest coated-vesicle lattices. Each triskelion is drawn as a "worm" extending from the hook-like representation of the terminal domain on the inside of the shell to the vertex of the triskelion at the outside. (Blue) One triskelion, in an orientation similar to the one in B. For further details see text in chapter 1.2.1. Obtained from (Kirchhausen, Owen et al. 2014).

Vertebrates also have two clathrin light chains, **LCa** (248 amino acids) and **LCb** (228 amino acids), differentially expressed in different tissues, with LCa being dominant in lymphoid tissue and LCb, in brain (reviewed in (Brodsky, 2012)). They share similar functions and bind and regulate CHC17, but do not functionally interact with CHC22 (Liu *et al.*, 2001). Contrary to the heavy chain, the CLCs have more divergent sequences. The human LCa and LCb share only 60% amino acid identity, despite their similar functionality. Yeast Clc1 is only 18% identical to mammalian LCb, but the domain organization and molecular functions are conserved (Brodsky *et al.* 1991).

As mentioned, cytosolic wild type clathrin is mostly (if not exclusively) assembled in triskelions composed of three heavy chains, each of them associated with a light chain. CHC comprises an N-terminal β-propeller domain and a long leg made of 8 α-solenoid repeats designated as clathrin heavy chain repeats (CHCR0-7) (Ybe, Brodsky et al. 1999). They form the ankle, the distal leg and proximal leg segments. The C-terminal end of CHCR7 contributes to trimerization (Ybe, Perez-Miller et al. 2007). The trimerization domain extends from CHCR7 below the triskelion vertex toward the cell membrane (Fotin, Cheng et al. 2004). Within this region, a QLMLT motif is involved in the recruitment of the Hsc70 chaperon, which participates in clathrin disassembly. The puckered vertex gives the CHC triskelion a characteristic orientation. The light chain binds to the proximal legs and imposes rigidity on the cytoskeleton. This portion of clathrin is also involved in the recruitment of the Hsc70 co-chaperon auxilin and HIP1R, a protein that links clathrin to actin (Senetar, Foster et al. 2004, Wilbur, Chen et al. 2008, Boettner, Friesen et al. 2011). The N-terminal domain (CHC TD) is a seven-bladed β-propeller, connected to CHCR0 by a linker region. An additional binding site for adaptors is localized between CHCR1 and CHCR2, in the ankle domain (Fig. 13 A and B)(Knuehl *et al*., 2006). The CHC TD represents the main interacting interface with adaptors and accessory proteins, with four different surface regions contributing to the described interactions. One of this consensus TD binding motifs is known as a clathrin box (LØXØ[DE]) (single letter amino acid code, where Ø represents a hydrophobic residue; alternative residues are in brackets) (Lemmon & Traub, 2012). Other sites that independently bind to the TD have been found in vertebrate proteins, such as the W-box site (PWXXW) (Miele *et al*., 2004). There are many other proteins that physically bind clathrin, but not all interaction motifs have precisely been mapped.

The clathrin light chains are linear arrays of functionally distinct domains. The N-termini of the light chains bear a conserved sequence, whose first three residues are negatively charged (EED). A number of studies revealed that this acidic region interacts with the central coiled-coil dimerization domain of Hip1R (Chen & Brodsky, 2005; Newpher *et al.*, 2006) and that this interaction regulates the assembly of triskelions into cages. Clathrin light chains are unstructured unless bound to heavy chains (Brodsky, 2012). The central region of all light chains contains 10 heptad repeats that form α-helical coiled-coils, and this central region is necessary and sufficient for the light-chain binding to the heavy chain (Scarmato & Kirchhausen, 1990). Light chain binds along the proximal domain of heavy chain through CHCR7 (Scarmato & Kirchhausen, 1990), although the C-terminus subunit of the heavy chain also contributes to the interaction (Ybe *et al*., 2007). The clathrin light chain binds calcium *in vitro* with low affinity, in mammals through residues 71-93/82-93. This residues form a calcium chelating loop similar to the EF-hand loop characteristic of other calcium-binding proteins (Mooibroek *et al*.,1987; Näthke *et al.*, 1990; Silveira *et al*., 1990). Importantly, this calcium-binding site is situated between the Hsc70 binding site and the heavy chain binding site (Brodsky, 1990), so it may have a role in regulating clathrin assembly, consistent with the observation that the *in vitro* self-assembling of clathrin coats requires calcium (Ungewickell & Ungewickell, 1991). Clathrin light chains

bind calmodulin through a region in their C-terminus but its functional role has not been assessed yet.

1.2.1.2 The Role of Clathrin and Clathrin Adaptors in the Formation of CCVs

The best characterized function of clathrin is the formation of CCVs (Fig. 14). This function is strongly dependent on the function of clathrin adaptors that simultaneously bind clathrin and cargo. Most of these adaptors also have domains that directly contact lipids, in particular PtdInsP_xs.

Purified triskelions can spontaneously form curved supra molecular structures under non-physiological conditions, which very much resemble those found on the surface of CCVs purified from cells (Kirchhausen 2000). This early observation lead to the widely accepted model that assembly of curved clathrin cages will impose curvature to the membrane. However, the opposite possibility, that curved membranes will impose curved assembly of clathrin cages was never discarded. Indeed, recent evidence indicates that clathrin assembles on a flat configuration, and only upon arrival of cargo adaptors it adopts a curved shape (Idrissi, Blasco et al. 2012, Kukulski, Schorb et al. 2012). Further, cell-free assays to measure coat assembly, invagination, receptor-sorting and vesicle fission (Schmid 1992), as well as biophysical modelling (Nossal 2001), suggest the requirement of additional components, such as clathrin adaptor proteins, to form functional clathrin lattices capable of curving cellular membranes.

The formation of CCVs is well documented for the internalization of material from the PM, where it functions with the heterotetrameric AP-2 and a number of cargo specific monomeric clathrin co-adaptors. Formation of CCVs is also well documented from the TGN, where it functions with either the monomeric GGA proteins or with the heterotetrameric AP-1 in subsequent waves of membrane vesiculation (Duncan, Costaguta et al. 2003). The heterotetrameric AP-3 adaptor is also involved in traffic from the Golgi apparatus and/or the ERC to the LE and lysosomes. Less clear is the role of clathrin forming *bona fide* CCVs from the endosomes. Clathrin and clathrin adaptors are found in the endosomal system, structures resembling clathrin coated pits have been identified on endosomes at the ultrastructural level, and they are known to definitely play important roles in retrograde transport events (Park and Guo 2014). However, the existence of CCVs unequivocally labelled with clathrin and clathrin adaptors and cargo retrieved from endosomes have not been demonstrated. Therefore, the effects observed upon depletion of clathrin or clathrin adaptors on endosomal retrieval might still be caused by a delay in endosome maturation (due to a delay in acquisition of material from the TGN), or by misfunction of endosomal clathrin as a scaffolding platform (see following chapter).

Early studies on isolated CCVs demonstrated that the native clathrin coat consisted of at least 12 pentagons, which introduce curvature, and a variable number of hexagons (Crowther & Pearse, 1981). The contour of a clathrin leg in a lattice reaches nearly three edges. When legs associate to form coats or cages, they incorporate pentagonal openings as well as hexagonal ones (Crowther & Pearse, 1981). 12 pentagons are required to form a closed shell, if all the other openings are hexagons. If all the openings were hexagonal, the lattice would be a flat array. The number of hexagonal openings and the distribution of pentagonal openings among them, define the size and shape of the overall structure (Crowther & Pearse, 1981; Fotin *et al.,* 2006; Kirchhausen *et al*., 2014; Pearse & Crowther, 1987). *In vitro*, these properties are determined by the presence or absence of

adaptors (Kirchhausen, 2000). Besides, the characteristics of the cargo could also influence the size and shape of a vesicle (Jackson *et al.*, 2010; Kirchhausen, 2000). The structures generated *in vitro* for cryo-electron microscopy studies are rather homogeneous showing a regular barrel-like coat structure with D6 symmetry (Fig. 13C). However, CCVs isolated from cells or tissues are found to be more heterogeneous in size and shape (Cheng *et al.* 2007). Clathrin coats derived from the PM are typically > 90 nm in diameter and contain about 35 to 40 triskelions, whereas coats derived from the Golgi apparatus or those in the synaptic terminal are 75 to 100 nm in diameter. They enclose a spherical vesicle whose size can vary according to the size of the coat. In contrast, the coat thickness remains relatively constant at ~22 nm (Pearse & Crowther, 1987). The gap between the coat and the vesicle can accommodate not only the various adaptors, but also the many other regulatory proteins that participate in cargo sorting, budding, and uncoating (Kirchhausen *et al.*, 2014).

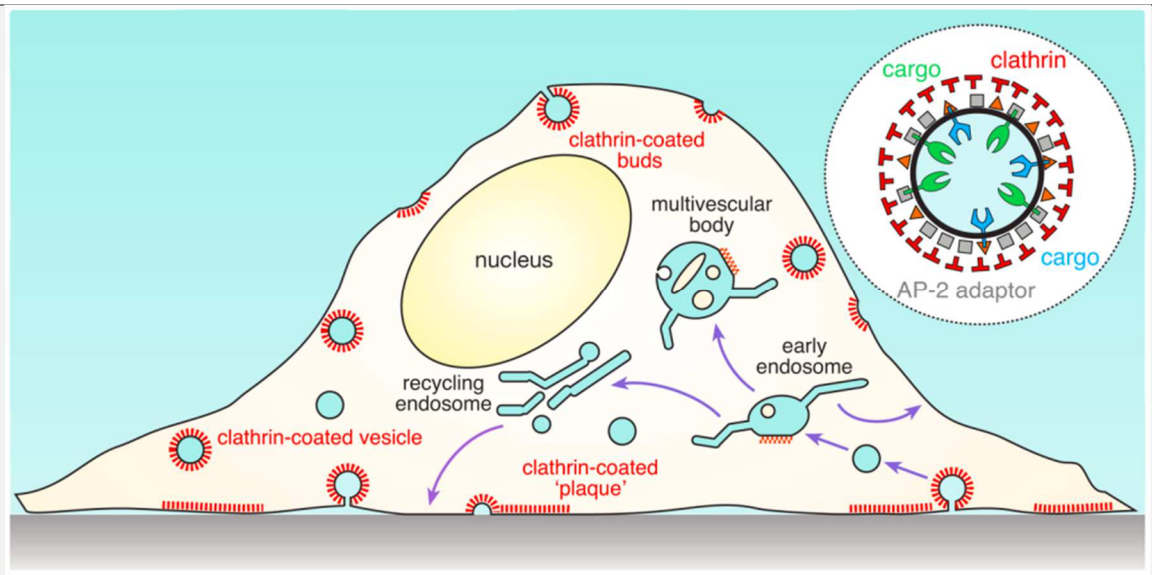

Figure 14. Cellular Sites of Clathrin Actions.
Schematic illustration of a cultured cell showing surface-positioned clathrin-coated buds, ventrally located large, flat clathrin ''plaques,'' and the major internal endosomal sorting stations. After clathrin coat uncoating, transport vesicles quickly fuse with the peripheral early endosome compartment, mingling incoming cargo molecules in this initial sorting endosome. Transmembrane cargo can return either directly to the PM from the EE, or be sorted into tubules that are delivered to the juxtanuclear recycling endosome compartment, from which cargo can also be directed back to the cell surface. The bulbous vacuolar portion of the EE, containing a flat, bilayered clathrin coat, matures into a multivesicular body for delivery of selected components to lysosomes for degradation. The inset shows the basic composition and organization of a CCV, with the three major layers: the inner membrane vesicle with various embedded transmembrane cargo (blue and green), an intermediate layer of adaptors including AP-2 (gray), and the outer clathrin polyhedral lattice (red). For further details, see text in chapter 1.2.1. Obtained from (Traub 2009).

A number of **clathrin adaptors for vesicle formation** that link clathrin to cargo on cellular membranes have been described. The adaptors are targeted to the appropriate membrane at least in part by interacting with PtdInsP_xs, and, once on the membrane, they form interconnected networks to get different types of cargo into the same vesicle. The best characterized clathrin adaptors are AP-1 and AP-2, which work for clathrin mediated vesicle budding at the TGN and the endosomes, and at the PM, respectively. They both promote clathrin assembly *in vitro* and they are composed of two large subunits of ~100 kDa (AP-1: γ & β1, AP-2: α & β2), one subunit of ~50 kDa (AP-1: μ1, AP-2: μ2) and one subunit of ~20 kDa (AP-1: σ1, AP-2: σ2). The 100 kDa subunits have a core and appendage (ear) domain, connected by a flexible and unstructured hinge region that binds the clathrin TD

through clathrin box motifs (Edeling, Mishra et al. 2006). The barrel-shaped core comprises the N-termini of adaptin-α and –β and the two smaller subunits, whereas the C-termini of the big subunits form protruding appendages resembling "ears" (Robinson and Bonifacino 2001). Many accessory endocytic proteins such as amphiphysin and other cargo co-adaptors such as epsins, AP180, or arrestins, simultaneously bind to the clathrin TD and the α and/or β ears, probably cooperating to build a dense clathrin coat (Brodsky 2012). AP-3, composed of δ, β3, μ3 and σ3 subunits is also involved in the formation of vesicles from the TGN or the ERC. The AP-3 vesicles are distinct from those carrying AP-2 (Esk, Chen et al. 2010, Brodsky 2012). Whether AP-3 functions with clathrin was a matter of discussion because AP-3 does not appeared enriched in CCVs preparations. However, increasing evidence indicates that it does: AP-3 has the clathrin binding box (Park and Guo 2014) and it can recruit clathrin on artificial liposomes and Golgi membranes *in vitro* (Drake, Zhu et al. 2000). Other two related heterotetrameric adaptors, AP-4 and AP-5 have been identified, but they do not seem to work with clathrin (Brodsky 2012), raising the question of whether there is another scaffolding protein that can fill the same role.

Another family of monomeric clathrin adaptors, the **GGAs** (Golgi-localized, γ-ear-containing, ARF-binding proteins), was identified more recently, again by the searching for AP subunit homologs in databases. GGAs are monomeric, but they have a C-terminal domain related to the appendage or 'ear' domain of the γ subunit of the AP-1 complex. Structurally, the GGAs are very different from the AP complexes, but their ear domains have similar folds, and both GGAs and APs have long, flexible linkers, often containing clathrin-binding sites, which connect the ear to the rest of the molecule (Robinson and Bonifacino 2001, Brodsky 2012). There is abundant evidence that the GGAs function together with clathrin in both mammalian cells and yeasts. Like AP-1, the GGAs are found on TGN and endosomal membranes, but reports vary as to the extent of co-localization between the two, and there is also some controversy about their functional relationship, even though recent evidence indicates that they function sequentially (Robinson 2004).

Recently, evidence has been emerging for another set of co-adaptors, which interact with the ear domain of either the α2 or the β2 subunit of AP-2, and which act together with AP-2 at the PM to bring different types of cargo into the same population of coated vesicles. Most of these adaptors also bind to the CHC TD, most likely contributing to the packing and bending of the endocytic coat. The first of these cargo-specific adaptors to be identified was **β-arrestin**, a protein originally isolated as an inhibitor of β-adrenergic receptor signalling, which was subsequently found to bind to several different G-protein-coupled receptors (Pavlos and Friedman 2017). Three other proteins, **Dab2** (disabled-2) **Numb**, and **ARH** (autosomal recessive hypercholesterolemia), have been implicated in the internalization of the LDL receptor and integrins (Ezratty, Bertaux et al. 2009, Wei, Fu et al. 2014). Other potential cargo adaptors on the endocytic pathway include **AP180/CALM,** involved in the recycling of a v-SNARE, the **epsins,** which recognize ubiquitinated cargo, **muniscins** or **Eps15** and Eps15 related proteins, which work as a scaffold for the CME of RTKs, among other adaptors (Robinson 2004). Not many co-adaptors have been identified for AP-1, with the exception of Eps15 and **epsinR,** which cooperate with the tetrameric adaptor in the transport of hydrolytic enzymes from the TGN to the endosomes (Hirst, Motley et al. 2003, Mills, Praefcke et al. 2003, van Bergen En Henegouwen 2009, Paczkowski, Richardson et al. 2015).

The μ-chains of AP-1, AP-2 and AP-3 all recognize and bind to YXXø-based signals present in the cytoplasmic tails of many transmembrane proteins, whereas the β-subunits recognize LL-based endocytic motifs [D/E]XXXL[L/I] (Kirchhausen 2000), raising the question on how each adaptor

recognizes its cargo on the adequate membrane. *In vitro,* the affinity of the μ- and β-subunits for transport signals is rather weak and it is unlikely that this interaction by itself accounts for the recruitment of the adaptor to the adequate cellular membrane. Instead, it seems that specificity for cargo binding and cooperativity is again provided by a double code which involves particular $PtdInsP_x$s. Thus, many clathrin adaptors that participate in cargo sorting at the PM bind **$PtdIns(4,5)P_2$** through different lipid binding domains, including the α- and β2-adaptins of AP-2, the ENTH and ANTH domains of epsins and AP180/CALM, respectively, the BAR domain of muniscins, or the PTB domain of Dab2 (Martin 2001) (Ungewickell and Hinrichsen 2007). On the contrary, AP-1 and epsinR bind **PtdIns(4)P**, which is enriched on the Golgi and ERC (Wang, Wang et al. 2003).

The mechanism whereby $PtdIns(4,5)P_2$ cooperatively triggers AP-2 cargo and clathrin binding has been well studied at the ultrastructural level (Collins, McCoy et al. 2002, Honing, Ricotta et al. 2005). AP-2 can adopt two very different conformations: open and closed. The open conformation is stabilized by binding to $PtdIns(4,5)P_2$ and cargo. In the closed conformation, AP-2 cannot bind to cargo and the clathrin binding site is sequestered in the interior of the AP-2 core. When AP-2 binds to $PtdIns(4,5)P_2$, the conformation opens, allowing cargo binding and the release of the clathrin box. A similar mechanism for PtdIn(4)P regulation of AP-2 is inferred (Maldonado-Baez and Wendland 2006).

1.2.1.3 The Role of Clathrin in the Formation of Scaffolding Structures

In addition to its role in vesicle formation, clathrin can form other **scaffolding flat structures** on membranes that either work as cargo sorting stations, such as those associated with the ESCRT machinery, or to recruit cytoskeleton elements, in particular the actin polymerization machinery or microtubules (Fig. 14). The molecular links involved and the mechanisms that regulate the assembly of non-vesicular clathrin platforms have not beendeciphered yet.

On the **basal surface of adherent cells, flat clathrin lattices**, also called plaques, can be observed at sites of integrin-substrate interaction (De Deyne, O'Neill et al. 1998). They are relatively long-lived clathrin arrays at the interface with the substrate. When studied by electron microscopy, these flat clathrin arrays correspond to extended lattices, which can be of substantially greater diameter than clathrin coated pits, and which have very different dynamics (Saffarian *et al.,* 2009). These large non-canonical structures, now termed “clathrin plaques,” can cover membranes and sequester cargo such as the TfnR. Nucleation of N-WASP-induced branched actin microfilaments drives internalization of clathrin plaques into the cell (Saffarian, Cocucci et al. 2009, Leyton-Puig, Isogai et al. 2017). Electron microscopy studies have shown that coated plaques have a high concentration of lattice defects that may be consequence of the resistance of the underlying support to curve, so that lattice defects will lead to a patchwork of hexagons unable to curve (Traub, 2009). These structures have been shown to be important integrin-adhesive structures (Chetrit, Ziv et al. 2009) and are essential for integrin endocytosis (Ezratty, Bertaux et al. 2009, Teckchandani, Mulkearns et al. 2012, Lampe, Vassilopoulos et al. 2016), a process that also requires the clathrin adaptors Dab2 and Numb as well as AP-2 (De Franceschi, Arjonen et al. 2016, Lampe, Vassilopoulos et al. 2016). It is unclear what coordinates the flat clathrin lattice arrangement, but it is possible that this different organization arises from an alternative arrangement of endocytic proteins. For example, epsin, which promotes membrane curvature via their ENTH domain, is distributed throughout the lattice in PM plaques, rather than being concentrated at the rim, as in classic clathrin coated pits (Humphries and Way

2013). In any case, the proteins and associated interactions that influence the structural configuration and function of clathrin remain unknown.

Clathrin has also been implicated in **phagocytosis** (Veiga and Cossart 2006). Clathrin is generally not considered to contribute to phagocytosis due to the size limitation of CCVs and *in vitro* reconstituted clathrin cages. However, clathrin was reported to act as a scaffold for actin remodelling, which is required for the internalization of pathogenic bacteria and virus (Bonazzi, Vasudevan et al. 2011). A prime example of this is clathrin exploitation by enteropathogenic *E. coli* (EPEC), a bacterial pathogen that adheres to the cell surface. On binding, EPEC inserts a bacterial protein, Translocated intimin receptor (Tir), into the PM, and the protein is subsequently clustered by intimin on the bacterial surface. Clustering of Tir leads to its phosphorylation by SRC and ABL family kinases, and in the recruitment of NCK and N-WASP. N-WASP then recruits the Arp2/3 complex, which stimulates actin polymerization to form a pedestal beneath the bacterium (Frankel and Phillips 2008). Dynamin and clathrin are also recruited to and have a role in EPEC pedestal formation (Unsworth, Mazurkiewicz et al. 2007, Bonazzi, Vasudevan et al. 2011). Clathrin is recruited downstream of NCK and was found to constitute part of the signalling complex required for actin polymerization. Subsequent studies demonstrated that AP-2 was neither recruited nor required for actin pedestal formation but it rather required Dab2 together with epsin and Eps15. A similar set of proteins and mechanisms to those involved in EPEC pedestal formation have also been shown to play a role in the internalization of the 'zippering' bacterium *Listeria monocytogenes* (Cossart and Toledo-Arana 2008). This has led to the proposal that Tyr phosphorylation of clathrin might stabilize its assembly at the inner surface of the PM and promote its association with the actin machinery. In support of this, SRC activation is also required for the **recruitment of clathrin to adherens junctions** (Cossart and Toledo-Arana 2008). It was observed that clathrin localizes to adherens junctions and regulates their maturation by creating a stable platform for the recruitment of cytoskeletal proteins, in a manner reminiscent of *L. monocytogenes* and EPEC. Clathrin has also been implicated in the internalization of certain large viruses (Ehrlich, Boll et al. 2004, Rust, Lakadamyali et al. 2004) and fungi (Moreno-Ruiz, Galan-Diez et al. 2009), as well as in the **disposal of apoptotic neurons by cells of the microglia** (Sullivan, Scheib et al. 2014). Clathrin also seems to play a scaffolding role for the recruitment of the actin machinery at the **immunological synapse**, a process also triggered by the phosphorylation of CHC by activated T cell receptors (Stoddart, Dykstra et al. 2002, Crotzer, Mabardy et al. 2004, Calabia-Linares, Robles-Valero et al. 2011). While the particular details of the function and regulation of clathrin as a scaffold recruiting the actin polymerization machinery have not been worked out for all cellular processes described, it is likely that they imply analogous actors.

Clathrin has been related with the function of the **microtubule cytoskeleton**. Clathrin is involved in mitosis via interaction with microtubules (Fu, Jiang et al. 2011). CHC forms a complex with the microtubule-binding protein TACC3 and the ch-TOG protein, which have roles in microtubule growth and stabilization. The complex is present at the mitotic spindle but also at centrosomes, and it contributes to centrosome integrity during early mitosis (Royle 2012). CHC also plays a role in endosomal membrane traffic during mitotic cell expansion and abscission (Foraker, Camus et al. 2012, Royle 2012).

In addition to its roles in recruiting the cytoskeleton machinery, clathrin is also known to form **scaffold structures** on the surface of endosomes (Brodsky 2012, Stehbens and Wittmann 2012). These structures seem to work as platforms **to concentrate cargo**. In this context, the **clathrin bilayered structures** associated to the ESCRT machinery are the best characterized. Clathrin

constitutes a characteristic flat bilayered structure on the surface of maturing SEs and MVBs (Sachse *et al.,* 2002), which is distinct from the "canonical" PM and TGN clathrin coats and PM clathrin plaques. At endosomes, these structures are not associated with actin and their generation is dependent on the presence of PtdIns(3)P ((Sachse *et al.,* 2002) and references therein), and the interaction with the ESCRT-0 subunit HRS (Raiborg *et al*., 2001). Clathrin bilayered plaques on endosomes seem to operate by sequestering cargo for their targeting to lysosomes (Raiborg *et al.*, 2006). The unusual appearance of bilayered clathrin coats could indicate inclusion of structural components that preclude lattice curvature (Traub, 2009). Interestingly, clathrin has also been implicated in budding of retroviruses at the PM (Brodsky 2012). The viral protein Gag plays a major part in budding and can produce virus-like particles when expressed alone in cells. Gag mediates budding by interacting with several components of the ESCRT machinery (Pincetic and Leis 2009). Interestingly, AP-2 also binds to Gag and cooperates with the Gag late domain to promote assembly and release of nascent equine infectious anaemia virions. Studies have additionally shown that AP-2 binding directs HIV-1 Gag to distinct domains and that an interaction of AP-1 with both Gag and ESCRT proteins also promotes retroviral budding. Nevertheless, the exact role of clathrin and clathrin adaptors in retroviral budding is still unclear.

Both **clathrin and retromer** seem to work in the same retrograde traffic route from endosomes to the TGN. However, clathrin has not been found to be part of the retromer tubes and a classical role for clathrin generating *bona fide* vesicles delivering material to an intermediate compartment where retromer might assemble has not been proven. Instead, increasing evidence suggests that clathrin might rather work as a platform that traps retromer destined cargo, and that this platform needs to disassemble to allow the formation of the actual retromer transport intermediates. RME-8 is an endosomal specific auxilin-like protein that has been described in mammalian cells, *D. melanogaster, C. elegans* and plants, which contains a DNA J-domain that stimulates the chaperone Hsc70 (Chang *et al.*, 2004; Girard *et al.,* 2005; Silady *et al.,* 2008; Zhang *et al.,* 2001). RME-8 strongly co-localizes with retromer components and it interacts with the retromer component SNX1 but does not bind clathrin (McGough & Cullen, 2013; Popoff *et al.*, 2009; Shi *et al.*, 2009). Loss of RME-8, Hsc70 or the retromer component SNX1 led to an increase in the amount of clathrin on endosomes, a slower turnover of endosomal clathrin, and cargo missorting into the degradative pathway (Popoff *et al.*, 2009; Shi *et al.*, 2009). However, loss of RME-8 did not increase the co-localization between retromer and clathrin, and tubules generated were still clathrin negative (McGough & Cullen, 2013). These data support a role of RME-8 in recruiting Hsc70 onto sites of retrograde tubule formation, thereby regulating clathrin dynamics that is critical for functional retrograde transport. In addition, it has also been recently suggested that other key role of RME-8 in endosomal trafficking is to coordinate WASH and sorting nexins activities for efficient retromer-mediated endosomal protein sorting (Freeman *et al.*, 2014). Upon deletion of RME-8, SNX1 maintains an abnormally tight association with the membrane, causing an exacerbated tubulation activity of its BAR domain (Freeman *et al.*, 2014). How the retromer associated clathrin relates to the ESCRT associated clathrin has not been elucidated yet, but of notice is that SNX1 also alternatively binds RME-8 and HRS - the ESCRT-0 subunit that interacts with clathrin.

1.2.2 Actin

The cellular cytoskeleton consists of three types of filamentous polymers - microtubules, intermediate filaments and actin filaments. Together, they help to organize the on a first glance chaotic cytoplasm and support structural integrity, but they are also indispensable to generate forces and determine the shape of cells and tissues.

Actin filaments, in particular, function as force-generating polymers, structural scaffolds and tracks for motor proteins. Actin plays an essential role in dynamic processes such as intracellular transport, cell division, cell migration, muscle contraction and a number of morphogenetic processes. It is conserved in all eukaryotes and homologs in prokaryotes have also been identified (reviewed in (Wickstead and Gull 2011)), pointing on the importance of actin during the evolution of life. Even after many decades of research on actin-mediated processes, new insights are still gained today. Thus, even though association of nuclear actin with DNA was already described in the 70s (Goldstein, Ko et al. 1977), the requirement of actin dynamics and formin activity for initiation of DNA replication has been just reported recently (Parisis, Krasinska et al. 2017).

1.2.2.1 Actin Structure and Biochemistry

Actin is one of the most abundant proteins in nearly all organisms. In humans, six different isoforms are expressed with many pseudogenes all over the genome (NCBI RefSeq, Aug 2017). Three main isoforms exist in higher eukaryotes: α-actin is found in muscle and is associated with muscle contraction, whereas β- and γ-actin are expressed in non-muscle cells. β-actin mainly polymerizes at the cell leading edge and γ-actin mainly associates with stress fibres. The monomer is relatively small (43 kDa) with a globular structure named G-actin. Actin has enzymatic ATPase activity and can self-assemble into microfilaments with a diameter of 4 – 7 nm. The actin conformation once polymerized is named F-actin. Actin filaments appear as two helices which twine slowly round each other (Holmes, Popp et al. 1990) with a head-to-tail orientation (Huxley 1963). The filaments are highly dynamic with an intrinsic polarity. The two ends of a filament are named barbed- and pointed-end based on the arrowhead pattern observed upon decoration with myosin fragments (Huxley 1963). Barbed ends are also called the (+) ends due to their higher growth and shrinking rate. Pointed ends are also called (-) ends and are less dynamic (Fig. 15) (Goley and Welch 2006).

The formation of new actin filaments starts with the assembly of an actin seed of two or three ATP-loaded actin monomers. After overcoming this thermodynamically unfavourable and therefore limiting step for the growth of new filaments, actin monomers are constantly added to the barbed-end (Sugino and Hatano 1982, Symons and Mitchison 1991, Pollard and Borisy 2003). Once an ATP-actin monomer is added, it promotes irreversible and fast hydrolysis of ATP. Phosphate is then released more slowly to produce ADP-actin, which shows less affinity to the neighbour subunit and consequently dissociates from the pointed end (Carlier, Pantaloni et al. 1988). The anew free ADP-actin undergoes nucleotide exchange and the recharged ATP-actin is ready to be recycled into another round of polymerization - a process commonly called treadmilling (Goldschmidt-Clermont, Furman et al. 1992).

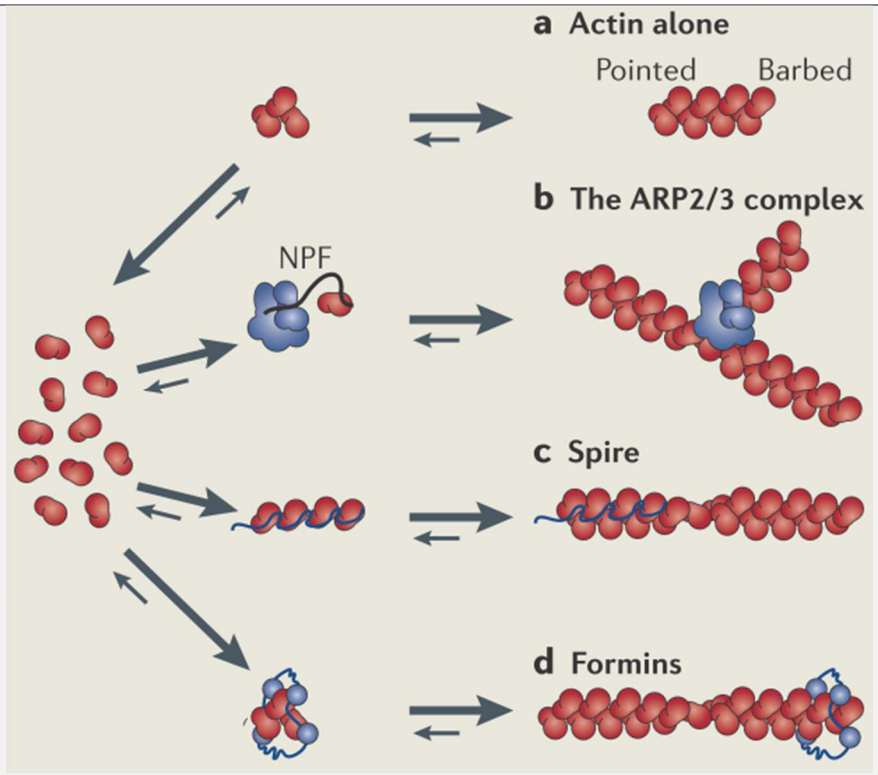

Figure 15. Paths to Actin Nucleation.
Spontaneous initiation of actin-filament assembly requires the formation of a trimeric nucleus in a process called nucleation (part **a**). Spontaneous nucleation is kinetically unfavourable and is the rate-limiting step in polymerization, because the actin dimer intermediate is very unstable. So far, three main classes of protein have been identified that bypass the energy threshold needed for spontaneous nucleation and promote the initiation of filament assembly. These factors, commonly referred to as nucleators, are the actin-related protein-2/3 (Arp2/3) complex, spire and formins. Each promotes nucleation by a distinct mechanism. The Arp2/3 complex is thought to mimic an actin dimer or trimer and to function as a template for the initiation of a new actin filament that branches off of an existing filament, generating y-branched actin networks (part **b**). Spire proteins, which are conserved among metazoan species, were recently discovered to nucleate actin assembly. Biochemical studies with *D. melanogaster* spire indicate that its four tandem WH2 domains mediate longitudinal association of four actin subunits and function as a scaffold for polymerization into an unbranched filament (part **c**). Spire might remain associated with the pointed end of the filament, as it can cap pointed ends and prevent their depolymerisation *in vitro*. Formins, which are conserved in most eukaryotes, also promote the nucleation of unbranched filaments. Biochemical and structural studies with yeast and mammalian formins indicate that a dimer of FH2 domains stabilizes an actin dimer or trimer to facilitate the nucleation event (part **d**). In contrast to spire and Arp2/3, formins remain associated with the growing barbed ends of filaments, and sequential binding and release interactions might allow formins to 'walk' with the polymerizing barbed end. The existence of multiple classes of nucleator gives the cell the flexibility to assemble distinct populations of actin filaments with particular geometries and polymerization characteristics. Obtained from (Goley and Welch 2006)

1.2.2.2 Cellular Regulation of Actin Dynamics

Actin polymerization and depolymerisation needs to be tightly controlled in cells in order to built a myriad of distinct actin structures with different architectures and dynamics. A striking number of actin binding proteins or protein complexes can modulate actin polymerization. They can be classified according to their biochemical activities: 1) Actin monomer sequestering; 2) Actin severing; 3) Actin Capping and 4) Actin nucleating. These proteins or protein complexes are tightly regulated by posttranslational modifications, calcium levels, PtdInsPxs binding and small regulatory GTPases, to spatiotemporally control actin polymerization in response to extracellular or intracellular signals.

Actin monomer sequestering proteins such as profilin or thymosin-β can either work by decreasing the actual concentration of free monomeric actin and as a consequence, lower the probability of filament assembly, or reciprocally, by promoting ATP loading on actin and targeting of actin monomers to cellular sites where increased actin polymerization is required.

Capping proteins prevent actin polymerization by binding to the fast growing end of actin filaments, namely the barbed ends, where most actin monomers would be effectively added. However, capping proteins can effectively stabilize filaments though by preventing the activity of depolymerizing factors.

Severing proteins, such as ADF/colfilin or gelsolin, work by binding to the ADP-F-actin and inducing breaks that generate filament ends prone to depolymerisation. However, the severing of filaments together with profilin can increase actin treadmilling by promoting rapid regeneration of actin monomers and/or by providing new barbed ends (McGough, Pope et al. 1997, Bobkov, Muhlrad et al. 2004).

Finally, **actin nucleators** such as formins or the Arp2/3 complex work by overcoming the energy barrier of actin filament nucleation, which is the most energy unfavourable step in actin polymerization (Fig. 15). Since during the course of this thesis, we found that kazrin C interacts with the Arp2/3 complex and several proteins that modulate its activity, the cellular mechanisms controlling actin nucleation will be discussed in detail. For excellent review discussing additional mechanisms regulating actin polymerization, please refer to (Campellone and Welch 2010).

1.2.2.2.1 Cellular Regulation of Actin Nucleation

To overcome the energetically unfavoured formation of actin seeds and to give rise to new microfilaments in a spatiotemporal regulated manner, **actin nucleators** assist this first step in a controlled manner. So far, five types of nucleators are identified - each of them work by a distinct mechanisms and trigger building of specialized actin-based structures: proteins of the formin family, spire proteins, cordon-bleu (COBL), leiomodin, and the Arp2/3 complex (Mullins, Kelleher et al. 1998, Pruyne, Evangelista et al. 2002, Sagot, Rodal et al. 2002, Quinlan, Heuser et al. 2005, Ahuja, Pinyol et al. 2007, Chereau, Boczkowska et al. 2008). Of those, only formins and the Arp2/3 complex are conserved in all species. Each type of actin nucleator work by distinct mechanisms and trigger building of specialized actin-based structures. Only the Arp2/3 complex is capable of producing branched actin networks, all others make linear actin filaments (Fig. 15) (Campellone and Welch 2010).

Formins are virtually present in all eukaryotes (Campellone and Welch 2010, Chesarone, DuPage et al. 2010). They assemble lineal structures including stress fibres, filopodia and the cytokinetic contractile ring. Their functions range from supporting cell polarity, cytokinesis or formation of tracks for polarized secretion and organelle inheritance, to DNA replication (Parisis, Krasinska et al. 2017). Most formins are able to nucleate and cap actin filaments and are associated with the fast-growing barbed end (Evangelista, Zigmond et al. 2003).

Spire, COBL and **leiomodin families** can be united as **WH2 domain-containing nucleators**. As their signature, they contain a tandem cluster of three or more G-actin-binding motifs, including WH2 domains. The WH2 element is shared with NPFs, but the tandem WH2 domain-containing nucleators

do not seem to bind Arp2/3 (Fig. 16) (Campellone and Welch 2010). As endocytic and endosomal processes involving the Arp2/3 will be of central importance for this thesis, the complex will be discussed in more detail in the following.

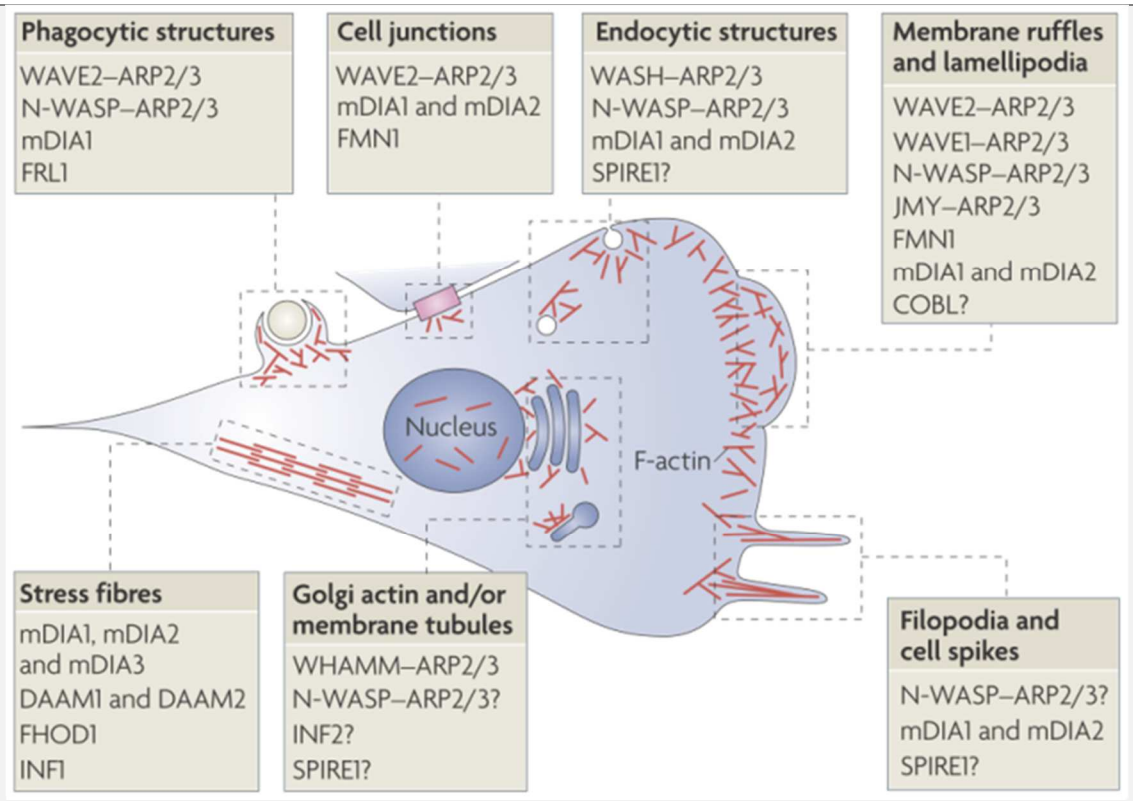

Figure 16. Localization and Function of Actin Nucleation Factors in Mammalian Cells.
F-actin (red) is nucleated and organized into branched networks by the Arp2/3 complex and its NPFs, or is generated in unbranched forms by formins and tandem WH2 domain-containing nucleators. Functional roles for different NPFs in a generic mammalian cell are depicted during phagocytosis, cell junction assembly, endocytosis, membrane ruffling and lamellipodia dynamics, filopodia formation, Golgi and tubulovesicular membrane dynamics, and stress fiber formation. Question marks indicate that the precise role for the nucleation factor is unclear. COBL, cordon-bleu; DAAM, Dishevelled-associated activator of morphogenesis; FHOD, formin homology domain; FMN, formin; FRL, formin-related in leukocytes; INF, inverted formin; JMY, junction-mediating regulatory protein; mDIA, murine Diaphanous; N-WASP, neuronal-WASP; WASP, Wiskott–Aldrich syndrome protein; WASH, WASP and SCAR homologue; WAVE, WASP-family verprolin homologue; WHAMM, WASP homologue associated with actin, membranes and microtubules. Obtained from (Campellone and Welch 2010).

1.2.2.2.1.1 The Arp2/3 Complex and its Nucleating Promoting Factors and Inhibitors

The **Arp2/3 complex** was the first actin nucleator identified in eukaryotic cells and it is still the only known to generate a branched actin network (Fig. 17A). Experiments with yeast mutants pointed out early a role for the Arp2/3 complex in the organization of the actin cytoskeleton and in the uptake step of endocytosis (Machesky and Gould 1999, Goley and Welch 2006). In general, the Arp2/3 complex is a central element in cell migration and adhesion but also plays a fundamental role in the intracellular movement of membranes and their cargoes from the PM, the endosomal system and the Golgi-apparatus, among others.

A great variety of studies showed that depletion of the Arp2/3 complex in many organisms, such as yeast, *C. elegans* or Drosophila, causes lethality (Lees-Miller, Henry et al. 1992, Winter, Podtelejnikov

et al. 1997, Morrell, Morphew et al. 1999, Hudson and Cooley 2002, Sawa, Suetsugu et al. 2003). In mouse fibroblasts, Arp2/3 is required for lamellipodia extension and directional cell migration (Suraneni, Rubinstein et al. 2012) and in neuron hippocampal cultures the complex is necessary for normal development (Spence, Kanak et al. 2016). In the intestinal epithelium of mice, loss of Arp2/3 leads to defects in vesicle trafficking, transcytosis and the organization of the endo-lysosomal system and the mice die within days of birth (Zhou, Sumigray et al. 2015). In human blood cells the loss of one subunit of the complex causes loss of a great proportion of the Arp2/3, leading to dramatic effects (Kahr, Pluthero et al. 2017). And in the human cancer cell line HeLa, the inactivation of a complex subunit is lethal (Harborth, Elbashir et al. 2001).

The Arp2/3 complex consists of seven subunits, considered as a single entity: two actin-related proteins Arp2 and Arp3 and five actin-related protein complex proteins Arpc1/p41, Arpc2/p34, Arpc3/p21, Arpc4/p20 and Arpc5/p16 (Fig. 17a). Arpc1 to 4 do not contain common sequence motifs. Arpc5 contains a WD-repeat and forms a seven-blade β propeller with an insertion that may associate with the side of an actin filament (Robinson, Turbedsky et al. 2001). Arp2 was first identified based on sequence similarity to actin, which also Arp3 shows (Lees-Miller, Henry et al. 1992, Schwob and Martin 1992). As actin, they have ATPase activity, and binding to ATP is required for a functional complex. Hydrolysis of the bound ATP might cause conformational changes enabling the onset of nucleation but the exact mechanism is not completely elucidated (Dayel, Holleran et al. 2001, Le Clainche, Didry et al. 2001, Robinson, Turbedsky et al. 2001, Goley, Rodenbusch et al. 2004, Egile, Rouiller et al. 2005, Martin, Xu et al. 2005, Goley and Welch 2006). Additionally, the phosphorylation of the Arp2 subunit is necessary for the activity of the complex (LeClaire, Baumgartner et al. 2008).

Two models for the complex based on cryo-electron microscopy propose that Arp2 and Arp3 interact with the pointed end of the daughter filament, and Arpc2 and Arpc4 make substantial contacts with the mother filament (Beltzner and Pollard 2004, Egile, Rouiller et al. 2005). Further, it is assumed that Arp2 and Arp3 act as the two first actin subunits of the new filament. The complex will generate a lateral branch on an existing mother filament with an angle of approximately 70°, forming the characteristic Y-shaped networks with the complex located at the junction. Apart from nucleation of new actin fibres, the Arp2/3 complex caps the new filament at its pointed end, leaving the more dynamic barbed end free (Fig. 17b) (Mullins, Kelleher et al. 1998, Svitkina and Borisy 1999, Egile, Rouiller et al. 2005, Rouiller, Xu et al. 2008). Binding of the complex to actin filaments increases the affinity for regulatory proteins, hence stimulates nucleation (Marchand, Kaiser et al. 2001). Coupling of nucleation and branching is also referred to as autocatalytic branching or dendritic nucleation.

The purified complex is able to start actin polymerisation *in vitro* but with pretty low activity on its own. An early crystal structure of the bovine purified complex showed that Arp2 and Arp3 are too far apart to form an actin dimer, suggesting an inactive state. So, it was proposed that regulatory proteins might promote a conformational change to close up the complex (Robinson and Bonifacino 2001, Goley, Rodenbusch et al. 2004, Egile, Rouiller et al. 2005, Rodal, Sokolova et al. 2005). Indeed, the addition of regulatory factors boosts the initiation of the filament formation several orders of magnitude (Welch, Rosenblatt et al. 1998, Machesky and Gould 1999, Rohatgi, Ma et al. 1999) and therefore, these factors are called nucleation promoting factors (NPF). In a cellular context, a fast and localized polymerization is necessary, which is coordinated by a meticulous regulation of the recruitment and activation of NPFs.

To accomplish the big variety of Arp2/3 dependent cellular tasks the complex needs to be activated in a spatio/temporal controlled manner. To this end, many regulatory cofactors evolved. One group are the Arp2/3 Nucleating Promoting Factors (NPFs). The NPFs can be divided into two classes by the type of actin they bind to. NPFs class I bind to monomeric G-actin and NPFs class II bind to existing actin filaments. The type I and type II NPFs activate the Arp2/3 complex by different mechanisms and show a diverse domain organization but they still share some common characteristics. One characteristic is that they all contain an Arp2/3-binding sequence called CA domain which consists of a Cofilin-homology, central or connecting region (C) plus an acidic sequence that includes a conserved tryptophan (A). The CA domain is necessary to activate the Arp2/3 complex but is not sufficient on its own (Rohatgi, Ma et al. 1999).

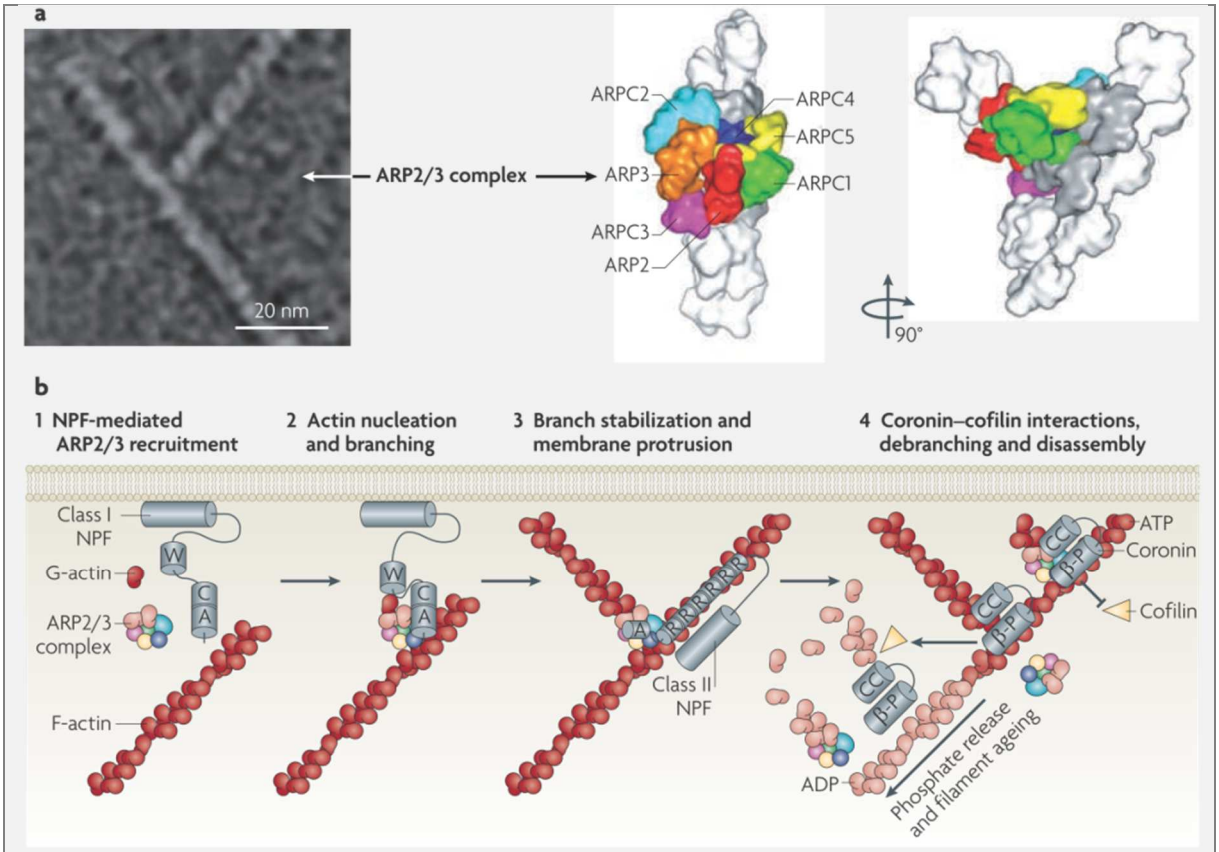

Figure 17. Structure of Arp2/3 in Y-branches and Model for Actin Nucleation and Branching.
a. The morphology of a Y-branched actin filaments and the Arp2/3 complex is shown in an electron micrograph and in structural models based on electron tomography. The Arp2/3 complex consists of Arp2 and Arp3 plus the additional subunits Arpc1–Arpc5. In this model, all seven subunits participate in binding to the existing filament and Arp2 and Arp3 act as the first two subunits of the nascent filament. **b.** Arp2/3 is recruited by the WCA domains of class I NPFs in proximity to cellular membranes (1). The collective activities of WASP homology 2 (WH2; W), connector (C) and acidic (A) segments serve the basic purpose of bringing Arp2/3 together with the first actin subunit in the new filament to generate a branch (2). Arp2/3 branch points can be stabilized by F-actin-binding class II NPFs, such as cortactin (3). Coronin family proteins interact with Arp2/3 and F-actin to prevent cofilin-mediated disassembly of newly formed filaments (4, top). Coronin can also replace Arp2/3 and synergize with cofilin to trigger debranching and disassembly of older ADP–actin filaments (4, middle). Disassembly of older branches can also occur spontaneously, following phosphate release from Arp2 and actin (4, bottom). β-P, β-propeller; CC, coiled coil; R, repeat. For further details see text in chapter 1.2.2.2.1.1 ff. Obtained from (Campellone and Welch 2010).

Class I NPFs are diverse in their overall domain organization but have two features in common (Fig. 18). They contain one or two actin monomer-binding WH2 (WASP homology 2) domains, also called V (verprolin homology) or W domains, usually found just before regions C and A, whichthat mediate binding to the Arp2/3. The WH2 domain positions the first actin to start the new filament. Most class

I NPFs contains the triple domain WCA and can activate the Arp2/3 complex by itself but some members might lack one of the typical sequences, which can be located in a separate molecule, therefore requiring reconstitution of a complex for activity (Lechler, Jonsdottir et al. 2001, Marchand, Kaiser et al. 2001, Goley, Rodenbusch et al. 2004, Chereau, Kerff et al. 2005, Rodal, Sokolova et al. 2005). Class I NPFs usually show low affinity for the Arp2/3 complex. The interaction is more of a transient nature, so probably they just stimulate, dissociate off and start over with a different complex. Typical members are the **WASP-family** , namely WASP and N-WASP (Symons, Derry et al. 1996) or **Scar/WAVE** proteins (suppressor of cyclic AMP repressor/WASP-family verprolin-homologous protein) (Machesky and Gould 1999, Rohatgi, Ma et al. 1999, Winter, Lechler et al. 1999, Yarar, To et al. 1999), **WHAMM** (WASP homolog associated to actin, membranes, and microtubules) (Campellone, Webb et al. 2008), the **WASH** complex (WASP and Scar homologue) (Derivery, Sousa et al. 2009, Gomez and Billadeau 2009), the p53 cofactor **JMY** (Zuchero, Coutts et al. 2009), the fungal **type I myosins** (Geli, Lombardi et al. 2000, Lee, Bezanilla et al. 2000, Lechler, Jonsdottir et al. 2001, Sun, Martin et al. 2006) and proteins from intracellular pathogens such as **ActA** from *Listeria monocytogenes*, RickA from *Rickettsia*, metazoan **CARMIL** (capping protein Arp2/3 and myosin-I linker)(Jung, Remmert et al. 2001) or **p78/83** from a baculovirus (Welch, Rosenblatt et al. 1998, Gouin, Egile et al. 2004, Jeng, Goley et al. 2004, Goley, Ohkawa et al. 2006). See below for more details about WASP and WASH.

Class II NPFs are far less powerful activators *in vitro* (Higgs and Pollard 2001, Sun, Martin et al. 2006). They also contain an acidic sequence for Arp2/3 binding but do not bind G-actin, instead they bind to actin filaments through F-actin binding domains. It is not clear how they activate the Arp2/3 complex since they lack a connecting region and cannot trigger the Arp2/3 conformational change necessary for complex activation (Goley, Rodenbusch et al. 2004). The mechanism might actually involve an enhancement of Arp2/3 association with the mother filament, which is itself an activator of the complex (Higgs and Pollard 1999, Machesky and Gould 1999). Typical members are **cortactin** (Uruno, Liu et al. 2001, Weaver, Karginov et al. 2001), **Abp1** (Goode, Rodal et al. 2001) and **Eps15** (Duncan, Cope et al. 2001).

Cortactin and N-WASP can bind simultaneously to the Arp2/3 complex but N-WASP is released after y-branching, whereas cortactin remains associated with the complex at the branching point to inhibit branch dissociation. Therefore, the most important function of class II NPFs might be to stabilize the y-branched organization of actin networks (Higgs and Pollard 2001).

In the last years, **negative modulators of the Arp2/3 complex** have also been identified. They are characterized by the presence of an acidic peptide, similar to that observed in NPFs, but the absence of other domains that are also required to promote actin nucleation, such as the WH2 domains. **Arpin** was the first Arp2/3 inhibitor to be identified (Dang, Gorelik et al. 2013). Arpin directly binds Arp2/3 and suppresses actin filament nucleation of the complex *in vitro* (Dang, Gorelik et al. 2013). It is recruited to the leading edge during migration of mouse embryonic fibroblasts by the small GTPase Rac1, which controls cell protrusion. Interestingly, arpin levels are inversely correlated with lamellipodium speed and persistence (Dang, Gorelik et al. 2013, Gorelik and Gautreau 2015). It is generally accepted that the strong accumulation of actin nucleation factors at the leading edge depends on positive feedback loops. To prevent a permanently activated state, the existence of a negative feedback loop with a relatively slow turnover was early proposed in cell migration models. Arpin now exits as a potent candidate for an antagonist to the many Arp2/3 activators (Dang, Gorelik et al. 2013, Veltman 2014). More recently, contradictory results display no obvious defect in

chemotaxis upon arpin depletion. In any case, these results do not rule out a potential role of arpin in other systems and cellular processes engaging the Arp2/3 complex (Dang, Linkner et al. 2017).

The existence of a second Arp2/3 inhibitor, **gadkin**, has also been suggested based on the presence of an acidic domain at its C-terminus, on its capacity to interact with the Arp2/3 complex and on the effects on actin polymerization upon gadkin overexpression or depletion. However, one has to mention that direct demonstration of its biochemical activity as an inhibitor of the Arp2/3 complex on pyrene-actin polymerization assays with purified components has not been possible to date. Gadkin was originally purified from AP-1 containing CCVs and shown to interact with the Arp2/3 complex and kinesin-1 (Neubrand, Will et al. 2005, Schmidt, Maritzen et al. 2009, Hirst, Edgar et al. 2015). When overexpressed, gadkin inhibits Arp2/3-dependent dendritic cell migration by sequestering the Arp2/3 complex on AP-1 containing vesicles, while loss of gadkin is associated with a partial redistribution of Arp2/3 to the PM and increased cell spreading and migration (Maritzen, Zech et al. 2012). In addition, it seems that an AP-1/gadkin/kinesin-1 complex controls the positioning and/or dynamics of rab4- and Tfn-positive recycling vesicle. This outward-directed microtubular transport may act synergistically with short-range actin- and myosinVb-dependent movement of endosomal vesicle (Fig. 4D) (Maritzen and Haucke 2010).

1.2.2.3 Function and Regulation of Actin within the Endocytic Pathway

Actin is involved in many different ways in the endocytic pathway, reaching from the support of cargo selection, to vesicle and tubule budding and/or fission, the movement of transport intermediates or the stabilisation of the organelle structure.

At the PM, mammalian cells assemble cortical actin, not only important for the formation of actin rich structures such as lamellipodia or filopodia, but also for the stabilisation of the cell shape and intercellular and cellular-matrix junctions, as well as for the positioning and regulation of cell surface receptors and other membrane proteins. During **endocytic uptake** from the PM, actin is involved in different steps. It is well established that CME in yeast occurs in an actin-dependent manner. An actin cup induced by N-WASP and the type-I myosins is require to stabilize membrane curvature and to sustain elongation of the endocytic profiles (Idrissi and Geli 2014). Further, it is likely to play a role in vesicle fission (Idrissi and Geli 2014). Epsins and the HIP1R homolog Sla2 play essential function linking the endocytic coat to actin filaments, a function that seems to be regulated by PtdIns(4,5)P_2 (Skruzny, Brach et al. 2012). What primarily brings and activates the endocytic Arp2/3 NPFs at the endocytic coats in yeast is not really known, even though mechanisms involving interactions with BAR-domain proteins, the biogenesis of PtdIns(4,5)P_2, the transfer of sterols, and calcium bursts have been proposed (Encinar Del Dedo, Idrissi et al. 2017, Sun, Leong et al. 2017).

By contrast, the role of actin in mammalian endocytosis has been somewhat controversial. Live imaging showed that actin is recruited near the end of the lifetime of the invaginating pit, suggesting it plays a part in vesicle scission (Merrifield, Perrais et al. 2005). In line with this, electron microscopy data show that actin filaments form a collar-like structure around the neck of the growing vesicle (Humphries and Way 2013). These data support a role for actin polymerization in neck elongation, vesicle scission and the subsequent movement of the vesicle into the cell.

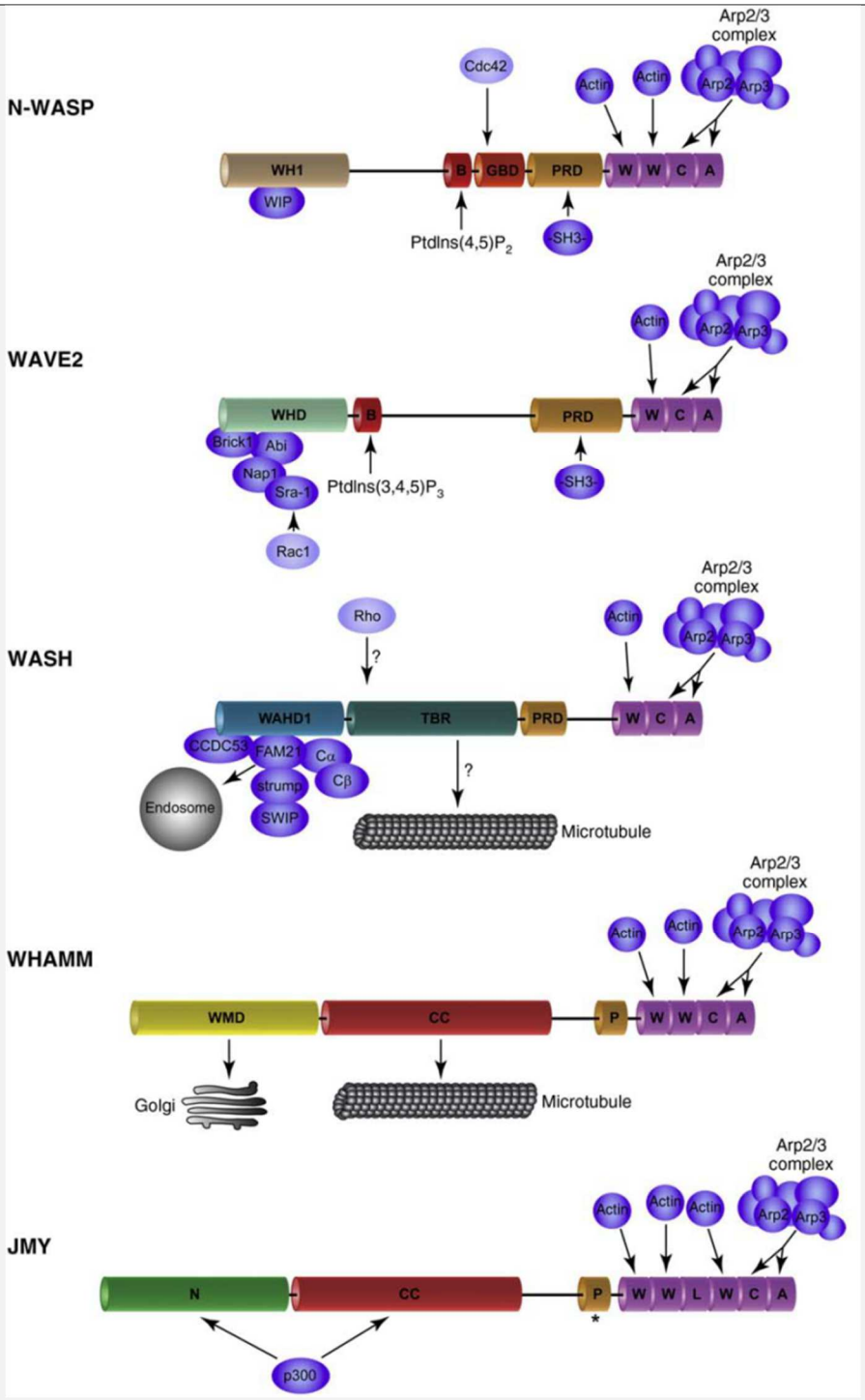

Figure 18. Domain Organization of Human Type I NPFs.

The C-termini of all shown NPFs are characterized by Arp2/3-binding CA-modules linked N-terminally to different numbers of actin monomer-binding WH2 domains (W). The N-termini are highly divergent and are thought to mediate subcellular targeting, Rho-GTPase-binding (Cdc42 in the case of N-WASP or a Rho subfamily member in the case of WASH) and associations with diverse regulators or into large protein complexes (i.e. WAVE2 and WASH). -SH3-, SH3-domain containing protein; A, acidic region; B, basic domain; C, connector region; Ca/Cb, a-/b-subunit of heterodimeric capping protein; CC, coiled-coil region; GBD, GTPase-binding domain; PRD, proline-rich domain; P, polyproline domain; L, monomer-binding linker (homologous to actin monomer-binding linker in Spir); N, N-terminus; strump, strumpellin; TBR, tubulin-binding region; WAHD1, WASH homology domain 1; WHD, WAVE homology domain (also known as SHD, Scar homology domain); WH1, WASP homology 1 domain; WIP, WASP interacting protein; WMD, WHAMM membrane interaction domain; * indicates the description of JMY isoforms lacking the polyproline domain. Obtained from (Rottner, Hanisch et al. 2010).

The controversy over the role of actin arose because of the varying degree of disruption of CME when actin polymerization was inhibited. Subsequent studies have now demonstrated that actin seems to be required only when membrane tension is high. Consistent with this tension-based dependence on actin, reducing the high turgor pressure eliminates the need for actin during endocytosis in yeast (Aghamohammadzadeh and Ayscough 2009). In mammalian cells, a number of proteins have been linked to the regulation of Arp2/3-dependent actin polymerization during endocytosis, including dynamin, cortactin, HIP1-related protein (HIP1R) and N-WASP. Dynamin might coordinate actin nucleation through its interaction with cortactin and through its indirect interaction with N-WASP mediated by a number of adaptors such as amphiphysin (Higgs 2002, Weaver, Heuser et al. 2002). Additional regulation of actin polymerization is provided by HIP1R (Engqvist-Goldstein, Zhang et al. 2004, Le Clainche, Pauly et al. 2007, Brady, Damer et al. 2010). HIP1R also interacts with cortactin and inhibits the interaction of this protein with N-WASP, dynamin and the Arp2/3 complex.

The connection between clathrin and the actin cytoskeleton was further reinforced with the identification of clathrin plaques at the PM. These structures are observed at the adherent surface of cells, suggesting that they only form in situations of high membrane tension. Consistent with this, their internalization is strongly dependent on N-WASP-induced actin polymerization (Schafer 2002).

After fission of the CCV, the early inward movement of the vesicle is probably actin dependent (Taylor, Perrais et al. 2011, Idrissi and Geli 2014), before a change of the transport system to microtubule based long distance transport takes place. Nascent pinosomes moving at the tip of actin tails have been reported on macrophages using live-cell microscopy (Merrifield, Moss et al. 1999). In addition, Tfn-labeled membrane profiles, possibly corresponding to primary clathrin-uncoated endocytic vesicles have also been observed moving at the tip of actin tails that co-localize with the Arp2/3 complex *in vivo* (Kaksonen, Peng et al. 2000). In addition, Tfn-labeled vesicles travel toward the cell centre in a myosin-VI-dependent manner. Myosin-VI transports vesicles away from the actin filament plus end and thus, away from the surface where actin filaments are nucleated (Aschenbrenner, Lee et al. 2003).

Purified mammalian **WASP and N-WASP** fold in an autoinhibited conformation, which can be cooperatively released by binding to **PtdInsPxs** and small GTPases to its basic and CRIB domains, respectively (Higgs and Pollard 2001). The WASP CRIB region interacts with **Cdc42**, a small GTPase involved in filopodium formation and the establishment of cell polarity (Miki, Sasaki et al. 1998, Takenawa and Suetsugu 2007). However, Cdc42 is not required for CME. Other small GTPases related to CDC42, such as Tc10, RhoT and Chp, activate N-WASP, but their involvement in CME has not been explored (Aronheim, Broder et al. 1998, Abe, Kato et al. 2003, Hemsath, Dvorsky et al. 2005). The binding of **SH3-domain-containing proteins** such as **TOCA-1** to the proline-rich region of WASP and N-WASP also activates its Arp2/3-dependet actin nucleating promoting activity, but the precise mechanism of this is not clear (Takenawa and Suetsugu 2007, Derivery and Gautreau 2010). A number of endocytic proteins such as **syndapins** or **endophilins** that bear curvature sensing domains such as BAR or EFC, also have SH3 domains that interact with WASP or N-WASP and are involved in CME (Simpson, Hussain et al. 1999, Kessels and Qualmann 2004, Frost, Unger et al. 2009). This has been used to propose that membrane curvature might modulate the recruitment and/or activation of these proteins, which in turn will engage the NPF (Galletta, Mooren et al. 2010). Finally, phosphorylation of WASP and N-WASP by the **Src** family of tyrosine kinases close to the CRIB region and by **casein kinase 2** (CK2) in a Serine or Threonine adjacent of the acidic peptide can also modulate their activity (Suetsugu, Hattori et al. 2002, Cory, Cramer et al. 2003, Martinez-Quiles, Ho

et al. 2004). Both Src and CK2 have been implicated in CME, and therefore, they might be modulating N-WASP activity for endocytic uptake (Cao, Chen et al. 2010, Galovic, Xu et al. 2011).

At the endosomes, as already described, internalized cargo is sorted for retrograde transport to the PM or to the TGN or is destined for degradation. For both retrograde transport pathways, cargo is concentrated into outgrowing tubulations and is packed into vesicular transport intermediates. In both pathways, engaging retromer or retriever, the Arp2/3 NPF WASH complex is involved to create actin networks necessary to form and stabilize the sorting platforms including the SNXs, as well as the emerging membrane tubules. The importance of WASH in endosome-related pathways could be demonstrated by the strong effects upon its depletion, as seen for the retromer-mediated endosome-to-Golgi retrieval of the CI-MPR (Gomez and Billadeau 2009), the endosome-to-cell surface recycling of the transferrin receptor (TfnR), α4β1-integrin (Zech, Calaminus et al. 2011), the GPCR β2-adrenoreceptor (Bear 2009, Temkin, Lauffer et al. 2011), the sorting into lysosomes of the EGFR (epidermal growth factor receptor) (Duleh and Welch 2010), for trafficking of glucose transporter Glut-1, or the T cell receptor and CD28 in T cells (Gomez, Gorman et al. 2012, Piotrowski, Gomez et al. 2013). Partial depletion of WASH caused accumulation of endosomal tubules (Derivery, Sousa et al. 2009, Gomez and Billadeau 2009) suggesting a participation in the fission of retromer generated tubules. On the other hand, a complete knockout showed enlarged endosomes but no excessive tubulation (Gomez, Gorman et al. 2012), indicating that WASH might also participate in the formation of retromer or retriever tubules. In addition, GPCRs have been shown to be trapped in endosomal actin and filamin A-enriched subdomains previous to loading in retromer tubes, indicating that actin subdomains might act as the endosomal clathrin platforms for cargo recruitment (Varandas, Irannejad et al. 2016, Pons, Izquierdo et al. 2017). In addition to endosome dynamics, WASH is implicated in exocytosis and in integrin-based invasive migration (Carnell, Zech et al. 2011, Zech, Calaminus et al. 2011).

WASH is, in contrast to WASP, constitutively active. As already mention though, WASH is held inactive *in vivo* as part of an >600 kDa complex composed of five subunits: FAM21, SWIP, strumpellin and CCDC53 plus associated F-actin barbed end capping proteins (Bear 2009, Derivery, Sousa et al. 2009, Gomez and Billadeau 2009, Campellone and Welch 2010, Jia, Gomez et al. 2010, Rottner, Hanisch et al. 2010, Seaman, Gautreau et al. 2013, Edwards, Zwolak et al. 2014). How its association with the complex and/or its activity is modulated is far from being understood. Interestingly, ubiquitination of WASH via the ubiquitin ligase MAGE-L2-TRIM27 is necessary for endosomal Arp2/3-mediated actin polymerisation and correct CI-M6PR trafficking (Hao, Doyle et al. 2013). The recruitment of both, the ubiquitin ligase and the WASH complex, happens via the VPS35 subunit of the retromer (Fig. 19) (Harbour, Breusegem et al. 2010, Hao, Doyle et al. 2013). In addition, RME-8, known to be involved in membrane traffic of EE, coordinates the activity of WASH and retromer and thereby endosomal tubulation (Freeman, Hesketh et al. 2014). RME-8 interacts with SNX1 from the SNX–BAR subcomplex and FAM21 of the WASH complex and thereby, might coordinately regulate their activity (Popoff, Mardones et al. 2009, Freeman, Hesketh et al. 2014, McGough, Steinberg et al. 2014). Further, SNX27 interacts with both SNX1 and WASH (Steinberg, Gallon et al. 2013), all together strengthening the link between the retromer and the WASH complex.

Besides WASH, other actin nucleators are necessary for the correct functionality of the elaborated endosomal system. The actin nucleator **spire** was found to co-localize with the G protein rab11, the master regulator of recycling from the ERC and exocytic vesicle transport processes (Kerkhoff,

Simpson et al. 2001, Wang and Riechmann 2008). Further, an actin nucleator complex composed of members of the spire family (Spir-1 and -2) and members of the **formin** family (Fmn-1 and -2) have been found to work cooperatively in the nucleation of actin filaments at endosomal and vesicle membranes (Pechlivanis, Samol et al. 2009, Dietrich, Weiss et al. 2013). Together with the **rab11** effector RAB11FIP2 linked to myosin Vb, rab11 might build another important node for vesicle transport from endosomal compartments employing actin (Lapierre, Kumar et al. 2001, Hales, Vaerman et al. 2002, Dietrich, Weiss et al. 2013). Additionally, actin patches nucleated on early endosomes via spire1 and annexin A2 seem to control endosome biogenesis, presumably by driving the membrane remodeling process (Morel, Parton et al. 2009).

On the other hand, **cortactin** has been shown to be necessary for the formation of F-actin networks that mediate endosome maturation and transport through the degradative pathway, whereas its depletion does not seem to affect retrograde trafficking pathways (Muriel, Tomas et al. 2016). Also supporting its role in the formation of endosomal actin networks, depletion of cortactin prevents the appearance of an actin shell upon interfering with the function of calmodulin (Llado, Timpson et al. 2008). On the endosomal context, cortactin seems to be negatively regulated by PtdIn(3,5)P_2. Cortactin binds PtdIns(3,5)P_2 via its actin filament-binding region and PtdIns(3,5)P_2 competes with actin filaments for binding to cortactin, thereby antagonizing cortactin activity. These findings suggest that PtdIn(3,5)P_2 formation on endosomes may remove cortactin from endosome-associated branched actin (Hong, Qi et al. 2015). Consistently, inhibition of PtdIn(3,5)P_2 production led to cortactin accumulation and actin stabilization on rab7-positive endosomes. Whether the cortactin and WASH actin networks coincide has not been investigated in detail, but the observation that cortactin depletion does not interfere with retrograde transport from the endosomes indicates that different actin platforms with distinct functions exist on endosomal membranes.

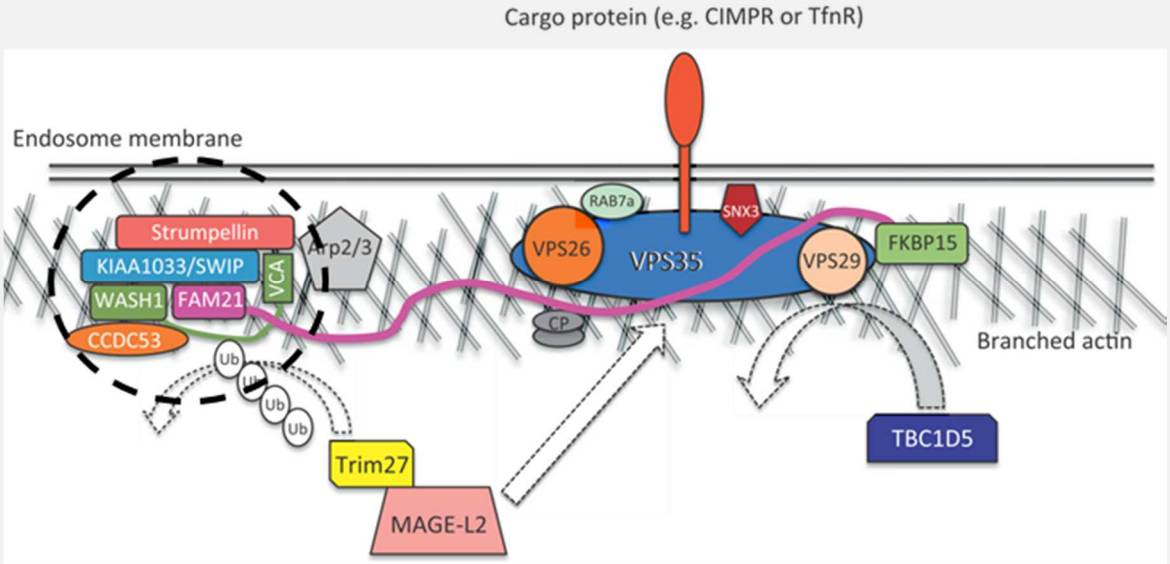

Figure 19. Diagram of the WASH Complex and the Retromer.
The retromer cargo-selective complex (CSC) comprising VPS35, VPS29 and VPS26 functions as an unit that is recruited to endosomes by rab7 and SNX3. The TBC1D5 protein acts antagonistically to rab7 to downregulate recruitment of the retromer CSC. Through an interaction between VPS35 and Fam21 mediated by numerous LFa motifs within the unstructured tail of Fam21, the retromer CSC recruits the WASH complex (dashed circle) to endosomes to drive the formation of branched actin patches. Additionally, MAGE-L2 connects VPS35 to TRIM27, which polyubiquitinates WASH1 and activates its NPF activity towards Arp2/3. Obtained from (Seaman, Gautreau et al. 2013).

Preliminary Results

2 Preliminary Results

2.1 Kazrin C was Identified in a Genetic Screening for Proteins Involved in CME

A genetic screening was designed in our laboratory to identify human proteins involved in CME (Schmelzl and Geli 2002). In this study, an expression library with partial cDNAs from human brain, with an average size of 1.2 kb was cloned in a vector bearing the SV40 origin of replication, which can be amplified in Cos-7 cells. One day upon transfection, cells were exposed to a fluorescently-labelled antibody against the Tfn receptor. In intact Cos-7 cells, the Tfn receptor is continuously internalized by CME and recycled back to the PM from SE and ERC following different pathways. Because internalization of the Tfn receptor is very efficient, most of the receptor accumulates in the recycling endosome at steady state. However, impairment of the uptake step of CME results in the accumulation of the receptor at the cell surface. Cells expressing human cDNAs that caused accumulation of the Tfn receptor at the PM were detected and selected by Fluorescence-Activated Cell Sorting (FACS) and the plasmids encoding such cDNAs were recovered by extraction and electroporation in *E. coli*, and further analysed individually (Fig. 20). One of the recovered cDNAs encoded for the thus far uncharacterized protein encoded by the KIAA102 locus, nowadays known as kazrin C.

Bioinformatical analysis of the amino acid sequence of the 327 aa of kazrin C, unveiled a putative coiled-coil region at the N-terminus showing weak homology to ERM proteins (Fig. 21). Further, the polypeptide carried two possible clathrin binding motifs and a cluster of positively charged amino acids resembling those that might interact with lipids and/or clathrin adaptors (Chapman, Desai et al. 1998), enforcing the possibility that kazrin C might directly interact with the CME machinery and therefore, participate in endocytic traffic. The positively charged poly basic stretch has also been proposed to be a nuclear localization signal (Groot, Sevilla et al. 2004). Additionally, we identified an acidic peptide at the C-terminus, similar to those found in NPFs such as N-WASP or WASH (Fig. 21), required for the interaction with the Arp2/3 complex. In later studies from other laboratories, kazrin was identified as a component of desmosomes and its N-terminal region was shown to be sufficient for direct binding to periplakin (aa 89 to 239; (Groot, Sevilla et al. 2004)). In agreement with its localization in desmosomes, overexpression of kazrin in human keratinocytes caused profound changes in cell shape and impaired assembly of intercellular junctions, associated with decreased Rho activity (Sevilla, Nachat et al. 2008). Interestingly, also reduced filamentous actin in cells overexpressing kazrin was noted in that study.

The cDNA discovered in our screening encodes for one of five splice variants of the gene locus KIAA1016 on the human chromosome 1 and on the mouse chromosome 4 (Fig. 22A). Exons 2 to 8 of human kazrin are spliced together, whereas four different first exons can be formed by alternative splicing. Coding sequences containing exon 1c or 1d begin at a start codon within exon 2 and result in kazrin C and D, which have an identical amino acid sequence and are referred to as kazrin C from now on. Kazrin A, B and F encode for slightly larger proteins with additional sequences at the N-terminus. Kazrin E shares most of its sequence with kazrin A but substitutes the last 15 amino acids by a fragment of 368 amino acids (Fig. 22B). Human kazrin C is 98% identical at the protein level to the amino acid sequence of mouse kazrin over the corresponding region (Groot, Sevilla et al. 2004). Taken together, all isoforms bear most of the sequence of kazrin C as their core, supplemented with additional fragments.

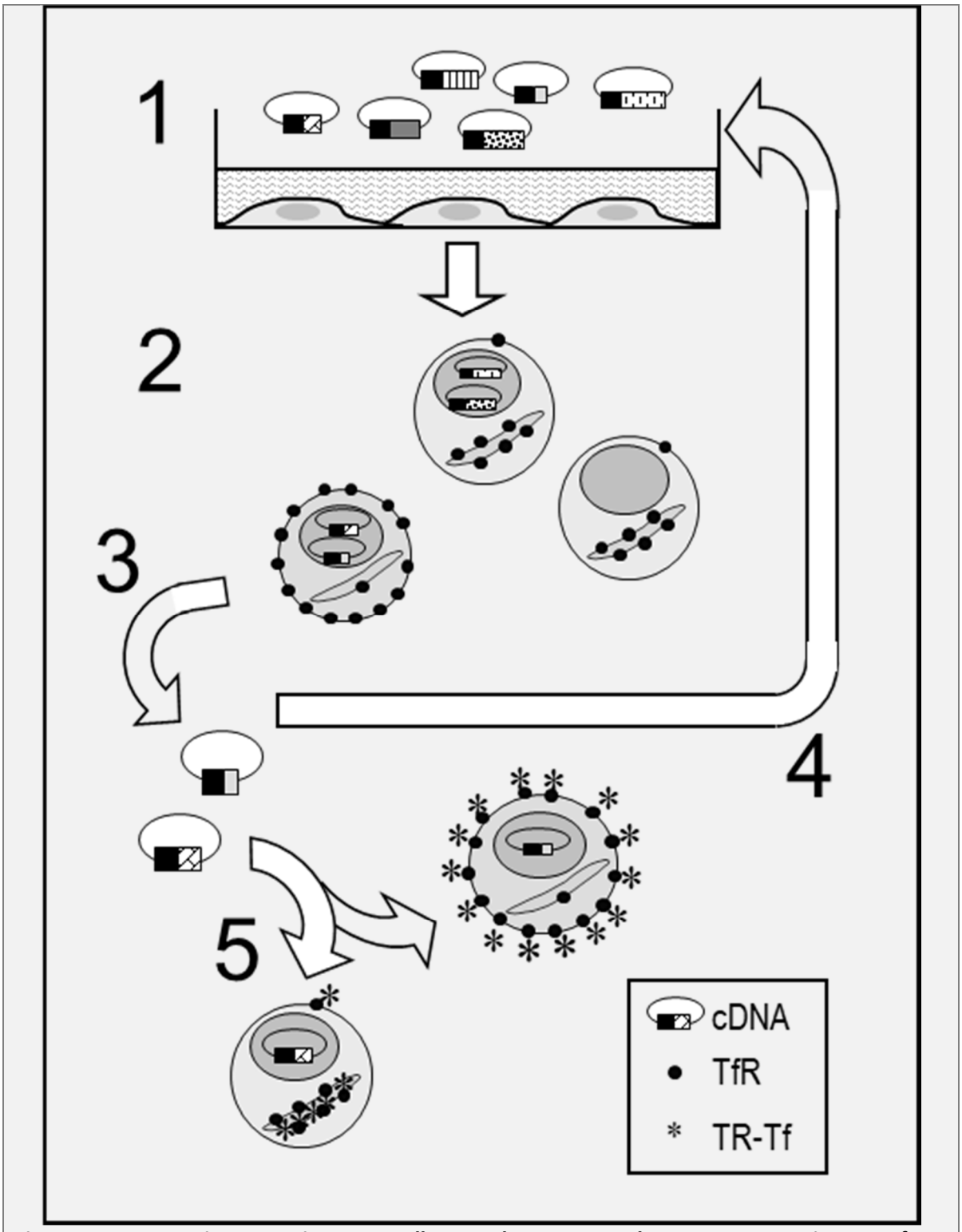

Figure 20. A Genetic Screen in Cos-7 Cells to Isolate cDNAs whose Overexpression Interferes with CME.

Cos-7 cells are transfected with a library of partial cDNAs fused to GFP (1). One day upon transfection, cells accumulating the transferrin receptor (TfnR) at the cell surface are selected using a monoclonal antibody against the TfnR and anti-mouse IgG antibody-coated dishes or CY5-labelled Tfn and FACS (2). Selected cells are lysed and plasmids are recovered by electroporation into *E. coli* (3). Plasmids from individual colonies are either pooled and subjected to a new round of selection (4) or they are separately purified to analyze the effect of overexpressing individual cDNA under the fluorescence microscope using TR-Tfn (5).

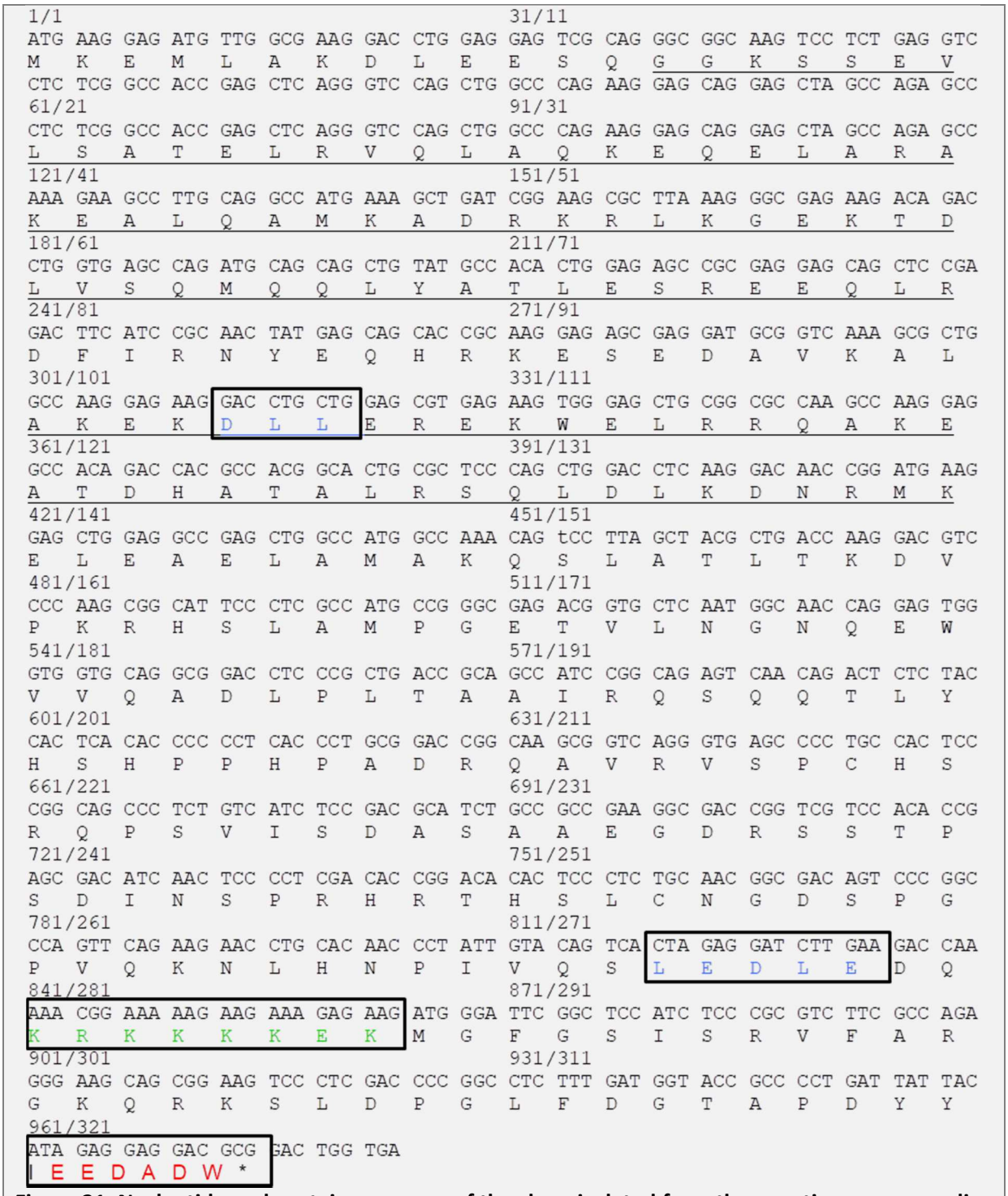

Figure 21. Nucleotide and protein sequence of the clone isolated from the genetic screen encoding Kazrin C.

The coding DNA sequence and the deduced amino acid sequence of the hB24 clone encoding kazrin C are shown. The putative coiled-coil region is underlined, conserved or degenerated clathrin binding motifs are shown in blue (1. and 2. box). The cluster of positively charged amino acids from a clathrin box is shown in green (3. box) and the acidic peptide at the C-terminus is shown in red (4. box).

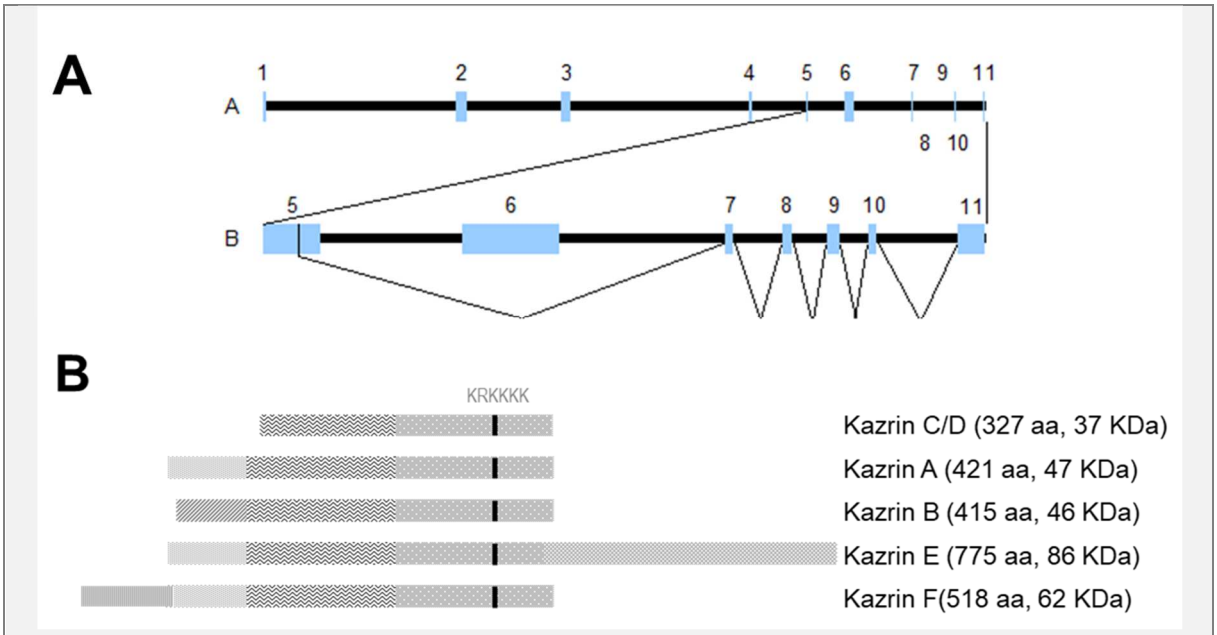

Figure 22. Structure of the Identified Human Splice Variants of KIAA1026.
A. Exon-intron structure of the KIAA1026 gene on human chromosome 1. The mRNA splicing resulting in the mRNA encoding kazrin C, encompassing part of exon 5 and exons 7 – 11, is indicated. **B.** Splice variants encoded by KIAA1026. All isoforms share a core structure that corresponds to kazrin C. All bear the C-terminal acidic peptide except for kazrin E. Kazrin A, E and F bear a BAR domain (light grey).

2.2 Overexpression of Kazrin C Inhibits the Uptake Step of CME

In order to investigate if overexpression of kazrin C increases the surface exposure of the Tfn receptor by inhibiting its endocytic internalization, Cos-7 cells were transfected with plasmids encoding GFP alone or GFP fused to either kazrin C or to a eps15 (EGFR pathway substrate clone 15) dominant negative mutant (eps15-EΔ95/295), known to inhibit CME (Benmerah, Bayrou et al. 1999). The next day, the cells were exposed to Tfn labelled with Texas Red (TR-Tfn) and allowed to internalize for 15 minutes at 37°C. In untransfected cells or cells expressing GFP, about 90 % of the cells accumulated TR-Tfn in the endosomal recycling compartments (ERC), which in Cos-7 cells is concentrated at the perinuclear region (Fig. 23A and B). In contrast, perinuclear accumulation of TR-Tfn was observed in only 20 % of the cells expressing either GFP-kazrin C or the GFP-eps15 mutant (Fig. 23 A and 4B). This observation indicated that the transient overexpression of kazrin C, either impaired the uptake of Tfn at the PM and/or altered its subsequent transport to the perinuclear region of the cells (Fig. 23 A and B).

To clarify the cause of this defect, the internalization of Biotin-labelled Tfn (B-Tfn) was analysed biochemically in cells transiently overexpressing GFP, GFP-kazrin C or GFP-eps15-EΔ95/295. B-Tfn was allowed to bind to the cell surface at 0°C and then the cells were enabled to internalize B-Tfn by shifting to 37°C for 2, 4, 8 or 12 minutes. To measure internalized B-Tfn, cells were washed with an acidic buffer to stripsurface-bound B-Tfn. Cells only washed with PBS were used to measure all cell-associated B-Tfn (surface-bound and internalized). In GFP-kazrin C and GFP-eps15-EΔ95/295 overexpressing cells, the uptake of B-Tfn was strongly reduced compared to the cells expressing GFP alone (Fig. 23C and D). This experiment demonstrated that the endocytic uptake of Tfn was strongly impaired by high cellular levels of kazrin C.

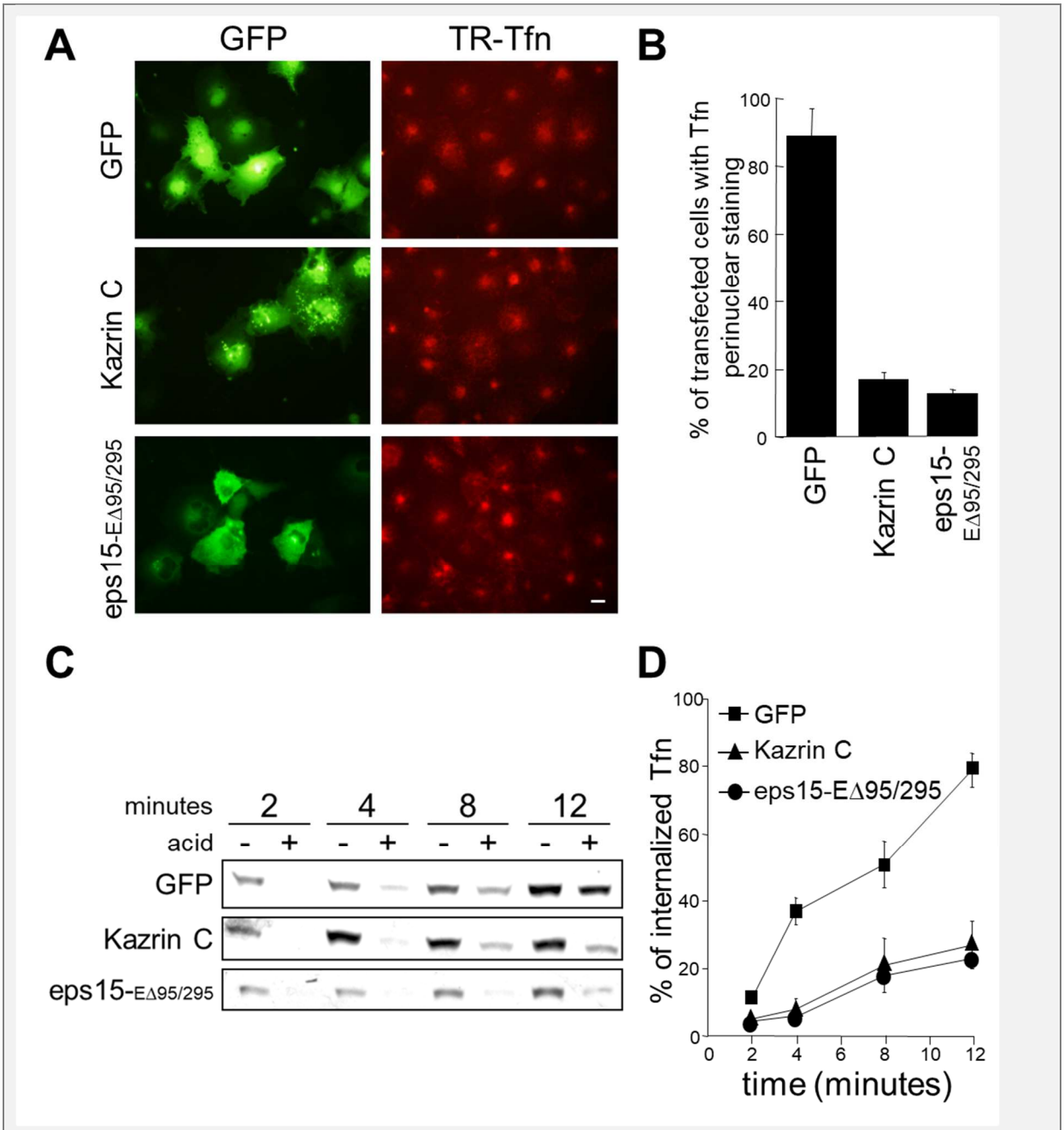

Figure 23. Overexpression of Kazrin C Inhibits CME of Tfn.

A. Fluorescence micrographs of Cos-7 cells transfected with plasmids encoding GFP (C) or GFP fused to kazrin C or eps15-EΔ95/295. Cells were exposed to Texas Red-transferrin (TR-Tfn) for 15 minutes before fixation. Scale bar = 10 µm. **B.** Graphs presenting the percentage of Cos-7 cells expressing GFP (C), GFP fused to kazrin C or eps15-EΔ95/295 showing perinuclear accumulation of TR-Tfn of cells described in A. The data indicate the average +/- SEM of 3 independent experiments (n = 50). **C.** Streptavidin-peroxidase decorated Western blots of protein extracts from Cos-7 cells transfected with GFP (C) or GFP fused to kazrin C or eps15-EΔ95/295, incubated with Biotin-conjugated Tfn for the indicated times, and either washed with PBS (-, total B-Tfn) or an acidic buffer (+, internalized B-Tfn). Same amount of protein for each sample were separated by SDS-PAGE and transferred by Western blot. Membranes were incubated with Streptavidin-Peroxidase and developed with a chemiluminescence detection kit. **D.** Graphs indicating the average ± SEM percentage of internalized B-Tfn, normalized to total B-Tfn as a function of the incubation time for Cos-7 cells under the experimental conditions described in C. The data indicates the average of 3 independent experiments.

2.3 Kazrin Interacts with the Clathrin-associated Machinery from Rat Brain Extracts

To deepen into the molecular mechanism behind the inhibition of endocytic uptake by kazrin C overexpression, the putative interaction of kazrin C with components of the machinery involved in CME was studied.

For this purpose, pull-down experiments from rat brain non-denaturing protein extracts were performed using glutathione-Sepharose beads coated with recombinant purified GST-kazrin C or GST as control. The co-precipitation of proteins implicated in CME was tested via immunoblot using a set of antibodies from a Coated Vesicle Sampler kit (BD Transduction Laboratories). A specific interaction of GST-kazrin C could be demonstrated with the CHC and with the β-adaptin subunits of the clathrin adaptor complexes of the AP-family, but not, for instance, with the BAR domain protein amphiphysin (Fig. 24A), among others.

To confirm that an interaction of kazrin C with clathrin and β-adaptins also occurred with the endogenous kazrin isoforms from brain, immunoprecipitations from rat brain extracts were performed. Polyclonal antibodies against the N- (aa 1 to 147) or C-terminus (aa 148 to 327) of kazrin C fused to GST were raised in rabbit. Specificity of the antibodies was validated by immunoblots with extracts from Cos-7 cells transfected with either the full length kazrin C, the N-terminal or the C-terminal portion fused to GFP. As expected, the serum against the N-terminus specifically recognized the full length kazrin C and the N-terminus, whereas the serum against the C-terminus recognized the full length kazrin C and the C-terminus (Fig. 24B). To test the detection of endogenous kazrin by the sera, rat brain extracts were Western blotted and immuno-probed. Both antibodies detected several putative splice variants of kazrin expressed in brain, although the antibody against the N-terminus seemed to be more sensitive. Four main bands could be detected by both sera, possibly corresponding to some of the isoforms shown in figure 22B (Fig. 24C).

Immunoprecipitation from rat brain non-denaturing protein extracts using sera against the N- or the C-terminus of kazrin C bound to Protein A-agarose, confirmed the specific interaction of β-adaptins and clathrin with endogenous kazrin, as compared to the immunoprecipitations with pre-immune serum (Fig. 24D). However, the signal from the immuno-precipitation with the antibody against the N-terminus was weaker as compared with the antibody against the C-terminus of kazrin C. Actually; clathrin could only be precipitated with the sera against the C-terminal portion of kazrin C. This was despite the fact that the antibody against the N-terminus detects kazrin isoforms from denatured brain extracts better. This might indicate a difference in the exposure of the N- and the C-terminal segment of endogenous, non-denatured kazrin (Fig. 24D).

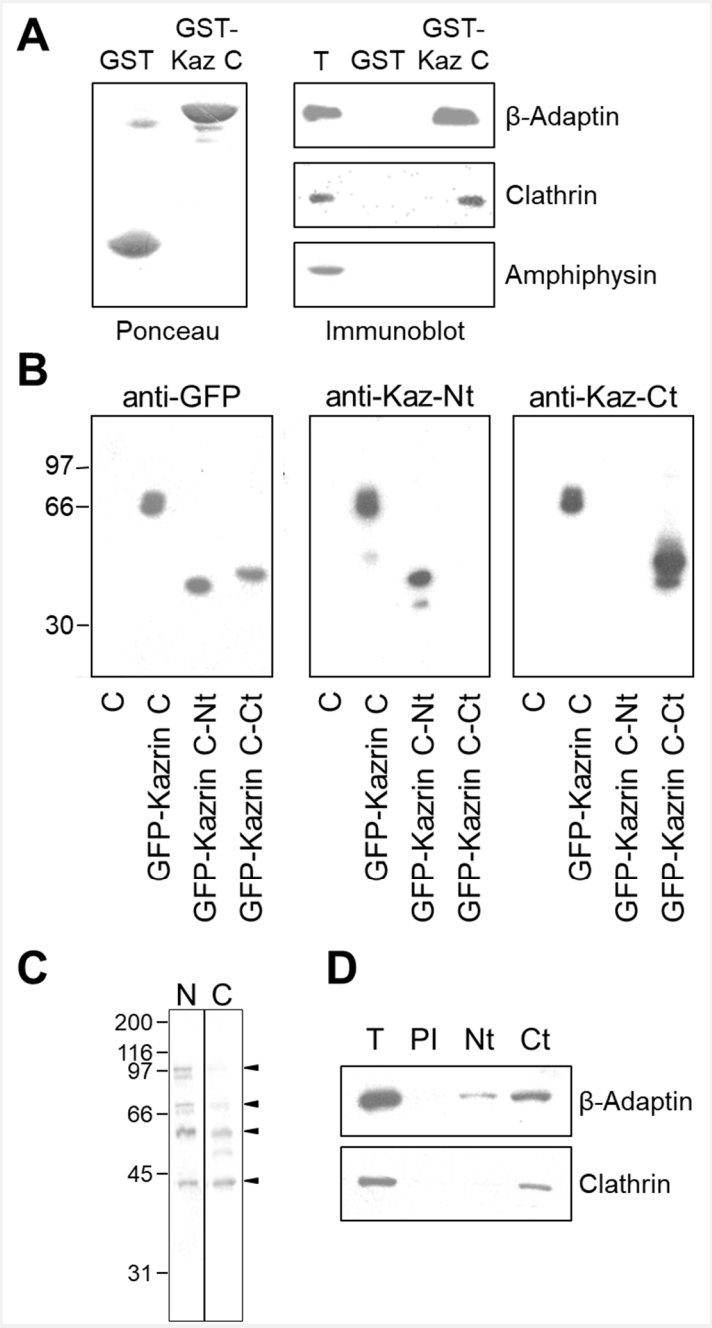

Figure 24. Kazrin C Interacts with the Clathrin Machinery from Rat Brain Extracts.

A. Immunoblot of glutathion-Sepharose pull downs from rat brain extracts. Beads coated with 10 µg of GST or GST fused to kazrin C (Kaz C) expressed and purified from *E. coli* were incubated with a rat brain protein extract. Proteins co-precipitating with the beads were analyzed by immunoblot using antibodies against the indicated proteins. 2 µg of the extract were loaded to monitor the input (T). Ponceau S was used to monitor the amount of loaded GST and GST-kazrin C. **B.** Immunoblot of Cos-7 cells either untransfected or transfected with GFP fused to the full length kazrin C, the N- or C-terminal domains of kazrin C. Membranes were decorated either with and antibody against GFP (Invitrogen A11122) or the polyclonal sera raised in rabbit against the N (aa 1 to 147) or the C-terminal domain (aa 148 to 327) of kazrin C. 10 µg of total protein were loaded per lane. **C.** Immunoblots of rat brain lysates decorated with sera raised against the N- or the C-terminus of kazrin C. 10 µg of total protein were loaded per lane. **D.** Immunoblot of proteins co-precipitating from rat brain lysates with agarose beads coated with preimmune sera (PI) or sera rose against the N- (αN) or the C-terminus (αC) of kazrin C. Nitrocellulose membranes were decorated with antibodies against the indicated proteins. 2 µg of the extract were loaded to monitor the input (T).

2.4 Depletion of Kazrin Accelerates CME and Recycling of Tfn but Impairs Arrival of Internalized Tfn to the Perinuclear ERC

The next step to gain more understanding about the cellular function of kazrin was to deplete the endogenous protein and to examine the effect of the loss of kazrin on endocytic uptake and recycling. For this purpose, Cos-7 cells were transfected with either a control small interfering RNA (siRNA; Ambion 4644) or a siRNA targeting kazrin (GGAGAUGUUGCGCAAGGACtt, Ambion *Silencer* Pre-designed siRNA, target gene KIAA1026) and the specific depletion of kazrin isoforms expressed in Cos-7 cells was tested by immunoblot of denatured protein extracts using the affinity purified serum against the N-terminus of kazrin C. A significant reduction of two protein bands recognized by the anti-kazrin sera, running slightly above or under the 45 kDa marker, was observed in cells transfected with the siRNA targeting kazrin, as compared to cells treated with the control siRNA. According to the molecular weights, the kazrin isoforms expressed in Cos-7 cells might correspond to the isoforms C, A and/or D (Fig. 25A).

We next inspected the effect of partially depleting kazrin on the capacity of Cos-7 cells to internalize TR-Tfn. For that purpose, cells transfected with either the control siRNA or the siRNA against kazrin were incubated at 37^{o}C in the presence of fluorescent-labelled Tfn for 15 minutes. Cells were fixed, immuno-stained for the ERC marker rab11 and analysed with the fluorescence microscope. Similar to the overexpression of kazrin C (see Fig. 23A), loss of endogenous kazrin prevented perinuclear accumulation of TR-Tfn in about half of the treated cells, even though the rab11 recycling compartment appeared intact (Fig. 25B and C). Surprisingly though, in contrast to the overexpression of kazrin C, depletion of endogenous kazrin did not prevent efficient uptake of B-Tfn when biochemically analysed (Fig. 25D and E, as compared with figures 23C and D). Indeed, B-Tfn uptake seemed faster in cells transfected with the siRNA against kazrin, as compared with those exposed to the control siRNA (see 8 minutes time point).

In order to find an explanation for this somehow contradictory observation, a recycling assay was performed. Kazrin depleted and control cells were exposed to B-Tfn at 16°C as to allow internalisation but prevent further intracellular trafficking. Upon stripping of surface-bound B-Tfn with an acidic buffer, and shift of the cells to 37°C, endosomal transport and recycling was monitored by following the B-Tfn fraction reaching back to the PM. Western blot analysis of protein extracts probed with Peroxidase-conjugated Streptavidin after acid-stripping of surface exposed B-Tfn at different time points, demonstrated a faster endocytic recycling rate in cells depleted of the endogenous kazrin, as compared to the control cells (Fig. 25F and G). Thus, most of the internalized B-Tfn was already lost 5 minutes after shift to 37^{o}C in cells treated with siRNA against kazrin, whereas control cells still retained more than 50 % of the internalized B-Tfn (Fig. 25F and G). Fluorescence microscopy analysis of the same protocol using TR-Tfn rendered similar results (Fig. 25H). Images taken 5 minutes after the shift to 37^{o}C showed that in kazrin-depleted cells TR-Tfn did not reach the perinuclear region that corresponds to the rab11 positive ERC, but rather returned to the PM, where it could be acid-stripped (Fig. 25H). Together, these results indicated that direct recycling of Tfn from EE, probably via the rab4 short-loop recycling circuit, was accelerated upon loss of kazrin, whereas transfer to the perinuclear ERC was impaired.

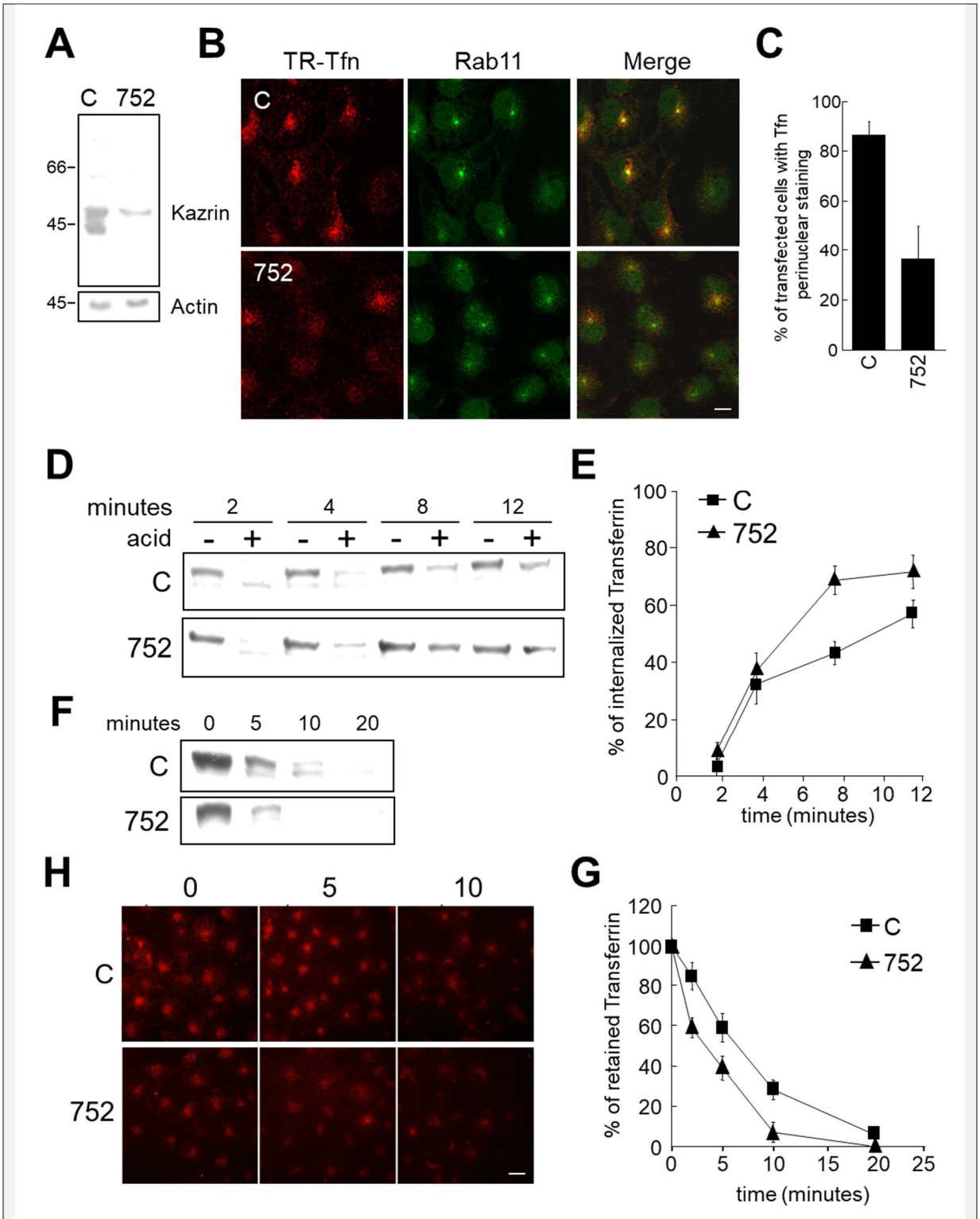

Figure 25. Depletion of Kazrin Accelerates Uptake and Recycling of Tfn but Prevents Perinuclear Accumulation.

A. Immunoblot of cell lysates from Cos-7 cells transfected with a siRNA against kazrin (752, Ambion Silencer) or a control siRNA (C, Ambion Silencer). Protein extracts from Cos-7 cells were separated by SDS-PAGE and Western blotted to nitrocellulose membranes. Membranes were decorated with an affinity-purified rabbit polyclonal sera against the N-terminus of kazrin C (aa 1-147) or a monoclonal antibody against actin (Roche 1378996) and the appropriate peroxidase-conjugated secondary antibodies. **B.** Fluorescence micrographs of Cos-7 cells transfected with a siRNA against kazrin (752, Ambion Silencer) or a control siRNA (C, Ambion Silencer), incubated for 15 minutes in the presence of TR-Tfn, fixed and stained with a mouse monoclonal antibody against rab11 (BD Transduction Laboratories 610656) and an adequate fluorescently labeled secondary antibody. Scale bar = 10 µm. **C.** Graphs indicating the average ± SEM percentage of Cos-7 cells

transfected either with the control siRNA (C, Ambion Silencer) or siRNA against kazrin (752, Ambion Silencer) showing perinuclear accumulation of TR-Tfn under the conditions described in C. The data indicates the average of 3 independent experiments (n = 50). **D.** Immunoblots of protein extracts from Cos-7 cells transfected with a control siRNA (C, Ambion Silencer) or a siRNA against kazrin (752, Ambion Silencer), incubated with B-Tfn for the indicated times and either washed with PBS (-, total B-Tfn) or an acidic buffer (+, internalized B-Tfn). Same amount of protein for each sample were separated by SDS-PAGE and transferred to nitrocellulose membranes. Membranes were incubated with Streptavidin-Peroxidase and developed with a chemiluminiscence detection kit. **E.** Graphs indicating the average ± SEM percentage of internalized B-Tfn normalized to the total B-Tfn as a function of the incubation time, under the experimental conditions described in E. The data indicates the average of 3 independent experiments. **F.** Immunoblots of protein extracts from Cos-7 cells transfected with a control siRNA (C, Ambion Silencer) or a siRNA against kazrin (752, Ambion Silencer), incubated with B-Tfn at 16ºC to allow internalization but not recycling. After shift to 37ºC, cells were incubated with excess of unlabeled Tfn for the indicated times and surface exposed B-Tfn recycled to the PM was stripped with an acidic buffer. The same amount of protein for each sample were separated by SDS-PAGE and transferred to nitrocellulose membranes. Membranes were incubated with Streptavidin-Peroxidase and developed with a chemiluminiscence detection kit. **G.** Graphs indicating the average ± SEM percentage of internal B-Tfn at the indicated time points, normalized to the internal B-Tfn at time 0, under the experimental conditions described in E. The data indicates the average of 3 independent experiments. **H.** Fluorescence micrographs of Cos-7 cells transfected with a siRNA against kazrin (752, Ambion Silencer) or a control siRNA (C, Ambion Silencer), incubated for 1 hour with TR-Tfn at 16ºC to allow internalization but not recycling, acid stripped of surface TR-Tfn and chased at 37ºC with excess of unlabeled Tfn for the indicated times. At the indicated time points, surface exposed TR-Tfn recycled to the PM was stripped with an acidic buffer, cells were fixed and visualized under the confocal fluorescence microscope. Scale bar = 10 µm.

2.5 Kazrin might Localize to SE together with Rab4, γ-Adaptin and EHD3

For a more detailed definition of the subcellular localization and function of the endogenous kazrin, Cos-7 cells were stained with the affinity purified antibody targeting the N-terminus of kazrin C. To test the specificity of our antibody in immunofluorescence staining, cells depleted of kazrin using siRNA or control cells were immunodecorated with the affinity purified anti-kazrin antibody and a fluorescently conjugated antibody against rabbit IgGs. In kazrin depleted cells, a clear reduction of the detected signal could be seen. However, several bright dots persistently remained in the cytoplasm of Cos-7 cells (Fig. 26A), which therefore could not be unequivocally ascribed to the endogenous kazrin. Since depletion of kazrin seemed to affect the endosomal trafficking of Tfn, we loaded Cos-7 cells with TR-Tfn for 15 minutes to investigate if a fraction of the endogenous kazrin might co-localize. Consistent with this hypothesis, a significant co-localization of the antibody recognizing kazrin was observed with internalized TR-Tfn, mostly at peripheral Tfn puncta (Fig. 26B), suggesting that endogenous kazrin might be at least partially localized to early SE.

To better define the nature of the endosomal compartments labeled with the antibody recognizing kazrin, its localization was inspected together with different endosomal markers. The small GTPases rab4 and rab5 were employed as well-established markers for SE and rab11 for the ERC. Kazrin was found to accumulate on enlarged structures formed by rab4 overexpression, but it did not seem to be recruited to rab5 subdomains and only scarcely to rab11 labeled structures (Fig. 26C), further indicating a possible localization of endogenous kazrin on EE.

Since AP-1 and clathrin have been involved in endosomal trafficking, and kazrin seemed to interact with clathrin and the AP adaptors from brain extracts, we analyzed the co-localization of kazrin with the AP-1 γ-adaptin subunit on endosomal compartments loaded with fluorescent Tfn. Interestingly, the antibody decorating endogenous kazrin co-localized with Tfn and γ-adaptin on peripheral structures but not in the perinuclear region where the Golgi apparatus and the ERC accumulate. (Fig. 27A). When overexpressing the endosomal proteins EHD1 and EHD3, kazrin displayed only a slight overlap with the recycling endosome-associated EHD1. In contrast, a significant localisation of kazrin at the base of EHD3 emanating tubules was found (Fig. 27B). EHD1 has been involved in the generation or fission of tubules trafficking from the ERC to the PM, whereas EHD3 is rather associated with a trafficking step between the sorting and recycling endosomes. Altogether, the phenotypes installed upon partial depletion of kazrin using siRNA and the tentative localization of endogenous kazrin using the affinity purified anti-kazrin antibody, seemed to point to a role of this protein regulating the rab4/rab11 recycling fork at SE, possibly by favouring traffic from sorting to ERC and/or inhibiting the short-loop rab4-asssociated pathway.

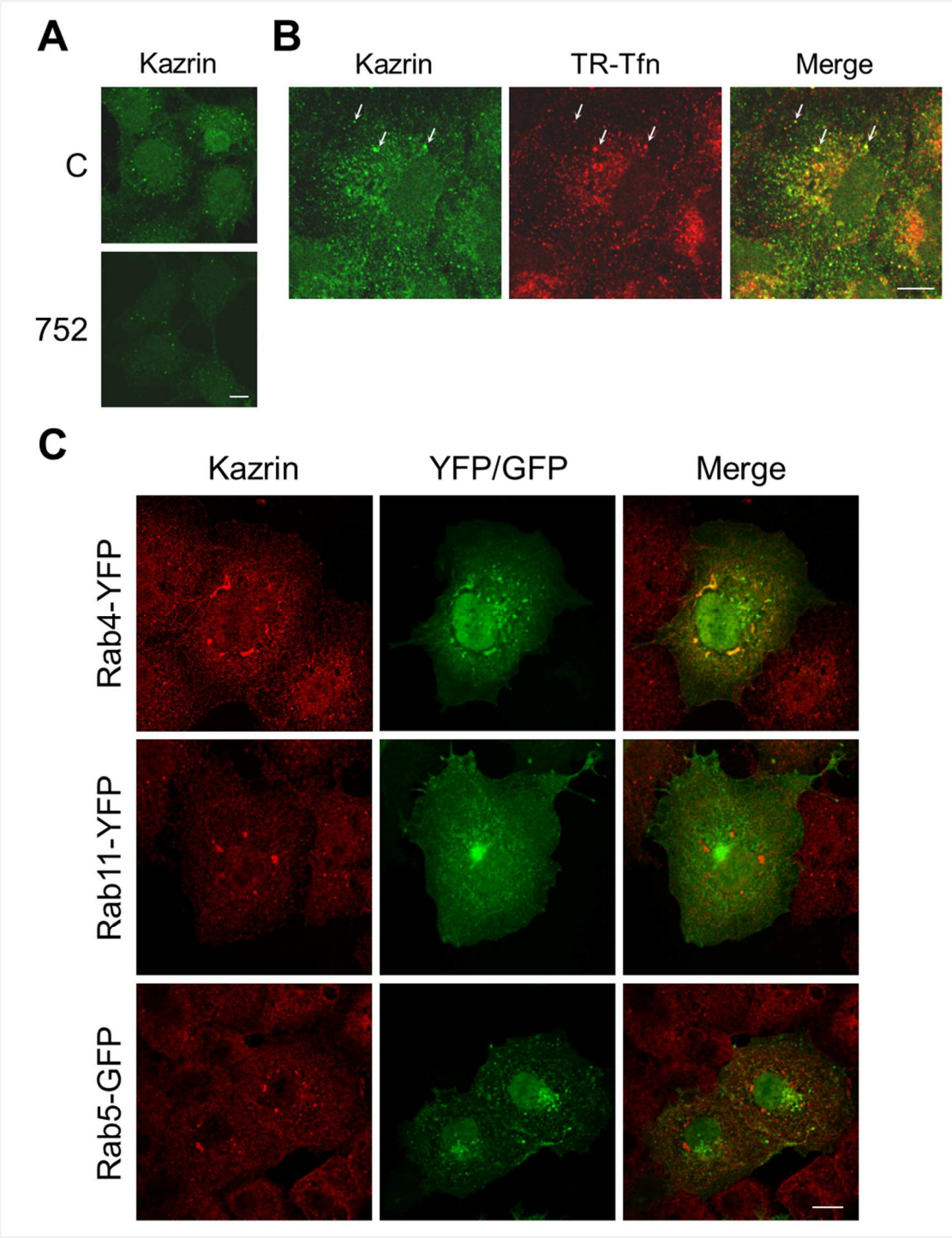

Figure 26. Endogenous Kazrin Might Localize to Sorting Endosomes.

A. Fluorescence micrographs of Cos-7 transfected with a control siRNA (C, Ambion Silencer) or a siRNA against kazrin (752, Ambion Silencer), fixed and stained with an affinity purified rabbit polyclonal antibody against the N-terminus of kazrin C (aa 1-147) and the adequate conjugated secondary antibody. Scale bars = 10 µm. **B.** Fluorescence micrographs of Cos-7 cells incubated with TR-Tfn for 15 min, fixed and stained with an affinity purified rabbit polyclonal antibody against the N-terminus of kazrin C (aa 1-147) and the adequate conjugated secondary antibody. Scale bar = 10 µm. **C.** Fluorescence micrographs of Cos-7 cells transfected with the indicated rab proteins either fused to YFP or GFP. Cells were fixed and decorated with an affinity-purified rabbit polyclonal antibody against the N-terminus of kazrin C (aa 1-147) and the adequate secondary antibody. Scale bar = 10 µm.

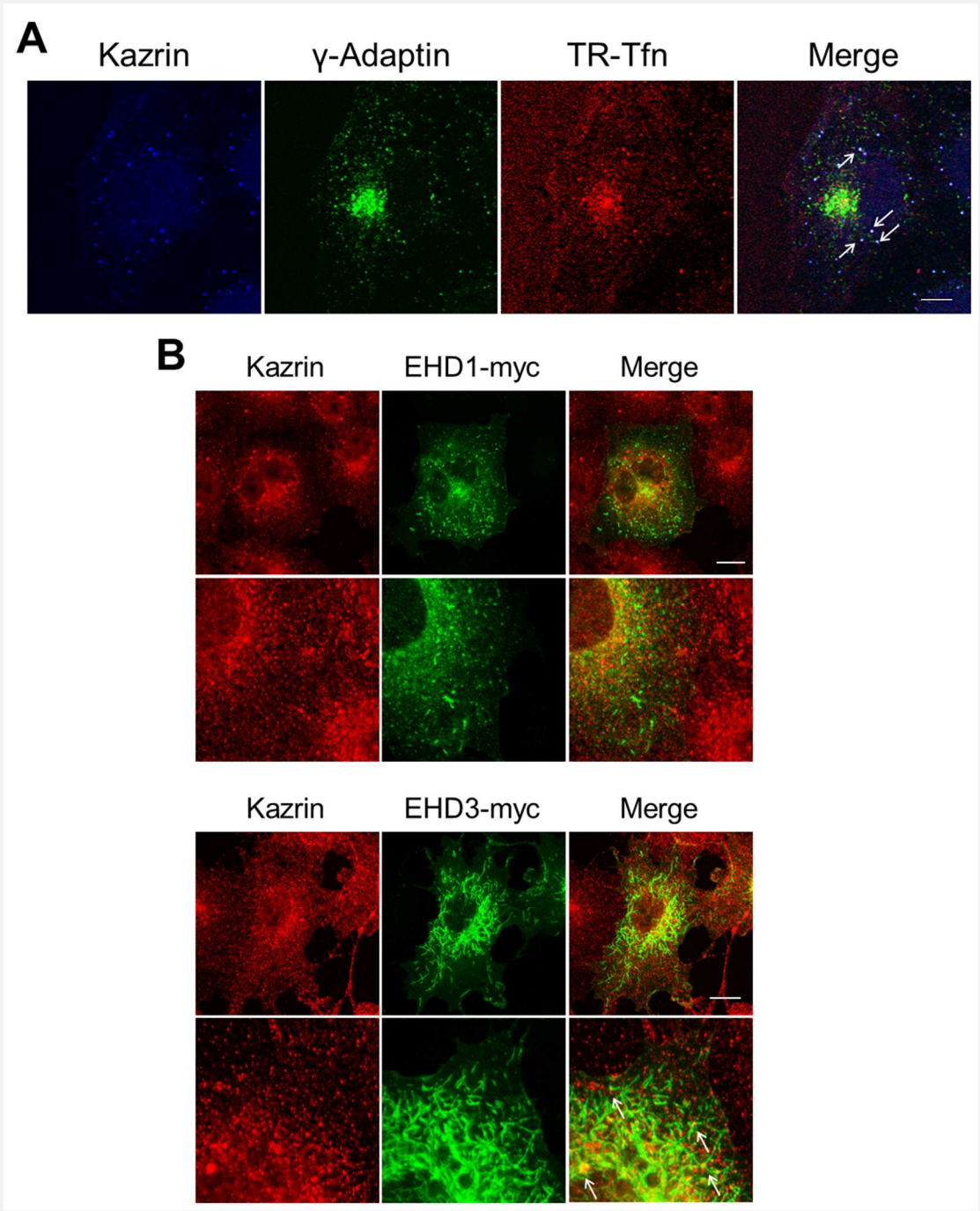

Figure 27. Endogenous Kazrin Might Co-localize with γ-Adaptin and EHD3 on Early Endosomes.
A. Fluorescence micrographs of Cos-7 cells incubated with TR-Tfn for 15 minutes, fixed and stained with an affinity purified rabbit polyclonal antibody against the N-terminus of kazrin C (aa 1-147), a mouse monoclonal antibody against the AP-1 γ-adaptin (BD Transduction Laboratories 610385) and the appropiate conjugated secondary antibodies. Arrows indicate cellular spots where the 3 signals co-localize. Scale bar = 10 µm. **B.** Fluorescence micrographs of Cos-7 cells transfected with plasmids encoding EHD1-myc and EHD3-myc, fixed one day upon transfection and stained with an affinity purified rabbit polyclonal antibody against the N-terminus of kazrin C (aa 1-147), a mouse monoclonal antibody against the MYC epitope and the appropiate conjugated secondary antibodies. Upper pannels show fluorescence micrographs of entire cells. Lower pannels show magnified fluorescence confocal micrographs of other cells. The arrows indicate cellular structures decorated with the anti-kazrin antibody from where EHD3 tubules emanate. Scale bar = 10 µm.

Objectives

3 Objectives

In light of the preliminary results described in the previous chapter, the objectives of this thesis were:

1. To confirm that kazrin is recruited to endosomes and that its depletion prevents perinuclear accumulation of Tfn but not its cellular uptake.

2. To investigate if the interaction between kazrin and clathrin is direct and define if kazrin interacts with a specific set of clathrin adaptors, in particular with AP-1.

3. To study the possible physical and functional interaction of kazrin with the Arp2/3 complex and with the NPFs that play roles in the endocytic pathway.

4. To analyse the effects of the overexpression and depletion of kazrin on the actin cytoskeleton with a particular focus on the endosomal actin.

Results

4 Results

4.1 Depletion of Kazrin Prevents Perinuclear Accumulation of Tfn but Increases Uptake

In order to discard off-target effects in the experiments showing that depletion of endogenous kazrin by siRNA technology in Cos-7 cells accelerates endocytic Tfn uptake, while it prevents endocytic transport to the perinuclear recycling endosomes (see Fig. 25), we decided to use another methodology for kazrin depletion, namely a stable transformation with an unrelated shRNA targeting this protein. We expected that this methodology will improve reproducibility, simplify the work flow and reduce costs in the long run, as compared with the siRNA technology. For this purpose, cell lines stably expressing anti-kazrin shRNA were generated via lentiviral transduction of plasmids carrying the shRNA against kazrin (pKLO.1_shKaz, see table I.) or a control shRNA (pLKO.1_CV/_SCR, see table I.), and a gene for puromycin resistance. Following transfection, cells were selected in media containing puromycin to isolate those bearing genomic integration of the shRNA constructs, and the levels of expression of endogenous kazrin in cells transfected with shKaz was compared with that of intact Cos-7 cells or cells transfected with shSCR by immunoblot using the antibody raised against the C-terminal portion of kazrin C (Fig. 28A).

To investigate if depletion of kazrin using the shRNA technology also impacts on the endocytic uptake and traffic of Tfn, intact Cos-7 cells or cells stably transfected with shSCR or shKaz were exposed to Tfn-Alexa647 for 2 hours and examined under the fluorescence microscope upon fixation. As observed previously for the depletion of kazrin using siRNA, loss of endogenous kazrin via shRNA also seemed to impair arrival of Tfn to the perinuclear region. Thus, the fraction of peripheral Tfn-labelled structures, as compared to the perinuclear staining, was much higher in cells expressing shKaz, as compared with those expressing shSCR or intact Cos-7 cells (Fig. 28B and D). Also, as previously observed for the siRNA kazrin depleted cells, the Tfn uptake was not compromised. Instead, it seemed rather exacerbated, since the overall Tfn-Al647 signal per cell was significantly higher as compared to cells expressing shSCR or intact cells (Fig. 28B and D). The number of Tfn-labelled structures per cell area was4- to 6-fold higher in shKaz Cos-7 cells as compared tointact Cos-7 cells or cells expressing shSCR, and the endosomal structures were bigger (average endosomal size of 0.34 μm^2 in shKaz cells, versus 0.12 μm^2 in intact cells) (Fig. 28B, C and D). Nevertheless, the effect on the endosomal size of the shKaz construct might be caused by off-target effects to a certain degree, since Cos-7 cells expressing shSCR also showed rather enlarged endosomal structures (average endosomal size of 0.24 μm^2 in shSCR cells, versus 0.12 μm^2 in intact cells) albeit still smaller as compared to the cells expressing shKaz (Fig. 28C and D).

In summary, in accordance to the data showed in preliminary results, depletion of endogenous kazrin in Cos-7 cells, seemed to prevent perinuclear accumulation of endosomal cargo while increasing its endocytic uptake.

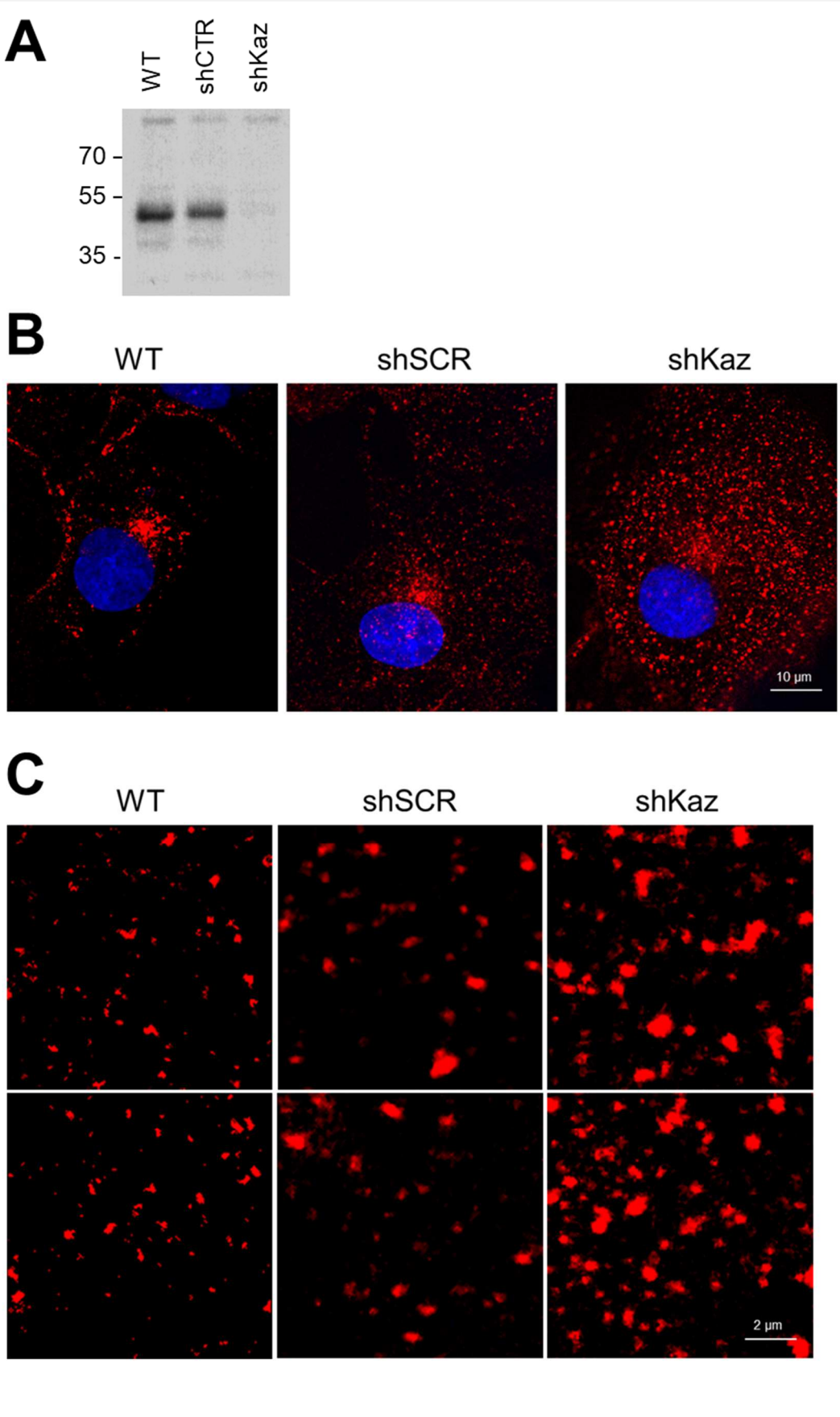
A
WT
shCTR
shKaz
70
55
35
B
WT
shSCR
shKaz
10 µm
C
WT
shSCR
shKaz
2 µm

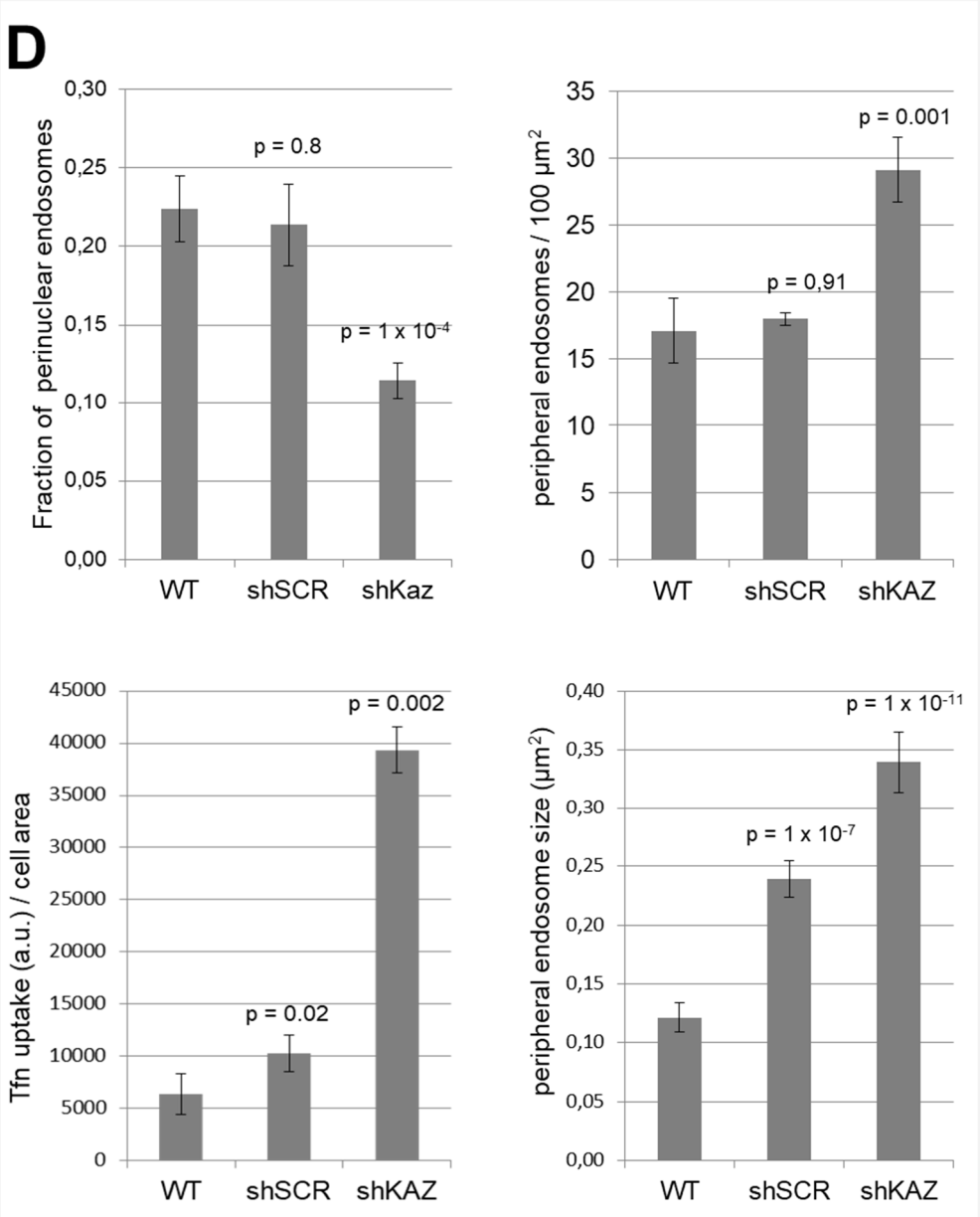

Figure 28. Depletion of Kazrin with shRNA Prevents Transferrin Accumulation at the Perinuclear Region but Increases Transferrin Uptake.

A. Immunoblot of protein extracts against kazrin (Abcam ab74114) from Cos-7 cells either wild type or stable cell lines expressing a non target control shRNA (shSCR) or a shRNA against kazrin (shKaz) confirming the depletion of kazrin in the Cos-7 shkazrin cell line. Proteins were extracted four days upon transduction and selection with puromycin. 18 µg of total protein extract was loaded per lane. **B & C.** Maximum intensity projections of confocal fluorescence micrographs (**B**), or a gallery of confocal micrographs of their peripheral endosomes (C), showing either wild type Cos-7 cells (WT), stable Cos-7 cell lines expressing a non target control shRNA (shSCR) or a shRNA against kazrin (shKaz). Cells were exposed to Tfn-Alexa647 for 2 hours before fixation. Images were acquired using a Leica TCS-SP5 microscope with a 63x/1.4NA objective and the emission filter LP590 for detection of Alexa-647 (far red). **D.** Graphs representing the average +/- SEM of the size of peripheral Tfn loaded endosomes, the Tfn signal normalized to the cellular area, the percentage of perinuclear Tfn loaded endosomes as compared to the total Tfn-loaded endosomes and the density of peripheral endosomes per cellular surface area of cells described in A and B. Images were analysed as described in 6.5.5 Image analysis. The Student´s T-test p value was used to assess the statistical significance.

4.2 Kazrin Co-fractionates with Endosomes

The results described in chapter 2.5 of the preliminary results indicated recruitment of endogenous kazrin to endosomal structures labelled with Tfn in Cos-7 cells. These results were based on immunofluorescence staining of Cos-7 cells using an antibody against kazrin. Co-localization seemed to mostly occur in peripheral structures rather in the perinuclear region, suggesting a role of kazrin on SEs (Fig. 26B). Further, a co-localization with the endosomal AP-1 complex at Tfn positive peripheral structures enforced the view that kazrin might be recruited to endosomes (Fig. 27A). However, since depletion of kazrin with siRNA did not completely eliminate the immunofluorescence signal and the co-localization with Tfn was only partial, we could not rule out that proteins other than kazrins, labelled by our antibody were the ones recruited on endosomal structures. To gain more evidence supporting the view that endogenous kazrin was recruited to endosomes, we further investigated the localization of kazrin by subcellular fractionation and immunoblot. For that purpose, cellular membranes were separated from the cytosol by ultracentrifugation at 100,000 g, and the membranes were gently resuspended and laid on a 10 to 30 % OptiPrep step density gradient. Upon ultracentrifugation, subcellular fractions were recovered and analysed by immunoblot using the antibodiy against kazrin or specific markers of the PM, the Golgi and the endosomal compartments (Fig. 29). To define bands corresponding to the endogenous kazrin isoforms, the previously described sera against the N- and the C-terminal portion of kazrin C (Fig. 28A) were used to compare the immunoblot signals of untransfected Cos-7 cells and cells expressing the shKaz. As described in figure 28A, the N- and C-terminal sera both mostly recognized a band of about 50 kDa, which partially disappeared in cells expressing shKaz (Fig. 29). The N-terminal serum detected better this band and therefore was used for the analysis of the gradient. A kazrin signal could be detected in the lighter fractions, co-localizing with the rab5 and PtdIns(3)P-binding protein EEA1, a tethering factor often used as a marker for SEs. Hrs, one of the two ESCRT-0 subunits that also recognizes PtdIns(3)P and is the gatekeeper of the entrance of ubiquitinated proteins to the degradative pathway at the SE, consistently fractionated with EEA1 (most in 12.5% and 15 %) (Raiborg, Bache et al. 2001) and kazrin, further supporting the view that kazrin is at least in part recruited to SEs. γ-Adaptin, a component of the Golgi and early endosomal AP-1 complex, accumulated in slightly denser fractions (Fig. 28). Nevertheless, a considerable overlap between the γ-adaptin and the signals for kazrin and the SE markers could still be detected (Fig. 29). Instead, α-adaptin, a component of the the PM-associated clathrin adaptor AP-2 , was found in heavier fractions, and showed little overlap with the kazrin signal and none with the SE markers Hrs and EEA1 (Fig. 28). The rab11-binding protein EHD1 often used as a marker of ERC was mostly found in the heaviest fractions overlapping with a very significant portion of a distinct pool of kazrin (Fig. 29). Interestingly though, the distribution of the EHD1 and kazrin signals in the heaviest fractions was strikingly different, with the EHD1 signal spreading towards the lighter fractions while kazrin concentrated only in the heaviest. This differential pattern could indicate that kazrin and EDH1 did not really co-localize to the same compartment but rather on distinct dense cellular membranes that could not be resolved with this particular methodology. Nevertheless, a small fraction of EHD1 could be detected co-localizing with γ-adaptin and kazrin in the lighter fractions.

Altogether, the subcellular fractionation data was consistent with our preliminary results shown in Fig. 26 and Fig. 27, suggesting that at least a portion of the endogenous kazrin is recruited to sorting and maybe also recycling endosomes.

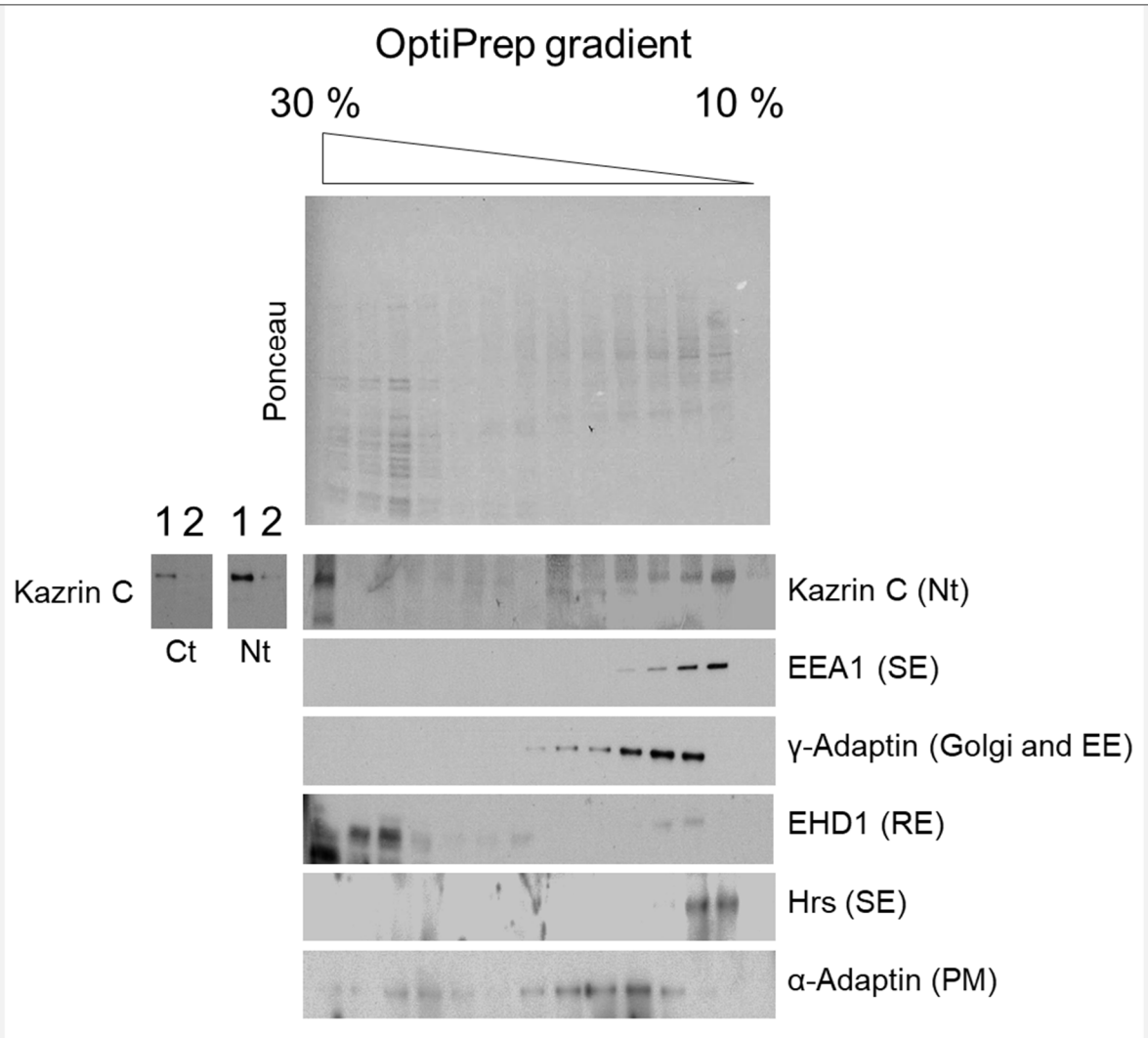

Figure 29. A Fraction of Kazrin C Co-fractionates with Sorting and Recycling Endosomes.

Ponceau S staining (upper panel) and immunoblots (lower panels) against the indicated proteins of Cos-7 cells membranes fractionated in a 10 to 30 % OptiPrep density gradient. (SE, sorting endosomes; EE, early endosomes; RE, recycling endosomes, usually called ERC; PM, Plasma membrane). The left panels correspond to immunoblots of protein extracts (5 µg) of either wild type Cos-7 cells (1) or a stable Cos-7 cell line expressing a shRNA against kazrin (2), probed with serums against the N-terminal (aa 1 to 176) or the C-terminal (aa 161 to 327) portions of kazrin C.

4.3 GFP-Kazrin C Forms Subdomains on Rab4 Endosomes

To gain deeper insight into the ability of kazrin C to localize to specific endosomal compartments, the fact that overexpression of rab4 causes formation of vacuolar endosomes in some cell types was exploited. One of these cell types is the human cell line HEK293, which can very efficiently be transfected. These cells were co-transfected with plasmids encoding YFP-rab4 and GFP-kazrin C and imaged *in vivo*. Many cells formed huge, presumably aberrant structures decorated with both, YFP-rab4 and GFP-kazrin C (Fig. 30A). Separate YFP-rab4-decorated endosomes could be observed to briefly dock for a few seconds on these huge structures before separation, similar to the kiss-and-run contacts occurring within LEs and lysosomes (Fig. 30A, arrow heads in magnification). The large rab4 endosomes were often completely decorated with kazrin C when both proteins were overexpressed. However, in the few cells expressing lower levels of these proteins, GFP-kazrin C subdomains could be observed on YFP-rab4-decorated vacuolar structures. YFP-rab4 also seemed to form engrossed structures on these vacuolar endosomes, presumably associated with the formation of tubular transport intermediates in transit to the PM. Interestingly, the GFP-kazrin C and YFP-rab4 engrossed subdomains often appeared adjacent but not overlapping, indicating that they might function in distinct, yet interconnected pathways (Fig. 30B and C).

Some vacuolar YFP-rab4 endosomes in cells co-transfected with GFP-kazrin C seemed to be bigger than in cells co-expressing only GFP, indicating a possible interference of the kazrin C overexpression with membrane traffic in or out of the EEs. However, the analysis of the luminal diameter of YFP-rab4 endosomes failed to show significant differences between cells expressing GFP-kazrin C, as compared to those only expressing GFP (Fig. 31).

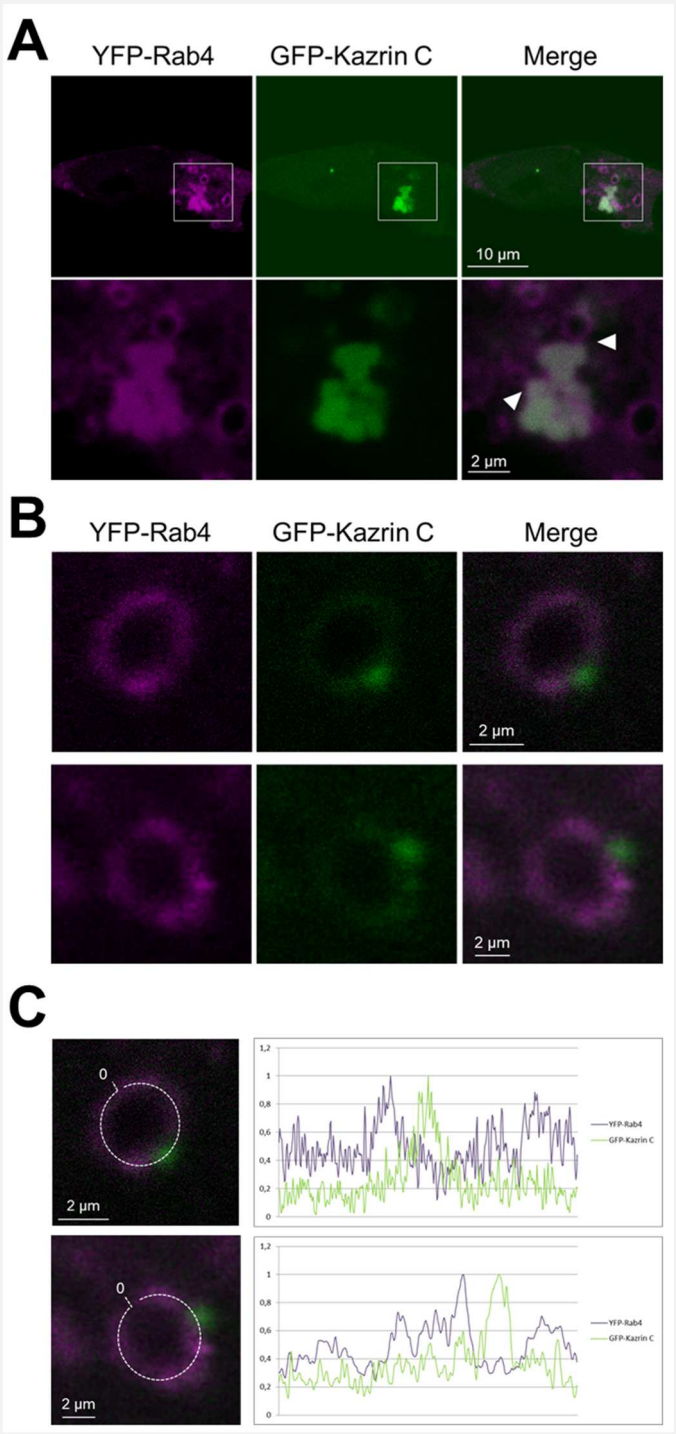

Figure 30. Kazrin Forms Subdomains on Rab4 Endosomes in HEK293 (EBNA) Cells.
A. Confocal fluorescence micrographs of a HEK293 (EBNA) cell overexpressing GFP-kazrin C and YPF-Rab4. The insets magnified in the lower panels show a presumably aberrant cellular structure decorated with GFP-kazrin C and YFP-rab4, where YFP-rab4 vacuolar endosomes (arrow heads) seem to kiss and run. **B.** Confocal fluorescence micrographs of selected vacuolar early endosomes from HEK293 (EBNA) cells expressing GFP-kazrin C and YFP-rab4, showing GFP-kazrin C labelled subdomains on vacuolar YFP-rab4 endosomes. Movies of the living cells for A and B were recorded one day upon transfection using a Leica TCS-SP5 microscope with a 63x/1.4NA objective, using the emission filter BP525/50 optimized for GFP for detection of the GFP signal, and using the emission filter LP515 for detection of YFP signal with the PMTs maximally closed to evoke bleed through. **C.** Plot profiles for the normalized intensity of the YFP-rab4 and GFP-kazrin C signals of the indicated segmented lines drawn on the surface of the endosomes shown in B. Data was acquired using FIJI ImageJ, transferred to an Excel file and normalized for the maximum intensity. «0» indicates where the profile starts (converging at the Y axes).

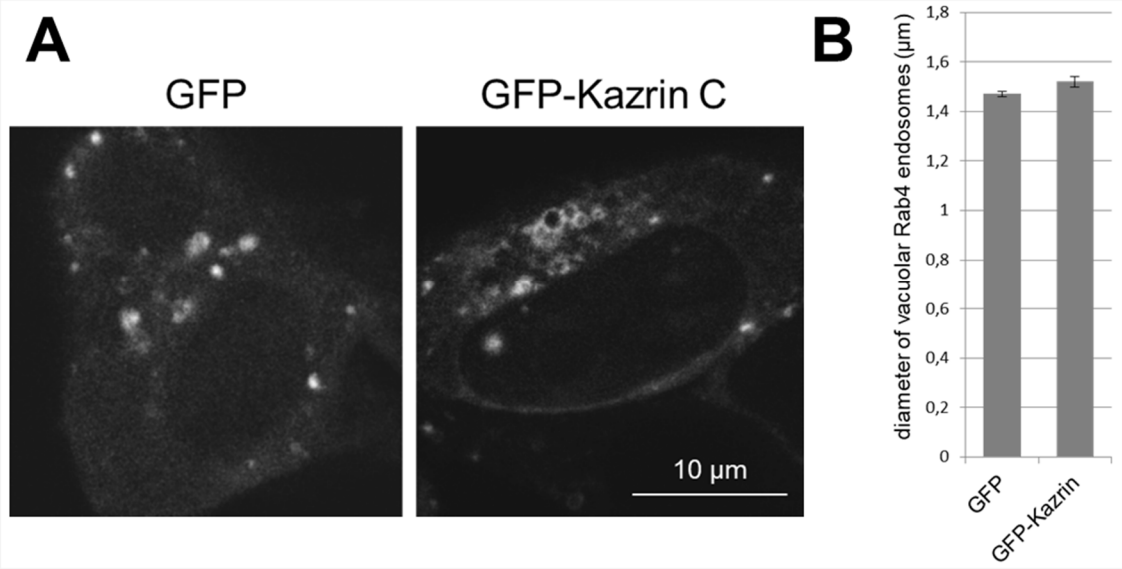

Figure 31. Overexpression of Kazrin C Does Not Significantly Affect the Diameter of the Rab4 Vacuolar Endosomes in HEK293 (EBNA) Cells.

A. Confocal fluorescence micrographs of HEK293 (EBNA) cells overexpressing YFP-rab4 and either GFP or GFP-kazrin C. Images of living cells were acquired one day upon transfection using a Leica TCS-SP5 microscope with a 63x/1.4NA objective, for detection of the GFP signal using the emission filter BP525/50 optimized for GFP, for detection of YFP signal using the emission filter LP515 with the PMTs maximal closed to evoke bleed through. **B.** Graph representing the average +/- SEM diameter of vacuolar YFP-rab4 endosomes in the cells described in A, more than 20 endosomes in at least 5 cells were analysed. The Student´s T-test p value was used to assess the statistical significance (p ~ 1).

4.4 Characterization of Kazrin Interactions with Endosomal Components

4.4.1 Rab4 does not Significantly Interact with Kazrin C

The preliminary results indicated that endogenous kazrin localizes on endosomal membranes that can be decorated with YFP-rab4, when the GTPase is overexpressed in Cos-7 cells (see Fig. 26). We also showed that, GFP-kazrin C formes subdomains on vacuolar YFP-rab4 vacuolar endosomes in HEK293 cells (see Fig. 30). The seen subdomains of kazrin C on vacuolar rab4 endosomes suggested a possible interaction between kazrin and rab4. To test this possibility a series of immunoprecipitations and pull down experiments were performed. Immunoprecipitation from native cell extracts of Cos-7 cells overexpressing GFP-kazrin C, or the C- or the N-terminal constructs (amino acids 1-176 and 161 to 327, respectively), could not co-precipitate significant amounts of endogenous rab4 (Fig. 32A). Further, glutathione-Sepharose pull down experiments with components purified from *E. coli* were performed and showed no significant interaction between GST-rab5, GST-rab11 or GST-rab4 and recombinant kazrin C in the presence of GDP (Fig. 32B). Loading of the GTPases with GTPγS to test if kazrin might be a specific rab4 effector, did not increase specific binding of kazrin to rab4, as compared with rab5 (Fig. 32C).

In summary, a specific interaction between kazrin C and rab4 could not be demonstrated under the experimental conditions used, suggesting that the partial co-localization observed by the fluorescence microscopy experiments might be the result of the overexpression of one or both proteins, and/or the result of an indirect interaction.

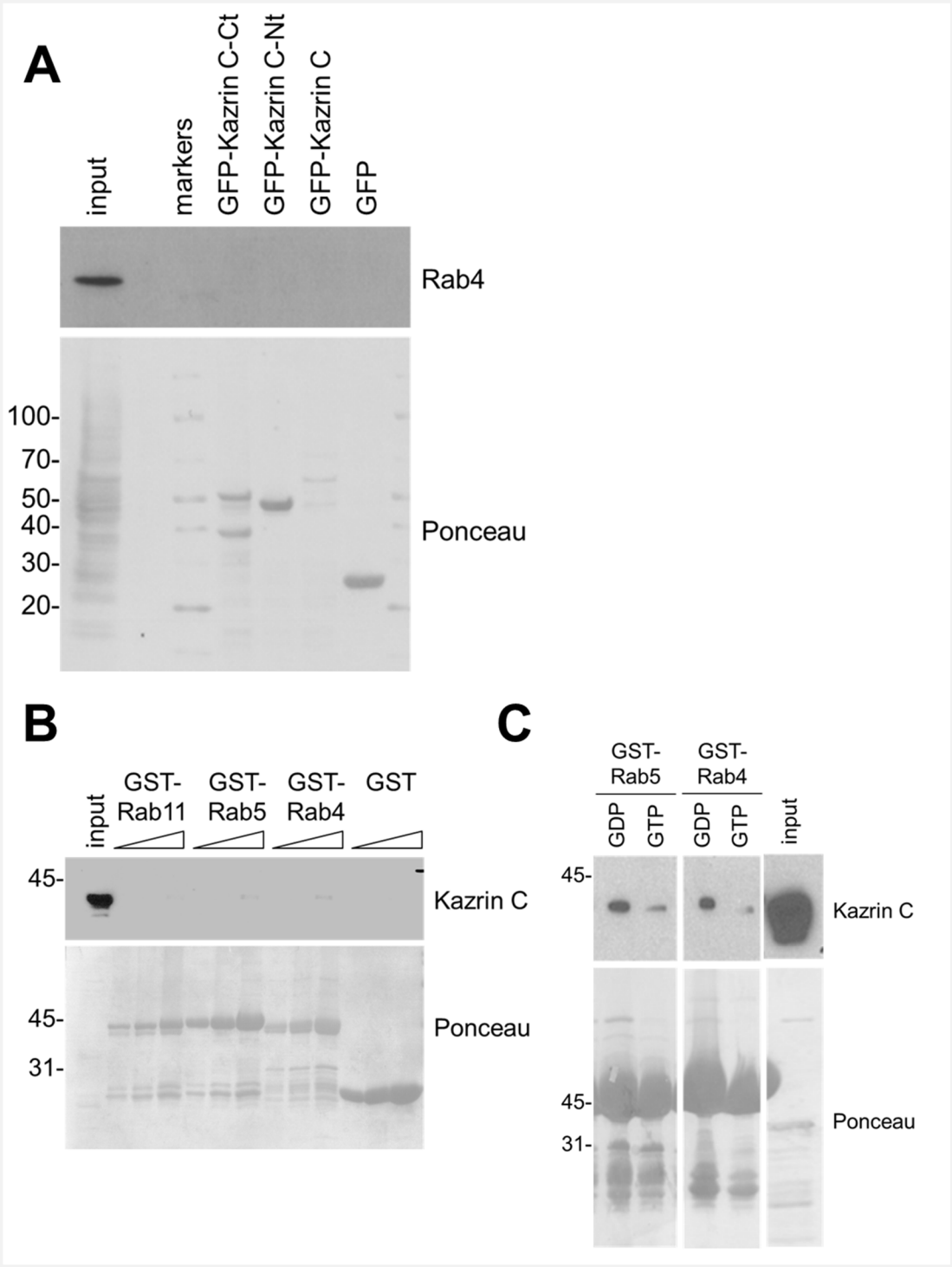

Figure 32. Kazrin C Does Not Specifically Interact with Rab4 Under the Experimental Conditions Used.

A. Ponceau S staining (lower panel) or immunoblot (upper panel) against rab4 (BD610888) of GFP-Trap (Chromotec) immunoprecipitations of native cell extracts from Cos-7 cells transfected with either pEGFP-C2, pEGPF-kazrin C, pEGFP constructs bearing the 1 to 176 N-terminal amino acids (kazrin C-Nt) or 161 to 327 C-terminal amino acids (kazrin C-Ct). 18 µg of total protein extract was loaded as input. **B.** Ponceau S staining (lower panel) or immunoblot (upper panel) against kazrin C (Abcam ab74114) of glutathione-Sepharose pull downs of either 5 µg GST or GST fused to the indicated rab GTPases incubated in the presence of GDP (Sigma) with 0.1 µg of purified kazrin C. 1:100 of the purified and digested kazrin used for the pull down was loaded as input. **C.** Ponceau S stainings (lower panels) or immunoblots (upper panels) against kazrin C (Abcam ab74114) of glutathione-Sepharose pull downs of 5 µg either of GST or GST fused to the indicated rab GTPases, either loaded with GDP (Sigma) or GTP (Sigma) and incubated with 0.1 µg of purified kazrin C. 1:10 of the purified and digested kazrin C used for the pull down was loaded as input.

4.4.2 Kazrin Directly Interacts with the Clathrin Heavy Chain Terminal Domain

Preliminary experiments already indicated that clathrin from rat brain extracts interacts with purified GST-kazrin C as well as with the endogenous kazrin rat brain isoforms (see Fig. 24A and D). Similar to the rat brain, immunoprecipitations from native protein extracts from Cos-7 cells confirmed that endogenous clathrin could be pulled down with the serum against the C-terminus of kazrin, but not against the N-terminus (Fig. 33A). Immunoprecipitation with a different commercially available antibody against kazrin (Abcam, ab74114), also indicated a specific interaction between the endogenous clathrin and kazrin isoforms in this cell type. To test if the human kazrin C interacts with clathrin in Cos-7 cells, plasmids encoding either GFP alone or GFP fused to the full length kazrin C or N- or C-terminal constructs (amino acids 1 to 176 and 161 to 327, respectively) were transfected. One day upon transfection, immunoprecipitations assays were performed from non-denaturing protein extracts, and the presence of clathrin in the precipitates was assessed by immunoblot. Even though clathrin was unspecifically bound to GFP in this assay, quantification of the clathrin signal, normalized for the amount of GFP or GFP-fusion proteins pulled down, indicated that the GFP-kazrin C full length might more efficiently co-precipitate endogenous clathrin, as compared to GFP alone or the N- and C-terminal kazrin constructs (Fig. 33B and C). Immuno-fluorescent staining for clathrin on fixed Cos-7 cells overexpressing GFP-kazrin C demonstrated a considerable overlap of both proteins, mainly in the perinuclear region (Fig. 33D), where the Golgi apparatus and the ERC are usually found, but also, in some peripheral structures close to the basal cell surface (Fig. 33D, left column). Most likely due to the abundance of clathrin and its involvement in many different cellular transport processes, only few of the clathrin structures co-localized with GFP-kazrin (Fig. 33D). Since most of the clathrin adaptors and endocytic accessory proteins that bind to clathrin are binding to the N-terminal clathrin Terminal Domain (TD) and the linker (Fig. 33E), we tested if recombinant purified 6xHis-kazrin C might directly interact with these clathrin domains expressed in and purified from *E. coli*. glutathione-Sepharose pull down experiments of GST or GST fused to the terminal and linker domains of human CHC17 demonstrated a specific and direct binding to recombinant 6xHis-kazrin C (Fig. 33F). This set of experiments enforced the view that kazrin binds to clathrin *in vivo* and *in vitro* and demonstrated that kazrin C can directly interact with the CHC17 terminal and linker domains.

To map the domains of kazrin C essential for interaction with the CHC TD (see Fig. 33F), a set of N-terminal kazrin C truncations fused to GST was generated (Fig. 34A) and tested in glutathione pull down assays with purified components. Even the N-terminal truncation of 250 amino acids still retained CHC17 binding activity. In contrast, loss of additional 37 amino acids (GST-kazrin C aa 289-327) resulted in complete loss of interaction, indicating the clathrin binding site of kazrin might lie within amio acid 250 to 289. Consistent with this view, C-terminal truncation of this fragment also prevented CHC17 binding (data not shown).

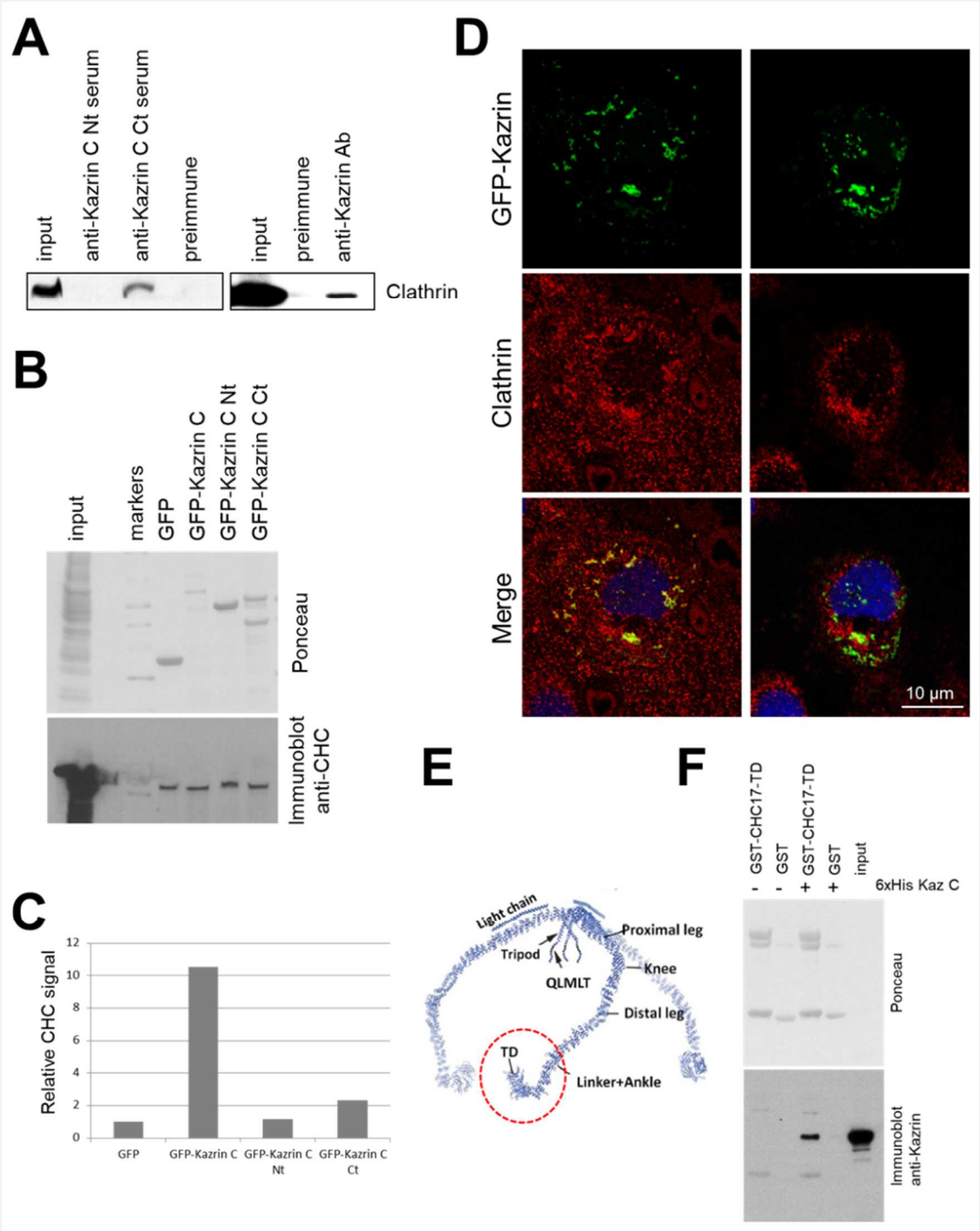

Figure 33. Kazrin Interacts with the Terminal Domain (TD) of the Clathrin Heavy Chain CHC17.

A. Anti-clathrin heavy chain (BD610499) immunoblots of Protein A-Sepharose immunoprecipitations from native Cos-7 extracts using either serums against the N-terminal (aa 1 to 176), the C-terminal (aa 161 to 327) portions of kazrin C, pre-immunisation serum (left panels) or an IgG against kazrin (Abcam ab74114) (right panel). Protein A-Sepharose bound to a preimmune serum was used as control. 10 or 18 µg of total protein were loaded as input in the left and right panels, respectively. **B.** Ponceau S staining (lower panel) or immunoblot (lower panel) against anti-clathrin heavy chain (BD610499) of GFP-Trap immunoprecipitations of native protein extracts of Cos-7 cells performed one day upon transfection with either GFP, GPF-kazrin C or GFP constructs bearing the 1 to 176 N-terminal amino acids (kazrin C Nt) or 161 to 327 C-terminal amino acids (kazrin C Ct). 21 µg of total protein was loaded as input. **C**. Graph representing the relative intensity of the clathrin signal in the blot shown in B normalized to the amount of GFP or GFP-kazrin constructs immunoprecipitated. **D.** Confocal fluorescence micrographs of different planes of a Cos-7 cell fixed one day upon transfetion with GFP-kazrin C and immunostained for the clathrin heavy chain using monoclonal anti-CHC17 IgGs (BD610499) and Alexa568-conjudgated secondary antibodies. The images were acquired with a

Zeiss LSM-780 confocal microscope using a 63x/1.4NA objective and the 32 PMT GaAsP array adjusted for detection of GFP and Alexa-568 (red). **E.** Scheme representing the clathrin triskelion. Encircled in red is the region (linker plus the terminal domain (TD)) fused to GST for expression in and purification from *E. coli*. **F.** Ponceau S staining (upper panel) and immunoblot (lower panel) against kazrin (Abcam ab74114) of glutathione-Sepharose pull downs of GST or GST fused to the linker and TD of human CHC17 (GST-CHC17-TD) incubated in the absence (-) or presence (+) of 200 ng/ml of purified 6xHis-kazrin. 1:100 of 6xHis-kazrin used for the pull down was loaded as input.

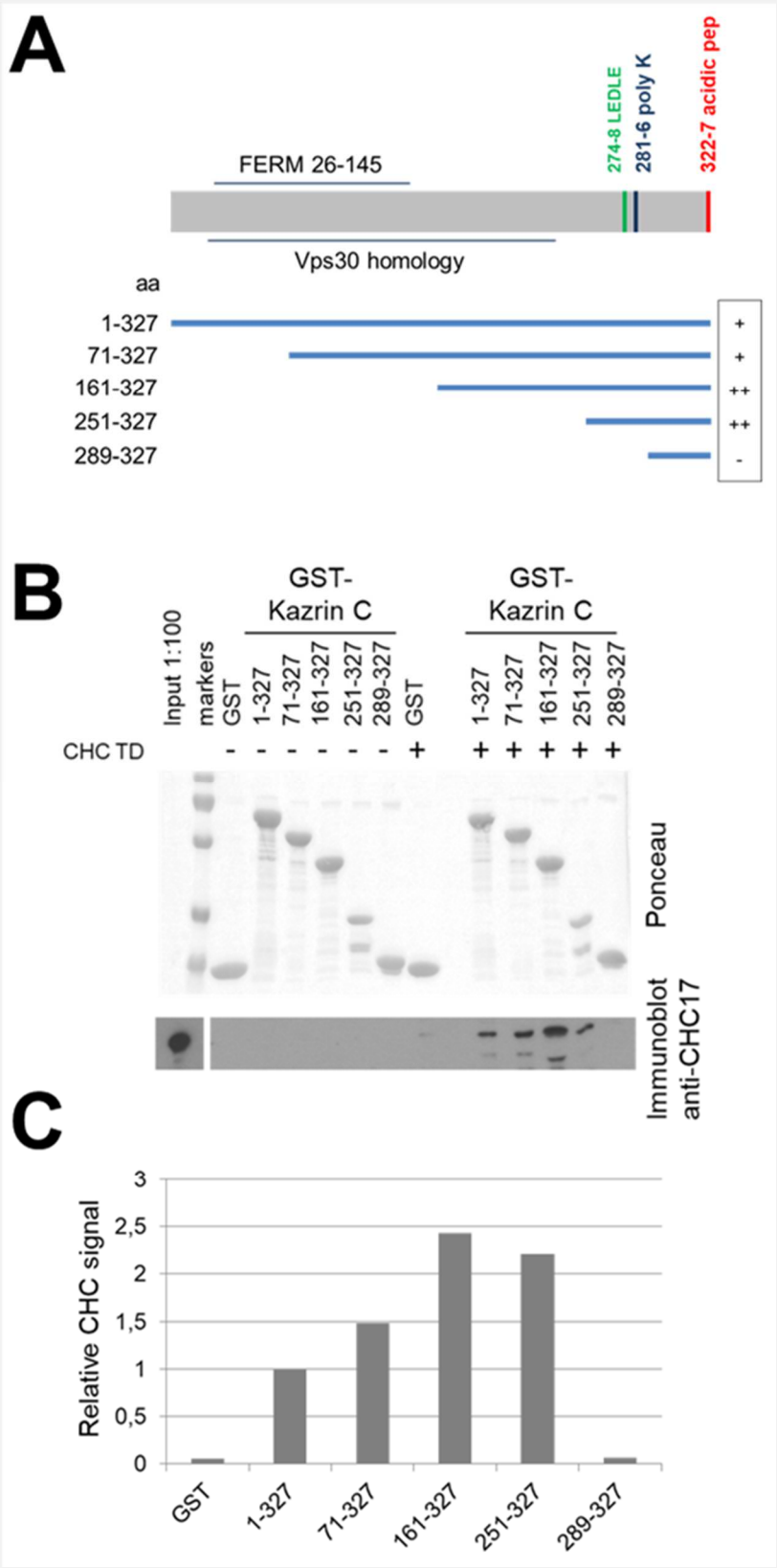

Figure 34. Kazrin C Directly Binds to the Clathrin Heavy Chain TD.

A. Scheme of kazrin constructs fused to GST, expressed in and purified from E. coli. Black (+) or (–) indicates the degree of interaction with the TD and linker domains of human CHC17 in the pull down. **B.** Ponceau S staining (upper panel) and immunoblot (lower panel) against clathrin (BD610499) of glutathione-Sepharose pull downs of purified GST or GST fused to the kazrin C constructs depicted above, incubated in the absence (-) or presence (+) of 200 ng/ml of the purified human CHC17 TD and linker domains (aa 1-483). 1:100 of CHC TD used for the pull down was loaded as input. **C.** Graph representing the relative intensity of the clathrin signal in the blot shown in B normalized to the amount of GST-kazrin constructs precipitated.

4.4.3 Kazrin Does not Significantly Interact with the VPS35 Subunit of Retromer or HRS of ESCRT-0

The next step was to clarify if kazrin might interact with endocytic machinery other than clathrin, in particular with that localized on SEs. For that purpose, we performed immunoprecipitations of native extracts from Cos-7 cells expressing GFP-kazrin or GFP alone using an antibody against GFP covalently bound to a matrix (GFP Trap). Co-precipitation of the HRS subunit of the ESCRT-0 complex involved in the degradative pathway and VPS35, a subunit of the retromer involved in retrograde trafficking from the endosomes to the Golgi and the PM, was probed by immunoblot. Both proteins did not appear to interact with kazrin in this assay (Fig. 35). Additionally, immunostainings of these proteins in cells expressing GFP-kazrin were done without showing a significant overlapping signal (data not shown).

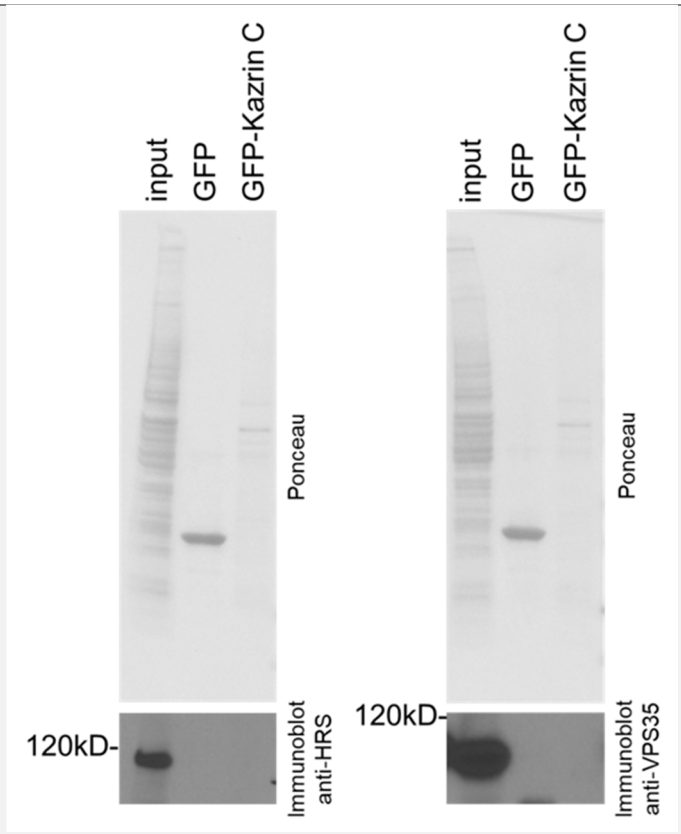

Figure 35. Kazrin C Does Not Interact with the Retromer Subunit VPS35 or the ESCRT-0 Subunit HRS Under the Experimental Conditions Used.
Ponceau S stainings (upper panels) and immunoblots (lower panels) against HRS (Santa Cruz sc-30221) or VPS35 (Santa Cruz sc-374372) of GFP-Trap immuoprecipitations of native protein extracts from Cos-7 cells one day upon transfection with GFP or GFP-kazrin C. 9 µg of total protein extract was loaded as input.

The negative results regarding the search for interaction partners among other endosomal components let us to intensify the study of the interplay with clathrin and clathrin adaptors of the adaptin family.

4.4.4 Kazrin Interacts with the Ear Domains of the β1- and γ-Adaptins Subunits of the AP-1 Complex

Preliminary data already indicated that kazrin might interact with tetrameric AP clathrin adaptors. Thus, we found that a generic antibody recognizing the β-adaptin subunits of the AP-family detected a specific band in the immunoprecipitates using the antibodies against kazrin C or in pull down experiments from native protein extracts, using glutathion-Sepharose bound to recombinant GST-kazrin C (see Fig. 24A and D). Further, immunofluorescence staining with an affinity purified antibody against kazrin suggested that endogenous kazrin partially co-localizes with the AP-1 γ-adaptin subunit on peripheral endosomal compartments loaded with Tfn in Cos-7 cells (see Fig. 27A).

For confirmation of the interactions detected in rat brain extracts, the immunoprecipitations were repeated with native extracts from Cos-7 cells using the sera against the N- and the C-terminus of kazrin. Again, the N- and C-terminal sera could precipitate a protein recognized by the generic anti-β-adaptin antibody. In addition, the sera against the C-terminus of kazrin precipitated the γ-subunit of the AP-1 complex, but not the α-subunit of AP-2 (data not shown), suggesting a specific interaction with AP-1.

To investigate if kazrin C might directly interact with AP-1, independently of clathrin, pull down assays with purified components expressed in *E. coli* were performed. Since most endocytic accessory proteins bind to the ears of the large subunits (γ- and β1-adaptin), the interactions of these domains fused to GST, with recombinant 6xHis-kazrin C were analyzed in glutathione-Sepharose pull down experiments. A specific interaction of kazrin C was detected with both AP-1 subunits, but the interaction with γ-adaptin seemed much stronger (Fig. 36B).

To map the domains required for interaction with γ-adaptin, the γ-adaptin ear was excised from GST by proteolytic digestion and binding with the set of N- and C-terminal kazrin C truncations fused to GST (Fig. 37A) was tested *in vitro,* in glutathione-Sepharose pull down experiments. C-terminal truncation of the 33 C-terminal amino acids encompassing the acidic peptide (Kaz aa1-294) or truncation of a larger fragment, also including the poly basic stretch and the putative clathrin box (Kaz aa 1-250) only partially reduced the interaction with γ-adaptin. However, complete inhibition of the interaction was observed in C-terminal truncations leaving less than 176 amino acids (Kaz aa 1-176, Kaz aa 1-148 and Kaz aa 1-70), indicating that the γ-adaptin binding site might lie within the 176 to 327 fragment. On the contrary, truncation of the 148 or 162 N-terminal amino acids (Kaz aa 148-327 and Kaz aa 161-327) very much increased the interaction with the ear of γ-adaptin in a reproducible manner, clearly pointing to an autoinhibitory effect of the N- versus the C-terminus of kazrin C in terms of γ-adaptin binding. Further, N-terminal truncation to amino acid 289 completely impeded binding (Kaz aa 289-327; Fig. 37B and C). Thus, the results with the N- and C-terminal truncations suggested that the hard core γ-adaptin binding site is located within amino acids 161 - 250, immediately upstream of the putative clathrin binding motif and positively charged poly lysine sequence (see Fig. 21), and that an N-terminal fragment comprised between amino acids 71 and 148 auto-inhibits the kazrin C / γ-adaptin interaction either in cis or in trans.

To answer the question of whether the observed autoinhibition of kazrin C also happens *in vivo*, GFP constructs of kazrin, transiently expressed in Cos-7 were immunoprecipitated. As seen in the pull down experiments, the N-terminus failed to co-precipitate endogenous γ-adaptin whereas the C-terminus attracted nearly twice adaptin than the full length protein (Fig. 38A and B). In order to corroborate the observations *in vivo*, Cos-7 cells were transfected with full length or the C-terminus

of kazrin fused to GFP. Immunostainings showed in many cells prominent perinuclear co-localization of γ-adaptin and the C-terminus. The full length kazrin only coincided in individual puncta (Fig. 38C).

In summary, the interaction between kazrin C and γ-adaptin could be demonstrated *in vitro and in vivo*, with the γ-adaptin binding domain being located at the C-terminus of kazrin, between amino acids 161 and 250. Further, the N-terminus of kazrin was not only unable to interact with γ-adaptin but it rather inhibited the interaction with the kazrin C-terminal fragment.

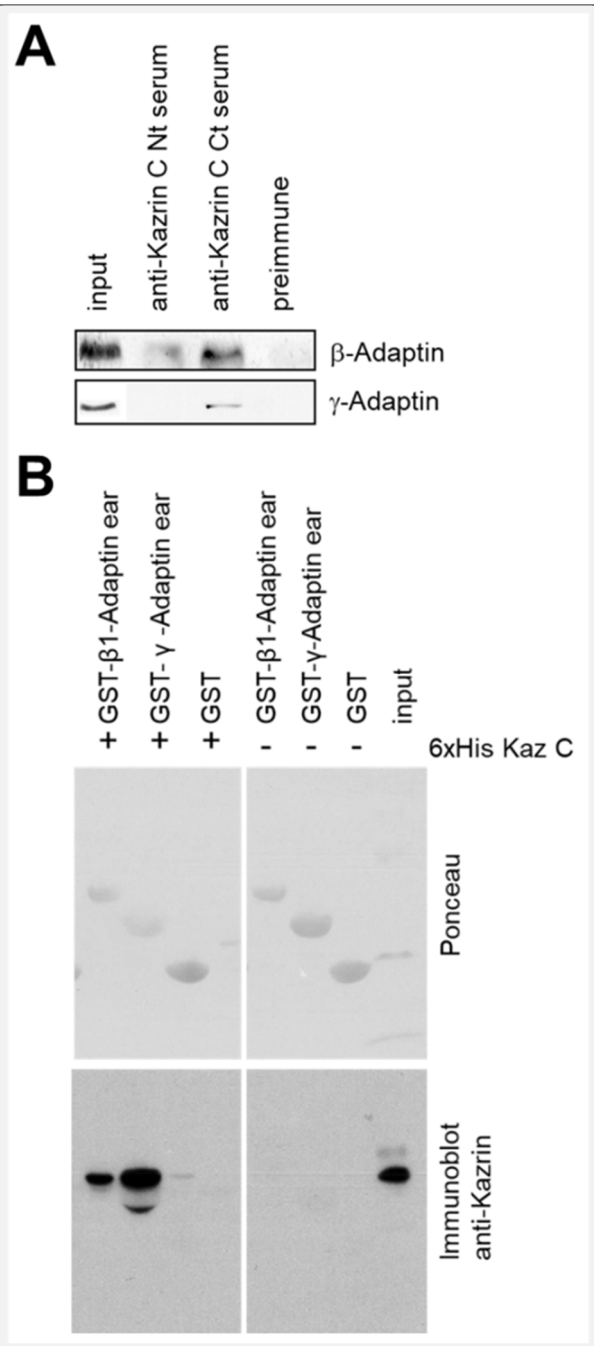

Figure 36. Kazrin C Directly Interacts with AP-1.

A. Immunoblots of Protein A-Sepharose immuoprecipitations of native protein extracts from Cos-7 cells using serums against the N-terminal (aa 1 to 176) or the C-terminal (aa 161 to 327) portions of kazrin C or pre-immunisation serum, probed with IgGs against clathrin (BD610499), β-adaptin (Clontech A35620) or γ-adaptin (BD 610385). 10 µg of total protein was loaded as input. **C.** Ponceau S stainings (upper panels) and immunoblots (lower panels) against kazrin (Abcam ab74114) of glutathione-Sepharose pull downs of purified GST or GST fused to the human γ- or β1-Adaptin ears, incubated in the absence (-) or presence (+) of 200 ng/ml of purified 6xHis-kazrin. 1:100 of the purified 6xHis-kazrin used for the pull down was loaded as input.

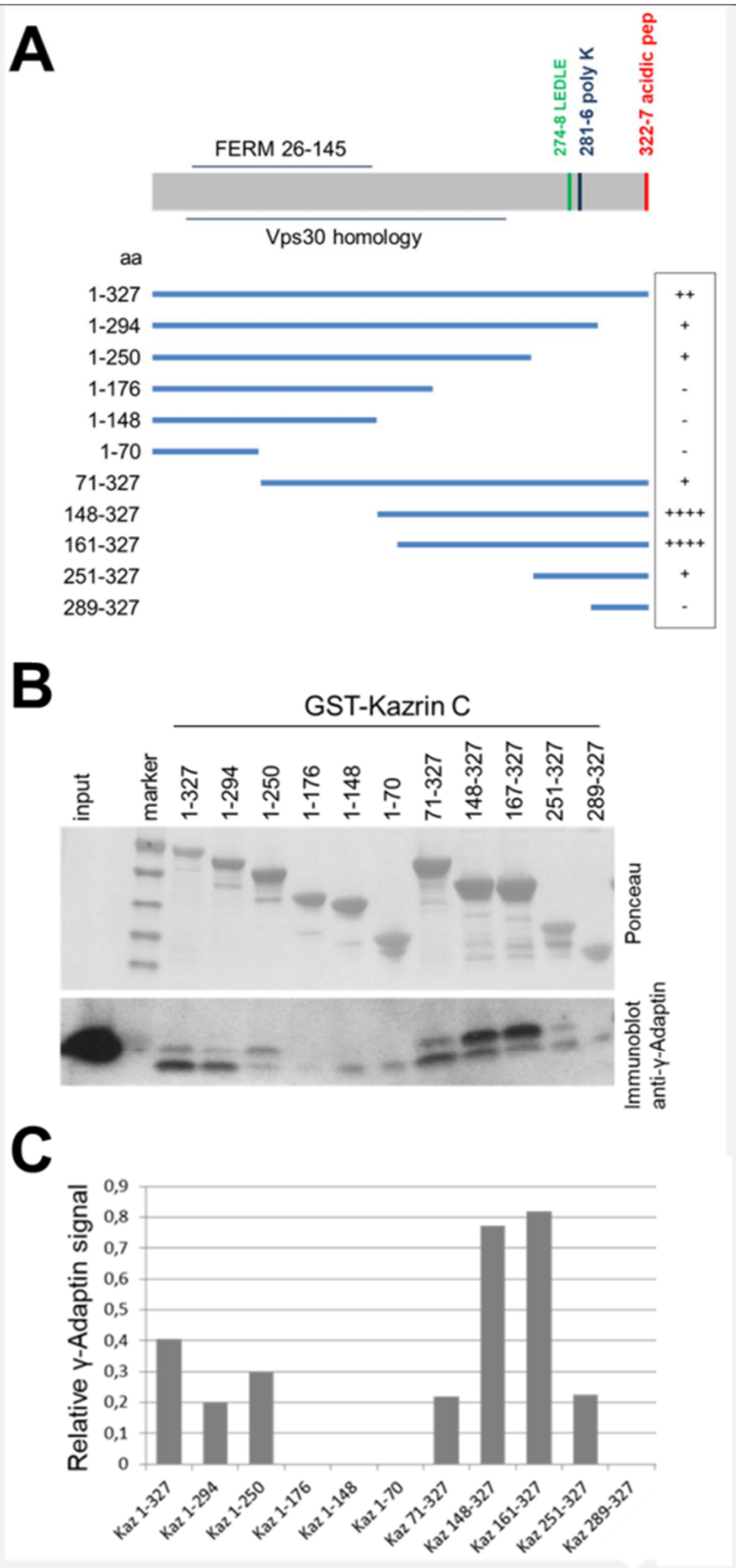

Figure 37. The Interaction Between Kazrin C and the γ-Adaptin Ear is Autoinhibited *In Vitro*.
A. Scheme of kazrin constructs fused to GST, expressed in and purified from E. coli. (+) or (–) indicates the degree of interaction with the γ-adaptin ear in the pull down shown in B. **B.** Ponceau S staining (upper panel) and immunoblot (lower panel) against γ-adaptin (BD 610385) of glutathione-Sepharose pull downs of purified GST or GST fused to the kazrin C constructs depicted above, incubated in the presence of 200 ng/ml of purified human γ-adaptin ear (aa 702-925). 1:10 of the purified γ-adaptin ear used for the pull down was loaded as input. **C.** Graph representing the relative intensity of the γ-adaptin signal in the blot shown in B normalized to the amount of GST-kazrin constructs precipitated.

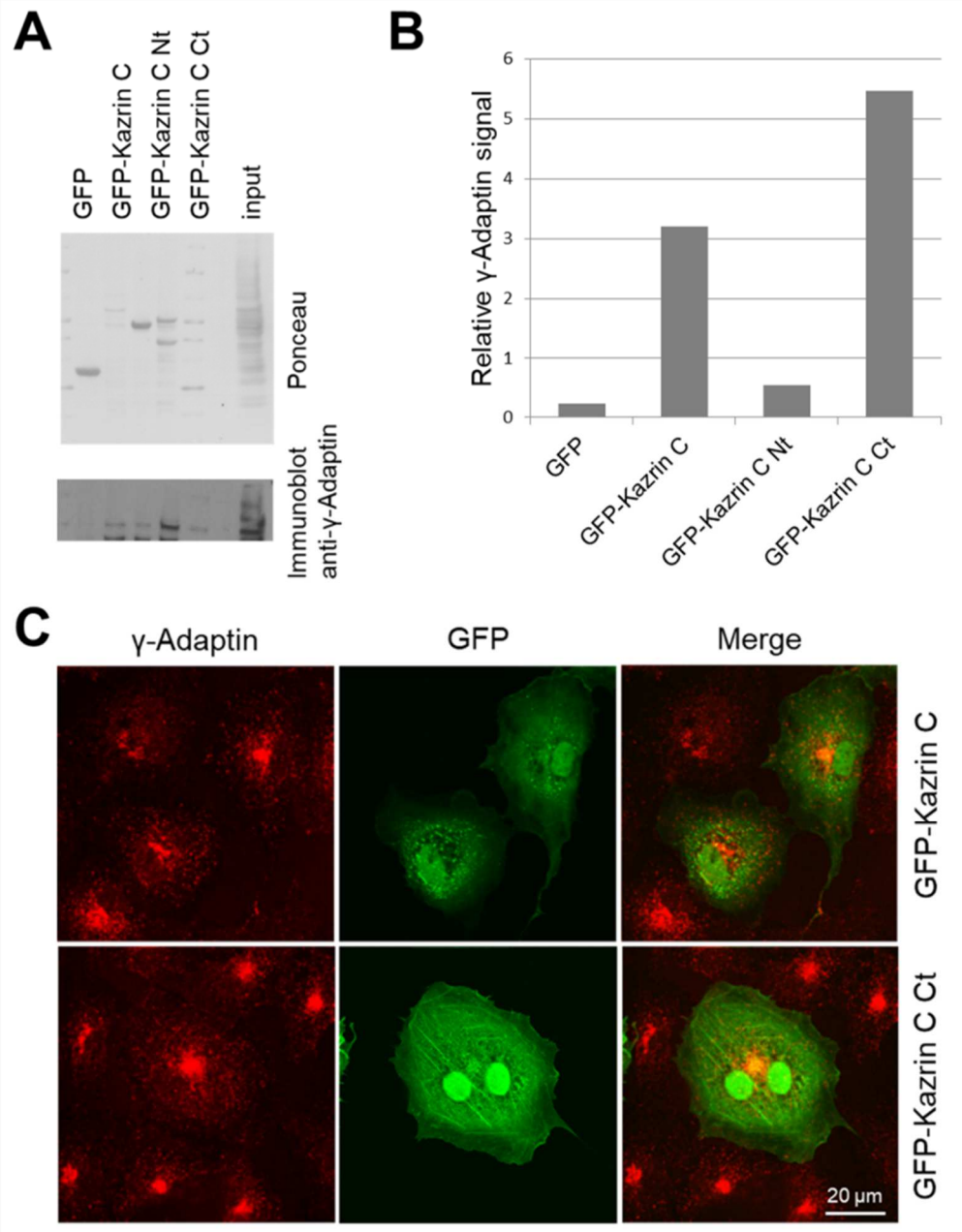

Figure 38. The Interaction Between Kazrin C and γ-Adaptin is Autoinhibited *In Vivo*.
A. Ponceau S staining (upper panel) and immunoblot (lower panel) against γ-adaptin (BD 610385) of GFP-Trap immunoprecipitations from native protein extracts of Cos-7 cells one day upon transfection with GFP, GPF-kazrin C or GFP constructs bearing the N-terminal amino acids 1 to 176 (kazrin C-Nt) or C-terminal amino acids 161 to 327 (kazrin C-Ct) of kazrin C. 18 µg of total protein extract was loaded as input. **B.** Graph representing the relative intensity of the γ-adaptin signal in the blot shown in A normalized to the amount of GFP constructs precipitated. **C.** Maximum intensity projections of confocal fluorescence micrographs of Cos-7 cells one day upon transfection with GFP-kazrin C or GFP fused to the C-terminal amino acids 161-327 of kazrin C and immunostained using a monoclonal anti-γ-adaptin antibody (BD 610385) and a Alexa568-conjudgated secondary antibody. Images of the fixed cells were acquired using a Leica TCS-SP5 microscope with a 63x/1.4NA objective and the emission filters BP525/50 for detection of GFP, and LP590 for detection of Alexa-568 (red).

4.5 Kazrin C Co-localizes with Endosomal Actin and Interacts with Arp2/3 and WASH

4.5.1 Kazrin Co-localizes with Actin on Early Endosomal Structures

In the process of analysing the localization of the GFP-kazrin C full length and its C-terminus, we noticed that a significant fraction of the GFP-kazrin C C-terminal construct appeared in filamentous structures reminiscent of actin fibres. Since overexpression and depletion of kazrin has previously been described to impact on the actin cytoskeleton (Sevilla, Nachat et al. 2008, Cho, Vaught et al. 2010), and actin polymerization plays important roles at different stages within the endocytic pathway, we decided to investigate if the GFP-kazrin C-terminal construct might be associated with endosomal actin structures. For that purpose, Cos-7 cells were co-transfected with plasmids encoding the kazrin C C-terminus fused to GFP and the actin binding protein LifeAct fused to RFP. One day upon transfection, cells were fixed and immuno-stained for the endosomal marker EEA1. LifeAct is a 17 amino acid, peptide that stains filamentous actin structures in eukaryotic cells and tissues and seems not to interfere with actin dynamics *in vitro* and *in vivo* (Riedl, Crevenna et al. 2008). The C-terminus of kazrin C localized to a great extent with cellular actin structures all over the cell and at the PM, including stress fibres (Fig. 39 upper panels). Many small actin structures were clearly decorated with kazrin, often shaping together (Fig. 39 central panels). Commonly, actin and kazrin co-labelled structures were associated with or emerge from EEA1 positive endosomes (Fig. 39 lower panels).

Also corroborating the association of kazrin with endosomal actin, we observed that in HEK293 cells that were co-transfected with plasmids expressing YFP-rab4, GFP-kazrin C and DsRed-cortactin, the GFP-kazrin C subdomains on YFP-rab4 vacuolar endosomes often co-localized with DsRed-cortactin (Fig. 40). Since cortactin mostly decorates Arp2/3-crosslinked actin networks (Schnoor, Stradal et al. 2018), we decided to investigate the possible interactions between kazrin C and the Arp2/3 complex, as well as its best characterized endosomal NPF, WASH.

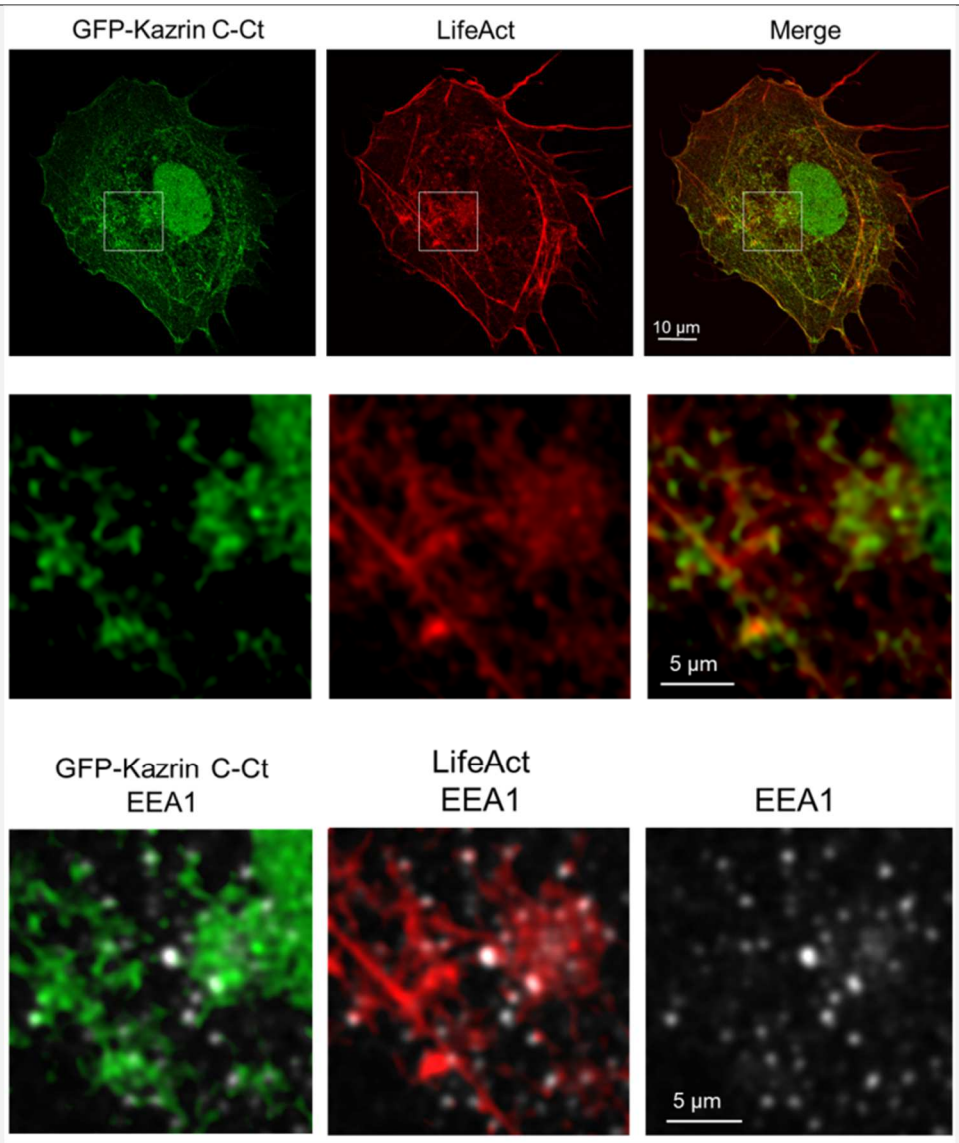

Figure 39. The C-terminus of Kazrin C Co-localizes with Actin and Early Endosomal Structures.
The upper panels show maximum intensity projections of confocal fluorescence micrograph of Cos-7 cells fixed one day upon transfection with RFP-LifeAct and GFP fused to the C-terminal amino acids 161 to 327 of kazrin C. The lower panels represent magnified single plains of the insets above, showing GFP-kazrin C-Ct and LifeAct-RFP positive structures stained with antibodies against EEA1 (Cell Signaling #3288) and Alexa647-conjugated secondary antibodies. The images were acquired with a Zeiss LSM-780 confocal microscope using a 63x/1.4NA objective, the 32 PMT GaAsP array adjusted for detection of GFP and RFP, and a conventional PMT for detection of Alexa-647 (far red).

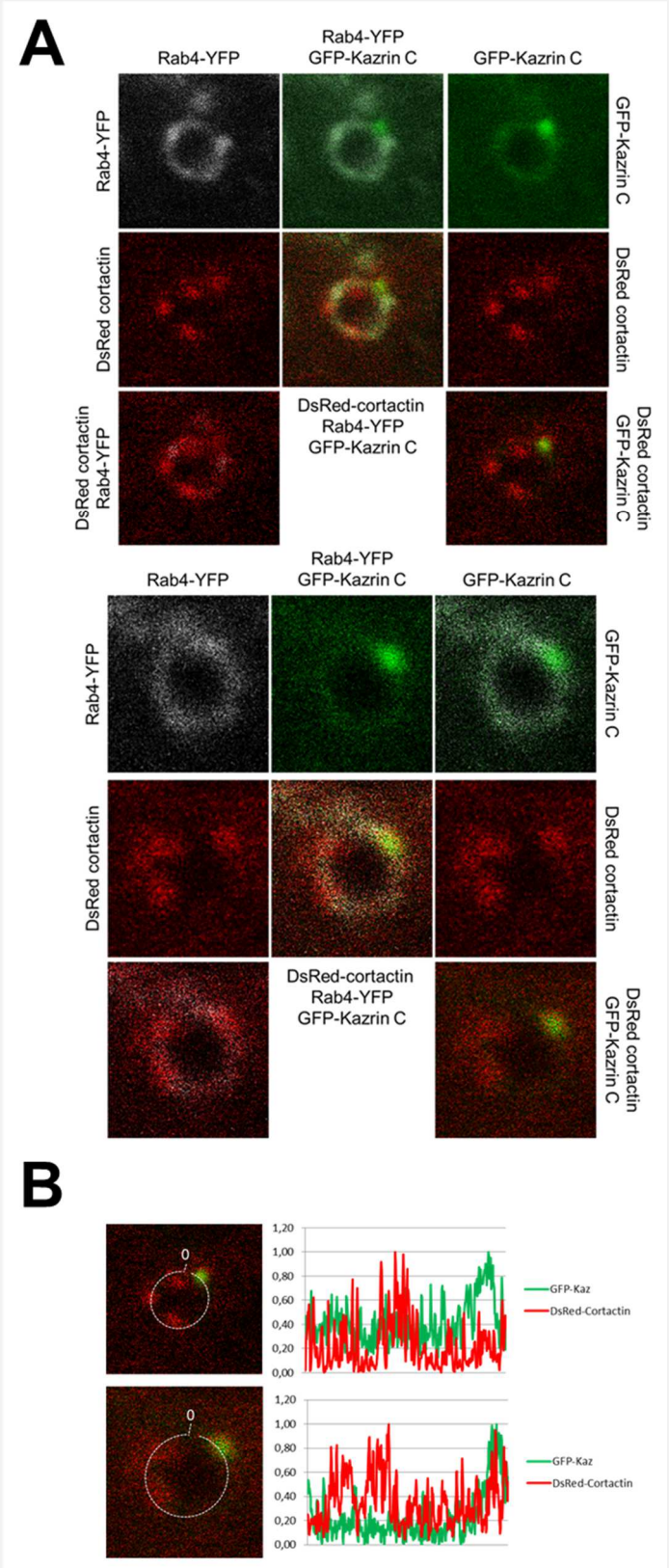

Figure 40. Kazrin C Co-localizes with Cortactin on YFP-Rab4 Vacuolar Endosomes in HEK293 (EBNA) Cells.

A. Confocal fluorescence micrographs of selected vacuolar early endosomes of a HEK293 (EBNA) cell expressing GFP-kazrin C, DsRed cortactin and YPF-rab4. **B.** Plot profiles for the normalized intensity of the YFP-rab4. DsRed cortactin and GFP-kazrin C signals of the indicated segmented lines drawn on the surface of the endosomes shown. Data was acquired using FIJI ImageJ, transferred to an Excel file and normalized for the maximum intensity. «0» indicates where the profile starts (converging at the Y axes).

4.5.2 Kazrin Directly Interacts with the Arp2/3 Complex Via its C-terminal Acidic Peptide

Alignment of the C-terminus from kazrin C with that of known type I Arp2/3 complex NPFs such as N-WASP and WASH1 or the newly identified Arp2/3 inhibitor arpin, evidenced the presence of an acidic peptide bearing a conserved W, which has been shown to participate in the interaction with the Arp2/3 complex (Rottner, Hanisch et al. 2010) (Fig. 41A). To test if the acidic peptide is able to directly interact with Arp2/3, pull down experiments with purified components were performed and analysed by immunoblot, using an antibody targeting the p41 subunit of the Arp2/3 complex. As shown in figure 41, the C-terminus of kazrin C (aa 161-327) could precipitate Arp2/3 whereas the C-terminus lacking the acidic peptide (GST-KazC Ct-aΔ, aa161-294) or the C-terminus bearing the acidic peptide mutated to alanins (GST-KazC Ct-EA, aa161-327-(322-EEDADW-327, AAAAAA)) lost the capacity to do so (Fig. 41B). Immunofluorescent staining for p41 of Cos-7 cells expressing full length kazrin C fused to GFP showed partial co-localization in dot-like structures, supporting the view that kazrin C interacts with the Arp2/3 complex *in vivo* (Fig. 41C). Immunoprecipitations from Cos-7 cells transiently expressing GFP-kazrin C constructs indicated that full length kazrin C as well as the C-terminus alone were equally able to precipitate the complex but not the N-terminus. Surprisingly though, depletion of the acidic peptide of the C-terminal construct only partially diminished co-precipitation of Arp2/3, as opposed to the complete inhibition of the interaction observed *in vitro* with purified components (Fig. 41C and D). The data suggested that kazrin C might bind other Arp2/3 interacting partners that indirectly bridge kazrin to the Arp2/3 complex, in addition to the direct interaction mediated by the acidic kazrin C peptide.

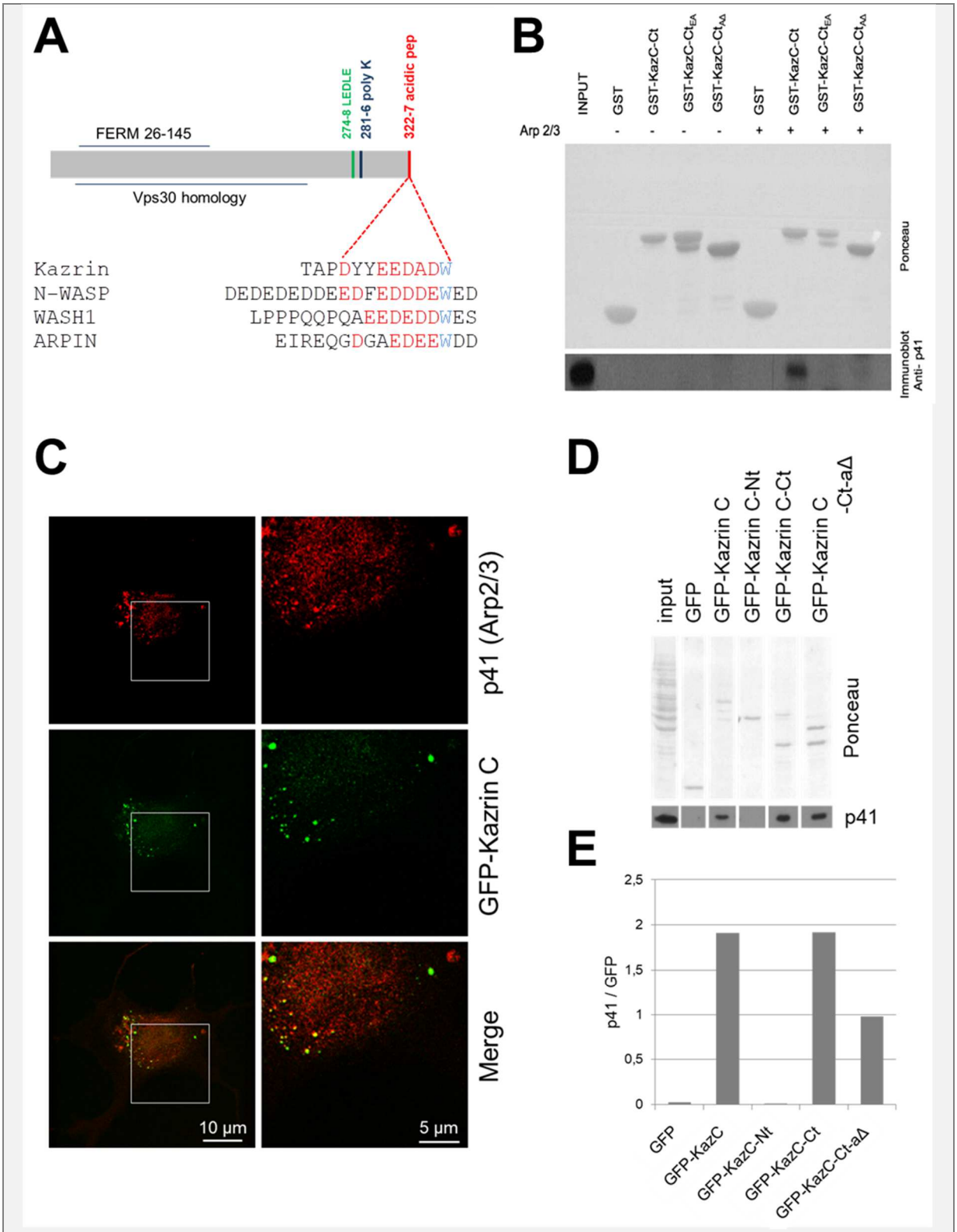

Figure 41. Kazrin C Directly Interacts with the Arp2/3 Complex Via its C-terminal Acidic Peptide.
A. Alignment of the acidic peptides required for the interaction of Arp2/3 complex activators (N-WASP, WASH1), the inhibitor (Arpin) and the C-terminal acidic peptide of kazrin C. **B.** Ponceau S staining (upper panel) and immunoblot (lower panel) against the p41 subunit (Santa Cruz sc-137125) of the Arp2/3 complex of glutathione-Sepharose pull downs of purified GST or the indicated kazrin C constructs fused to GST, incubated in the absence (-) or presence (+) of 4 µg of purified Arp2/3 complex (Cytoskeleton). 1:100 of the purified Arp2/3 complex used for the pull down was loaded as input. **C.** Ponceau S staining (upper panel) and immunoblot (lower panel) against the p41 subunit (Santa Cruz sc-137125) of the Arp2/3 complex of GFP-Trap immunoprecipitation of native protein extracts from Cos-7 cells one day upon transfection with GFP or the indicated kazrin constructs fused to GFP. 10 µg of total protein was loaded as input. **D.** Graph representing the

relative intensity of the p41 signal in the blot shown in C, normalized to the amount of GFP constructs precipitated. **E.** Confocal fluorescence micrographs of Cos-7 cells fixed one day upon transfection with GFP-kazrin C and stained for the p41 subunit (Santa Cruz sc-137125) of the Arp2/3 complex and an Alexa568-conjugated secondary antibody. The right panels are magnifications of the insets. The images were acquired using a Leica TCS-SP5 microscope with a 63x/1.4NA objective and the emission filters BP525/50 for detection of GFP, and LP590 for detection of Alexa-568 (red).

4.5.3 Kazrin Interacts with the Endosomal NPF WASH

Since WASH activates the Arp2/3 complex on endosomes, we decided to investigate if kazrin C might interact with this NPF. For this purpose, immunoprecipitations from Cos-7 cells transfected with GFP-kazrin constructs were performed. Strikingly, we found that the full length kazrin C as well as both, the N- and the C-terminus of kazrin C, strongly interacted with WASH in these assays (Fig. 42A, B and C). No significant interaction could be observed when Cos-7 cells were transfected with a plasmid encoding GFP alone. Analogous immunoprecipitations with spire, an NPF found on rab11 endosomes, or N-WASP, an NPF mainly involved in CME at the PM, could not demonstrate a significant interaction with the full length kazrin C, nor with the N- or C-terminal truncations, strengthening the view that kazrin C specifically interacts with WASH (Fig. 42D). Further supporting this hypothesis, glutathione-Sepharose pull downs of purified WASH fragments fused to GST and recombinant 6xHis-kazrin C demonstrated strong binding of kazrin C to both the N- and C-terminal portions of human WASH1 including the VCA domains, whereas little interaction could be demonstrated between the N-WASP VCA domain and kazrin C in analogous experiments (Fig. 42D, E and additional data not shown).

Further corroborating the interaction *in vivo*, co-localization of WASH with GFP-kazrin C on enlarged peripheral structures could be observed in immunofluorescence experiments in Cos-7 cells (Fig. 42F). To investigate if these structures might be of endosomal nature, we tried to load the cells with Tfn-Alexa647, but the potent negative effect of the overexpression of kazrin C on the Tfn uptake precluded the experiment with this construct (data not shown). Some loading could be achieved in cells overexpressing the GFP-kazrin C C-terminal construct, even though again, the C-terminal construct also partially impeded uptake. In this cells, Tfn-Alexa647 loaded structures decorated with GFP-kazrin C C-terminus could be observed, which could also be immuno-labelled with antibodies against WASH (Fig. 43A). The overexpression of the N-terminal fragment of kazrin C did not prevent Tfn-Alexa647 uptake but co-localization of Tfn labelled structures with this kazrin C construct was difficult to evaluate because, besides Tfn and WASH-loaded structures, it also labelled many other cellular structure within the cytosol (Fig. 43B).

Altogether the results indicated that kazrin C extensively interacts with WASH *in vivo* and *in vitro*, the interaction involving several kazrin C and WASH domains. Further, the fluorescence microscopy results indicated that the interaction occurred, at least to a certain extent, when kazrin C and WASH sit on endosomal membranes.

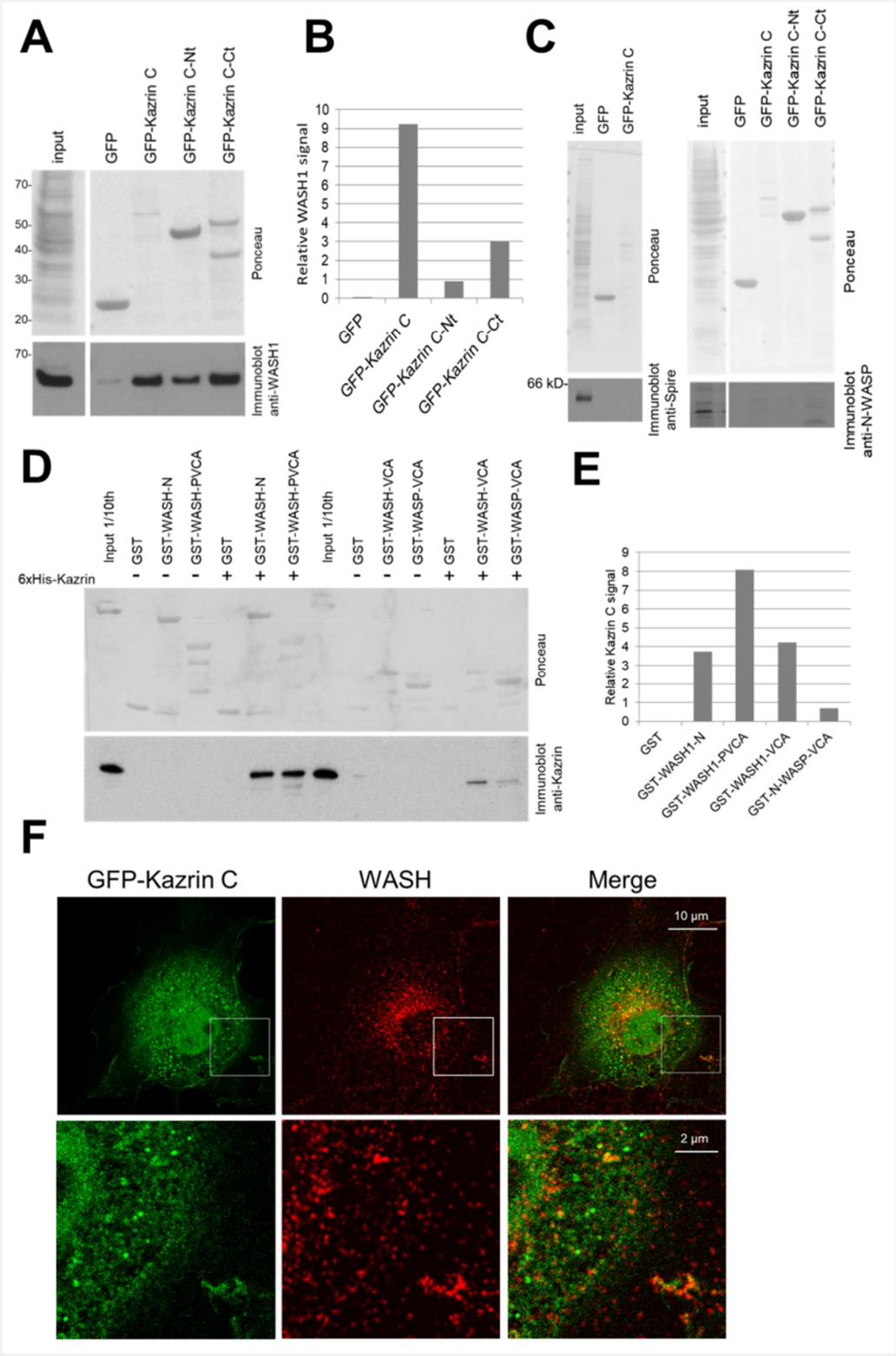

Figure 42. Kazrin C Directly Interacts with WASH.

A. Ponceau S staining (upper panel) and immunoblot (lower panel) against WASH1 (Millipore ABS72) of GFP-Trap immunoprecipitations of native protein extracts from Cos-7 cells one day upon transfection with plasmids encoding GFP or the indicated kazrin C constructs fused to GFP. 18 µg of total protein was loaded as input. **B.** Graph representing the relative intensity of the WASH signal in the blot shown in A, normalized to the amount of GFP constructs precipitated. **C.** Ponceau S stainings (upper panels) and immunoblots (lower panels) against spire (Abnova H00056907-M01) and N-WASP (Santa Cruz sc-20770) of GFP-Trap immunoprecipitations of native protein extracts from Cos-7 cells, one day upon transfection with plasmids encoding either GFP or the indicated kazrin C constructs fused to GFP. 18 µg of total protein was loaded as input. **D.** Ponceau S staining (upper panel) and immunoblot (lower panel) against kazrin C (Abcam ab74114) of

glutathione-Sepharose beads pull downs of GST alone or GST fused to the indicated fragments of human WASH1 or N-WASP, incubated in the absence (-) or presence (+) of 200 ng/ml of 6xHis-kazrin, expressed in and purified from *E. coli*. 1:10 of the purified 6xHis-kazrin used for the pull down was loaded as input. **E.** Graph representing the relative intensity of the kazrin signal in the blot shown in D, normalized to the amount of GST constructs precipitated. **F.** Maximum intensity projections of confocal fluorescence micrographs of Cos-7 cells fixed one day upon transfection with GFP-kazrin C and stained with antibodies against WASH1 (Millipore ABS72) and an Alexa568-conjugated secondary antibody. The lower panels show magnified single plains of the insets above. The images were acquired with a Leica TCS-SP5 microscope with a 63x/1.4NA objective and the emission filters BP525/50 for detection of GFP and LP590 for detection of Alexa-568 (red).

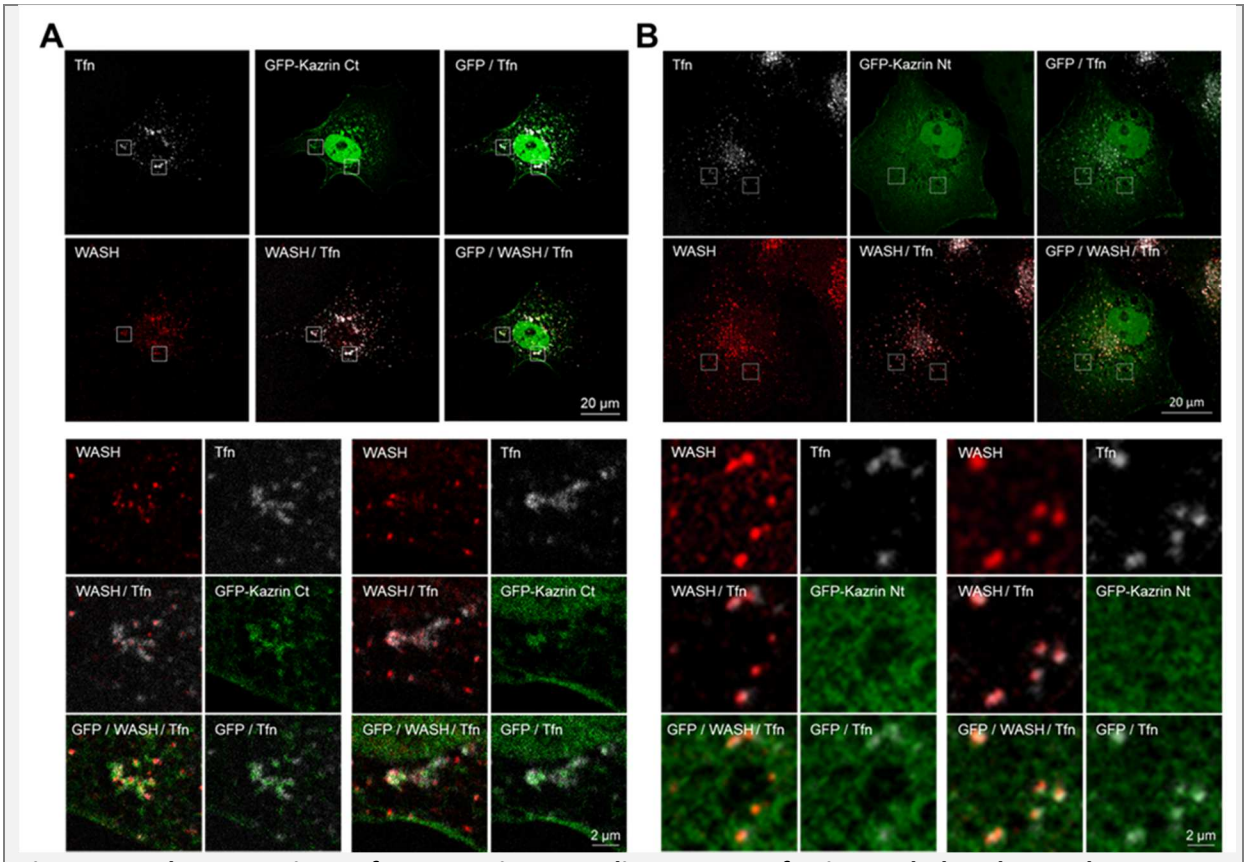

Figure 43. The C-terminus of GFP-Kazrin C Localizes to Transferrin Loaded Endosomal Structures that Can also Be Decorated with WASH1.

A. Maximum intensity projections of confocal fluorescence micrographs of a Cos-7 cell (upper panels) one day upon transfection with plasmids encoding GFP fused to the C-terminal amino acids 161 to 327 of kazrin C, loaded with 20 µg/ml Tfn-Alexa647 for 2 hours before fixation, and staining with an antibody against WASH1 (Millipore ABS72) and an Alexa-568-conjugated secondary antibody. The lower panels represent magnification of single plains of the insets from above, showing Tfn loaded endosomal structures co-localizing with GFP-kazrin-Ct and WASH1. **B.** Maximum intensity projections of confocal fluorescence micrographs of a Cos-7 cell one day upon transfection with a construct endocding GFP fused to the N-terminal amino acids 1 to 176 of kazrin C, loaded with 20 µg/ml Tfn-Alexa647 for 2 hours before fixation and staining with an antibody against WASH1 (Millipore ABS72) and an Alexa-568-conjugated secondary antibody. The images were acquired using a Leica TCS-SP5 microscope with a 63x/1.4NA objective and the emission filters BP525/50 for detection of GFP and LP590 for detection of Alexa-568 (red) and Alexa-647 (far red).

4.6 Impact of Overexpression or Depletion of Kazrin on Cellular Actin

4.6.1 Depletion of Kazrin Alters the Actin Cytoskeleton in Cos-7 and MEF Cells

To gain insight into the impact of kazrin depletion on cellular actin, untransfected Cos-7 cells or those transfected with the shKaz or shSCR constructs, were fixed and stained with TRICT-phalloidin. As observed in figure 44, depletion of kazrin had a major impact on the cytoskeleton of Cos-7 cells with most actin collapsing around the nucleus, the stress fibres being scarce and a numbers of small dot-like, elongated and circular actin structures appearing in the cytosol (Fig. R44). A similar effect was observed when depletion of kazrin was achieved by treatment of the cells with an unrelated siRNA (data not shown). An analogous experiment performed in MEFs (Mouse Embrionic Fibroblast) demonstrated a major effect of kazrin depletion on the actin cytoskeleton, with stress fibres disappearing and small dot-like structures accumulating in the cytosol. In this respect, the effect was more prominent in MEF than in Cos-7 cells. In addition, the small cytosolic structures did not seem to collapse around the nucleus in MEFs, making their analysis easier (Fig. 45A). Analysis of intensity plot profiles across the cell, excluding stress fibres, indicated an increase in the number and intensity of the cytosolic dot-like structures relative to the cortical actin in kazrin-depleted MEF cells, as compared to untransfected cells or cells expressing the shSCR (Fig. 45B and C).

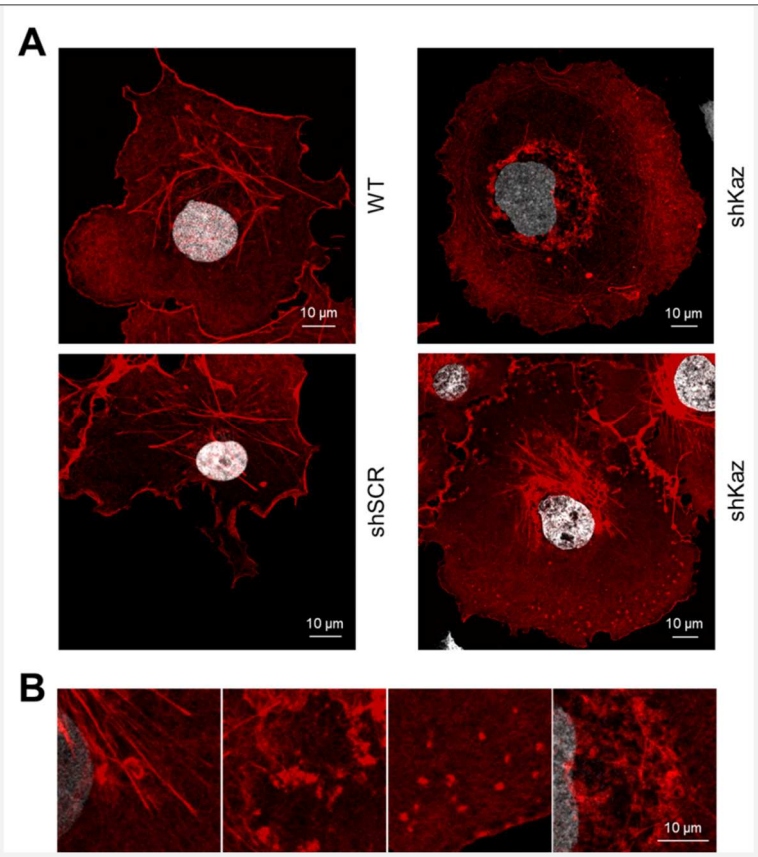

Figure 44. Depletion of Kazrin Alters the Actin Cytoskeleton in Cos-7 Cells.
A. Confocal fluorescence micrographs of Cos-7 cells either unransfected (WT) or transfected with plasmids encoding a shRNA against Kazrin C (shKaz) or a control shRNA (shSCR), fixed and stained with TRICT-phalloidin and DAPI. **B.** Enlarged areas of kazrin depleted cells showing small cytosolic actin structures not detectable in untransfected cells. The images were acquired using a Leica TCS-SP5 microscope with a 63x/1.4NA objective and the emission filter LP590 for detection of Alexa-568 (red).

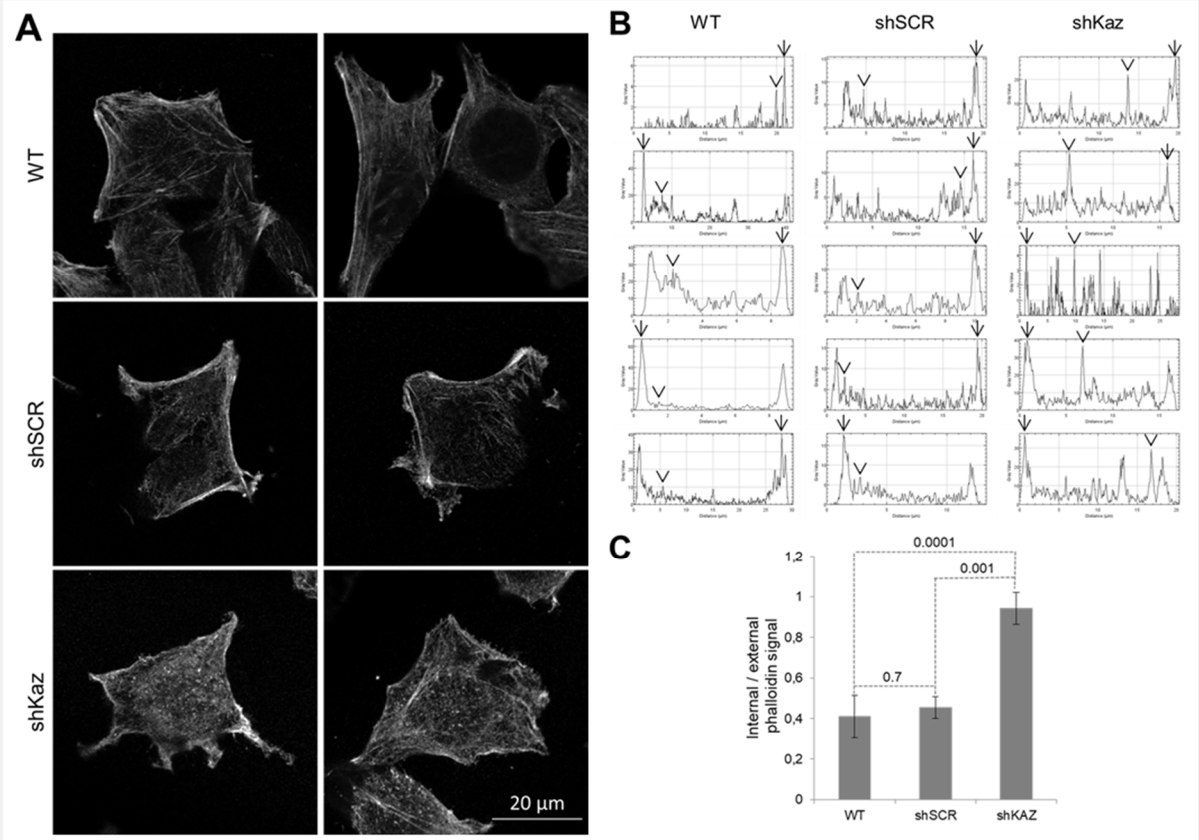

Figure 45. Depletion of Kazrin in MEF Cells also Increases the Number of Internal Actin Structures Versus the Cortical Actin or the Stress Fibres.

A. Maximum intensity projections of confocal fluorescence micrographs of wild type MEF cells (WT) and stable MEF cell lines expressing a non target control shRNA (shSCR) or a shRNA against kazrin (shKaz), fixed and stained with TRICT-phalloidin. The immunoblot confirming the depletion of kazrin from the used cell lines is shown in Fig. 46C. The images were acquired with a Zeiss LSM-780 confocal microscope using a 63x/1.4NA objective and the 32 PMT GaAsP array adjusted for detection of TRITC (red). **B.** Intensity plot profiles of cross sections from randomly chosen images of MEF cells as described above. The maximum intensity peak at the cortex (arrows) and the maximum intensity peak across the cell (arrowheads) are indicated. **C.** Graph representing the average +/- SEM of the internal TRICT-Phalloidin signal on small cytosolic structures normalized to the cortical signal. The maximum intensity peak across the cell (arrowheads) was divided for the maximum intensity peak at the cortex (arrows) (n = 5). Stress fibers were excluded from the analysis. The Student´s T-test p value was used to assess the statistical significance.

4.6.2 Endosomal Actin is Altered Upon Kazrin Depletion

To analyse the effects of kazrin depletion on endosomal actin, we decided to use MEF instead of Cos-7 cells because in MEFs, the internal actin structures appearing upon kazrin depletion did not collapse around the nucleus and therefore, their characterization as endosomal structures would be easier. For this purpose, untransfected cells, and cells expressing shKaz or shSCR were exposed to fluorescently labelled Tfn for 2 hours, fixed and stained for F-actin with TRICT-phalloidin. Analysis of endosomes in peripheral areas allowed evaluation of the impact of loosing kazrin on the associated actin. As previously seen in Cos-7 cells, the average endosome size significantly increased in kazrin-depleted MEFs (shKaz), relative to untransfected MEFs or MEFs expressing shSCR. Consequently, even though the average density of Tfn loaded per endosome was indistinguishable between the three cell types, the total amount of Tfn loaded on endosomes was higher in cells lacking kazrin (Fig 46A and B), as compared to the control cells. When the phalloidin signal per endosome was

measured, the actin associated per endosome appeared 2.5-fold higher in cells expressing shKaz, as compared to cells expressing shSCR or untransfected cell. This was in part the result of the increased endosomal size, but also, of an increase in actin density on Tfn loaded structures (Fig. 46A and B).

Together with the observation that kazrin interacts with WASH and the Arp2/3 complex and co-localizes with WASH and actin on endosomal membranes, we hypothesised that kazrin might act by negatively controlling WASH and Arp2/3-dependent actin polymerization, which in turn might inhibit retromer, retriever and sorting nexin-dependent recycling from the SEs to the PM.

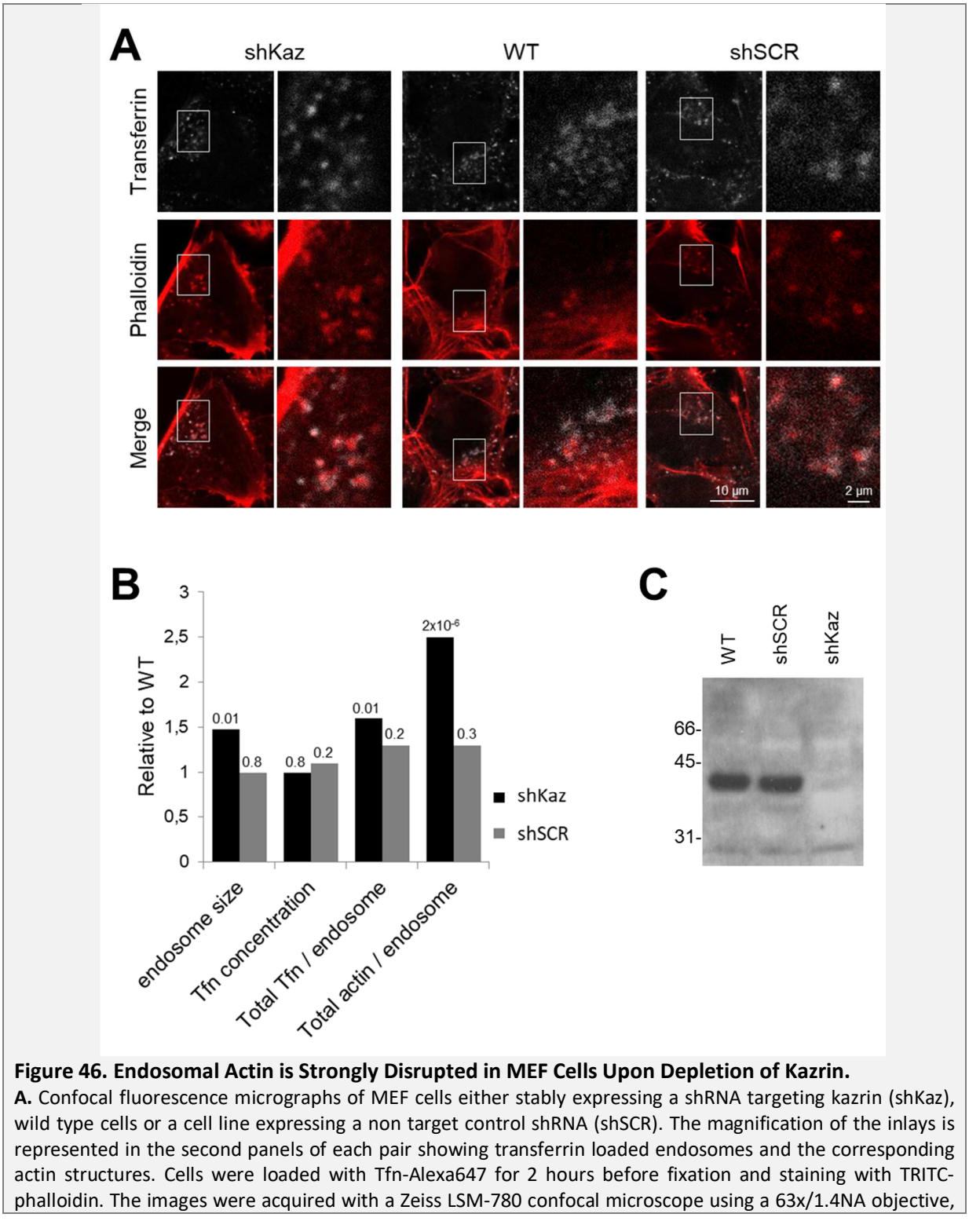

Figure 46. Endosomal Actin is Strongly Disrupted in MEF Cells Upon Depletion of Kazrin.
A. Confocal fluorescence micrographs of MEF cells either stably expressing a shRNA targeting kazrin (shKaz), wild type cells or a cell line expressing a non target control shRNA (shSCR). The magnification of the inlays is represented in the second panels of each pair showing transferrin loaded endosomes and the corresponding actin structures. Cells were loaded with Tfn-Alexa647 for 2 hours before fixation and staining with TRITC-phalloidin. The images were acquired with a Zeiss LSM-780 confocal microscope using a 63x/1.4NA objective,

the 32 PMT GaAsP array adjusted for detection of TRITC (red) and a conventional PMT for detection of Alexa-647 (far red). **B.** Graph representing the average endosome size, the average Tfn concentration per endosome, the total Tfn per endosome and the total actin per endosome, relative to the wild type cells, of 43 to 46 peripheral endosomes each, from three (WT, shSCR) or four (shKaz) cells analysed. The Student´s T-test p value was used to assess the statistical significance. **C.** Immunoblot of protein extract from MEF cells against kazrin (Abcam ab74114) of either wild type MEF or stable cell lines expressing a non target control shRNA (shSCR) or a shRNA against kazrin (shKaz). Proteins were extracted four days upon transduction and selection with puromycin. 18 µg of total protein were loaded per lane.

4.6.3 Overexpression of the Kazrin C C-terminus Induces Actin Polymerization on Endosomes

To investigate if kazrin C might actually be a negative regulator of endosomal actin polymerization and explore if this effect might depend on its interaction with the Arp2/3 complex and WASH, we decided to test the effect of overexpressing the C-terminal fragment of the wild type kazrin C, the 322-EEDADW-327 to AAAAAA mutant, and a C-terminal truncation lacking the amino acids 295 to 327, which includes the acidic peptide. Given the inhibitory effect on Tfn uptake of the overexpression of the kazrin C C-terminus, we used instead YFP-rab4 as an endosomal marker. One day upon transfection, cells were fixed and stained with TRITC-phalloidin.

In contrast to what we expected, we observed that overexpression of the kazrin C C-terminus significantly increased the amount of actin associated with rab4-endosomes. This effect did not seem to require the acidic peptide mediating direct interaction with the Arp2/3 complex, but it did require the very C-terminal fragment bearing the amino acids 295 to 327 (Fig. 47A and B), which is involved in the interaction with clathrin.

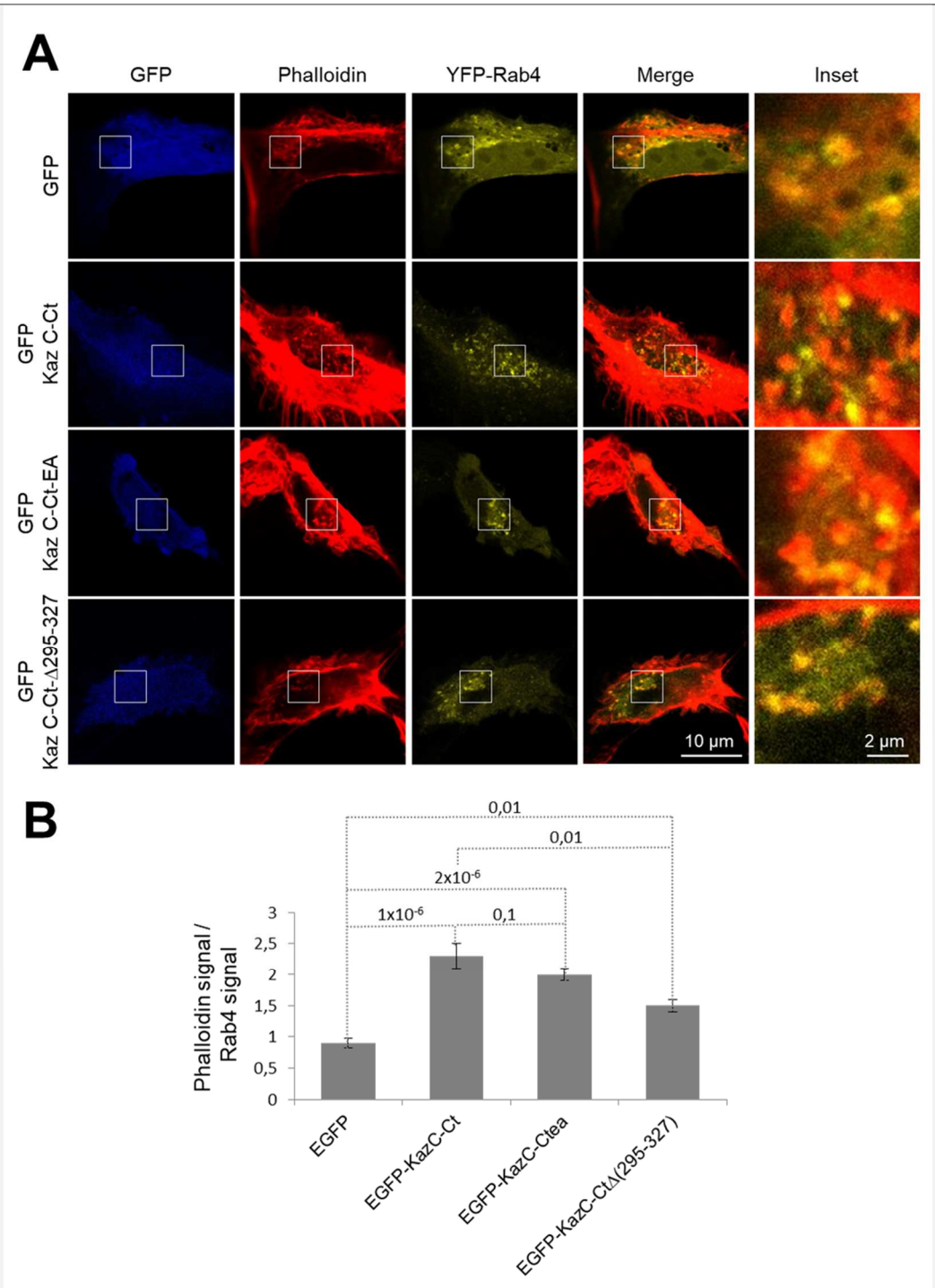

Figure 47. Overexpression of the C-terminus of Kazrin C Increases the Formation of Actin Structures on Rab4-Endosomes.

A. Maximum intensity projections of confocal fluorescence micrographs of MEF cells fixed one day upon transfection with YFP-rab4 and either GFP, GFP fused to the C-terminus of kazrin C (aa 161 to 327) (Kaz C C-t), the C-terminus of kazrin C with the final acidic peptide mutated in amino acids 322 - 327 EEDADW to AAAAAA (Kaz C-Ct-EA) or the C-terminus of kazrin C missing the final amino acids 295-327 including the acidic peptide (aa 322 - 327) (aa 161 - 294, Kaz C-ΔAc-Ct). The insets magnified in the last column show actin structures associated with Rab4. The images were acquired with a Zeiss LSM-780 confocal microscope using a 63x/1.4NA objective and the 32 PMT GaAsP array adjusted for detection of TRITC and conventional PMTs for detection of GFP and YFP. **B.** Graph representing the average +/- SEM of the TRICT-phalloidin signal normalized to the YFP-rab4 signal. The Student´s T-test p value was used to assess the statistical significance.

4.6.4 The C-terminus of Kazrin C Does Not Activate Arp2/3-dependent Actin Polymerization *In Vitro*

To investigate if kazrin C might act as a direct activator of Arp2/3-dependent actin polymerization, *in vitro* fluorimetry-based pyrene-actin polymerization assays were established in our laboratory. This assay measures the increase in fluorescence emission that results from the incorporation of monomeric pyrene-actin into filamentous polymers. When actin polymerization is followed in time in the absence of activators of the Arp2/3 complex (NPFs), there is a lag phase caused by the energy threshold required to overcome the unfavourable actin nucleation. When NPFs such as WASH or WASP are added to the mixture, they induce a conformational change in the Arp2/3 complex that mimics the actin nucleus, therefore overcoming this energetic threshold and eliminating the lag phase.

To investigate if kazrin C might act as a direct activator of the Arp2/3 complex, C-terminal kazrin C fragments, either the wild type isoform or mutants with the acidic peptide mutated or deleted, were added to a mixture containing pyrene-actin and purified Arp2/3, and actin polymerization was followed in a time course. As controls, samples only containing actin; actin and the Arp2/3 complex; or actin, the Arp2/3 complex and the N-WASP VCA domain were included. As observed in figure 48, actin alone or in the presence of the Arp2/3 complex polymerized slowly. Also as expected, the addition of the N-WASP VCA very much accelerated the initial actin polymerization rate. Thus, the solid grey line (B + WASH) shows the usual graph of activation by a VCA domain with a quick and heavy onset of actin polymerization until reaching a stable plateau. The grey dashed line (actin 10 % + Arp2/3) shows the negative control that contains only actin and Arp2/3 but no NPF. No effect on the polymerization rate of actin in the presence or absence of the Arp2/3 complex could be observed upon addition of the kazrin C C-terminal constructs, even when kazrin was added in much higher concentrations than the N-WASP VCA. The data indicated that the kazrin C C-terminus is unable to directly activate Arp2/3-dependent actin polymerization in the absence of other factors.

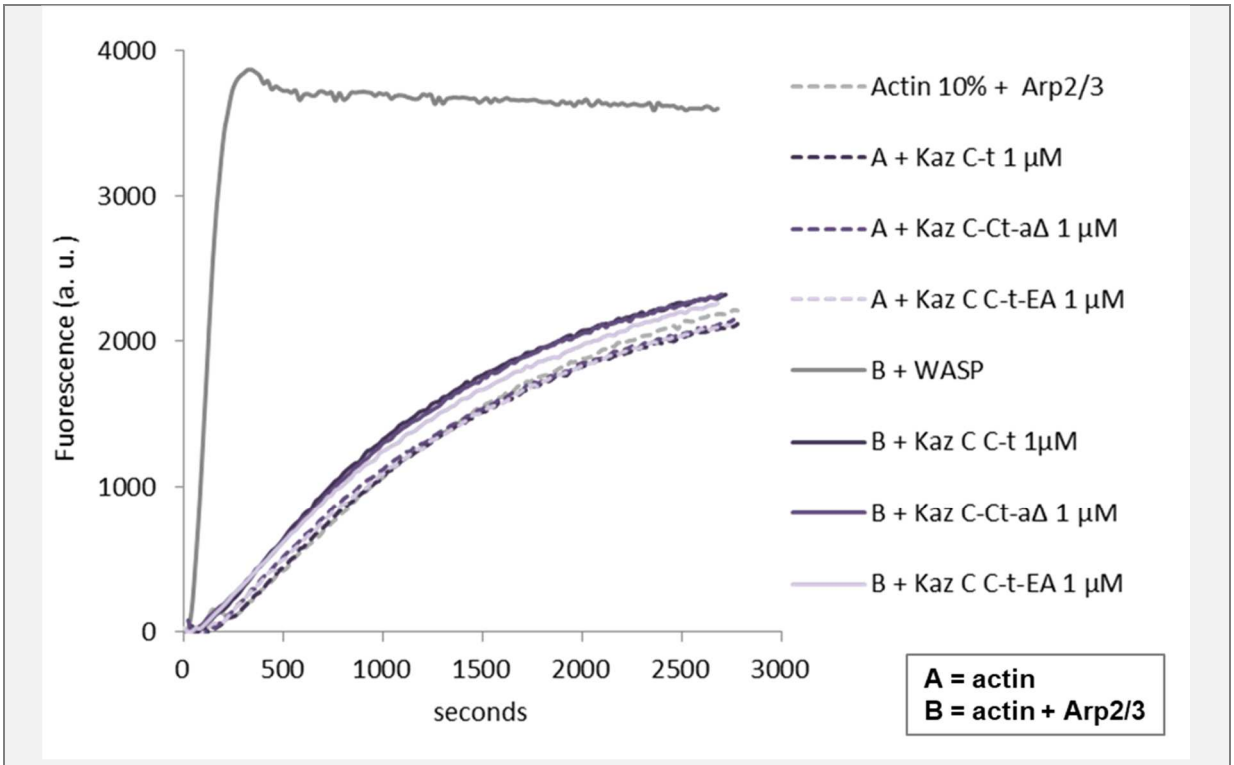

Figure 48. The C-terminus of Kazrin C Does Not Activate Arp2/3-Dependent Actin Polymerization.
Graph representing the fluorescence emitted by polymerized pyrene-actin over the reaction time. 1 µM G-actin (10 % pyrene-actin) was incubated in the presence (B) or absence (A) of 10 nM Arp2/3 complex, in the absence or presence of 185 nM of the VCA domain of the human N-WASP fused to GST or of the indicated concentration of the C-terminus of kazrin C (aa 161 to 327) (Kaz C C-t), the C-terminus of kazrin C missing the final amino acids 295 - 327 including the acidic peptide amino acids 322 - 327 (aa 161 - 294, Kaz C C-t-aΔ) or the C-terminus of kazrin C with the final acidic peptide mutated in amino acids 322 - 327 EEDADW to AAAAAA (Kaz C C-t-EA), fused to GST. a.u., arbitrary units.

4.6.5 The C-terminus of Kazrin C Does Not Alter the WASP or WASH VCA NPF Activity

Since kazrin was found to directly interact with the WASH PVCA domain (see Fig. 42D and E), we decided to also test the possibility that it might function as a regulator of the WASH activity. For that purpose, *in vitro* pyrene-actin polymerization assays in the presence of the WASH VCA or the N-WASP VCA as control were performed in the presence of increasing concentration of the kazrin C C-terminal fragment. The latest described Arp2/3 complex inhibitor arpin showed at a concentration of 100 nM a slight inhibitory effect and at 400 nM a clear reduction in polymerization velocity with the N-WASP VCA (Dang, Gorelik et al. 2013). Therefore, we decided to explore the effect of the kazrin C C-terminus in a similar range of concentrations. Up to 1 µM kazrin C C-terminus, we could not detect any effect on the NPF activity of neither the WASH (Fig. 49 lower graph) nor the N-WASP VCA domains (Fig. 49 upper graph).

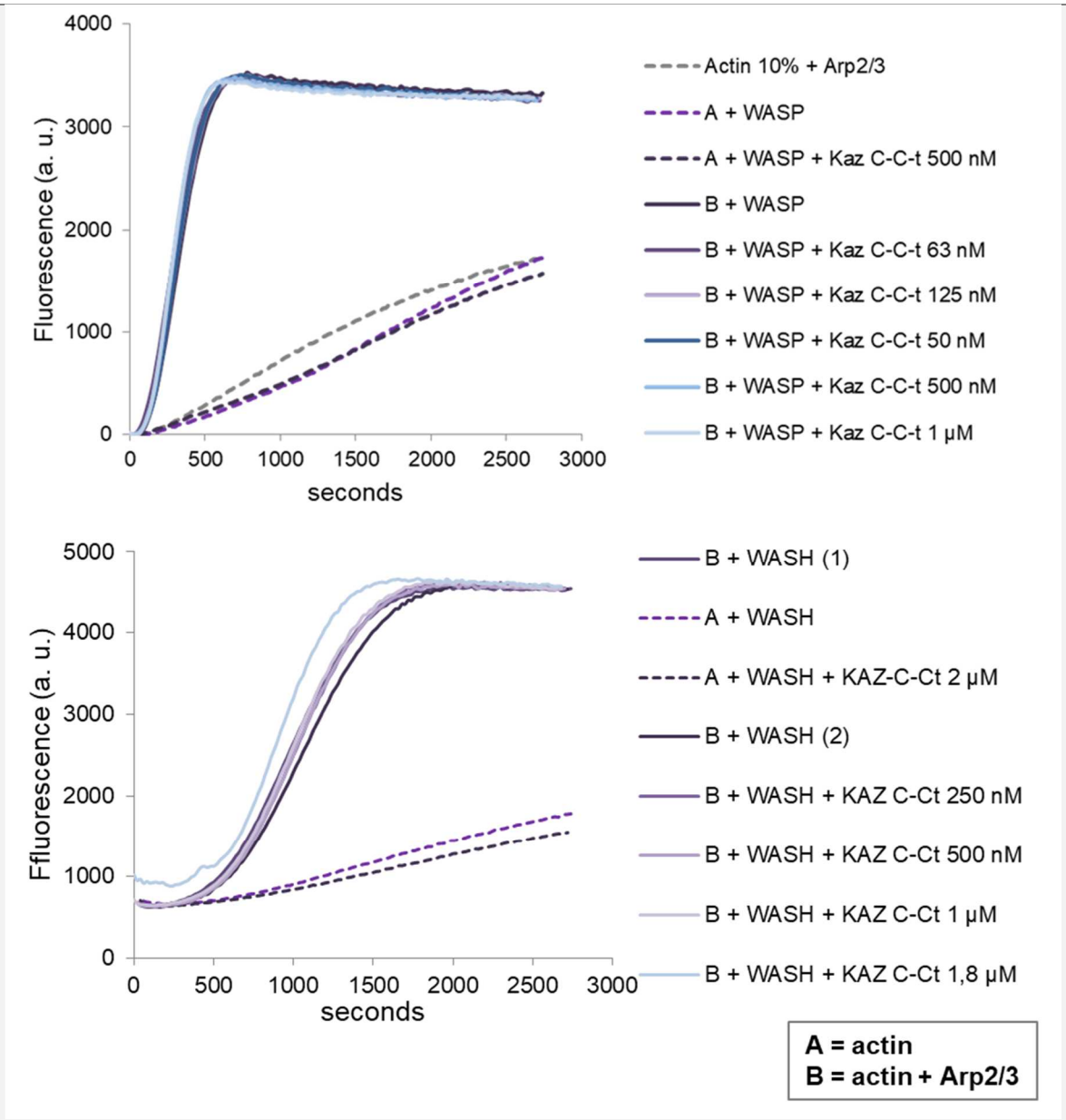

Figure 49. The C-terminus of Kazrin C Does Not Inhibit the NPF Activity of the WASH or N-WASP VCA.

Graphs representing the fluorescence emitted by polymerized pyrene-actin over the reaction time. 1µM G-actin (10 % pyrene-actin) was incubated in the presence (B) or absence (A) of 10 nM Arp2/3 complex, in the absence or presence of 185 nM of the VCA domains of the human N-WASP (upper graph) or WASH (lower graph) fused to GST, in the absence or presence of the indicated concentration of the C-terminus of kazrin C (amino acids 161 to 327) fused to GST. a.u., arbitrary units.

Discussion

5 Discussion

Our previous results showed that overexpression of human kazrin C inhibits the uptake step of Tfn via CME in Cos-7 cells. Further, the data indicated a possible interaction between kazrin and the clathrin-associated machinery from rat brain extracts, in particular, the CHC and the β-adaptin subunits of the AP clathrin adaptors. In addition, the preliminary data showed that depletion of kazrin from Cos-7 cells using siRNA technology accelerates CME and recycling of Tfn, but impairs arrival of internalized Tfn to the perinuclear ERC *in vivo*. Finally, immunofluorescence microscopy experiments indicated that endogenous kazrin might localize to SE together with rab4, γ-adaptin and EHD3.

During the course of this study, we confirmed that kazrin can be recruited to early SE and that it directly interacts with clathrin and the endosomal clathrin adaptor AP-1. On the other hand, we identified and characterized the interaction of kazrin with the Arp2/3 complex and its endosomal activator WASH. *In vivo*, we could observe partial co-localization of GFP-kazrin C with these proteins when overexpressed. Additionally, we confirmed that kazrin depletion prevents Tfn accumulation at the perinuclear region but increases Tfn uptake. Further, we demonstrated that kazrin depletion causes enlargement of early endosomal structures and accumulation of endosomal actin. Interestingly, we also see increased actin polymerization on endosomal membranes when the kazrin C-terminal fragment is overexpressed.

5.1 Kazrin C Regulates Endosomal Traffic

We extensively studied the effects of kazrin depletion on Tfn uptake and recycling. Under standard conditions, internalized Tfn is transported to the SE and the main portion of the receptor continues its journey to the perinuclear ERC before returning to the PM for another cycle of iron uptake. Only a small portion normally undergoes direct recycling from the SE or even earlier compartments.

We found that when kazrin was depleted, most Tfn failed to reach the perinuclear region even though TGN and ERC markers were still perinuclearly located. In our previous experiments using siRNAs to deplete kazrin, we could demonstrate using a biochemical assay with biotinylated Tfn, that this phenotype was not caused by preventing internalization. Instead, uptake and recycling of Tfn were slightly accelerated. With the results presented in this thesis, we could confirm these observations using a different technology, namely depletion of kazrin with a shRNA stably expressed in Cos-7 cells. Using this approach, we found that upon loss of kazrin, the overall Tfn uptake per cell area at steady state was increased, but Tfn accumulated within larger and more peripheral endosomes and was unable to reach the perinuclear region. Altogether, the results indicated an implication of kazrin at the sorting endosomal trafficking crossroad favouring transport towards the ERC versus the short loop recycling path to the PM. Whether depletion of kazrin also alters the degradative pathway to the late endosome and lysosomes or the retrograde transport to the TGN still remains to be elucidated.

Maturation of SE to LE has strongly been linked to the ability of endosomes to move towards the cell center, where lysosomes are often concentrated (Driskell, Mironov et al. 2007). The transport from SE to ERC also generally implies displacement of the cargo to the cell center, towards the ERC, but the nature of this displacement is not well understood. Either tubular subdomains emanating from

the SE mature to ERC, or *bona fide* transport intermediates are generated from SE and eventually fuse with pre-existing ERC. In context of the first hypothesis, the accumulation of enlarged peripheral endosomes in kazrin depleted cells could be the result of interfering with the endosome motility and maturation, which will cause the enlargement of the organelles because the endosomes would continuously accept incoming material from the PM and fail to move to the cell center. However, no obvious differences in the motility of YFP-rab4 endosomes has been detected in our life cell imaging experiments (data not shown). In the context of the second model, depletion of kazrin could be preventing the formation of transport intermediates to the ERC. The inefficient budding from the endosomes would then be the main cause of the enlargement of the peripheral endosomes. The formation of GFP-kazrin enriched subdomains on YFP-rab4a vacuolar endosomes and its interaction with clathrin and AP-1 (see bellow), coat components capable of generating transport intermediates from EE, may point into this direction.

In addition to its requirement for transport form SE to ERC, kazrin could also have a direct inhibitory effect on the internalization and the short-loop recycling pathway to the PM. However, we cannot rule out that acceleration of this pathway is an indirect consequence of the blocked transport from SE to ERC. Indeed, a slight acceleration of recycling has also been observed upon interference with the rab4b function (Perrin, Lacas-Gervais et al. 2013). Reciprocally, acceleration of endocytic uptake and the short loop recycling pathway might prevent arrival of Tfn to the recycling compartments. However, this being the primary effect of kazrin depletion could hardly explain why enlarged early endosomes accumulate in cells lacking kazrin. Extended studies on the fate of other endosomal cargo, including for instance integrins, GPCRs, Glut-1, Cholera toxin B or EGFR, are necessary to elucidate the pathways controlled by kazrin and to clarify its exact role within these transport routes.

To decipher what the primary function of kazrin C was in endosomal traffic, we made the effort to define where it is mainly localized. Initial immunofluorescence microscopy experiments with an affinity purified antibody recognizing the N-terminus of kazrin C suggested the recruitment of the endogenous protein to peripheral structures that could be loaded with Tfn, as well as some PM and nuclear staining, which has also been described previously (Groot, Sevilla et al. 2004, Sevilla, Nachat et al. 2008). Further, we found that endogenous kazrin C could be loaded on YFP-rab4a vacuolar structures, which have been previously shown to co-localize with the EE marker EEA1 (D'Souza, Semus et al. 2014). Consistent with these data, we found that endogenous kazrin co-fractionates with the SE markers EEA1 and HRS in OptiPrep gradients and that it shows some overlap with the TGN and EE clathrin adaptor AP-1, but only residually coincide with the PM clathrin adaptor AP-2. In addition, a portion of kazrin C fractionated at the heaviest OptiPrep gradient fraction, which might correspond to the nucleus or the recycling endosomes since it partially co-fraccionated with the rab11 binding protein EHD1.

The co-localization and formation of prominent GFP-kazrin C subdomains on YFP-rab4a vacuolar endosomes fits well into the emerging picture suggesting that kazrin works on SEs. Further supporting the localization of kazrin to SE is the observed co-localization of the GFP-kazrin C C-terminal construct on Tfn loaded endosomes with WASH and its co-localization with EEA1. Of notice is that WASH has previously been reported to strongly associate with EEs labelled with EEA1, (Derivery, Sousa et al. 2009, Duleh and Welch 2010). All results together provide a solid line of evidence suggesting that a fraction kazrin C is recruited to SE (Figure 60A).

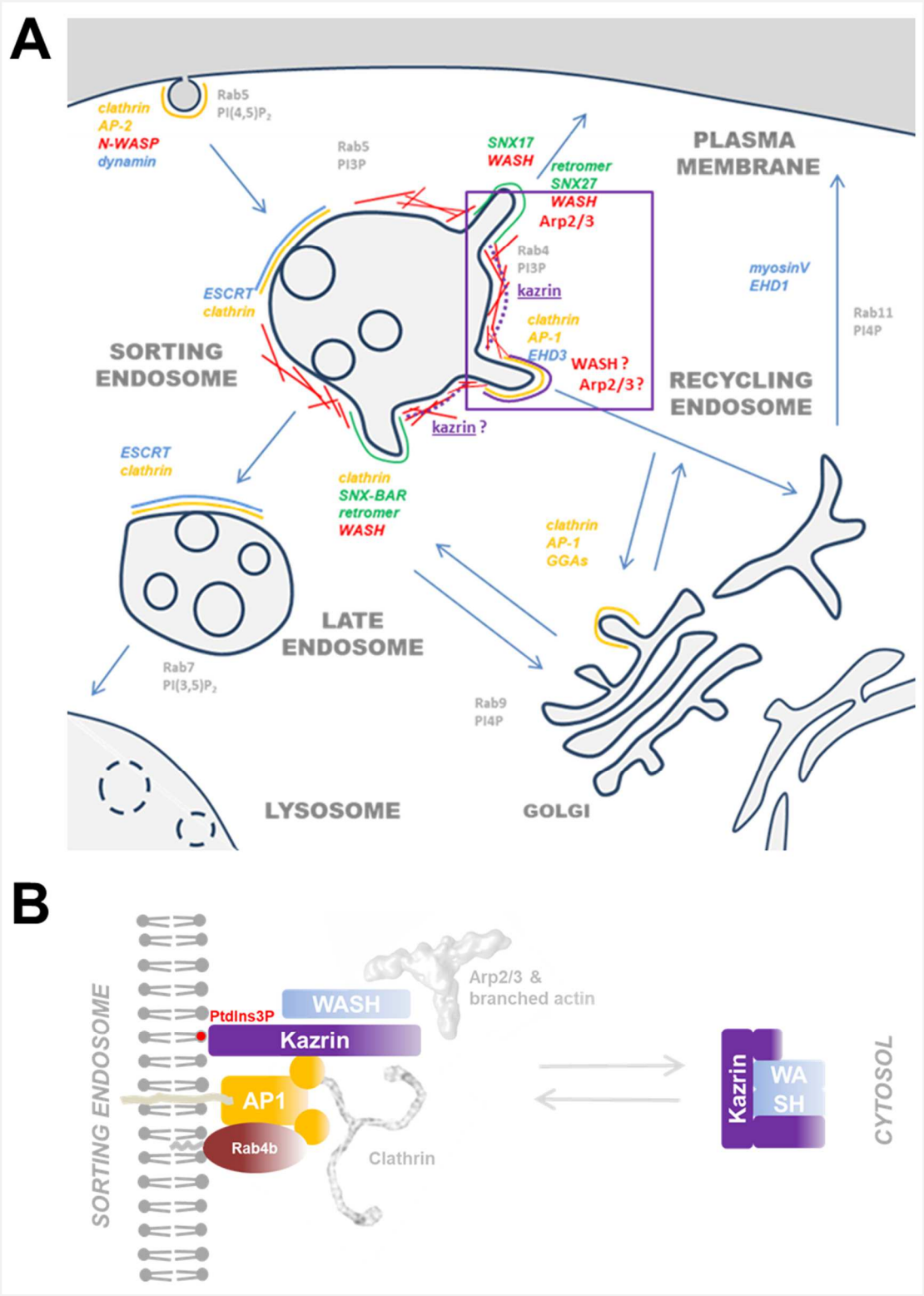

Figure 50. Kazrin in the Endocytic Pathways.

A. Putative model for the role of kazrin on endosomal traffic. Based on the molecular interactions of kazrin, the effects of kazrin depletion and overexpression, and the localization of endogenous kazrin and GFP-kazrin C constructs, we would like to propose that kazrin plays a role in the AP-1 and clathrin-dependent generation of transport intermediates between the SE and the ERC/RE. This is mainly based on the observations that 1. kazrin can be recruited to early endosomes, where it seems to co-localize with γ-adaptin; 2. its depletion interferes with transport of the TfnR to the ERC (similar to depletion of AP-1); and 3. kazrin directly interacts with AP-1 and clathrin. In this context, kazrin might simply work as a co-adaptor for AP-1 on endosomal membranes. However, based on the observations that GFP-kazrin C forms subdomains on SE that co-localize with cortactin, that it interacts with WASH, and that overexpression of its C-terminus increases endosomal

actin, we rather favour the hypothesis that kazrin might link endosomal clathrin subdomains to WASH-induced actin polymerization for the formation of transport intermediates to the ERC. The role of WASH in the formation of AP-1 and clathrin-dependent transport intermediates to the ERC has not been demonstrated at this point though. In addition, we need to demonstrate in triple labelling experiments that AP-1, kazrin and WASH co-localize in the same endosomal subdomains, and that depletion of kazrin interferes with this link. On the other hand, based on the effects of kazrin depletion and overexpression on endocytic uptake and recycling, we cannot discard that kazrin also has an inhibitory role on clathrin-dependent endocytosis at the PM and/or on the short recycling loop from the SE to the PM, which could be mediated by inhibition of WASH. However, no direct or indirect links between kazrin and the PM clathrin adaptor AP-2, or the machinery specifically involved in short-loop recycling pathways (retromer or rab4a) other than WASH could be established in the present work, suggesting that those effects might be indirect. **B. Putative molecular model for the kazrin recruitment and function on endosomal membranes.** Based on the observation that depletion of rab4b phenocopies the effects of depletion of kazrin on endosomal traffic (Perrin, Lacas-Gervais et al. 2013), and that both proteins directly interact with AP-1, we would like to propose that these proteins might work together in the formation of transport intermediates in this pathway. Activation of rab4b could recruit AP-1 as previously proposed (Perrin, Lacas-Gervais et al. 2013), which in turn could bring kazrin. Binding of kazrin to $PtdIns_3P$ on endosomal membranes could pre-activate kazrin and ensure that it interacts with AP-1 on the SE, but not at the TGN or in the cytosol. In this way, a double code composed of a small GTPase and a PtdInsP would ensure specificity as shown for other membrane traffic events. On endosomal membranes, kazrin could link AP-1 to WASH-induced actin polymerization. Experiments demonstrating the co-localization of kazrin with rab4b and γ-adaptin on the same endosomal subdomains would be required to initially test this hypothesis. The effect of rab4b or Vps34 depletion on the recruitment of kazrin would also need to be tested. On the cytosol, ”inactive” kazrin might not bind AP-1, but it might extensively interact with WASH and inhibit its NPF activity. This would explain why depletion of kazrin increments actin on endosomal membranes, presumably on retromer–associated domains. Pyrene-actin polymerization assays with the full-length WASH and kazrin would be required to test this hypothesis.

5.2 Functional and Physical Interaction of Kazrin with AP-1 and Clathrin

In order to dissect the molecular function of kazrin in endosomal trafficking, we decided to look for relevant interacting partners known to play important roles on SE. Our efforts did not identify interactions of kazrin C with any of the rab GTPases tested (rab4a, rab11, rab5 or rab7), neither in pull down assays with purified components nor in immunoprecipitations from cell extracts. Also, we could not detect any interaction with components of the versatile retromer or the ESCRT machinery. Instead though, our results provided striking evidence for specific and direct interactions of kazrin C with AP-1 and clathrin as well as WASH and the Arp2/3 complex.

Our preliminary data demonstrated that recombinant GST-kazrin C was able to pull down clathrin from rat brain extracts and that clathrin was pulled down with an antibody raised against the C-terminus of kazrin C. In this thesis, we confirmed the results with immunoprecipitations from Cos-7 cell extracts using the same antibody, as well as with a second unrelated commercially available antibody. Even though the GFP-trap precipitation experiments from cells overexpressing GFP-kazrin C were not conclusive due to unspecific binding in the control cells only expressing GFP, the pull down experiments with recombinant components purified from *E. coli* demonstrated that a specific and direct interaction of kazrin C with the terminal and linker domains of the CHC occurs *in vitro*. These pull down experiments also indicated that the main kazrin C clathrin binding site is situated within the last C-terminal 76 amino acids of kazrin C, which bear a putative clathrin binding motif (LEDLE, (Dell’Angelica 2001)). Point mutations in this motif are being performed to investigate its contribution to the interaction. The presented immunoprecipitation data strongly suggested that the kazrin/clathrin interaction can occur *in vivo*. However, complementary immunofluorescence

experiments showing co-localization of clathrin with endogenous kazrin or with moderately expressed functional GFP-kazrin C are needed to unequivocally demonstrate the interaction *in vivo*.

In addition to the interaction with clathrin, we also provided strong evidence supporting that kazrin C interacts with the clathrin adaptor AP-1. The γ-adaptin AP-1 subunit could be specifically co-precipitated with GFP-kazrin C in GFP-Trap immunoprecipitation assays. Further, immunofluorescence microscopy experiments showed co-localization of antibodies labelling endogenous γ-adaptin and kazrin on Tfn-loaded peripheral ensdosomal structures. Finally, the overexpressed GFP-kazrin C C-terminus extensively co-localized with the perinuclear γ-adaptin staining. The discrepancies between the localization of the endogenous protein in peripheral structures versus the GFP-kazrin C C-terminal fragment in the perinuclear region, where most of the γ-adaptin signal accumulates associated with the Golgi apparatus, might be caused by the overexpression of the C-terminus of kazrin C and/or by the release of the autoinhibitory kazrin C conformation observed in this construct, which might trigger promiscuos γ-adaptin binding. In this context, we showed in pull down experiments of recombinant fragments purified from *E. coli* that the C-terminus of kazrin C binds better to the γ-adaptin ear as compared to the full length kazrin C. This effect did not seem to be caused by missfolding of the full length construct, since WASH interacted better with the full length kazrin C than with the C-terminus. The preferred binding of γ-adaptin to the C-terminal fragment of kazrin, as compared to the full length protein, was also observed in GFP-Trap immunoprecipitations from Cos-7 cells overexpressing GFP-kazrin C constructs. The data suggested that the N-terminal fragment can in *cis* or *trans* inhibit binding of the C-terminal fragment of kazrin C to γ-adaptin. A detailed analysis with several GST-kazrin C N- and C-terminal truncations indicated that γ-adaptin binds to a kazrin C fragment comprised between amino acids 161 and 250, immediately upstream of the clathrin binding site. The autoinhibitory domain was mapped instead to a region comprised between the amino acids 71 to 148. How specific the binding of kazrin C to AP-1 is, still needs to be thoroughly analysed. We detected considerable interaction of kazrin C with the α-adaptin ear of the AP-2 complex in pull down experiments with purified components (data not shown). However, we failed to detect any co-localization or interaction between the α-adaptin with GFP-kazrin C or with the endogenous kazrin in immunofluorescence microscopy experiments or immunoprecipitations assays, respectively. Further we could only detect residual co-fractionation of kazrin and the α-adaptin on OptiPrep density gradients. Altogether, the data suggest the kazrin/AP-2 interaction is either not functionally relevant *in vivo* or only very transient in Cos-7 cells.

How the interaction between kazrin C and γ-adaptin might be controlled is an interesting question to be answered in the future. Data from I. Hernandez in the laboratory indicates that kazrin strongly and specifically interacts with $PtdIns_3P$, a phosphoinositide particularly enriched on early endosomes (Wallroth and Haucke 2018). It is therefore tempting to speculate that $PtdIns_3P$ binding to kazrin, maybe in concert with an endosomal GTPase, might trigger kazrin C interaction with AP-1 (Figure 60B). Such a double code mechanism would prevent unwanted binding of AP-1 and kazrin in the cytosol or the Golgi apparatus to occur. On the other hand, cooperative interaction of proteins with the terminal domain of clathrin and the ears of AP clathrin adaptors is a widespread feature of clathrin co-adaptors, which bring distinct cargo to AP/clathrin transport intermediates (Owen, Vallis et al. 2000, Brodsky, Chen et al. 2001). In this context, cargo binding to kazrin C could also contribute to regulate AP-1 binding. It will be very interesting in the future to try indentifying cargo recognized by a putative kazrin/AP-1 adaptor on early endosomal membranes. Of notice in this context is the described interactions of the N-terminus of kazrin with proteins present in desmosomes and tight

junctions such as the ARVCF-catenin and periplakin, respectively (Groot, Sevilla et al. 2004, Cho, Vaught et al. 2010). Thus, an interesting possibility is that kazrin regulates the internalization and turn over of cell-cell contacts. Consistent with this view overexpression of kazrin A in human keratinocytes alters the distribution of both, desmosomes and tight junctions (Sevilla, Nachat et al. 2008). Finally, we could also envision that post translational modifications such as phosphorylation or ubiquitination might influence kazrin C autoinhibition in response to extracellular or intracellular signals.

Even though the recruitment and function of AP-1 was originally associated with the formation of CCVs at the Golgi apparatus (Nakatsu, Hase et al. 2014), the recruitment of AP-1 to early endosomal membranes is well established. Structural studies have localized AP-1 and clathrin on tubular structures emanating from EE, and AP-1 co-localizes with EEA1 in untransfected cells and with dynamic GFP-rab4a tubular structures (Stoorvogel, Oorschot et al. 1996, D'Souza, Semus et al. 2014). Indeed, a detailed pathway for the recruitment of AP-1 on early endosomal membranes has been described, emanating from rab4a to the small GTPase Arl1, which in turn recruits the Arf GEF BIG1 and BIG2, and activates the small GTPases Arf1 and Arf3 (D'Souza, Semus et al. 2014). Further, the γ-adaptin ear directly interacts with rabaptin-5, a rab5 and rab4 effector (Shiba, Takatsu et al. 2002), and rab4 and AP-1-dependent budding from endosomal membranes has been reconstituted *in vitro* (Pagano and Spiess 2005). Similar to depletion of kazrin C, depletion of Arl1 or Arf1/3 results in the enlargement of early endosomes (D'Souza, Semus et al. 2014), altogether suggesting that AP-1 and kazrin C might operate together mediating budding from SE. Interestingly though, we have found that kazrin C patches on the endosomes rarely coincide with YFP-rab4a engrossed microdomains, presumably containing AP-1 and clathrin, but they rather appeared adjacent. Further, we failed to demonstrate any interaction with rab4a. The experimental conditions used did not allow us to follow membrane budding from the YFP-rab4a endosomes and therefore, the possibility exists that kazrin C is recruited on the YFP-rab4a tubules as the rab4a signal fades away and therefore, the interaction is too transient to be biochemically demonstrated. Under these conditions, the overlapping signal on steady micrographs might be residual, as it has been observed for endocytic proteins sequentially recruited at the PM (Kaksonen, Sun et al. 2003, Kaksonen, Toret et al. 2005, Taylor, Perrais et al. 2011). Alternatively, kazrin might be specifically recruited to tubular structures generated by rab4b but not rab4a, the isoform we have used in our GST-rab4 pull downs and YFP-rab4 experiments *in vivo*. Rab4b is a rab4 isoform encoded by a different gene , which is also recruited to early endosomes. The phenotype resulting from depletion of rab4b even more closely recapitulates that observed upon kazrin depletion, as compared to rab4a depletion. Namely, depletion of rab4b prevents transport of Tfn from SE to ERC, while it accelerates Tfn uptake and Tfn short-loop recycling (Perrin, Lacas-Gervais et al. 2013). On the contrary, rab4a induced budding seems to be responsible for the fast recycling of Tfn to the PM, together with NECAP2 (van der Sluijs, Hull et al. 1992, Chamberland, Antonow et al. 2016). Interestingly, the rab4b pathway also relies on the recruitment of AP-1 but in contrast to rab4a, which indirectly recruits AP-1 via the activation of Arl1 and Arf1/3, rab4b directly interacts with the γ-adaptin ear (Chamberland, Antonow et al. 2016). To finally elucidate which pathway kazrin participates in, we need to image GFP-kazrin C dynamics in concert with AP-1 on rab4a and rab4b endosomes and analyse the tubulation activity induced by these two rab GTPases in the presence or absence of kazrin.

Finally, it is interesting to mention in the context of membrane budding and endosomal subdomain organization that kazrin E contains 3 tandem repeats of the so called SAM domain (Steril Alpha Motif), a protein feature that can induce the formation of head to tail polymers. The SAM domains of

kazrin E have indeed been shown to form rod-shaped polymers of about 100-200 nm in length, which can be visualize by negative staining on EM grids (Knight, Leettola et al. 2011). If kazrin polymers are formed upon binding to cellular membranes, kazrin could induce membrane deformation by molecular crowding (Chen, Atefi et al. 2016) or generate membrane subdomains where other proteins might be trapped. In addition, in silico analysis, predicts that kazrin A, E and F bear N-terminal BAR domains, banana shape structures capable of detecting and inducing curvature, with well established roles in membrane budding. Altogether, strongly pointing to roles of the kazrin isoforms in membrane traffic.

5.3 Functional and Physical Interaction of Kazrin with WASH and the Arp2/3 Complex

Besides the described interaction of kazrin C with clathrin and the AP-1 complex, in this thesis we provided solid evidence for an interaction between kazrin C and the Arp2/3 complex and its endosomal activator WASH. Published data already pointed to a functional relation between kazrin and the actin cytoskeleton. Kazrin was found on actin rich structures (Groot, Sevilla et al. 2004, Sevilla, Nachat et al. 2008) and overexpression of kazrin A in keratinocytes disrupted the actin cytoskeleton and lowered the ammount of polymerrized actin (Sevilla, Nachat et al. 2008). The presence of an acidic peptide in the C-terminus of kazrin C, conserved in known activators and inhibitors of the Arp2/3 complex, prompted us to explore the possibility that kazrin might interact with the actin filament nucleator. Indeed, we observed that the recombinant purified C-terminal fragment of wild type kazrin C, but not a mutant bearing point mutations to alanines in the acidic strech, interacted with purified Arp2/3 complex. GFP-Trap pull down experiments from Cos-7 cells expressing GFP alone, GFP-kazrin C or its N- and C-terminal truncations confirmed the interaction between the C-terminus of kazrin C and the Arp2/3 complex. However, deletion of the acidic strech did not completely prevent binding of GFP-kazrin C to the Arp2/3 complex in Cos-7 cell extracts, indicating that other proteins might stabilize the interaction *in vivo*. Also consistent with the functional cooperation of kazrin C and the Arp2/3 complex, we could demonstrate co-localization of GFP-kazrin C with the endogenous p41 subunit of the complex in immunofluorescence microscopy experiments and we observed co-localization of GFP-kazrin C with the branched actin marker cortactin on vacuolar YFP-rab4 endosomes.

The localization of kazrin C on SE, the observation that the interaction of kazrin C with the Arp2/3 complex might be stabilized by other proteins *in vivo*, and the co-localization of kazrin C with cortactin, whose endosomal recruitment is at least in part WASH-dependent (Derivery, Sousa et al. 2009, Ohashi, Tanabe et al. 2011) led us to investigate the possible interaction of kazrin C with WASH. Indeed, we found that WASH robustly co-precipitates with GFP-kazrin C, but not with GFP, in GFP-Trap immunoprecipitation experiments from extracts of Cos-7 cells overexpressing the indicated constructs. The interaction seemed to be specific for WASH, since GFP-kazrin C did not co-precipitate significant amounts of N-WASP or spire in similar experiments. Pull down experiments also indicated that both, the N- and the C-terminus of kazrin C contributed to the interaction with WASH, albeit the interaction with the C-terminus seemed stronger. Confirming the interaction of kazrin C with WASH *in vivo*, we also found that the C-terminal fragment of kazrin C fused to GFP co-localized with endogenous WASH on Tfn-loaded endosomal subdomains. Finally, pull downs with recombinant purified components demonstrated extensive, direct interactions betweeen kazrin C and the N- and C-terminal domains of WASH.

At this point, we wanted to investigate whether kazrin influences endosomal actin polymerization. Our initial hypothesis was that kazrin might be an inhibitor of WASH-induced Arp2/3 dependent actin polymerization. This hypothesis was based in 3 observations: 1) Overexpression of kazrin A (which encodes a protein similar to kazrin C but with a short N-terminal extension) inhibits actin polymerization when overexpressed in keratinocytes (Sevilla, Nachat et al. 2008); 2) kazrin depletion seemed to favour the short loop recycling from SE to the PM, which mainly relies on retromer, retriever and WASH, and 3) similar to the Arp2/3 complex inhibitor Arpin (Dang, Gorelik et al. 2013), kazrin has and acidic peptide that binds to the Arp2/3 complex, but lacks the WH2 domains required to induce actin polymerization. Consistent with this hypothesis, we indeed observed that depletion of kazrin in Cos-7 cells increases the amount of filamentous actin associated to EEs. However, when we overexpressed the C-terminus of kazrin C, we observed an unexpected increase of endosomal actin as compared to cells overexpressing GFP. Mutation of the acidic stretch responsible for the interaction with the Arp2/3 complex did not abolish this effect indicating that kazrin does not act as a direct activator of the Arp2/3 complex. An alternative hypothesis would be that kazrin C might trigger actin polymerization on endosomal membranes by recruiting active WASH to AP-1 enriched subdomains. This hypothesis would actually fit well with the observation that the kazrin C enriched subdomains on YFP-rab4 endosomal membranes co-localize with cortactin, a marker of branched actin recruited to endosomes by WASH (Derivery, Sousa et al. 2009). How could we reconcile all these observations?

We have seen that binding of kazrin to WASH is strong, does not seem to be autoinhibited and it implicates binding to both, the N- and C-terminal portions of WASH. It is therefore possible that kazrin C binds to the N- and C-terminal portions WASH in the cytosol and acts as a clamp that inhibits the otherwise constitutively active WASH (Duleh and Welch 2010), preventing ectopic actin polymerization, similar to what has been shown for the WAVE and the WASH complexs (Jia, Gomez et al. 2010). In this context, depletion of kazrin could have a general effect, increasing WASH-induced actin polymerization on endosomal membranes by allowing recruitment of constitutively active WASH to retromer enriched subdomains via Fam21. This effect could in turn accelerate the short loop retromer and/or retriever recycling pathway. On the other hand, kazrin can bind to AP-1 but not retromer on endosomal membranes. Further, GFP-kazrin C-enriched subdomains on YFP-rab4 vacuolar endosomes co-localizes with cortactin. In this context, one might envision that upon release of the kazrin autoinhibition on endosomal membranes, kazrin could release the WASH VCA domain, while still binds to its N-terminus, and link WASH-induced actin polymerization to endosomal AP-1 and clathrin subdomains to assist fission of SE to ERC transport intermediates (Figure 60B). This is an exciting hypothesis that would explain why the constitutively activated C-terminus of kazrin C can trigger actin polymerization on endosomal membranes, while overexpression of the full length kazrin might sequester and inhibit WASH.

Much work needs to be done now in order to test this hypothesis. We need to demonstrate that the effects observed upon overexpression or depletion of kazrin on the endosomal actin are indeed dependent on WASH and the Arp2/3 complex. Further, we would need to show that WASH is associated not only with retromer- and retriever-enriched endosomal subdomains, but also with AP-1, and that this association depends on kazrin. *In vitro* data demonstrating that kazrin can inhibit WASH-induced actin polymerization when the full length proteins, WASH and kazrin C, are used in the pyrene-actin polymerization assay is still missing. Also *in vitro*, we will have to show that the C-terminus of kazrin can link active WASH to γ-adaptin or the clathrin terminal domain. It is maybe pertinent to mention in this context that our pyrene-actin polymerization assay results, showing that

the C-terminus of kazrin can neither inhibit nor activate WASH-induced actin polymerization, are not inconsistent with the final hypothesis. Thus, if kazrin works as a clamp to inhibit WASH, as it has been proposed for the WAVE complex (Chen, Borek et al. 2010), kazrin will only inhibit WASH if the full length NPF is used in the assay. On the other hand, according to our hypothesis, the C-terminus of kazrin C would not activate WASH-induced actin polymerization *in vitro per se*, but rather serve to localize WASH on AP-1 and clathrin enriched subdomains *in vivo*. Still, we also need to understand the relevance of kazrin binding to the Arp2/3 complex. Experimental evidence indicates that at least two acidic peptides from WASP or WAVE are needed to promote Arp2/3 dependent actin nucleation (Padrick, Doolittle et al. 2011). In this context, the acidic peptide of kazrin could contribute to WASH induced actin polymerization on endosomal membranes. Alternatively, kazrin could hold together WASH and Arp2/3 in an inactive cytosolic complex which could then be more efficiently recruited and activated on particular cellular locations. In spite we still lack all these evidence to support our final hypotheis, the data strongly point to a functional relevant interaction between kazrin and the endosomal machinery controlling actin polymerization.

Based on our present results, the working model proposed for the function of kazrin in endosomal traffic would be as follows: 1) In the cytosol, kazrin binds to WASH and maybe the Arp2/3 complex and maintain them inactive; 2) Binding of kazrin to endosomal $PtdIns_3P$ and rab4b, would release kazrin´s autoinhibition, liberate the WASH VCA domain and allow binding to AP-1, which in turn also binds to rab4b; 3) rab4b, AP-1, kazrin and WASH would then cooperate to generate transport intermediates that travel between SE and ERC (Figure 60B).

5.4 Kazrin and Human Disease

Defects in endocytosis are strongly linked to a number of human diseases, including neurodegenerative and metabolic pathologies or cancer. Still, in many cases, the molecular bases explaining the contribution of endocytic traffic alteration to the development of human syndromes are not well understood and as a consequence, opportunities for therapeutically intervention are surely being lost. We initially decided to seek for human endocytic proteins accessory to the essential core machinery in the hope that those might lead to putative therapeutic targets for neurodegeneration or cancer. Our initial screen for proteins that when overexpressed interfere with CME led to the identification of kazrin. In the curse of this thesis, we have been able to provide evidence suggesting that kazrin might indeed be a accessory protein to the AP-1 and clathrin endocytic core machinery, which regulates endosomal recycling by also controlling WASH-induced actin polymerization. Evidence that links kazrin to different human disease is now also starting to emerge.

Kazrin, has the ability to regulate adhesion and differentiation of keratinocytes and can bind to periplakin, a protein found in the epidermal cornified envelope, localized to desmosomes (Groot, Sevilla et al. 2004, Sevilla, Nachat et al. 2008). Kazrin is up-regulated during keratinocyte differentiation and it is included in the cornified envelope, a cell layer essential for the integrity of the epidermis and mucosa (Groot, Sevilla et al. 2004). Overexpression of kazrin in keratinocytes leads to changes in morphology and impaired assembly of intercellular junctions, an effect that might be linked to its role in endocytic traffic (Sevilla, Nachat et al. 2008). Altogether, the data suggest that disregulation of kazrin might lead to dermatological diseases. Consistent with this view, expression of kazrin is downregulated in biopsies from oral and genital Lichen Planus lesions as compared to

controls. Lichen Planus is a chronic recurrent inflammatory disease affecting both skin and mucosa, mainly in oral and/or genital regions (Danielsson, Ebrahimi et al. 2017).

On the other hand, the *Xenopus* kazrin A binds to ARVCF (Cho, Vaught et al. 2010), a member of the catenin family and one of the genes deleted in the Velo Cardiac Facial Syndrome in humans, a relatively common human disorder with phenotypic features including cleft palate, conotruncal heart defects and facial dysmorphology. Consistent with this view, depletion of kazrin in *Xenopus* embryos induced malformation of the craneofacial cartilage, similar to depletion of ARVCF. The defects installed upon kazrin or ARVCF depletion seemed to derive from defective neural crest migration, which might in turn be caused by altered regulation of cell-cell contacts (Cho, Lee et al. 2011).

In addition to the phenotypes directly link to the alterations in the expression levels of kazrin, our data places kazrin at the crossroad controlling endocytic recycling pathways with important implications in neurodegeneration and cancer. Thus, a strong link between mutations in the WASH complex or retromer with a number of inherited neuropathies already exists. For example, autosomal dominant mutations in Strumpellin causes hereditary spastic paraplegia (Valdmanis, Meijer et al. 2007) and recessive mutations in SWIP results in inherited intellectual disability (Ropers, Derivery et al. 2011) and are also linked to late-onset Alzheimer disease (LOAD)(Vardarajan, Bruesegem et al. 2012). On the other hand, also retromer is strongly related to LOAD and Parkinson. Early works demonstrated a link between LOAD and VPS35 using model guided microarrays and showed that depletion of VPS35 increases the production of the neuropathogenic Amyloid β peptide (Aβ)(Small, Kent et al. 2005). Recently, it was shown that interfering with VPS35 in hippocampal neurons increases the levels of the neuropathogenic Aβ concomitant with enhanced co-localization of Amyloid Precursor Protein (APP) with β-site Amyloid precursor protein Cleaving Enzyme 1 (BACE1)(Bhalla, Vetanovetz et al. 2012). In addition, interfering with retromer function in heterozygous mice for different retromer subunits causes hypocampal dysfunction, neurodegeneration and accumulation of Aβ in the brain (Muhammad, Flores et al. 2008). Further, VPS35 haplo insufficiency increases AD neuropathology in a mouse model (Wen, Tang et al. 2011). Finally, genetic analysis also links SNX1 and VPS26 to AD (Rogaeva, Meng et al. 2007). Regarding the involvement of WASH and retromer in Parkinson, it has been shown that the VPS35 D620N mutation causing a rare form of autosomal-dominant Parkinson disease specifically disrupts the interaction of VPS35 with WASH (McGough, Steinberg et al. 2014). Since depletion of kazrin accelerates the short-loop recycling pathway, interfering with its activity might alleviate diseases associated to missfunction of the retromer and WASH-dependent pathways.

Finally, depletion of kazrin seems to interfere with the long-loop recycling pathway through the rab11 compartment, a recycling route strongly linked to cell invasion and metastasis. Endocytic traffic impacts cell migration and invasion in different ways. The effects observed upon depletion of kazrin on neural crest cell behavior (Sevilla, Rana et al. 2008, Cho, Lee et al. 2011) might be explained by its primary function in endocytic recycling of cargo relevant for cell migration and invasion. Thus, in the context of cancer and metastasis, expression of a dominant negative GDP-bound inactive rab11-S25N, decreases invasion of MDA-231 breast cancer cells induced by hypoxia. Further, the amplification of the rab25 locus, a constitutively active epithelial-specific member of the rab11 family, occurs in approximately half of ovarian and breast cancers and RNAi-mediated depletion of rab25 inhibits tumor growth *in vitro* and *in vivo*. In ovarian cancer cells, rab25 directly interacts with the cytoplasmic tail of the β1-integrin to promote the delivery of the $\alpha_5\beta_1$-integrin to pseudopodial tips during cell migration and invasion. Moreover, RCP, a rab25 efector, coordinates recycling of $\alpha_5\beta_1$-

integrin and EGFR to membrane protrusions during fibronectin-mediated cell migration, and increased RCP-mediated $\alpha_5\beta_1$-integrin and EGFR recycling correlates with enhanced invasion and metastasis (Zhang, Liu et al. 2009). Thus, in this context, interfering with kazrin functions could potentially lower the probability of cancer metastasis. Interestingly, kazrin F is highly expressed in cervix cancer tissues compared with the adjacent noncancerous tissues and promotes cell proliferation, colony formation, migration and invasion in HeLa and the Cervix cancer cell line C33A by suppressing apoptosis and facilitating epithelial-to-mesenchymal transition (EMT). Kazrin F expression upregulated by the micro RNA miR-186 influences malignancy in prostate cancer, endometrial- and medulloblastomas (Myatt, Wang et al. 2010, Lv, Kim et al. 2012, Erdmann, Kaulke et al. 2014, Liu, Wang et al. 2017).

In summary, kazrin might be directly or indirectly linked to a number of human diseases and therefore it might have a potential as a therapeutic target. In this context, one can envision that deciphering in the future the differential expression, physiological functions and interactomes of specific kazrin isoforms in healthy and pathological situations will have an important biomedical interest.

Conclutions

6 Conclutions

- ✓ Kazrin can be recruited to the EE and partially co-localizes there with actin, Arp2/3 and cortactin.
- ✓ Kazrin depletion increase endosomal actin and alters the actin cytoskeleton.
- ✓ Kazrin C C-terminus overexpression increases endosomal actin.
- ✓ Kazrin directly interacts with the Arp2/3 complex via its C-terminal acidic peptide.
- ✓ Kazrin directly interacts with WASH.
- ✓ The purified Kazrin C C-terminus does not activate Arp2/3-dependent actin polymerization *in vitro*.
- ✓ The purified Kazrin C C-terminus does not alter the WASH or WASP VCA NPF activity *in vitro*.
- ✓ Kazrin directly interacts with the CHC TD.
- ✓ The interaction of Kazrin C and the CHC TD requires the sequence comprised between amino acids between amino acids 250 to 289 of Kazrin C
- ✓ Kazrin directly interacts with the β1- and γ-adaptin subunits of the AP-1 complex.
- ✓ The Kazrin C interaction with γ-adaptin requires the sequence comprised between amino acids 161 to 250 of Kazrin C and it is autoinhibited in cis or trans by the Kazrin C sequence comprised between amino acids 71 to 148.
- ✓ Kazrin depletion interferes with transport towards the ERC and slightly accelerates the short loop recycling path to the PM.

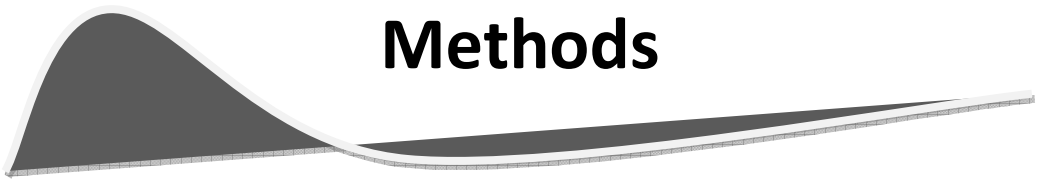

Methods

7 Methods

7.1 Cell Culture

7.1.1 Cell Culture of *Escherichia coli*

E. coli cell culture was done according to standard protocols (Sambrook and Russell 2001). The DH5α strain was used for molecular cloning and plasmid amplification. The BL21 strain was used for the expression of GST- or 6xHis-fusion proteins (see chapter 7.3.3 Protein Purification). Cells were grown at 37°C in LB media (0.5% yeast extract, 1% bacto tryptone, 0.5% NaCl) supplemented with 50 mg/l ampicillin or kanamycin (Sigma-Aldrich) when plasmid selection was required. *E. coli* strains were stored at -80°C in LB media bearing 10 % glycerol.

7.1.2 Cell Culture of Mammalian Cells

Mammalian cell lines were grown in DMEM medium (10% (v/v) FCS, 100 u/ml Penicillin, 100 µg/ml Streptaminicin, 2 mM L-Glutamine; Thermo Fisher) at 37°C in a humidified atmosphere containing 5% CO_2. The medium was renewed every 2 - 5 days. About 10, 5 or 2.5 ml of DMEM was used for plates of 10, 6 or 3.5 cm in diameter, respectively. For subcultivation, the cells were grown until they reached confluency around 80% in 10 cm plates. Cells were resuspended by incubating at 37^{o}C up to 5 minutes (depending on the cell type) in the presence of 1 ml PBS (137 mM NaCl, 2.7 mM KCl, 10 mM Na_2HPO_4 , 2 mM KH_2PO_4, pH 7.4) containing 0.05 % (v/w) Trypsin and 0.02 % (v/w) EDTA (Thermo Fisher). Cells were diluted in DMEM, as appropriate for each experiment, and seeded in the adequate plates.

7.1.3 Freezing and Thawing of Mammalian Cells

Cells were grown in 10 cm culture dishes in DMEM medium up to 70 – 90 % confluency and trypsinized as usual. After centrifugation at 300 g for 10 minutes, the cell pellet was resuspended in 0.5 - 1 ml DMEM medium supplemented with 10 % DMSO (Sigma-Aldrich) and transfered to cryogenic vials (Nuc CryoTubes, Sigma-Aldrich). The cryotubes were frozen slowly in a freezing container (Mr. Frosty, Sigma-Aldrich) filled with isopropanol (-1°C/minute) at -80°C, and the next day, the cells were transferred to liquid nitrogen for long-term storage. To thaw the cells, the tubes were transferred into a 37°C water bath followed by resuspension in 10 ml DMEM medium for cultivation.

7.1.4 Cell Lines

Cos-7 cells were obtained from the DSMZ, Germany. MEFs, HEK293 and HEK293**T** were kindly provided by Anna Aragay, IBMB-CSIC Barcelona.

Cos-7: African green monkey kidney fibroblast-like cells; tissue: kidney; morphology: fibroblasts; adherent. Cells express the simian virus 40 (SV40) large T antigen.

ATCC: COS-7 (ATCC CRL-1651).

MEF: Mouse embryonic fibroblasts; tissue: embryo; morphology: fibroblasts; adherent.

ATCC: MEF (CF-1) (ATCC SCRC-1040).

HEK293: Human embryonic kidney cells; tissues: embryonic kidney; morphology: epithelia; adherent.

ATCC: 293 [HEK293] (ATCC CRL1573).

HEK293T: Human embryonic kidney cells; tissues: embryonic kidney; morphology: epithelia; adherent; cells constitutively express the simian virus 40 (SV40) large T antigen.

ATCC: 293T/17 [HEK 293T/17] (ATCC CRL-11268).

7.2 Genetic Techniques

7.2.1 Transformation of *Escherichia coli*

Transformation of *E. coli* strains was performed according to standard protocols (Sambrook and Russell 2001). The $CaCl_2$ protocol was used to transform intact plasmids in BL21 cells and DH5α cells. Electroporation was used to transform DNA ligations in DH5α cells, using a BioRad Gene Pulser Xcell electroporation system (BioRad) and compatible 2.5 mm cuvettes (Cell Projects Ldt).

7.2.2 DNA and RNA Techniques and Plasmid Construction

7.2.2.1 Standard Molecular Biology Techniques: Amplification and Purification of Plasmids in *E. coli*, Enzymatic Restriction of DNA, PCRs, Agarose Gels, Purification of DNA Fragments, and DNA Sequencing

Standard DNA manipulations, such as polymerase chain reaction (PCR), gel electrophoresis, enzymatic digestion, DNA ligation, and plasmid purification were performed as described, using standard techniques (Sambrook and Russell 2001). Standard PCRs were performed with a DNA polymerase with proof reading activity (Vent polymerase, NEB) and a TRIO-thermoblock (Biometra GmbH). Oligonucleotides were synthesized by Fisher Scientific. Restriction endonucleases were obtained from New England Biolabs. DNA was purified using PCR or gel extraction kits from Macherey-Nagel. Analytical agarose gel electrophoresis was performed using Sub-Cell cells from Bio-Rad Laboratories. Cloning of DNA fragments into plasmid vectors was performed with the T4 DNA

ligase (New England Biolabs). Plasmids were amplified and purified from *E. coli* with a Nucleospin plasmid purification kit according to the manufacturers protocol (Macherey-Nagel). DNA sequencing was performed by Macrogen Inc.

7.2.3 Construction of Plasmids for this Study

A list of plasmids used in this study is included in Table I. When plasmids were constructed during the course of this project, the strategy used for the construction is defined bellow. Recombinant DNA manipulations were carried out using standard protocols (Sambrook and Russell 2001). A list of oligonucleotides used for the corresponding clonings, specifying their nucleotide sequence, is included in Table II. All restriction enzymes were obtained from New England Biolabs and restriction digests were done following the suggested standard conditions for the appropriate enzyme combinations. Ligations were performed using T4 DNA ligase according to the suppliers standard protocol in T4 DNA ligase buffer for 10 hours at room temperature followed by heat inactivation of the ligase at 65°C for 10 minutes. The constructs were confirmed by sequencing (Macrogen Inc).

Plasmid Name	Insert, Description	Back-bone	Source	Reference	Primer	acces. #
pACT2-adaptin α	Rattus norvergicus AP2-A2	pACT2	n.a.	n.a.	n.a.	831
pACT2-adaptin β2	Rattus norvergicus AP2-B1	pACT2	n.a.	n.a.	n.a.	832
pcDNA3.1	empty mammalian expression vector, CMV promotor, no tag.	pcDNA3.1	Invitrogen life technologies	#A-150228	n.a.	812
pcDNA3.1-Rab1(myc)	Rab1-myc	pcDNA3.1	Matin Lowe	n.a.	n.a.	999
pcDNA5´-Rab11a (myc)	Rab11a (myc)	pcDNA5´	Peter van der Sluijs	n.a.	n.a.	986
pCMV-dR8.2 dvpr	Packaging plasmid for Lentivirus	n.a.	C. Gallego	Addgene plasmid # 8455	n.a.	1016
pCMV-hsCLTC	human clathrin heavy chain CLTC = CHC17 = CLH7 = KIAA0034	pCMV-SPORT6	Open Biosystems	MHS1010-925173	n.a.	1017
pCMV-LifeAct-RFP	LifeAct-RFP	n.a.	C. Gallego /IBIDI #60102	IBIDI #60102	n.a.	n.a.
pCMV-VSV-G	Envelope plasmid for Lentivirus	n.a.	C. Gallego	Addgene plasmid # 8454	n.a.	n.a.
pcSralpha296(pX2)EDH1	EHD1 + myc	pX2	Steve Kaplan	n.a.	n.a.	995
pcSralpha296(pX2)EDH3	EHD3 + myc	pX2	Steve Kaplan	n.a.	n.a.	996
pDsRed1-cortactin	cortactin + dsRed	pDsRed1-N1	M. Kaksonen	GenBank Acc. NM_001184740	n.a.	
pEGFP-C1-Rab1	Rab1	pEGFP-C1	Martin Lowe	n.a.	n.a.	990
pEGFP-C1-Rab11a	Rab11a	pEGFP-C1	Mitsundri Fukuda	n.a.	n.a.	998
pEGFP-C1-Rab4a	Rab4a	pEGFP-C1	Mitsundri Fukuda	n.a.	n.a.	997
pEGFP-C2	GFP	pEGFP-C2	BD Biosciences clontech's Living Colors	GenBank Acc. #: U57607	n.a.	743

pEGFP-C3	GFP	pEGFP-C3	BD Biosciences clontech's Living Colors	GenBank Acc. #: U57607	n.a.	744
pEGFP-Rab11	GFP + Rab11	pEGFP	Peter van der Sluijs	n.a.	n.a.	985
pEGFP-Rab11S25NI (DN)	GFP + Rab11S25NI (DN)	pEGFP	Peter van der Sluijs	n.a.	n.a.	983
pEGFP-Rab5	GFP + Rab5a	pEGFP	Peter van der Sluijs	n.a.	n.a.	982
pEYFP-Rab4a	YFP + Rab4a	pEYFP	Peter van der Sluijs	n.a.	n.a.	984
pEYFP-Rab4N121I (DN)	YFP + Rab4N121I (DN)	pEYFP	Peter van der Sluijs	n.a.	n.a.	981
pGDAGH-adaptin γ	human adaptin γ	n.a.	n.a.	n.a.	n.a.	833
pGEX-4T-2	GST	pGEX-4T-2	GE Healthcare	pGEX-4T-2 #28-9545-50	n.a.	457
pGEX-5X-3	GST	pGEX-5X-3	GE Healthcare	pGEX-5X-3 #28-9545-55	n.a.	25
pGEXRab11a	GST + Rab11a	pGEX	Peter van der Sluijs	n.a.	n.a.	979
pGEXRab27a	GST + Rab27a	pGEX	Peter van der Sluijs	n.a.	n.a.	980
pGEXRab4a	GST + Rab4a	pGEX	Peter van der Sluijs	n.a.	n.a.	977
pGEXRab5a	GST + Rab5a	pGEX	Peter van der Sluijs	n.a.	n.a.	978
pGFP-KazC	GFP + kazrin C from humans (KIAA1026), aa1-327	pEGFP-C2	B. Schmelzl	(Schmelzl and Geli 2002)	n.a.	746
pGFP-KazC-Ct	GFP + kazrin C C-terminus, aa 161-327	pEGFP-C2	this study	n.a.	#597, #598	727
pGFP-KazC-Ct251	GFP + kazrin C C-terminus spliced, aa251-327	pEGFP-C2	this study	n.a.	#599, #598	728
pGFP-KazC-Ct-aΔ	GFP + kazrin C C-terminus minus the acidic peptide, aa 161-294	pEGFP-C2	this study	n.a.	#597, #601	730
pGFP-KazC-Ct-EA	GFP + kazrin C C-terminus acidic peptide mutated to Alanines, (aa 161-327)-(322-EEDADW-327, AAAAAA)	pEGFP-C2	this study	n.a.	#597, #1137	1200
pGFP-KazC-Ct-kΔ	GFP + kazrin C C-terminus minus the poly K, (aa 161-327)-(281-288)	pEGFP-C2	this study	n.a.	1. (#599, #603), 2. (#602, #604)	731
pGFP-KazC-Nt	GFP + kazrin C N-terminus FERM like domain, aa 1-176	pEGFP-C2	this study	n.a.	n.a.	726
pGFP-KazC-Nt148	GFP + kazrin C N-terminus, aa1-148	pEGFP-C2	B. Schmelzl	n.a.	subcloned form plasmid #746	817
pGST-β1-ear	GST + human AP1 Adaptin B1 ear (aa 709-939)	pGEX-5X-3	this study	n.a.	#1134, #1135	1208
pGST-CHC17-TDLk	GST + human CHC17-aa1-483 (CHC TD + linker)	pGEX-5X-3	this study	n.a.	#1017, #1125, #1126	1190
pGST-γ-Adaptin-ear	GST + human AP1 Adaptin G1	pGEX-5X-3	this study	n.a.	#1132,	1207

	ear (aa 702-925)				#1133	
pGST-hB24	GST + kazrin C, human gene KIAA1026	pGEX-4T-2	B. Schmelzl	n.a.	#595, #604	747
pGST-KazC-Ct	GST + kazrin C C-terminus, aa 161-327	pGEX-5X-3	this study	n.a.	#597, #598	694
pGST-KazC-Ct251	GST + kazrin C C-terminus spliced, aa251-327	pGEX-5X-3	this study	n.a.	#599, #598	695
pGST-KazC-Ct289	GST + kazrin C C-terminus afte poly K, aa289-327	pGEX-5X-3	this study	n.a.	#600, #604	696
pGST-KazC-Ct-aΔ	GST + kazrin C C-terminus minus the acidic peptide, aa 161-294	pGEX-5X-3	this study	n.a.	#597, #601	697
pGST-KazC-Ct-EA	GST + kazrin C C-terminus acidic peptide mutated to Alanines, (aa 161-327)-(322-EEDADW-327, AAAAAA)	pGEX-5X-3	this study	n.a.	#597, #1137	1198
pGST-KazC-Ct-KA	GST + kazrin C C-terminus (aa 161-327) -(281-KRKKKK-286-AAAAAA)	pGEX-5X-3	this study	n.a.	1. (#1141, #1140 (KA)), 2. (#597, #598)	1201
pGST-KazC-Ct-KR	GST + kazrin C C-terminus (aa 161-327) -(281-KRKKKK-286-RRRRRR)	pGEX-5X-3	this study	n.a.	1. (#1139, #1138), 2. (#598, #597)	1202
pGST-KazC-Ct-kΔ	GST + kazrin C C-terminus minus the poly K, (aa 161-327)-(281-288)	pGEX-5X-3	this study	n.a.	1. (#599, #603), 2. (#602, #604)	698
pGST-KazC-EA	GST + kazrin C acidic peptide mutated to Alanines, (aa 1-327) -(322-EEDADW-327, AAAAAA)	pGEX-5X-3	this study	n.a.	#595, #1137	1206
pGST-KazC-KA	GST + kazrin C, (aa 1-327) -(281-KRKKKK-286-AAAAAA)	pGEX-5X-3	this study	n.a.	1. (#1141, #1140), 2. (#595, #598)	1204
pGST-KazC-KR	GST + kazrin C , (aa 1-327) -(281-KRKKKK-286-RRRRRR)	pGEX-5X-3	this study	n.a.	1. (#1139, #1138), 2. (#595, #598)	1203
pGST-KazC-Nt	GST + kazrin C N-terminus FERM like domain, aa 1-176	pGEX-5X-3	this study	n.a.	#595, #596	693
pGST-KazC-Nt(aa148-327)	GST + kazrin C N-terminus, aa148-327	pGEX-4T-2	this study	n.a.	n.a.	820
pGST-KazC-Nt(aa161-250)	GST + kazrin C N-terminus, aa161-250	pGEX-5X-3	this study	n.a.	#597, #1017	1186
pGST-KazC-Nt(aa71-327)	GST + kazrin C N-terminus, aa71-327	pGEX-5X-3	this study	n.a.	#598, #1119	1185
pGST-KazC-Nt250	GST + kazrin C N-terminus aa1-250	pGEX-5X-3	this study	n.a.	#595, #1017	1183
pGST-KazC-Nt294	GST + kazrin C N-terminus aa1-294	pGEX-5X-3	this study	n.a.	#595, #601	1182
pGST-KazC-Nt70	GST + kazrin C N-terminus aa1-70	pGEX-5X-3	this study	n.a.	#595, #1018	1184
pGST-Kaz-Ct-WA	GST + kazrin C C-terminus (aa 161-327) -(W327A)	pGEX-5X-3	this study	n.a.	#597, #1136	1199
pGST-KazC-WA	GST + kazrin C Tryptophan aa327 mutated to Alanin, (aa1-327)-(W327A)	pGEX-5X-3	this study	n.a.	#595, #1136	1205

pGST-N-WASP-VCA	GST + N-WASP aa402-505 from humans	pGEX-5X-3	this study	n.a.	#1127, #1128	1191
pGST-Rn.AP2.A2.ear	GST + AP2.A2 ear alfa-adaptin ear from Rattus norvergicus variant A2 (aa 710 to 940)	pGEX5X-3	M.I.Geli	n.a.	n.a.	715
pGST-Rn.AP2.B1.ear	GST + AP2.B1 ear beta-adaptin ear from Rattus norvergicus variant A2 (aa 713 to 952)	pGEX5X-3	M.I.Geli	n.a.	n.a.	716
pGST-WASH1-N	GST + WASH1 from humans, aa1-301	pGEX-5X-3	this study	n.a.	#1120, #1121	1187
pGST-WASH1-PVCA	GST + WASH1 PolyP + VCA domain from humans, aa302-468	pGEX-5X-3	this study	n.a.	#1122, #1123	1188
pGST-WASH1-VCA	GST + WASH1 VCA domain from humans, aa361-468	pGEX-5X-3	this study	n.a.	#1193, #1124	1189
pHIS-kazrin C	6xHistidine + kazrin C from humans (KIAA1026), aa1-327	pQE11	this study	n.a.	#595, hB24.Pst1.984U	1168
pKLO.1_shKaz	Sigma MISSION shRNA targeting all 3 mouse Isoforms of kazrin and human kazrin.	pLKO.1	Sigma Mission Libary 2007	cloneID TRCN0000182832	n.a.	n.a.
pLKO.1_CV/_SCR	Sigma MISSION pLKO.1-puro Non-Mammalian shRNA non target control.	pLKO.1	Sigma Mission Libary 2007	SHC002	n.a.	n.a.
pLKO.1_shRNA	Vector for shRNAs with puromycin resistence	pLKO.1	Sigma Mission Libary 2007	https://doi.org/10.1016/j.cell.2006.01.040	n.a.	n.a.
pLL3.7-GFP	empty shRNA vector for Lentivirus, only GFP	pLL3.7	J. Lüders	http://www.nature.com/ng/journal/v33/n3/full/ng1117.html	n.a.	n.a.
pN-WASP	N-WASP complete cDNA from humans	pBlueScript	Harvard plasmid ID data base	Gene ID 8976	n.a.	1192
pQE11	6 x histidine	pQE11	QIAGEN	pQE-11	n.a.	29
pWASH1	WASH1 complete cDNA from humans	pBlueScript	Harvard plasmid ID data base	Gene ID 100287171	n.a.	1193
n.a. = not available						

Table I. Plasmids.

#oMIG	Name, Restriction Sites	Sequence
595	hB24.BamHI.EcoRI.1D	aaccaaggatccccgaattcATGAAGGAGATGTTGGCGAAGG
596	hB24.XhoI.SmaI.528U	aaccaactcgagcccgggTCAGCCATTGAGCACCGTCTC
597	hB24.BamHI.EcoRI. 481D	aaccaaggatccccgaattcATGCCCAAGCGGCATTCCCTC
598	hB24.XhoI.SmaI.984U	aaccaactcgagcccgggTCACCAGTCCGCGTCCTC
599	hB24.BamHI.EcoRI. 751D	aaccaaggatccccgaattcATGCACTCCCTCTGCAACGGC
600	hB24.BamHI.EcoRI. 865D	aaccaaggatccccgaattcATGGGATTCGGCTCCATC
601	hB24.XhoI.SmaI.882U	aaccaactcgagcccgggTCAGATGGAGCCGAATCCCAT
602	hB24.SphI.865D	aaccaagcatgcATGGGATTCGGCTCCATC

603	hB24.SphI.840U	aaccaagcatgcTTGGTCTTCAAGATCCTCTAGTG
604	pEGFP-C2.1417U	ttatctagatccggtgg
611	RnAP2.B1.BamHI.EcoRI.2137D	aaccaaggatccccgaattcATGGGGATAGGCATGGCAGG
612	RnAP2.A2.BamHI.EcoRI.2101D	aaccaaggatccccgaattcATGGGCTCTGAAGACAACTTTGCC
613	RnAP2.B1.XhoI	aaccaactcgagTCATTAGTTTTTCAAAATGCTGTCGTAGACC
614	RnAP2.A2XhoI	aaccaactcgagTCATTAGAACTGTTCCGACAGCAATTC
1017	hB24.XhoI.SmaI.750U	aaccaactcgagcccgggTCAGGCATACAGCTGCTGCATC
1018	hB24.XhoI.SmaI.210U	aaccaactcgagcccgggTCATGTCCGGTGTCGAGGGGAC
1119	hB24.BamHI.EcoRI.1D.211D	aaccaaggatccccgaattcATGACACTGGAGAGCCGCGAG
1120	WASH.1D.EcoRI.BglII	Aaccaaccgaattccagatctctatgactcctgtgaggatg
1121	WASH.903U.HindII.XhoI	ccaaccaagcttctcgagctatagtaccccatcttgtag
1122	WASH.904D.EcoRI.BglII	aaccaagaattccagatctctatgacagcaccaccaccaccc
1123	WASH.1404U.HindII.XhoI	ccaaccaagcttctcgagctacgattcccagtcgtcctc
1124	WASH.1081D.EcoRI.BglII	aaccaagaattccagatctctatgccctccggtggccgggcc
1125	CHC17.1D.BamHI	aaccaaggatccccatggcccagattctgccaattc
1126	CHC17.1449U.HindIII.XhoI.	Ccaaccaagcttctcgagctacgttagcccttaggtacacactaag
1127	N-WASP.1204D.EcoRI.XhoI	sequence missing in collection list
1128	N-WASP.1515U.XhoI	ccaaccctcgagctagtcttcccactcatcatc
1132	AP1.G1.2134D.EcoRI.BamHI	aaccaagaattccggatccctatggatattgctgcaggcatcccc
1133	AP1.G1.2478U.HindII.XhoI	ccaaccaagcttctcgagtcattgccaggactgaggggg
1134	AP1.B1.2130D.EcoRI.BglII	aaccaagaattccagatctctatgtatgtggcccccaaagc
1135	AP1.B1.2820U.HindII.XhoI	ccaaccaagcttctcgagtcagttcttgaggatggtctc
1136	hB24.XhoI.SmaI.984U.W327A	aaccaactcgagcccgggTCACGCGTCCGCGTCCTCCTC
1137	hB24.XhoI.SmaI.984U.EEDADW.AAAAAA	aaccaactcgagcccgggTCACGCGGCCGCGGCCGCCGC TATGTAATAATCAGGGGC
1138	hB24.841D.PolyK-R	AGACGGAGAAGGAGGAGAGACAGGATGGGATTCGGCTCCATC
1139	Hb24.864U.polyK-R	CCTGTCTCTCCTCCTTCTCCGTCTTTGGTCTTCAAGATCCTC
1140	hB24.841D.PolyK-A	GCAGCGGCAGCGGCGGCAGCGGCGATGGGATTCGGCTCCATC
1141	Hb24.864U.polyK-A	CGCCGCTGCCGCCGCTGCCGCTGCTTGGTCTTCAAGATCCTC
n.a.	hB24.Pst1.984U	AaccaaCC ctgcag TCACCAGTCCGCGTCCTC

Table II. Oligonucleotides.

pGST-KazC-Ct-kΔ (#698), pGST-KazC-Nt (#693), pGST-KazC-Ct (#694), pGST-KazC-Ct251 (#695), pGST-KazC-Ct-EA (#1198), pGST-Kaz-Ct-WA (#1199), pGST-KazC-EA (#1206), pGST-KazC-WA (#1205), pGST-KazC-Nt250 (#1183), pGST-KazC-Nt294 (#1184), pGST-KazC-Nt70 (#1184)

The DNA fragments were obtained by PCR using pGFP-KazC (#746) as template with the corresponding oligonucleotides (see Table I. (primers). and II. (oligonucleotides)). The obtained DNA fragments and the target plasmid for insertion, pGEX5X-3 (#25), were digested using the restriction enzymes BamHI and XhoI. pGST-γ-Adaptin-ear (#1207)

The DNA fragment was obtained by PCR using pGDAGH-Adaptin-γ (#833) as template with the corresponding oligonucleotides (see Table I. (primers). and II. (oligonucleotides)). The obtained DNA

fragment and the vector, pGEX5X-3 (#25), were digested using the restriction enzymes BamHI and XhoI.

pGST-KazC-Ct251 (#695)

The DNA fragment was obtained by PCR using pGFP-KazC (#746) as template with the corresponding oligonucleotides (see Table I. (primers). and II. (oligonucleotides)). The obtained DNA fragment and the target plasmid for insertion, pGEX5X-3 (#25), were digested using the restriction enzymes BamHI and SmaI.

pGST-KazC-Nt (#693)

The DNA fragment was obtained by PCR using pGST-KazC-Nt (#693) as template with the corresponding oligonucleotides (see Table I. (primers). and II. (oligonucleotides)). The obtained DNA fragment and the vector, pEGFP-C2 (#743), were digested using the restriction enzymes EcoRI and SmaI.

pGST-hB24 (#747)

The DNA fragment was obtained by PCR using pGFP-KazC (#746) as template with the corresponding oligonucleotides (see Table I. (primers). and II. (oligonucleotides)). The obtained DNA fragment and the vector, pGEX-4T-2 (#457), were digested using the restriction enzymes BamHI and SmaI.

pGST-KazC-Ct-kΔ (#698)

The DNA fragments were obtained using a double PCR strategy using pGFP-KazC (#746) as template with the the oligonucleotides #599 and #603, and #602 and #604. A second PCR using the obtained DNA fragments was done using the oligonucleotides #599 and #604. The final DNA fragment and the vector, pGEX5X-3 (#25), were digested using the restriction enzymes BamHI and SmaI.

pGFP-KazC-Ct (#727)

The DNA fragment was obtained by PCR using pGST-KazC-Ct (#694) as template with the corresponding oligonucleotides (see Table I. (primers). and II. (oligonucleotides)). The obtained DNA fragment and the vector, pEGFP-C2 (#743), were digested using the restriction enzymes EcoRI and SmaI.

pGFP-KazC-Ct251 (#728)

The DNA fragment was obtained by PCR using pGST-KazC-Ct251 (#695) as template with the corresponding oligonucleotides (see Table I. (primers). and II. (oligonucleotides)). The obtained DNA

fragment and the vector, pEGFP-C2 (#743), were digested using the restriction enzymes EcoRI and SmaI.

pGFP-KazC-Ct-aΔ (#730)

The DNA fragment was obtained by PCR using pGST-KazC-Ct-aΔ (#697) as template with the corresponding oligonucleotides (see Table I. and II.). The obtained DNA fragment and the vector, pEGFP-C2 (#743), were digested using the restriction enzymes EcoRI and SmaI. Ligation was done using T4 DNA ligase (NEB), according to the supplier standard protocol (see above).

pGFP-KazC-Ct-kΔ (#731)

The DNA fragment was obtained by PCR using pGST-KazC-Ct-kΔ (#698) as template with the corresponding oligonucleotides (see Table I. (primers). and II. (oligonucleotides)). The obtained DNA fragment and the vector, pEGFP-C2 (#743), were digested using the restriction enzymes EcoRI and SmaI.

pGFP-KazC-Ct-EA (#1200)

The DNA fragment was obtained by PCR using pGST-KazC-Ct-EA (#1198) as template with the corresponding oligonucleotides (see Table I. (primers). and II. (oligonucleotides)). The obtained DNA fragment and the target plasmid for insertion, pEGFP-C2 (#743), were digested using the restriction enzymes EcoRI and SmaI.

pHIS-kazrin C (#1168)

The DNA fragment was obtained by PCR using pGFP-KazC (#746) as template with the corresponding oligonucleotides (see Table I. (primers). and II. (oligonucleotides)). The obtained DNA fragment and the vector, pQE11 (#29), were digested using the restriction enzymes BamHI and PstI.

pGST-WASH1-N (#1187), pGST-WASH1-PVCA (#1188), pGST-WASH1-VCA (#1189)

The DNA fragment was obtained by PCR using pWASH1 (#1193) as template with the corresponding oligonucleotides (see Table I. (primers). and II. (oligonucleotides)). The obtained DNA fragment and the vector, pGEX5X-3 (#25), were digested using the restriction enzymes BglII and XhoI.

pGST-N-WASP-VCA (#1191)

The DNA fragment was obtained by PCR using pN-WASP (#1192) as template with the corresponding oligonucleotides (see Table I. (primers). and II. (oligonucleotides)). The obtained DNA fragment and the vector, pGEX5X-3 (#25), were digested using the restriction enzymes BglII and XhoI.

pGST-CHC17-TDLk (#1190)

The DNA fragment was obtained by PCR using pCMV-hsCLTC (#1017) as template with the corresponding oligonucleotides (see Table I. (primers). and II. (oligonucleotides)). The obtained DNA fragment and the vector, pGEX5X-3 (#25), were digested using the restriction enzymes BamHI and XhoI.

pGST-β1-ear (#1208)

The DNA fragment was obtained by PCR using the gene encoding Adaptin β1 (HS, HS.CD000431697 Genebank accesion CVO12936) as template with the corresponding oligonucleotides (see Table I. (primers). and II. (oligonucleotides)). The obtained DNA fragment and the vector, pEGFP-C2 (#743), were digested using the restriction enzymes XhoI and BglII.

pGST-Rn.AP2.A2.ear (#715)

The DNA fragment was obtained by PCR using pACT2-adaptin α (#831) as template with the corresponding oligonucleotides (see Table I. (primers). and II. (oligonucleotides)). The obtained DNA fragment and the target plasmid for insertion, pGEX5X-3 (#25), were digested using the restriction enzymes BamHI and XhoI.

pGST-Rn.AP2.B1.ear (#716)

The DNA fragment was obtained by PCR using pACT2-Adaptin β2 (#832) as template with the corresponding oligonucleotides (see Table I. (primers). and II. (oligonucleotides)). The obtained DNA fragment and the target plasmid for insertion, pGEX5X-3 (#25), were digested using the restriction enzymes BamHI and XhoI.

pGST-kazrin C-KA (#1200)

The DNA fragment with the mutation was obtained by site-directed mutagenesis applying the overlap extension PCR. In the first step, two fragments containing the mutations were obtained using pGFP-KazC (#746) as template with the primers #595/#1141 or #1140/#598. The two DNA products were then used as template in the second step with the flanking oligonucleotides #595/#598. The final DNA fragment bearing the mutations and the vector, pGEX5X-3 (#25), were digested using the restriction enzymes XhoI and BamHI.

pGST-kazrin C-Ct-KA (#1201)

The DNA fragment with the mutation was obtained by site-directed mutagenesis applying the overlap extension PCR. In the first step, two fragments containing the mutations were obtained using

pGFP-KazC (#746) as template with the primers #597/#1141 or #1140/#598. The two DNA products were then used as template in the second step with the flanking oligonucleotides #597/#598. The final DNA fragment bearing the mutations and the target plasmid for insertion, pGEX5X-3 (#25), were digested using the restriction enzymes XhoI and BamHI.

pGST-kazrin C-KR (#1203)

The DNA fragment with the mutation was obtained by site-directed mutagenesis applying the overlap extension PCR. In the first step, two fragments containing the mutations were obtained using pGFP-KazC (#746) as template with the primers #595/#1139 or #1138/#598. The two DNA products were then used as template in the second step with the flanking oligonucleotides #595/#598. The final DNA fragment bearing the mutations and the vector, pGEX5X-3 (#25), were digested using the restriction enzymes XhoI and BamHI.

pGST-kazrin C-Ct-KR (#1202)

The DNA fragment with the mutation was obtained by site-directed mutagenesis applying the overlap extension PCR. In the first step, two fragments containing the mutations were obtained using pGFP-KazC (#746) as template with the primer #597/#1139 or #1138/#598. The two DNA products were then used as template in the second step with the flanking oligonucleotides #597/#598. The final DNA fragment bearing the mutations and the vector, pGEX5X-3 (#25), were digested using the restriction enzymes XhoI and BamHI.

7.2.4 Mammalian Cell Manipulation: Protein Overexpression and Protein Depletion

7.2.1 Transient DNA Transfection

7.2.2 Calcium Phosphate DNA Transfection

For calcium phosphate transfection, HEK293 cells were freshly plated and grown to 80-100% confluency, except for virus production that cells were grown only to 60% confluency. 60 minutes before treatment, the cell media was renewed. The transfection was performed with a total amount of 10 µg of precipitated DNA, per 10 cm cell culture plate. To precipitate the DNA, 250 µl of 256 mM $CaCl_2$, containing 3 µg of the plasmid DNA of interest and 7 µg of carrier DNA (pcDNA3) was dropwise added under constant mixing to 250 µl of 2 x HBS buffer (280 mM NaCl, 1.5 mM Na_2HPO_4, 50 mM HEPES, pH 7.05) and incubated for 30 minutes at room temperature before adding it to the cells. The mixture was then added to the cells drop wise under constant shacking and the media was changed 5 – 16 hours post transfection. The cells were harvested about 24 hours after transfection. For the

control, empty vectors (pEGFP-C2 or pcDNA3.1), 1.5 µg of the plasmid DNA and 8.5 µg of the carrier DNA was used.

7.2.3 Liposome-based DNA Transfection

Lipofectamine 2000 (Invitrogen, by life technologies) was used for liposome-mediated transfection, according to the manufacturer´s instructions. In brief, freshly plated cells were grown to 80 % (for biochemical analysis) or 60 % confluency (for fluorescence microscopy). Previous to transfection, the media was removed and half of the usual volume fresh DMEM was added to the cells. An appropriate amount of plasmid DNA and Lipofectamine 2000 were resuspended separately in OptiMEM (Invitrogen, by life technologies) and incubated for 5 minutes at room temperature. Both solutions were combined and incubated for 30 minutes at room temperature. The mixture was then added to cells drop-wise under constant gentle shaking. The media was changed 12 hours post transfection. 16-24 hours after transfection, the cells were analyzed. For immunofluorescence, cells were transfected with half the amount of DNA and Lipofectamine 2000.

Transfection Mix	µg DNA / µl OptiMEM	to	µl Lipofecta. 2000 / µl OptiMEM
10 cm diameter plates	20 µg / 400 µl	to	32 µl / 400 µl
6 cm diameter plates	7.5 µg / 150 µl	to	12 µl / 150 µl
3.5 cm diameter plates	2.5 µg / 50 µl	to	4 µl / 50 µl

7.2.4 Silencing of Protein Expression with Small Interfering RNA (siRNA), Short Hairpin RNA (shRNA) and Generation of Stable Cell Lines

7.2.4.1 Silencing of Protein Expression with Small Interfering RNA (siRNA)

One day before transfection, Cos-7 cells were seeded at 30 – 35 % confluency. The next day siRNA (control siRNA Ambion Silencer 4644 or siRNA targeting kazrin (GGAGAUGUUGCGCAAGGACtt, Ambion Silencer Pre-designed siRNA, target gene KIAA1026, Ambion Silencer) and Lipofectamine 2000 (Invitrogen) were diluted in OptiMEM (Invitrogen) in two separate 1.5 ml RNAse free micro reaction tubes (see table below for amounts).

Culture vessel	siRNA (50 µM) / OptiMEM	Lipfectamine 2000 / OptiMEM
12-well	0.5 µl (25 pmol) / 50 µl	1 µl / 50 µl
6-well	1.0 µl (50 pmol) / 100 µl	2 µl / 100 µl

6 cm	2.0 µl (100 pmol) / 200 µl	4 µl / 200 µl
10 cm	4.5 µl (222 pmol) / 440 µl	8.9 µl / 440 µl

The prepared solutions were incubated 5 minutes at room temperature before joining them and letting them to chill for 20 minutes. In the meanwhile, the cell medium was changed to DMEM with FCS without antibiotics, adding half of the usual volume. After 20 minutes, the reaction mix was added to the cells and distributed homogenously. The cells were incubated for 2 days before further analysis.

7.2.4.2 Lentivirus Production, Transduction of shRNA and Generation of Stable Cell lines

HEK293**T** cells were co-transfected with either the pLL3.7 encoding GFP, for virus production control and infection efficiency monitoring, or with pLKO.1 encoding the desired shRNA (see Table I. Plasmids), and the viral packaging (pCMV-dR8.2 dvpr) and envelope (pCMV-VSV-G) plasmids, using calcium phosphate transfection (see chapter 7.2.2). About 16 hours after transfection, the medium was changed and half of the usual volume was added. During the two following days, medium containing the virus was collected and filtered with a 0.45 µm filter (Millipore). The filtered virus solution was directly used for the infection of cell lines or stored in aliquots at -80°C without prior concentration of the virus. Infection and selection of stably infected cells were done in the presence of the appropriate concentration of puromycin (Sigma-Aldrich) titrated by using the minimum antibiotic concentration sufficient to kill untransfected cells, but to maintain cells transfected with the pLL3.7 GFP-containing plasmid. Actual depletion of kazrin or the protein of interest was analyzed by immunoblot (see chapter 7.3.1).

7.3 Biochemistry Techniques

7.3.1 SDS-PAGE, Immunoblot

SDS-PAGE was performed as described in (Laemmli 1970) using a Minigel system (Bio-Rad Laboratories). High Range, Low Range and PageRuler prestained SDS-PAGE molecular weight standards (Bio-Rad Laboratories) were used for determination of the molecular weights. Protein concentration was determined with the Bio-Rad Protein assay (Bio-Rad Laboratories), according to the manufacturer´s instructions. Coomassie Brilliant Blue (Sigma-Aldrich) (0.25% Coomassie Brilliant Blue, 7.5% Acetic Acid, 50% Methanol) was used for detection of total protein on Acrylamide gels. Laemmli sample buffer 2x (4% SDS, 200 mM DTT, 20% glycerol, 120 mM Tris-HCl pH 6.8, Bromophenol blue) was added to the samples, heated up at 95°C for 8 minutes, quickly spinned at room temperature and analysed by SDS-PAGE and Immunoblot after Westernblot.

Immunoblot was performed as described in (Geli and Riezman 1998). After polypeptide transfer to nitrocellulose membranes of 0.45 µm pore (GE Healthcare), membranes were stained with Ponceau S (Sigma-Aldrich) (0.3% Ponceau S, 3% TCA) for detection of total protein. After rising with PBS (137 mM NaCl, 2.7 mM KCl, 10 mM Na_2HPO_4 , 2 mM KH_2PO_4, pH 7.4), membranes were blocked for 30 minutes on blocking buffer (PBS, 3% (w/v) non-fat lyophilized milk, 0.1% (v/v) Nonidet P-40), followed by incubation for 1 hour with the primary antibody, dissolved in blocking buffer, washing with blocking buffer twice for 15 minutes and incubation with the peroxidase-conjugated secondary antibody for 1 hour in blocking buffer. Membranes were then washed 3 times for 20 minutes with blocking buffer and 3 times for 20 minutes with PBS and developed using an enhanced chemoluminiscence (ECL) detection kit (Amersham Biosciences), together with Super RX radiograph films (Fujifilm).

The primary and secondary antibodies used for detection of the indicated proteins are listed in Table III. Antibodies.

7.3.2 Antibody Affinity Purification

Polyclonal sera against kazrin were generated in rabbit using an N-terminal (aa 1 to 147) fragment of human kazrin C fused to GST, expressed in and purified from *E. coli*. Affinity purification of the serum was performed using a reactive ester agarose (Affi-Gel-10, Bio-Rad) covalently linked to the 6xHis-kazrin C (aa 1-327). In brief, purification of 6xHis-kazrin C was performed as described in chapter 6.3.3.2. The binding of 6xHis-kazrin to Affi-Gel-10 was done in 0.1 M MOPS pH 7.2 for 4 hrs at 4°C in head-over-shoulder rotation followed by stripping of not-covalently bound kazrin in 0.1 M citrate pH 2.5 and blocking of the remaining reactive esters in 1 M Tris pH 8 for 2 hours. For affinity purification of the antibody, 15 µl of the kazrin loaded beads were incubated with 1.5 ml of the serum for 2 hrs at 4°C in head-over-shoulder rotation. The beads were washed 5 times with PBS and the purified antibodies were eluted several times with 15 µl 0.1 M citrate pH 2.5, and immediately neutralized with appropriate volume of 1 M Tris pH 9.

7.3.3 Protein Purification

7.3.3.1 Protein Purification of Recombinant GST-fusion Proteins from *E. coli* by Affinity Chromatography and Cleavage of GST-tag

Recombinant glutathione-S-transferase-tagged proteins (GST-fusion proteins) were purified from BL21 *E. coli* cells according to (Geli, Lombardi et al. 2000). Briefly, a 1/100 dilution of an overnight *E. coli* culture transformed with the adequate vector was inoculated into LB media containing 50 mg/l Ampicillin (Sigma-Aldrich). The culture was grown at 37°C to an 600 nm Optical Density (OD) of 0.4. Cells were shifted to 24°C and the expression was induced at an OD 600 of 0.6 - 0.8 with 0.1 mM isopropyl-beta-D-thiogalactopyranoside (IPTG) (Sigma-Aldrich) for 2 hours. Cells were harvested at 5000 g for 30 minutes and frozen at -20°C.

For protein purification, cells were thawed in pre-chilled PBSTw (PBS buffer (137 mM NaCl, 2.7 mM KCl, 10 mM Na_2HPO_4 , 2 mM KH_2PO_4, pH 7.4), 0.5% Tween) in the presence of protease inhibitors (1 tablet cOmplete Protease Inhibitor Cocktail Tablets (Roche)/50 ml of buffer), and lysed by sonication at 30% amplitude with a Branson Ultrasonic Microtip Sonifier on ice, for 2 minutes per bacteria pellet derived from 1 litre of culture, at pulse intervals of 20 seconds, followed by a 20 second pause, to avoid excessive heating of the sample. Cell debris were removed by centrifugation at 15000 g and the supernatant was recovered for further processing.

Depending on whether the GST-fusion proteins were subjected to pull down, digest and removal of the GST-tag, or used for the *in vitro* actin polymerization assay, purification was performed as follows:

1. For pull down assays, 15 µl of 50% glutathione-Sepharose beads (GSH-beads) (GE Healthcare) equilibrated in PBSTw were added to the protein extracts obtained from *E. coli* cultures of 100 ml expressing the GST-constructs (unless indicated differentially) in 15 ml of PBSTw in the presence of protease inhibitors, and incubated for 1 hour at 4°C in head-over-shoulder rotation. In permanent presence of protease inhibitors, beads were recovered and washed twice with 15 ml of PBSTw, once with 15 ml of the appropriate buffer of the following experiment and transferred to siliconized polypropylene 1.5 ml tubes (Sigma-Aldrich) or to Mobicol columns (MoBiTec).

2. For digestion with Factor Xa protease (NEB) to remove of the GST-tag (plasmid pGEX-5X-3), 30 µl of glutathione-Sepharose beads (GE Healthcare), equilibrated in PBSTw were added to the protein extracts derived from 1 liter *E. coli* cultures expressing the GST-construct of interest (unless otherwise indicated) in 50 ml PBSTw in the presence of protease inhibitor, and incubated for 1 hour at 4°C in head-over-shoulder rotation. In absence of protease inhibitors, beads were washed with PBSTw, recovered to siliconized 1.5 ml polypropylene tubes and washed with 1 ml of Factor Xa buffer (20 mM Tris-HCl, 100 mM NaCl, 2 mM $CaCl_2$, pH 8.0). Beads were resuspended in 30 µl of Factor Xa buffer and 1 µl of Factor Xa protease (1mg/ml) was added. The constructs were digested for the adequate time and temperature as titrated, followed by inactivation of Factor Xa with 5 µl of 20 µM Dansyl-Glu-Glu-Arg-chloromethyl ketone (CALBIOCHEM) for a minimum one 1 minute at room temperature. The digested protein was recovered and glycerol was added to a final concentration of 10% (v/v). Aliquots were snap frozen in liquid nitrogen and stored at -80°C until use. Gel electrophoresis and Coomassie staining was performed to confirm final protein concentration.

Factor Xa protease digestion conditions for each GST-fusion protein used were:

Protein	**Temperature**	**Time**
GST-kazrin C-Ct	18°C	45 minutes
GST-CHC17-lTD	24°C	2 hours
GST-Ϋ-Adaptin	24°C	2 hours
GST-WASH-VCA	4°C	45 minutes

3. For digestion with Thrombin protease (Novagen) for removal of the GST-tag (plasmid pGEX-4T-2), 30 µl of glutathione-Sepharose beads (GE Healthcare), equilibrated in PBSTw were added to the protein extracts derived from 250 ml *E. coli* cultures expressing the GST-construct of interest (unless otherwise indicated) in 50 ml PBSTw in the presence of protease inhibitor, and incubated for 1 hour at 4°C in head-over-shoulder rotation. In absence of protease inhibitors, beads were washed with PBSTw, recovered to siliconized 1.5 ml polypropylene tubes and washed with 1 ml of Thrombin buffer (20 mM Tris-HCl, 150 mM NaCl, 2,5 mM CaCl 2 , pH 8.4). Beads were resuspendend in 60 µl of Thrombin buffer and 1 µl of Thrombin-biotin (1mg/ml) (Novagen) was added. The GST-kazrin C was digested for 1 hour at room temperature, followed by addition of 16 µl Strepdavidin-beads (Novagen) for 30 minutes at room temperature on shaker to remove the Thrombin-biotin. The digested protein was recovered and used directly. Gel electrophoresis and Coomassie staining was performed to confirm final protein concentration.

4. For the *in vitro* actin polymerization assay, 50 µl of 50% glutathione-Sepharose beads (GE Healthcare) equilibrated in PBSTw were added to the protein extract (see above) derived from 100 ml *E. coli* culture expressing GST-kazrin C-terminus (aa 161 – 327, #694) or GST-WASH-(P)VCA, and incubated for 45 minutes at 4°C in head-over-shoulder rotation. The beads were washed 3 times with 10 ml PBSTw in the presence of proteinase inhibitors and transferred into Mobicol columns bearing 35 µm pore filters (MoBiTec). The GST-constructs were eluted by incubating the beads 3 times in 75 µl of EB (50 mM Tris pH 8.0, 10 mM glutathione) at 22°C for 10 minutes, and recovering the supernatant after centrifugation at 500 g for 2 minutes. The supernatant was collected into fresh 1.5 ml polypropylene tubes. The buffer was then exchanged using a G-25 column (GE Healthcare) equilibrated with TKMES buffer (20 mM Tris, 25 mM KCl, 1 mM MgCl2, 0.5 mM EDTA, 2% sucrose, pH 7.5), followed by a concentration of the sample, using Vivaspin filters (cut of: 30.000 mwco) (VIVAproducts), according to the manufacturer's instructions. The protein was snap frozen in liquid nitrogen and stored in aliquots of 10 µl at -80°C. Gel electrophoresis and Coomassie staining was performed to determine final protein concentration.

7.3.3.2 Protein Purification of Recombinant 6xHis-fusion Proteins from *E. coli* by Affinity Chromatography

Recombinant 6xHis-tagged fusion proteins were purified from BL21 *E. coli* cells using Ni-NTA Superflow beads (Qiagen) according to the manufacturer´s protocol for purification under native conditions (The QIAexpressionist). In brief, protein expression was induced as indicated for the GST-fusion constructs, except that 1 mM IPTG (Sigma-Aldrich) was used instead of 0.1 mM. Cells were lysed as indicated for the GST-fusion constructs (see previous section) except that lysis buffer (50 mM NaH_2PO_4, 300 mM NaCl, 10 mM imidazole, pH 8) supplemented with EDTA-free protease inhibitor (1 tablet cOmplete Protease Inhibitor Cocktail Tablets (Roche)/50 ml of buffer) was used instead of PBSTw. 30 µl Ni-beads equilibrated in lysis buffer were added to the protein extracts obtained from *E. coli* cultures of 1 liter and incubated 1 hour at 4°C in head-over-shoulder rotation. After three washes with wash buffer (50 mM NaH_2PO_4, 300 mM NaCl, 20 mM imidazole, pH 8) in the presence of protease inhibitors, the 6xHis tagged protein was eluted two times with a bead volume of elution buffer (50 mM NaH_2PO_4, 300 mM NaCl, 250 mM imidazole, 0.05 % Tween, pH 8.0) for 30 minutes on ice. Glycerol was added to a final concentration of 10 % (v/v), proteins were snap frozen in liquid nitrogen and stored in aliquots at -80°C until use. Gel electrophoresis and Coomassie staining was performed to asses protein concentration.

7.3.4 Protein Extraction from Mammalian Cells

Cells from a confluent 10 cm culture dish were harvested, washed with cold PBS and transferred into 1.5 ml polypropylene tubes. After 10 minutes centrifugation with 500 g at 4°C, the supernatant was discarded, the cell pellet was resuspended in 50 - 100 µl of PBS supplemented with 1% Triton X-100 and protease inhibitors (Roche cOmplete) and left 10 minutes on ice for cell lysis. The lysate was centrifuged at 4°C for 10 minutes with 10,000 g to remove the cell debris. The supernatant was recovered and the protein concentration was determined with the BioRad Protein assay (see chapter 7.3.1). The sample was diluted 1/2 with in Laemmli sample buffer x 2 (2% SDS, 200 mM DTT, 20% glycerol, 120 mM Tris-HCl pH 6.8, Bromophenol blue) and usually 18 µg protein were analysed by SDS-PAGE and WB (see chapter 7.3.1).

7.3.5 Analysis of Protein-Protein Interactions

7.3.5.1 Pull Down Assays

For the pull down assay with purified components (for pull downs with Rab-GTPases see below), 20 µl of 50% glutathione-Sepharose covered with 0.5-1 µg of the indicated purified GST-construct (see chapter 7.3.3.1) were resuspended in 1 ml of Binding Buffer (PBSTw + 0.5% (w/v) BSA), or for pull down assays with the Arp2/3 complex, in IP buffer WASH (HEPES-KOH 20 mM, KAc 50 mM, EDTA 2 mM, Sorbitol 200 mM, TritonX-100 0.1%, pH 7.2) with 0.5% (w/v) BSA, supplemented with protease inhibitors, in the presence or absence of the putative purified binding partners of interest, for 1 hour at 4°C. After incubation, beads were recovered by centrifugation at 700 g for 1 minute and washed 3 times with 1 ml of Binding Buffer or IP buffer WASH with BSA, 2 times with 1 ml of PBSTw or IP buffer WASH w/o BSA, and 2 times with 1 ml of PBS. Beads were drained and resuspended in 30 µl of SDS-PAGE Laemmli buffer. Samples were incubated at 95°C for 5 minutes and 5-10 µl were analysed by SDS-PAGE and immunoblot. For analysis of interactions with proteins purified upon protease digestion of GST-fussion constructs, the proteins were pre-cleaned from residual GST or uncut GST-fusion protein by incubation for 30 minutes with 20 µl of 50% naked glutathione-Sepharose at 4°C in head-over-shoulder rotation.

Quantifications of the band intensity of the proteins pulled down (prey) by the GST-fused proteins (bait) were performed with ImageJ (see chapter 7.3.7). The average band intensity of the prey obtained from immunoblot analysis was normalized with respect to the band intensity of the

corresponding bait obtained from the Ponceau S staining. The signal from the prey pulled down by the GST control was subtracted from the result. At least 3 independent experiments were performed for each sample. Average percentage, standard error of the mean (SEM) and p-values for the two-tailed Student's t-test were calculated with Microsoft Excel.

7.3.5.2 Pull Down Assays with Rab-GTPases

In the pull down assay with Rab-GTPases the buffers and incubation times from (Popa, Deneka et al. 2005) were used. The Rab-GTPases were purified as described above. The proteins bound to GSH-beads were washed with NE buffer (20 mM HEPES, pH 7.5, 100 mM NaCl, 10 mM EDTA, 5 mM $MgCl_2$, 1 mM DTT) supplemented with protease inhibitors and either 10 µM GDP (Sigma) or GTPγS (Sigma) and incubated for 30 minutes at room temperature under rotation. Beads were recovered by centrifugation at 700 g for 1 minute. The incubation steps are repeated twice to ensure optimal nucleotide loading. Beads were washed once with NS buffer (20 mM HEPES, pH 7.5, 100 mM NaCl, 5 mM MgCl_2, 1 mM DTT) containing protease inhibitors and either 10 µM GDP or GTPγS and further incubated with NS buffer containing either 1 µM GDP or 10 µM or GTPγS for 20 minutes at room temperature and immediately used in binding assays.

5 µg of either GST or GST-Rab-GTPases were incubated for 2.5 hours at 4°C with 0.1 µg of purified and Thrombin digested kazrin C. After incubation, beads were recovered by centrifugation at 700 g for 1 minute and washed 3 times with 1 ml NS buffer containing either 1 µM GDP or 10 µM GTPγS. Beads were drained and resuspended in 30 µl of SDS-PAGE Laemmli buffer. Samples were incubated at 95^{o}C for 5 minutes and 5-15 µl were analysed by SDS-PAGE and immunoblot.

7.3.5.3 Immunoprecipitation of Proteins from Mammalian Cell Extracts

Cells of 2 - 4 confluent 10 cm cell culture plates were used per immunoprecipitation (IP), depending on the cell type and on the transfection efficiency, if transient protein expression was required. Cells were harvested and resuspended in 500 µl IP buffer WASH (HEPES-KOH 20 mM, KAc 50 mM, EDTA 2 mM, Sorbitol 200 mM, TritonX-100 0.1%, pH 7.2, supplemented with protease inhibitor Roche cOmplete 1 Tab/50 ml) and incubated for 10 minutes on ice. From now on all steps were performed with IP buffer WASH with protease inhibitors unless otherwise mentioned. The cell lysate was cleared by centrifugation at 4°C for 5 minutes at 10000 g and the cell extract was recovered.

- For precipitation of GFP-constructs the GFP-Trap beads (Chromotec) were used. Beads were washed in Mobicol columns bearing 35 µm pore filters (MoBiTec) with IP buffer WASH and resuspended in the cell extract.

- For immunoprecipitations of endogenous proteins, specific antibodies pre-coupled to Proein A-Sepharose beads (GE Healthcare) were used. For pre-binding of antibodies, 15 µl Protein A-Sepharose beads washed and resuspended in 1 ml of the appropriate IP binding buffer and incubated either with 60 µl of polyclonal sera against kazrin or 10 µg of commercial antibodies for 1 hour at 4°C in head-over-shoulder rotation. The beads were recovered by centrifugation at 700 g for 1 minute and washed 3 times with 1 ml of the IP binding buffer before addition of the cell extract. For immunoprecipitations with the endogenous proteins the cell extracts were pre-cleaned with 15 µl of 50% Protein A-Sepharose for 30 minutes at 4°C in head-over-shoulder rotation.

Immunoprecipitations were done for 1 hour at 4°C in head-over-shoulder rotation. Afterwards, the beads were washed six times with the IP binding buffer and recovered into a fresh tube. 15 µl of Laemmli SDS-PAGE sample buffer was added to the beads and samples were analysed by Immunoblot (see chapter 7.3.1).

7.3.6 OptiPrep Density Gradient

Subcellular fractionation of Cos-7 cells using Optiprep density gradients was performed as described in (Li and Donowitz 2008). Briefly, for each cell type, six confluent plates of cells were rinsed twice with ice-cold PBS and scraped in 1 ml ice cold PBS. Cells were harvested by centrifugation at 700 g for 10 minutes and resuspended in 2 ml of ice cold Lysis buffer (LyB: Hepes 25 mM pH 7.4, 150 mM NaCl, 1 mM DTT, 2 mM EGTA), containing protease inhibitors (PI: PMSF 1 mM, Pepstatin 1 µg/ml, Aprotinin 1 µg/ml, Antipain 2.5 µg/ml, Leupeptin 5 µg/ml). 1 ml of the cell suspension was then passed 10 times through a 27 age syringe needle using a 1 ml syringe to lyse the cells. The lysate was cleared by centrifuging twice at 3,000 g for 15 minutes. The supernatant (approx. 1 µg protein/µl) was subsequently centrifuged in a TLA-55 rotor in a table top Beckman Coulter Optima MAX-XP

ultracentrifuge at 200.000 g for 1 hour at 4°C to fractionate cellular membranes from cytosol. The membrane pellet was then carefully resuspended in 200 µl LyB containing PI (approx. 1 µg protein/µl) by passing them 10 times though a 27 age syringe needle, and carefully laid on a 12 x 1 ml OptiPrep step gradient (see table IV), prepared beforehand in Ultra-Clear tubes (Beckman Coulter 344059, Thin wall, Ultra-Clear™, 13.2 mL, 14 x 89 mm) for the Beckman Coulter SW41Ti rotor. 37.5% to 10% OptiPrep mixtures were prepared by mixing the following amounts of OptiPrep (60 %, Sigma D-1556), 3-fold concentrated LyB (3xLyB) and double distilled water (ddH_2O):

OptiPrep mixture	OptiPrep (60%)	3xLyB	ddH_2O
10 %	2 ml	4 ml	8 ml
12.5%	2.5 ml	4 ml	7.5 ml
15%	3 ml	4 ml	7 ml
17.5%	3.5 ml	4 ml	6.5 ml
20%	4 ml	4 ml	6 ml
22.5%	4.5 ml	4 ml	5.5 ml
25%	5 ml	4 ml	5 ml
27.5%	5.5 ml	4 ml	4.5 ml
30%	6 ml	4 ml	4 ml
32.5%	6.5 ml	4 ml	3.5 ml
35%	7 ml	4 ml	3 ml
37.5%	7.5 ml	4 ml	2.5 ml

Table IV. OptiPrep step gradient.

Mixtures were prepared and left over night at 4°C in 15 ml polypropylene tubes. Before cell lysis, the OptiPrep gradient was prepared by mixing 1 ml of each solution with 10 µl of 100 x PI and laying each mixture carefully with a Pasteur pipette starting from the heavier solution (37.5%) at the bottom, to the lightest (10%) at the top. The step gradient was carefully deposited on ice and stored until the membrane fraction was laid.

Once the membranes were laid on the top of the gradient, the tube was filled (if necessary) with LyB including PIs and samples were spun for 16 hours at 100.000 g at 4°C, in a SW41Ti rotor in a Optima L-90K ultracentrifuge. The gradient was carefully placed on ice and 0.6 ml fractions were carefully collected from the top into 1.5 ml polypropylene tubes. Samples were then precipitated by adding 66 µl of 100% TCA (Sigma-Aldrich), incubating on ice for 1 hour and centrifuging at 4°C for 30 minutes at 20.000 g., pellets were rinsed once with 1ml of 10% TCA, spun for 20 minutes, and rinsed again with 1 ml of -20°C pre-cooled acetone (Sigma-Aldrich). After centrifugation for 20 minutes at 4°C, the supernatant was removed, the pellets were air-dried and resuspended in 30 µl of SDS-PAGE sample buffer. After boiling, 10 µl were loaded for immunoblot analysis (see chapter 7.3.1).

7.3.7 Quantification of Immunoblots

The quantification of Immunoblots was performed with the FIJI distribution of the ImageJ software (NIH) according to http://lukemiller.org/index.php/2010/11/analyzing-gels-and-western-blots-with-image-j/. Briefly, the radiograph films of the immunoblots were scanned and converted with ImageJ into an 8-bit gray-scale image. The analysis was done using the ImageJ Gel Analyzer tool. The individual lanes were selected and added to the Analyzer. Next, the profiles of the selections were plotted (Analyze>Gels>Plot Lanes). Due to the natural background, noise of the peaks do not reach to the baseline and need to be closed manually by drawing a straight line at the bottom of the curve above the noise signal. Afterwards, all individual peaks were selected with the Wand tool and the corresponding values from the Results window were copied to Microsoft Excel for further calculations.

7.4 *In vitro* Actin Polymerization Assay (Pyrene assay)

In vitro actin polymerization assays were performed as previously described in (Doolittle, Rosen et al. 2013). Briefly, a mix of cold muscle actin (Cytoskeleton) and 10% pyrene-labelled muscle actin (Cytoskeleton) was prepared from stock solutions to a final concentration of 0.053 µg/µl (1.25 µM, to have a 1 µM in the assay) in G-buffer (5 mM Tris pH 8.0, 0.2 mM CaCl2, 0.2 mM ATP, 0.5 mM DTT). The mixture was incubated over night at 4°C protected from light, followed by centrifugation with 14,000 g for 1 hour at 4°C to remove small actin filaments. The supernatant was directly added to the reaction mixture to obtain a final concentration of 1 µM.

The lyophilized Arp2/3 complex (Cytoskeleton) was reconstituted with 10 µl of cold ddH_2O to obtain a solution with a concentration of 5 mg/ml in 20 mM Tris pH 7.5, 25 mM KCl, 1 mM $MgCl_2$, 0.5 mM EDTA, 0.1 mM ATP, 1.0% (v/v) dextran and 5% (v/v) sucrose, and it was stored at -80°C in aliquots of 2 µl. For the assay, the complex was diluted to 0.25 mg/ml (1.11 µm) in TKMES buffer (20 mM Tris, 25 mM KCl, 1 mM $MgCl_2$, 0.5 mM EDTA, 2% sucrose, pH 7.5). 2.25 µl were used for a final reaction mix of 250 µl to obtain the concentration of 10 nM.

The test proteins were purified from *E. coli* BL21 cells as described in chapter 6.3.3.1. N-WASP VCA was purchased from Cytoskeleton. The lyophilized protein was restored with 500 µl of cold ddH_2O to obtain a solution of 1 mg/ml in 20 mM Tris pH 7.5, 25 mM KCl, 1 mM $MgCl_2$, 0.5 mM EDTA, 0.2% dextran and 2% sucrose, and stored in aliquots at -80°C. For the quantities used in the experiments

see corresponding figure legends. For the assay, the test proteins were diluted in TKMES and supplemented with 10x actin Polymerization Buffer (APB) (100 mM Tris pH 7.5, 500 mM KCl, 20 mM $MgCl_2$, 50 mM guanidine carbonate, 10 mM ATP, stored in aliquots at -80°C).

Two separate solutions were prepared and mixed just before starting the measurement:

Mix 1:

	A	**B**
G-actin 1.25 µM	200 µl	200 µl
Arp2/3 1.11 µM	2.25 µl	0
TKMES	3.75 µl	6 µl

Mix 2:

GST-VCA and/or Test protein	x
TKMES	V till 19 µl
APB	25 µl

Upon polymerization, the pyrene-actin shows an emission at 407 nm that was measured with a Tecan Safire2 fluorimeter using the following settings: fluorescence mode; kinetic analysis; Costar 96 wells-black; measurement with previously adjusted settings using excitation 365 nm, emission 407 nm, bandpass of 20 nm; manual gain of 70; 10 reads, High sensitivity mode; manual Z-position optimized for this assay; 135 kinetic cycles with an interval of 20 seconds and shake between cycles for 2 seconds at room temperature. Up to 12 samples were measured at once.

Analysis of the obtained data was performed with Microsoft Excel as described in (Doolittle, Rosen et al. 2013) under 3.3, with minor adaptations. Briefly, the time values of the obtained raw data for each sample were corrected by the constantly kept delay between mixing of Mix 1 and Mix 2 (e.g. 5 seconds between each pipetting step, sample 5 started 25 seconds delayed in respect to sample 1). The intensity data was plotted as a function of the corrected time.

The minimum intensity (I_{min}) was calculated for each data set. The average of the 10 time points associated with the highest intensities was calculated to estimate the time when the maximum intensity (t_{max}) occurs.

The average of the 10 data points closest to t_max was used to calculate the maximum intensity (I_max).

Next, $t_{1/2}$ was calculated. The lower data point to find $t_{1/2}$ were usually determined with the equation (0.5-0.1)x(I_{max} - I_{min})+ I_{max}.

The upper data point to find $t_{1/2}$ were usually determined with the equation (0.5+0.1)x(I_{max} - I_{min})+ I_{max}. Using the values from the data set between these upper and lower point, a line was drawn and the slope $m_{t1/2}$ and intercept $b_{t1/2}$ were recorded. The used points and obtained lines were visually inspected in respect to the dataset. The $t_{1/2}$ was then found using $t_{1/2}$ = (0.5x(Imax - I_{min})+Imin)-$b_{t1/2}$)/$m_{t1/2}$. Important note: only subtraction of $b_{t1/2}$, instead of addition as indicated in (Doolittle, Rosen et al. 2013), gave realistic results and might be mistaken in the publication: f(x) = m x x + b <=> x = y - b / m.

7.5 Immunofluorescence and Microscopy Techniques

The primary and secondary antibodies used for detection of the indicated proteins are listed in Table III. Antibodies.

7.5.1 Live Cell Fluorescence Imaging

Cells were seeded and transfected with adequate density as described before (see chapter 7.2.4) either on 22-mm clean glass cover slips for imaging in Attofluor cell chamber coverslip holder (Invitrogen Molecular Probes) or in 35-mm µ-Dish (Ibidi) plates with polymer coverslips for high end microscopy. Before imaging, the medium was renewed with pre-warmed culture medium (fully supplemented DMEM). The image acquisition was usually done (unless differently described) with a Perkin Elmer Ultraview ERS confocal spinning disc microscope as described below (see chapter 7.5.4). The microscope was equipped for environmental control (temperature and CO_2) and the cells were kept during the imaging at 37°C with 5% CO_2.

7.5.2 Transferrin Uptake

Cells were plated 16 - 24 hours before fixation on glass coverslips (acidic acid cleaned) and grown up to 80% confluency. Before the transferrin (Tfn) uptake, cells were starved for 45 minutes in internalization medium (InMed) (DMEM, 0.5% BSA, 10 mM Hepes, pH 7.4) at 37°C. Fluorescently labelled Tfn (Sigma-Aldrich), stored in aliquots at -80°C, was centrifuged with 10,000 g at 4°C for 10 minutes before preparation of appropriate dilutions. For Tfn uptake, cells were incubated with pre-

warmed In-Med supplemented with 20 µg/ml Tfn (unless otherwise mentioned) for the indicated times. The uptake was stopped by washing the cells three times with ice cold PBS on ice. The cells were fixed with 4% paraformaldehyde (PFA) (Merck) diluted in PBS pH 7.4 bearing 0.02% Natrium Azide for 30 minutes on ice. All further steps were performed as described in next section.

7.5.3 Immunofluorescence, Phalloidin and DAPI Stainings

Cells were plated 16 - 24 hours before fixation on glass coverslips (acidic acid cleaned) and grown up to 80% confluency. Cells were fixed with 4% paraformaldehyde (PFA) (Merck) (PBS pH 7.4, 4% PFA, 0.02% Natrium Azide) for 15 minutes at room temperature. Cover slips were washed between each step with PBS. Cells were permeabilized and blocked with PBS-BTx (PBS pH 7.4, 1% (w/v) BSA, 0.2% Triton X-100) (or PBS-BGTx (PBS-BTx, 5% goat serum) if secondary antibodies were from goat) for 30 minutes. All following steps were performed with PBS-BTx, if not otherwise mentioned. All antibodies, Phalloidin and DAPI stock solution were centrifuged at 4°C for 10 minute with 10,000 g before use. For details about dilutions and references of antibodies and fluorescently labelled reagents see Table III. Antibodies. Primary antibodies were incubated for 1 hour at room temperature or overnight at 4°C. Secondary antibodies were added for 45 minutes at room temperature. If necessary, nuclear staining was done with DAPI for 2 minutes. Final washes were done with PBS at room temperature for 45 minutes or over night at 4°C. Coverslips were dipped in ddH2O and air-dried before mounting. Finally, the samples were mounted on a clean object carrier with the indicated mounting medium and kept at room temperature over night before imaging and storage at 4°C. Phalloidin staining of endosomes was analysed one day after preparation.

7.5.4 Image Acquisition

For further information about the used microscope system see corresponding figure legends. The available hardware was equipped as described below. Image aquisiton on the Zeiss LSM-780 was mainly done together with Elena Rebollo combined with advanced experimental design.

The Zeiss LSM-780 confocal microscope system was equipped with Diode Laser (405 nm), Multiline Argon Laser (458/488/514 nm), Solide State DPSS Laser (561 nm), HeNe Laser (594 nm) and HeNe Laser (633 nm), and a 63x/1.4NA Oil DIC Plan-Apochromat (1.40 OIL DIC PLAN-APOCHROMAT

∞/0.18) objective. The internal detectors of the LSM-780 system had 3 channels, 2 usual PMTs (photomultiplier tubes) and a 32 PMT GaAsP array that can be used for photon counting, all PMTs usable for fluorescence and reflection and an additional PMT for transmitted light allowing simultaneously detection of fluorescence and brightfield/DIC images. The system was controlled with the LSM software Zen2.1 (for exact technical details see web page http://www.ibmb.csic.es/groups/molecular-imaging-platform).

The Leica TCS-SP5 confocal microscope was equipped with Diode Laser (405nm), Multiline Argon (458nm, 476nm, 488nm, 496nm, 514nm), Solid State DPSS Laser (561nm) and HeNe Laser (633nm), and emission filters (excitation filter, dichroic mirror) LP425(BP340-380,400)/BP525/50(BP470/40,500) optimized for GFP/LP515(450-490,510)/LP590(BP515-560,580) and a 63x/1.4NA Oil HCX Plan-Apochromat objective (HCX PL APO 63x/1.40-0.60 OIL λ BL ∞/0.17/E). The spectral detection system was composed of an Acousto Optical Beam Splitter, a Spectral Detector SP and with three PMTs (photomultiplier tubes). The system was controlled with the Leica Application Suite Advanced Fluorescence (LAS AF) (for exact technical details see web page http://www.ibmb.csic.es/groups/molecular-imaging-platform).

The Perkin Elmer Ultraview ERS confocal spinning disc microscope was used for some life imaging. The microscope was equipped with Argon multiline gas laser (Melles Griot) (488nm, 514nm), DPSS solid state laser (Coherent) (568nm), Solid State Diode lasers (Melles Griot) (405nm, 440nm, 640nm), and a scan head with dichroic mirrors 405/488/568/640, 405-440/514/640 and 488/568 customized for increased detection in the red emission. The objectives 40x/1.3NA (1.30 OIL DIC PLAN-NEOFLUAR ∞/0.17), a 63x/1.4NA (1.40 OIL DIC PLAN-APOCHROMAT ∞/0.17) and 100x/1.4NA (1.40 OIL DIC PLAN-APOCHROMAT) were used. Images were taken with a Hamamatsu C9100-50 EMCCD camera. The system was controlled with the Volocity 6.1 software (Perkin Elmer) (for exact technical details see web page http://www.ibmb.csic.es/groups/molecular-imaging-platform).

7.5.5 Image Analysis

All images were processed and quantified using the FIJI distribution of the ImageJ software (NIH). For all fluorescence intensity measurements, background signal was measured in an adjacent area and subtracted. Analysis was usually performed on single z-layers unless otherwise mentioned. Semi-automated Macros were written to execute repetitive steps of the analysis process.

Images for figure 28 (Depletion of kazrin with shRNA prevents transferrin accumulation at the perinuclear region but increases transferrin uptake.) were analysed as follows:

The boundaries of the cells were drawn and saved as ROI set.

To determine the **peripheral endosome size (µm^2)** a general threshold defining the peripheral endosomes was determined and applied to all images after running a Gaussian blur with radius 1. Peripheral endosomes adjacent to the previously marked cell boundaries were added to the ROI manager by the "Analyze Particles" tool and revised afterwards, or simply with the "Wand (tracing)" tool as far as possible. Afterwards, the endosome size (Area) was measured on the background substracted original image by applying "Multi Measure" on the generated ROI set. The obtained data were further processed with Microsoft Excel.

To determine the **Tfn uptake / cell area,** the total signal of Tfn within the previously drawn cell boundaries was divided by the corresponding cell area and the average of all measured cells per condition calculated.

To determine the **percentage of perinuclear endosomes**, first, a proper diameter for a circle enclosing most perinuclear Tfn in wt cells was chosen. For easier visualization of Tfn accumulation the LTU was changed to the LTU Fire. Next, for all cells, the Tfn signal within the previously drawn cell boundaries and the perinuclear Tfn signal were measured. Finally, the percentage of perinuclear endosomes was calculated in Microsoft Excel by dividing the perinuclear signal by the total signal of the cell.

To determine **the peripheral endosomes / 100 µm²,** the peripheral endosome size (µm²) was normalized to the cell area of each cell and calculated for a 100 µm² cell area.

Images for figure 31 (Overexpression of GFP-kazrin C does not significantly affect the diameter of the YFP-Rab4 vacuolar endosomes in HEK293 (EBNA) cells.) were analysed as follows:

Single confocal micrographs of cells showing vacuolar Rab4 endosomes with a clear lumen (doughnut shape) were selected. The most stretched inner diameter of the endosomes was measured by drawing lines and using the ImageJ tool "Measure". The obtained results were exported to Microsoft Excel and the average of the length was calculated.

Images for figure 45 (Depletion of kazrin in MEF cells also increases the number of internal actin structures versus the cortical actin or the stress fibres.) were analysed as follows:

The maximum intensity projection from three not overlapping planes intersecting each cell close to the coverslip, in the cell centre and in an upper area, was generated. Next, a straight line was drawn crossing the most representative diagonal of each cell (cross section). The intensity profile as shown in figure 45B was plotted and the highest peak in the cytoplasm and the cell cortex was labelled by arrowheads or arrows, respectively. The corresponding plot values were obtained from the plot values list in ImageJ and saved to Excel as basis of the calculation of the internal/external phalloidin signal shown in figure 45C.

Images for figure 46 (Endosomal actin is strongly disrupted in MEF cells upon depletion of kazrin.) were analysed as follows:

After running a "Gaussian blur" with radius 1, a general threshold defining the peripheral endosomes was determined and applied to all images. A square with fixed size for all images was defined and endosomes inside the selection analysed. Single endosomes were added to the ROI manager with the "Analyze Particles" tool and revised afterwards, or simply with the "Wand (tracing)" tool as far as possible, in some special cases endosomes were selected by "Freehand" selection. Afterwards, the endosome size (Area) and the Tfn concentration (RawIntDent) were measured on the background subtracted original image by applying "Multi Measure" on the generated ROI set. Next, the selected endosomes were projected as masks on the filtered images, a threshold for endosomal actin was defined and the actin structures corresponding to each endosome were selected and added to the

ROI manager with the “Wand (tracing)” tool as far as possible, in special cases “Freehad” selection was necessary. The actin signal was measured on the background subtracted original image by applying “Multi Measure” on the generated ROI set. The obtained data were further processed with Microsoft Excel to calculate the average endosome size, the average Tfn concentration per endosome, the total Tfn per endosome and the total actin per endosome relative to the wild type cells.

In parallel the images were analyzed in collaboration with Elena Rebollo who designed and wrote an advanced semi-automated macro for the analysis of actin on endosomes that confirmed the data obtained by our manual analysis.

7.6 Antibodies

Antigen	Animal	Source, Ref., Product Number	Modification
Actin	mouse	Roche 1378996	primary
adaptin alpha	mouse	Clontech A43920	primary
adaptin beta	mouse	Clontech A35620	primary
adaptin delta	mouse	Clontech A91120	primary
adaptin gamma	mouse	BD Transduction Laboratories #610385	primary
alpha adaptin AC1-M11	mouse	M. Robinson	primary
amphiphysin	mouse	Clontech A59420	primary
anti-goat Alexa568	donkey	Thermo Fisher A11057	Alexa568
anti-mouse Alexa488	donkey	Thermo Fisher A21202	Alexa488
anti-mouse Alexa568	donkey	Thermo Fisher A10037	Alexa568
anti-mouse Alexa647	goat	Thermo Fisher A21236	Alexa647
anti-mouse HRP	n.a.	Jackson Immuno Research 315-035-048	HRP
anti-rabbit Alexa488	donkey	Thermo Fisher A21206	Alexa488
anti-rabbit Alexa568	goat	Thermo Fisher A11036	Alexa568
anti-rabbit Alexa647	goat	Thermo Fisher A21245	Alexa647
anti-rabbit HRP	n.a.	Jackson Immuno Research 111-035-045	HRP
anti-rat Alexa488	goat	Thermo Fisher A21212	Alexa488
anti-rat Alexa568	goat	Thermo Fisher A11077	Alexa568
AP180	mouse	Clontech A41820	primary
Arp3	rabbit	Upstate/Millipore	primary
ARP3 mammalian	sheep	Cytoskeleton AAR01	primary
CI-M6PR	mouse	Abcam ab8093	primary
CHC	mouse	BD Transduction Laboratories #610499	primary
CLC	goat	Abcam ab77542	primary

dynamin	rabbit	H. McMahon	primary
EEA1	mouse	Clontech E41120	primary
EEA1	rabbit	Cell Signaling #3288	primary
eps15	mouse	Clontech E41120	primary
Fam21	rabbit	Santa Cruz sc-137993	primary
FITC-Phalloidin	n.a.	Sigma-Aldrich P5282	FITC
GFP	mouse	Roche 1814 460	primary
GFP	rabbit	Invitrogen A11122, Lot. 699301	primary
GFP	rabbit	Serum 17.03.2000	primary
Goat IgG	rabbit	Sigma-Aldrich A4174	HRP
GST	goat	Amersham 27-45777 (GE)	primary
Hrs/Vps27	rabbit	Santa Cruz sc-30221	primary
Kazrin C-term	rabbit	Abcam ab74114	primary
Kazrin C-term Serum (aa 148 to 327)	rabbit	EMBL Heidelberg, Germamy	primary
Kazrin full length	mouse	Abcam ab88752	primary
Kaz N-term Serum (aa 1 to 147)	rabbit	EMBL Heidelberg, Germamy	primary
Mouse IgG	goat	Sigma-Aldrich A2554	HRP
MYC	mouse	Roche 1 1814 150	HRP
MYC	mouse	Roche 1 667 203	primary
N-WASP	rabbit	Santa Cruz sc-20770	primary
p41	mouse	Santa Cruz sc-137125	primary
Phalloidin-Alexa488	n.a.	Thermo Fisher A12379	Alexa488
Phalloidin-Alexa555	n.a.	Thermo Fisher A340555	Alexa555
Protein A	rabbit	Sigma-Aldrich P3775	primary
Rab11	mouse	BD Transduction Laboratories #610656	primary
Rab11	mouse	BD Transduction Laboratories #610656	primary
Rab4a	mouse	BD Transduction Laboratories #610888	primary
Rab4b	mouse	SantaCruz	primary
Rab5	mouse	BD Transduction Laboratories #610281	primary
Rab5	mouse	BD Transduction Laboratories #610281	primary
Rab7	mouse	Abcam ab50533	primary
Rabaptin-5	mouse	BD Transduction Laboratories #610676	primary
Rabbit IgG	goat	Sigma-Aldrich A0545	HRP
Rabbit IgG	goat	Jackson ImmunoResearch 111-035-145	HRP
Rat IgG	rabbit	Sigma-Aldrich A5795	HRP
Sheep IgG	donkey	Sigma-Aldrich A3415	HRP
Spire1	mouse	Abnova H00056907-M01	primary
Tfn-Alexa488	n.a.	Jackson Immuno Research 009-540-050	Alexa488
Tfn-Alexa647	n.a.	Jackson Immuno Research 009-	Alexa647

		600-050	
TGN38 (TGN46, TGN48)	mouse	Thermo Fisher 2F7.1	primary
TRITC-Phalloidin	n.a.	Sigma-Aldrich P1951	TRITC
VPS35	mouse	Santa Cruz sc-374372	primary
WASH	rabbit	A. Gautreu aliquot (Derivery, E., et al. (2009))	primary
WASH (C-term.)	rabbit	Millipore ABS72	primary
WASH (N-term)	mouse	Sigma SAB4200552	primary
YFP (Lucifer Yellow)	rabbit	Invitrogen A5750 Lot 490241A	primary

Table III. Antibodies

References

8 References

Abe, T., M. Kato, H. Miki, T. Takenawa and T. Endo (2003). "Small GTPase Tc10 and its homologue RhoT induce N-WASP-mediated long process formation and neurite outgrowth." J Cell Sci **116**(Pt 1): 155-168.

Aghamohammadzadeh, S. and K. R. Ayscough (2009). "Differential requirements for actin during yeast and mammalian endocytosis." Nat Cell Biol **11**(8): 1039-1042.

Ahuja, R., R. Pinyol, N. Reichenbach, L. Custer, J. Klingensmith, M. M. Kessels and B. Qualmann (2007). "Cordon-bleu is an actin nucleation factor and controls neuronal morphology." Cell **131**(2): 337-350.

Albertson, R., B. Riggs and W. Sullivan (2005). "Membrane traffic: a driving force in cytokinesis." Trends Cell Biol **15**(2): 92-101.

Allaire, P. D., B. Ritter, S. Thomas, J. L. Burman, A. Y. Denisov, V. Legendre-Guillemin, S. Q. Harper, B. L. Davidson, K. Gehring and P. S. McPherson (2006). "Connecdenn, a novel DENN domain-containing protein of neuronal clathrin-coated vesicles functioning in synaptic vesicle endocytosis." J Neurosci **26**(51): 13202-13212.

Angers, C. G. and A. J. Merz (2011). "New links between vesicle coats and Rab-mediated vesicle targeting." Seminars in cell & developmental biology **22**(1): 18-26.

Antonescu, C. N., T. E. McGraw and A. Klip (2014). "Reciprocal regulation of endocytosis and metabolism." Cold Spring Harb Perspect Biol **6**(7): a016964.

Apaja, P. M., H. Xu and G. L. Lukacs (2010). "Quality control for unfolded proteins at the plasma membrane." J Cell Biol **191**(3): 553-570.

Aronheim, A., Y. C. Broder, A. Cohen, A. Fritsch, B. Belisle and A. Abo (1998). "Chp, a homologue of the GTPase Cdc42Hs, activates the JNK pathway and is implicated in reorganizing the actin cytoskeleton." Curr Biol **8**(20): 1125-1128.

Aschenbrenner, L., T. Lee and T. Hasson (2003). "Myo6 facilitates the translocation of endocytic vesicles from cell peripheries." Mol Biol Cell **14**(7): 2728-2743.

Avinoam, O., M. Schorb, C. J. Beese, J. A. Briggs and M. Kaksonen (2015). "ENDOCYTOSIS. Endocytic sites mature by continuous bending and remodeling of the clathrin coat." Science **348**(6241): 1369-1372.

Baetz, N. W. and J. R. Goldenring (2013). "Rab11-family interacting proteins define spatially and temporally distinct regions within the dynamic Rab11a-dependent recycling system." Mol Biol Cell **24**(5): 643-658.

Balderhaar, H. J. and C. Ungermann (2013). "CORVET and HOPS tethering complexes - coordinators of endosome and lysosome fusion." J Cell Sci **126**(Pt 6): 1307-1316.

Balklava, Z., S. Pant, H. Fares and B. D. Grant (2007). "Genome-wide analysis identifies a general requirement for polarity proteins in endocytic traffic." Nat Cell Biol **9**(9): 1066-1073.

Banach-Orlowska, M., E. Szymanska and M. Miaczynska (2015). "APPL1 endocytic adaptor as a fine tuner of Dvl2-induced transcription." FEBS Lett **589**(4): 532-539.

Barbero, P., L. Bittova and S. R. Pfeffer (2002). "Visualization of Rab9-mediated vesicle transport from endosomes to the trans-Golgi in living cells." J Cell Biol **156**(3): 511-518.

Bear, J. E. (2009). "Sorting out endosomes in the WASH." Dev Cell **17**(5): 583-584.

Belenkaya, T. Y., Y. Wu, X. Tang, B. Zhou, L. Cheng, Y. V. Sharma, D. Yan, E. M. Selva and X. Lin (2008). "The retromer complex influences Wnt secretion by recycling wntless from endosomes to the trans-Golgi network." Dev Cell **14**(1): 120-131.

Beltzner, C. C. and T. D. Pollard (2004). "Identification of functionally important residues of Arp2/3 complex by analysis of homology models from diverse species." J Mol Biol **336**(2): 551-565.

Benmerah, A., M. Bayrou, N. Cerf-Bensussan and A. Dautry-Varsat (1999). "Inhibition of clathrin-coated pit assembly by an Eps15 mutant." J Cell Sci **112 (Pt 9)**: 1303-1311.

Bhalla, A., C. P. Vetanovetz, E. Morel, Z. Chamoun, G. Di Paolo and S. A. Small (2012). "The location and trafficking routes of the neuronal retromer and its role in amyloid precursor protein transport." Neurobiol Dis **47**(1): 126-134.

Bilodeau, P. S., J. L. Urbanowski, S. C. Winistorfer and R. C. Piper (2002). "The Vps27p Hse1p complex binds ubiquitin and mediates endosomal protein sorting." Nat Cell Biol **4**(7): 534-539.
Bobkov, A. A., A. Muhlrad, A. Shvetsov, S. Benchaar, D. Scoville, S. C. Almo and E. Reisler (2004). "Cofilin (ADF) affects lateral contacts in F-actin." J Mol Biol **337**(1): 93-104.
Boettner, D. R., R. J. Chi and S. K. Lemmon (2011). "Lessons from yeast for clathrin-mediated endocytosis." Nat Cell Biol **14**(1): 2-10.
Boettner, D. R., H. Friesen, B. Andrews and S. K. Lemmon (2011). "Clathrin light chain directs endocytosis by influencing the binding of the yeast Hip1R homologue, Sla2, to F-actin." Mol Biol Cell **22**(19): 3699-3714.
Bonazzi, M., L. Vasudevan, A. Mallet, M. Sachse, A. Sartori, M.-C. Prevost, A. Roberts, S. B. Taner, J. D. Wilbur and F. M. Brodsky (2011). "Clathrin phosphorylation is required for actin recruitment at sites of bacterial adhesion and internalization." J Cell Biol **195**(3): 525-536.
Bonazzi, M., L. Vasudevan, A. Mallet, M. Sachse, A. Sartori, M. C. Prevost, A. Roberts, S. B. Taner, J. D. Wilbur, F. M. Brodsky and P. Cossart (2011). "Clathrin phosphorylation is required for actin recruitment at sites of bacterial adhesion and internalization." J Cell Biol **195**(3): 525-536.
Bonifacino, J. S. and A. Hierro (2011). "Transport according to GARP: receiving retrograde cargo at the trans-Golgi network." Trends Cell Biol **21**(3): 159-167.
Bonifacino, J. S. and R. Rojas (2006). "Retrograde transport from endosomes to the trans-Golgi network." Nat Rev Mol Cell Biol **7**(8): 568-579.
Bottcher, R. T., C. Stremmel, A. Meves, H. Meyer, M. Widmaier, H. Y. Tseng and R. Fassler (2012). "Sorting nexin 17 prevents lysosomal degradation of beta1 integrins by binding to the beta1-integrin tail." Nat Cell Biol **14**(6): 584-592.
Boustany, R. M. (2013). "Lysosomal storage diseases--the horizon expands." Nat Rev Neurol **9**(10): 583-598.
Brady, R. J., C. K. Damer, J. E. Heuser and T. J. O'Halloran (2010). "Regulation of Hip1r by epsin controls the temporal and spatial coupling of actin filaments to clathrin-coated pits." J Cell Sci **123**(Pt 21): 3652-3661.
Bright, N. A., L. J. Davis and J. P. Luzio (2016). "Endolysosomes Are the Principal Intracellular Sites of Acid Hydrolase Activity." Curr Biol **26**(17): 2233-2245.
Bright, N. A., M. J. Gratian and J. P. Luzio (2005). "Endocytic delivery to lysosomes mediated by concurrent fusion and kissing events in living cells." Curr Biol **15**(4): 360-365.
Brodsky, F. M. (2012). "Diversity of clathrin function: new tricks for an old protein." Annu Rev Cell Dev Biol **28**: 309-336.
Brodsky, F. M., C. Y. Chen, C. Knuehl, M. C. Towler and D. E. Wakeham (2001). "Biological basket weaving: formation and function of clathrin-coated vesicles." Annu Rev Cell Dev Biol **17**: 517-568.
Burden, J. J., X. M. Sun, A. B. Garcia and A. K. Soutar (2004). "Sorting motifs in the intracellular domain of the low density lipoprotein receptor interact with a novel domain of sorting nexin-17." J Biol Chem **279**(16): 16237-16245.
Calabia-Linares, C., J. Robles-Valero, H. de la Fuente, M. Perez-Martinez, N. Martin-Cofreces, M. Alfonso-Perez, C. Gutierrez-Vazquez, M. Mittelbrunn, S. Ibiza, F. R. Urbano-Olmos, C. Aguado-Ballano, C. O. Sanchez-Sorzano, F. Sanchez-Madrid and E. Veiga (2011). "Endosomal clathrin drives actin accumulation at the immunological synapse." J Cell Sci **124**(Pt 5): 820-830.
Callaghan, J., A. Simonsen, J. M. Gaullier, B. H. Toh and H. Stenmark (1999). "The endosome fusion regulator early-endosomal autoantigen 1 (EEA1) is a dimer." Biochem J **338 (Pt 2)**: 539-543.
Campellone, K. G., N. J. Webb, E. A. Znameroski and M. D. Welch (2008). "WHAMM is an Arp2/3 complex activator that binds microtubules and functions in ER to Golgi transport." Cell **134**(1): 148-161.
Campellone, K. G. and M. D. Welch (2010). "A nucleator arms race: cellular control of actin assembly." Nat Rev Mol Cell Biol **11**(4): 237-251.
Campelo, F. and V. Malhotra (2012). "Membrane fission: the biogenesis of transport carriers." Annu Rev Biochem **81**: 407-427.

Cao, H., J. Chen, E. W. Krueger and M. A. McNiven (2010). "SRC-mediated phosphorylation of dynamin and cortactin regulates the "constitutive" endocytosis of transferrin." Mol Cell Biol **30**(3): 781-792.
Caplan, S., E. C. Dell'Angelica, W. A. Gahl and J. S. Bonifacino (2000). "Trafficking of major histocompatibility complex class II molecules in human B-lymphoblasts deficient in the AP-3 adaptor complex." Immunology letters **72**(2): 113-117.
Carlier, M. F., D. Pantaloni, J. A. Evans, P. K. Lambooy, E. D. Korn and M. R. Webb (1988). "The hydrolysis of ATP that accompanies actin polymerization is essentially irreversible." FEBS Lett **235**(1-2): 211-214.
Carnell, M., T. Zech, S. D. Calaminus, S. Ura, M. Hagedorn, S. A. Johnston, R. C. May, T. Soldati, L. M. Machesky and R. H. Insall (2011). "Actin polymerization driven by WASH causes V-ATPase retrieval and vesicle neutralization before exocytosis." J Cell Biol **193**(5): 831-839.
Carroll, K. S., J. Hanna, I. Simon, J. Krise, P. Barbero and S. R. Pfeffer (2001). "Role of Rab9 GTPase in facilitating receptor recruitment by TIP47." Science **292**(5520): 1373-1376.
Chamberland, J. P., L. T. Antonow, M. Dias Santos and B. Ritter (2016). "NECAP2 controls clathrin coat recruitment to early endosomes for fast endocytic recycling." J Cell Sci **129**(13): 2625-2637.
Chapman, E. R., R. C. Desai, A. F. Davis and C. K. Tornehl (1998). "Delineation of the oligomerization, AP-2 binding, and synprint binding region of the C2B domain of synaptotagmin." J Biol Chem **273**(49): 32966-32972.
Chen, Z., E. Atefi and T. Baumgart (2016). "Membrane Shape Instability Induced by Protein Crowding." Biophys J **111**(9): 1823-1826.
Chen, Z., D. Borek, S. B. Padrick, T. S. Gomez, Z. Metlagel, A. M. Ismail, J. Umetani, D. D. Billadeau, Z. Otwinowski and M. K. Rosen (2010). "Structure and control of the actin regulatory WAVE complex." Nature **468**(7323): 533-538.
Chereau, D., M. Boczkowska, A. Skwarek-Maruszewska, I. Fujiwara, D. B. Hayes, G. Rebowski, P. Lappalainen, T. D. Pollard and R. Dominguez (2008). "Leiomodin is an actin filament nucleator in muscle cells." Science **320**(5873): 239-243.
Chereau, D., F. Kerff, P. Graceffa, Z. Grabarek, K. Langsetmo and R. Dominguez (2005). "Actin-bound structures of Wiskott-Aldrich syndrome protein (WASP)-homology domain 2 and the implications for filament assembly." Proc Natl Acad Sci U S A **102**(46): 16644-16649.
Chesarone, M. A., A. G. DuPage and B. L. Goode (2010). "Unleashing formins to remodel the actin and microtubule cytoskeletons." Nat Rev Mol Cell Biol **11**(1): 62-74.
Chetrit, D., N. Ziv and M. Ehrlich (2009). "Dab2 regulates clathrin assembly and cell spreading." Biochem J **418**(3): 701-715.
Chia, P. Z. and P. A. Gleeson (2011). "The regulation of endosome-to-Golgi retrograde transport by tethers and scaffolds." Traffic **12**(8): 939-947.
Chishti, A. H., A. C. Kim, S. M. Marfatia, M. Lutchman, M. Hanspal, H. Jindal, S. C. Liu, P. S. Low, G. A. Rouleau, N. Mohandas, J. A. Chasis, J. G. Conboy, P. Gascard, Y. Takakuwa, S. C. Huang, E. J. Benz, Jr., A. Bretscher, R. G. Fehon, J. F. Gusella, V. Ramesh, F. Solomon, V. T. Marchesi, S. Tsukita, S. Tsukita, K. B. Hoover and et al. (1998). "The FERM domain: a unique module involved in the linkage of cytoplasmic proteins to the membrane." Trends Biochem Sci **23**(8): 281-282.
Cho, K., M. Lee, D. Gu, W. A. Munoz, H. Ji, M. Kloc and P. D. McCrea (2011). "Kazrin, and its binding partners ARVCF- and delta-catenin, are required for Xenopus laevis craniofacial development." Dev Dyn **240**(12): 2601-2612.
Cho, K., T. G. Vaught, H. Ji, D. Gu, C. Papasakelariou-Yared, N. Horstmann, J. M. Jennings, M. Lee, L. M. Sevilla, M. Kloc, A. B. Reynolds, F. M. Watt, R. G. Brennan, A. P. Kowalczyk and P. D. McCrea (2010). "Xenopus Kazrin interacts with ARVCF-catenin, spectrin and p190B RhoGAP, and modulates RhoA activity and epithelial integrity." J Cell Sci **123**(Pt 23): 4128-4144.
Choudhury, A., D. K. Sharma, D. L. Marks and R. E. Pagano (2004). "Elevated endosomal cholesterol levels in Niemann-Pick cells inhibit rab4 and perturb membrane recycling." Mol Biol Cell **15**(10): 4500-4511.

Christoforidis, S., M. Miaczynska, K. Ashman, M. Wilm, L. Zhao, S. C. Yip, M. D. Waterfield, J. M. Backer and M. Zerial (1999). "Phosphatidylinositol-3-OH kinases are Rab5 effectors." Nat Cell Biol **1**(4): 249-252.
Collins, B. M., A. J. McCoy, H. M. Kent, P. R. Evans and D. J. Owen (2002). "Molecular architecture and functional model of the endocytic AP2 complex." Cell **109**(4): 523-535.
Collins, B. M., S. J. Norwood, M. C. Kerr, D. Mahony, M. N. Seaman, R. D. Teasdale and D. J. Owen (2008). "Structure of Vps26B and mapping of its interaction with the retromer protein complex." Traffic **9**(3): 366-379.
Collins, B. M., C. F. Skinner, P. J. Watson, M. N. Seaman and D. J. Owen (2005). "Vps29 has a phosphoesterase fold that acts as a protein interaction scaffold for retromer assembly." Nat Struct Mol Biol **12**(7): 594-602.
Cory, G. O., R. Cramer, L. Blanchoin and A. J. Ridley (2003). "Phosphorylation of the WASP-VCA domain increases its affinity for the Arp2/3 complex and enhances actin polymerization by WASP." Mol Cell **11**(5): 1229-1239.
Cossart, P. and A. Toledo-Arana (2008). "Listeria monocytogenes, a unique model in infection biology: an overview." Microbes and Infection **10**(9): 1041-1050.
Cremona, O. and P. De Camilli (1997). "Synaptic vesicle endocytosis." Curr Opin Neurobiol **7**(3): 323-330.
Crotzer, V. L., A. S. Mabardy, A. Weiss and F. M. Brodsky (2004). "T cell receptor engagement leads to phosphorylation of clathrin heavy chain during receptor internalization." J Exp Med **199**(7): 981-991.
D'Souza, R. S., R. Semus, E. A. Billings, C. B. Meyer, K. Conger and J. E. Casanova (2014). "Rab4 orchestrates a small GTPase cascade for recruitment of adaptor proteins to early endosomes." Curr Biol **24**(11): 1187-1198.
Dang, I., R. Gorelik, C. Sousa-Blin, E. Derivery, C. Guerin, J. Linkner, M. Nemethova, J. G. Dumortier, F. A. Giger, T. A. Chipysheva, V. D. Ermilova, S. Vacher, V. Campanacci, I. Herrada, A. G. Planson, S. Fetics, V. Henriot, V. David, K. Oguievetskaia, G. Lakisic, F. Pierre, A. Steffen, A. Boyreau, N. Peyrieras, K. Rottner, S. Zinn-Justin, J. Cherfils, I. Bieche, A. Y. Alexandrova, N. B. David, J. V. Small, J. Faix, L. Blanchoin and A. Gautreau (2013). "Inhibitory signalling to the Arp2/3 complex steers cell migration." Nature **503**(7475): 281-284.
Dang, I., J. Linkner, J. Yan, D. Irimia, J. Faix and A. Gautreau (2017). "The Arp2/3 inhibitory protein Arpin is dispensable for chemotaxis." Biol Cell **109**(4): 162-166.
Danielsson, K., M. Ebrahimi, E. Nylander, Y. B. Wahlin and K. Nylander (2017). "Alterations in Factors Involved in Differentiation and Barrier Function in the Epithelium in Oral and Genital Lichen Planus." Acta Derm Venereol **97**(2): 214-218.
Dannhauser, P. N., S. M. Camus, K. Sakamoto, L. A. Sadacca, J. A. Torres, M. D. Camus, K. Briant, S. Vassilopoulos, A. Rothnie, C. J. Smith and F. M. Brodsky (2017). "CHC22 and CHC17 clathrins have distinct biochemical properties and display differential regulation and function." J Biol Chem.
Darsow, T., S. E. Rieder and S. D. Emr (1997). "A multispecificity syntaxin homologue, Vam3p, essential for autophagic and biosynthetic protein transport to the vacuole." J Cell Biol **138**(3): 517-529.
Dayel, M. J., E. A. Holleran and R. D. Mullins (2001). "Arp2/3 complex requires hydrolyzable ATP for nucleation of new actin filaments." Proc Natl Acad Sci U S A **98**(26): 14871-14876.
De Deyne, P. G., A. O'Neill, W. G. Resneck, G. M. Dmytrenko, D. W. Pumplin and R. J. Bloch (1998). "The vitronectin receptor associates with clathrin-coated membrane domains via the cytoplasmic domain of its beta5 subunit." J Cell Sci **111 (Pt 18)**: 2729-2740.
De Franceschi, N., A. Arjonen, N. Elkhatib, K. Denessiouk, A. G. Wrobel, T. A. Wilson, J. Pouwels, G. Montagnac, D. J. Owen and J. Ivaska (2016). "Selective integrin endocytosis is driven by interactions between the integrin alpha-chain and AP2." Nat Struct Mol Biol **23**(2): 172-179.
De Luca, M., L. Cogli, C. Progida, V. Nisi, R. Pascolutti, S. Sigismund, P. P. Di Fiore and C. Bucci (2014). "RILP regulates vacuolar ATPase through interaction with the V1G1 subunit." J Cell Sci **127**(Pt 12): 2697-2708.
De Matteis, M. A. and A. Luini (2011). "Mendelian disorders of membrane trafficking." N Engl J Med **365**(10): 927-938.

de Renzis, S., B. Sonnichsen and M. Zerial (2002). "Divalent Rab effectors regulate the sub-compartmental organization and sorting of early endosomes." Nat Cell Biol **4**(2): 124-133.
Del Conte-Zerial, P., L. Brusch, J. C. Rink, C. Collinet, Y. Kalaidzidis, M. Zerial and A. Deutsch (2008). "Membrane identity and GTPase cascades regulated by toggle and cut-out switches." Mol Syst Biol **4**: 206.
del Pozo, M. A., N. Balasubramanian, N. B. Alderson, W. B. Kiosses, A. Grande-Garcia, R. G. Anderson and M. A. Schwartz (2005). "Phospho-caveolin-1 mediates integrin-regulated membrane domain internalization." Nat Cell Biol **7**(9): 901-908.
Dell'Angelica, E. C. (2001). "Clathrin-binding proteins: Got a motif? Join the network!" TRENDS in Cell Biology.
Deneka, M., M. Neeft, I. Popa, M. van Oort, H. Sprong, V. Oorschot, J. Klumperman, P. Schu and P. van der Sluijs (2003). "Rabaptin-5alpha/rabaptin-4 serves as a linker between rab4 and gamma(1)-adaptin in membrane recycling from endosomes." Embo j **22**(11): 2645-2657.
Derivery, E. and A. Gautreau (2010). "Generation of branched actin networks: assembly and regulation of the N-WASP and WAVE molecular machines." Bioessays **32**(2): 119-131.
Derivery, E., C. Sousa, J. J. Gautier, B. Lombard, D. Loew and A. Gautreau (2009). "The Arp2/3 activator WASH controls the fission of endosomes through a large multiprotein complex." Dev Cell **17**(5): 712-723.
Di Fiore, P. P. and M. von Zastrow (2014). "Endocytosis, signaling, and beyond." Cold Spring Harb Perspect Biol **6**(8).
Di Paolo, G. and P. De Camilli (2006). "Phosphoinositides in cell regulation and membrane dynamics." Nature **443**(7112): 651-657.
Dietrich, S., S. Weiss, S. Pleiser and E. Kerkhoff (2013). "Structural and functional insights into the Spir/formin actin nucleator complex." Biol Chem **394**(12): 1649-1660.
Diggins, N. L. and D. J. Webb (2017). "APPL1 is a multifunctional endosomal signaling adaptor protein." Biochem Soc Trans **45**(3): 771-779.
Donaldson, J. G. and C. L. Jackson (2011). "ARF family G proteins and their regulators: roles in membrane transport, development and disease." Nat Rev Mol Cell Biol **12**(6): 362-375.
Doolittle, L. K., M. K. Rosen and S. B. Padrick (2013). "Measurement and analysis of in vitro actin polymerization." Methods Mol Biol **1046**: 273-293.
Drake, M. T., Y. Zhu and S. Kornfeld (2000). "The assembly of AP-3 adaptor complex-containing clathrin-coated vesicles on synthetic liposomes." Mol Biol Cell **11**(11): 3723-3736.
Driskell, O. J., A. Mironov, V. J. Allan and P. G. Woodman (2007). "Dynein is required for receptor sorting and the morphogenesis of early endosomes." Nat Cell Biol **9**(1): 113-120.
Duleh, S. N. and M. D. Welch (2010). "WASH and the Arp2/3 complex regulate endosome shape and trafficking." Cytoskeleton (Hoboken) **67**(3): 193-206.
Duncan, M. C., M. J. Cope, B. L. Goode, B. Wendland and D. G. Drubin (2001). "Yeast Eps15-like endocytic protein, Pan1p, activates the Arp2/3 complex." Nat Cell Biol **3**(7): 687-690.
Duncan, M. C., G. Costaguta and G. S. Payne (2003). "Yeast epsin-related proteins required for Golgi-endosome traffic define a gamma-adaptin ear-binding motif." Nat Cell Biol **5**(1): 77-81.
Edeling, M. A., S. K. Mishra, P. A. Keyel, A. L. Steinhauser, B. M. Collins, R. Roth, J. E. Heuser, D. J. Owen and L. M. Traub (2006). "Molecular switches involving the AP-2 beta2 appendage regulate endocytic cargo selection and clathrin coat assembly." Dev Cell **10**(3): 329-342.
Edwards, M., A. Zwolak, D. A. Schafer, D. Sept, R. Dominguez and J. A. Cooper (2014). "Capping protein regulators fine-tune actin assembly dynamics." Nat Rev Mol Cell Biol **15**(10): 677-689.
Egile, C., I. Rouiller, X. P. Xu, N. Volkmann, R. Li and D. Hanein (2005). "Mechanism of filament nucleation and branch stability revealed by the structure of the Arp2/3 complex at actin branch junctions." PLoS Biol **3**(11): e383.
Ehrlich, M., W. Boll, A. Van Oijen, R. Hariharan, K. Chandran, M. L. Nibert and T. Kirchhausen (2004). "Endocytosis by random initiation and stabilization of clathrin-coated pits." Cell **118**(5): 591-605.
Eichel, K. and M. von Zastrow (2018). "Subcellular Organization of GPCR Signaling." Trends Pharmacol Sci **39**(2): 200-208.

Encinar Del Dedo, J., F. Z. Idrissi, I. M. Fernandez-Golbano, P. Garcia, E. Rebollo, M. K. Krzyzanowski, H. Grotsch and M. I. Geli (2017). "ORP-Mediated ER Contact with Endocytic Sites Facilitates Actin Polymerization." Dev Cell **43**(5): 588-602.e586.
Engqvist-Goldstein, A. E., C. X. Zhang, S. Carreno, C. Barroso, J. E. Heuser and D. G. Drubin (2004). "RNAi-mediated Hip1R silencing results in stable association between the endocytic machinery and the actin assembly machinery." Mol Biol Cell **15**(4): 1666-1679.
Erdmann, K., K. Kaulke, C. Thomae, D. Huebner, M. Sergon, M. Froehner, M. P. Wirth and S. Fuessel (2014). "Elevated expression of prostate cancer-associated genes is linked to down-regulation of microRNAs." BMC Cancer **14**: 82.
Esk, C., C.-Y. Chen, L. Johannes and F. M. Brodsky (2010). "The clathrin heavy chain isoform CHC22 functions in a novel endosomal sorting step." The Journal of Cell Biology **188**(1): 131-144.
Esk, C., C. Y. Chen, L. Johannes and F. M. Brodsky (2010). "The clathrin heavy chain isoform CHC22 functions in a novel endosomal sorting step." J Cell Biol **188**(1): 131-144.
Evangelista, M., S. Zigmond and C. Boone (2003). "Formins: signaling effectors for assembly and polarization of actin filaments." J Cell Sci **116**(Pt 13): 2603-2611.
Ezratty, E. J., C. Bertaux, E. E. Marcantonio and G. G. Gundersen (2009). "Clathrin mediates integrin endocytosis for focal adhesion disassembly in migrating cells." J Cell Biol **187**(5): 733-747.
Farsad, K. and P. De Camilli (2003). "Mechanisms of membrane deformation." Curr Opin Cell Biol **15**(4): 372-381.
Ferreira, A. P. A. and E. Boucrot (2018). "Mechanisms of Carrier Formation during Clathrin-Independent Endocytosis." Trends Cell Biol **28**(3): 188-200.
Fischer, J. A., S. H. Eun and B. T. Doolan (2006). "Endocytosis, endosome trafficking, and the regulation of Drosophila development." Annu Rev Cell Dev Biol **22**: 181-206.
Fischer von Mollard, G. and T. H. Stevens (1999). "The Saccharomyces cerevisiae v-SNARE Vti1p is required for multiple membrane transport pathways to the vacuole." Mol Biol Cell **10**(6): 1719-1732.
Fjorback, A. W., M. Seaman, C. Gustafsen, A. Mehmedbasic, S. Gokool, C. Wu, D. Militz, V. Schmidt, P. Madsen, J. R. Nyengaard, T. E. Willnow, E. I. Christensen, W. B. Mobley, A. Nykjaer and O. M. Andersen (2012). "Retromer binds the FANSHY sorting motif in SorLA to regulate amyloid precursor protein sorting and processing." J Neurosci **32**(4): 1467-1480.
Foraker, A. B., S. M. Camus, T. M. Evans, S. R. Majeed, C. Y. Chen, S. B. Taner, I. R. Correa, Jr., S. J. Doxsey and F. M. Brodsky (2012). "Clathrin promotes centrosome integrity in early mitosis through stabilization of centrosomal ch-TOG." J Cell Biol **198**(4): 591-605.
Forgac, M. (2007). "Vacuolar ATPases: rotary proton pumps in physiology and pathophysiology." Nat Rev Mol Cell Biol **8**(11): 917-929.
Fotin, A., Y. Cheng, P. Sliz, N. Grigorieff, S. C. Harrison, T. Kirchhausen and T. Walz (2004). "Molecular model for a complete clathrin lattice from electron cryomicroscopy." Nature **432**(7017): 573-579.
Franch-Marro, X., F. Wendler, S. Guidato, J. Griffith, A. Baena-Lopez, N. Itasaki, M. M. Maurice and J. P. Vincent (2008). "Wingless secretion requires endosome-to-Golgi retrieval of Wntless/Evi/Sprinter by the retromer complex." Nat Cell Biol **10**(2): 170-177.
Frankel, E. B. and A. Audhya (2017). "ESCRT-dependent cargo sorting at multivesicular endosomes." Semin Cell Dev Biol.
Frankel, G. and A. D. Phillips (2008). "Attaching effacing Escherichia coli and paradigms of Tir-triggered actin polymerization: getting off the pedestal." Cell Microbiol **10**(3): 549-556.
Freeman, C. L., G. Hesketh and M. N. J. Seaman (2014). "RME-8 coordinates the activity of the WASH complex with the function of the retromer SNX dimer to control endosomal tubulation." Journal of Cell Science **127**(9): 2053-2070.
Frost, A., R. Perera, A. Roux, K. Spasov, O. Destaing, E. H. Egelman, P. De Camilli and V. M. Unger (2008). "Structural basis of membrane invagination by F-BAR domains." Cell **132**(5): 807-817.
Frost, A., V. M. Unger and P. De Camilli (2009). "The BAR domain superfamily: membrane-molding macromolecules." Cell **137**(2): 191-196.
Fu, W., Q. Jiang and C. Zhang (2011). "Novel functions of endocytic player clathrin in mitosis." Cell Res **21**(12): 1655-1661.

Galletta, B. J., D. Y. Chuang and J. A. Cooper (2008). "Distinct roles for Arp2/3 regulators in actin assembly and endocytosis." PLoS Biol **6**(1): e1.
Galletta, B. J., O. L. Mooren and J. A. Cooper (2010). "Actin dynamics and endocytosis in yeast and mammals." Current opinion in biotechnology **21**(5): 604-610.
Galletta, B. J., O. L. Mooren and J. A. Cooper (2010). "Actin dynamics and endocytosis in yeast and mammals." Curr Opin Biotechnol **21**(5): 604-610.
Gallon, M., T. Clairfeuille, F. Steinberg, C. Mas, R. Ghai, R. B. Sessions, R. D. Teasdale, B. M. Collins and P. J. Cullen (2014). "A unique PDZ domain and arrestin-like fold interaction reveals mechanistic details of endocytic recycling by SNX27-retromer." Proc Natl Acad Sci U S A **111**(35): E3604-3613.
Gallon, M. and P. J. Cullen (2015). "Retromer and sorting nexins in endosomal sorting." Biochem Soc Trans **43**(1): 33-47.
Galovic, M., D. Xu, L. B. Areces, R. van der Kammen and M. Innocenti (2011). "Interplay between N-WASP and CK2 optimizes clathrin-mediated endocytosis of EGFR." J Cell Sci **124**(Pt 12): 2001-2012.
Galvez, T., J. Gilleron, M. Zerial and G. A. O'Sullivan (2012). "SnapShot: Mammalian Rab proteins in endocytic trafficking." Cell **151**(1): 234-234 e232.
Garcia-Alai, M. M., J. Heidemann, M. Skruzny, A. Gieras, H. D. T. Mertens, D. I. Svergun, M. Kaksonen, C. Uetrecht and R. Meijers (2018). "Epsin and Sla2 form assemblies through phospholipid interfaces." Nat Commun **9**(1): 328.
Geli, M. I., R. Lombardi, B. Schmelzl and H. Riezman (2000). "An intact SH3 domain is required for myosin I-induced actin polymerization." EMBO J **19**(16): 4281-4291.
Geli, M. I. and H. Riezman (1998). "Endocytic internalization in yeast and animal cells: similar and different." J Cell Sci **111 (Pt 8)**: 1031-1037.
Gershlick, D. C. and M. Lucas (2017). "Endosomal Trafficking: Retromer and Retriever Are Relatives in Recycling." Curr Biol **27**(22): R1233-R1236.
Ghai, R., M. Mobli, S. J. Norwood, A. Bugarcic, R. D. Teasdale, G. F. King and B. M. Collins (2011). "Phox homology band 4.1/ezrin/radixin/moesin-like proteins function as molecular scaffolds that interact with cargo receptors and Ras GTPases." Proc Natl Acad Sci U S A **108**(19): 7763-7768.
Ghosh, P., N. M. Dahms and S. Kornfeld (2003). "Mannose 6-phosphate receptors: new twists in the tale." Nature reviews Molecular cell biology **4**(3): 202.
Goldenring, J. R. (2015). "Recycling endosomes." Curr Opin Cell Biol **35**: 117-122.
Goldschmidt-Clermont, P. J., M. I. Furman, D. Wachsstock, D. Safer, V. T. Nachmias and T. D. Pollard (1992). "The control of actin nucleotide exchange by thymosin beta 4 and profilin. A potential regulatory mechanism for actin polymerization in cells." Mol Biol Cell **3**(9): 1015-1024.
Goldstein, L., C. Ko and J. Errick (1977). "Nuclear actin: an apparent association with condensed chromatin." Cell Biol Int Rep **1**(6): 511-515.
Goley, E. D., T. Ohkawa, J. Mancuso, J. B. Woodruff, J. A. D'Alessio, W. Z. Cande, L. E. Volkman and M. D. Welch (2006). "Dynamic nuclear actin assembly by Arp2/3 complex and a baculovirus WASP-like protein." Science **314**(5798): 464-467.
Goley, E. D., S. E. Rodenbusch, A. C. Martin and M. D. Welch (2004). "Critical conformational changes in the Arp2/3 complex are induced by nucleotide and nucleation promoting factor." Mol Cell **16**(2): 269-279.
Goley, E. D. and M. D. Welch (2006). "The ARP2/3 complex: an actin nucleator comes of age." Nat Rev Mol Cell Biol **7**(10): 713-726.
Gomez, T. S. and D. D. Billadeau (2009). "A FAM21-containing WASH complex regulates retromer-dependent sorting." Dev Cell **17**(5): 699-711.
Gomez, T. S., J. A. Gorman, A. A. de Narvajas, A. O. Koenig and D. D. Billadeau (2012). "Trafficking defects in WASH-knockout fibroblasts originate from collapsed endosomal and lysosomal networks." Mol Biol Cell **23**(16): 3215-3228.
Goode, B. L., A. A. Rodal, G. Barnes and D. G. Drubin (2001). "Activation of the Arp2/3 complex by the actin filament binding protein Abp1p." J Cell Biol **153**(3): 627-634.
Gorelik, R. and A. Gautreau (2015). "The Arp2/3 inhibitory protein arpin induces cell turning by pausing cell migration." Cytoskeleton (Hoboken) **72**(7): 362-371.

Goud, B. and P. A. Gleeson (2010). "TGN golgins, Rabs and cytoskeleton: regulating the Golgi trafficking highways." Trends in cell biology **20**(6): 329-336.
Gouin, E., C. Egile, P. Dehoux, V. Villiers, J. Adams, F. Gertler, R. Li and P. Cossart (2004). "The RickA protein of Rickettsia conorii activates the Arp2/3 complex." Nature **427**(6973): 457-461.
Grant, B., Y. Zhang, M.-C. Paupard, S. X. Lin, D. H. Hall and D. Hirsh (2001). "Evidence that RME-1, a conserved C. elegans EH-domain protein, functions in endocytic recycling." Nature Cell Biology **3**: 573.
Grant, B. D. and S. Caplan (2008). "Mechanisms of EHD/RME-1 protein function in endocytic transport." Traffic **9**(12): 2043-2052.
Grant, B. D. and J. G. Donaldson (2009). "Pathways and mechanisms of endocytic recycling." Nat Rev Mol Cell Biol **10**(9): 597-608.
Groot, K. R., L. M. Sevilla, K. Nishi, T. DiColandrea and F. M. Watt (2004). "Kazrin, a novel periplakin-interacting protein associated with desmosomes and the keratinocyte plasma membrane." J Cell Biol **166**(5): 653-659.
Gruenberg, J. and F. G. van der Goot (2006). "Mechanisms of pathogen entry through the endosomal compartments." Nat Rev Mol Cell Biol **7**(7): 495-504.
Hales, C. M., J. P. Vaerman and J. R. Goldenring (2002). "Rab11 family interacting protein 2 associates with Myosin Vb and regulates plasma membrane recycling." J Biol Chem **277**(52): 50415-50421.
Hao, Y. H., J. M. Doyle, S. Ramanathan, T. S. Gomez, D. Jia, M. Xu, Z. J. Chen, D. D. Billadeau, M. K. Rosen and P. R. Potts (2013). "Regulation of WASH-dependent actin polymerization and protein trafficking by ubiquitination." Cell **152**(5): 1051-1064.
Harborth, J., S. M. Elbashir, K. Bechert, T. Tuschl and K. Weber (2001). "Identification of essential genes in cultured mammalian cells using small interfering RNAs." J Cell Sci **114**(Pt 24): 4557-4565.
Harbour, M. E., S. Y. Breusegem, R. Antrobus, C. Freeman, E. Reid and M. N. Seaman (2010). "The cargo-selective retromer complex is a recruiting hub for protein complexes that regulate endosomal tubule dynamics." J Cell Sci **123**(Pt 21): 3703-3717.
Harrison, M. S., C. S. Hung, T. T. Liu, R. Christiano, T. C. Walther and C. G. Burd (2014). "A mechanism for retromer endosomal coat complex assembly with cargo." Proc Natl Acad Sci U S A **111**(1): 267-272.
Harterink, M., F. Port, M. J. Lorenowicz, I. J. McGough, M. Silhankova, M. C. Betist, J. R. T. van Weering, R. van Heesbeen, T. C. Middelkoop, K. Basler, P. J. Cullen and H. C. Korswagen (2011). "A SNX3-dependent retromer pathway mediates retrograde transport of the Wnt sorting receptor Wntless and is required for Wnt secretion." Nat Cell Biol **13**(8): 914-923.
Haucke, V. (2005). "Phosphoinositide regulation of clathrin-mediated endocytosis." Biochem Soc Trans **33**(Pt 6): 1285-1289.
Hemsath, L., R. Dvorsky, D. Fiegen, M. F. Carlier and M. R. Ahmadian (2005). "An electrostatic steering mechanism of Cdc42 recognition by Wiskott-Aldrich syndrome proteins." Mol Cell **20**(2): 313-324.
Hierro, A., D. C. Gershlick, A. L. Rojas and J. S. Bonifacino (2015). "Formation of Tubulovesicular Carriers from Endosomes and Their Fusion to the trans-Golgi Network." Int Rev Cell Mol Biol **318**: 159-202.
Hierro, A., A. L. Rojas, R. Rojas, N. Murthy, G. Effantin, A. V. Kajava, A. C. Steven, J. S. Bonifacino and J. H. Hurley (2007). "Functional architecture of the retromer cargo-recognition complex." Nature **449**(7165): 1063-1067.
Higgs, H. N. (2002). "Actin nucleation: cortactin caught in the act." Curr Biol **12**(17): R593-595.
Higgs, H. N. and T. D. Pollard (1999). "Regulation of actin polymerization by Arp2/3 complex and WASp/Scar proteins." J Biol Chem **274**(46): 32531-32534.
Higgs, H. N. and T. D. Pollard (2001). "Regulation of actin filament network formation through ARP2/3 complex: activation by a diverse array of proteins." Annu Rev Biochem **70**: 649-676.
Hirst, J., J. R. Edgar, G. H. Borner, S. Li, D. A. Sahlender, R. Antrobus and M. S. Robinson (2015). "Contributions of epsinR and gadkin to clathrin-mediated intracellular trafficking." Mol Biol Cell **26**(17): 3085-3103.

Hirst, J., A. Motley, K. Harasaki, S. Y. Peak Chew and M. S. Robinson (2003). "EpsinR: an ENTH domain-containing protein that interacts with AP-1." Mol Biol Cell **14**(2): 625-641.
Holmes, K. C., D. Popp, W. Gebhard and W. Kabsch (1990). "Atomic model of the actin filament." Nature **347**(6288): 44-49.
Hong, N. H., A. Qi and A. M. Weaver (2015). "PI(3,5)P2 controls endosomal branched actin dynamics by regulating cortactin-actin interactions." J Cell Biol **210**(5): 753-769.
Honing, S., D. Ricotta, M. Krauss, K. Spate, B. Spolaore, A. Motley, M. Robinson, C. Robinson, V. Haucke and D. J. Owen (2005). "Phosphatidylinositol-(4,5)-bisphosphate regulates sorting signal recognition by the clathrin-associated adaptor complex AP2." Mol Cell **18**(5): 519-531.
Hopkins, C. R. (1983). "Intracellular routing of transferrin and transferrin receptors in epidermoid carcinoma A431 cells." Cell **35**(1): 321-330.
Horiuchi, H., R. Lippe, H. M. McBride, M. Rubino, P. Woodman, H. Stenmark, V. Rybin, M. Wilm, K. Ashman, M. Mann and M. Zerial (1997). "A novel Rab5 GDP/GTP exchange factor complexed to Rabaptin-5 links nucleotide exchange to effector recruitment and function." Cell **90**(6): 1149-1159.
Hudson, A. M. and L. Cooley (2002). "A subset of dynamic actin rearrangements in Drosophila requires the Arp2/3 complex." J Cell Biol **156**(4): 677-687.
Hullin-Matsuda, F., T. Taguchi, P. Greimel and T. Kobayashi (2014). Lipid compartmentalization in the endosome system. Seminars in cell & developmental biology, Elsevier.
Humphries, A. C. and M. Way (2013). "The non-canonical roles of clathrin and actin in pathogen internalization, egress and spread." Nature Reviews Microbiology **11**(8): 551-560.
Humphries, A. C. and M. Way (2013). "The non-canonical roles of clathrin and actin in pathogen internalization, egress and spread." Nat Rev Microbiol **11**(8): 551-560.
Huotari, J. and A. Helenius (2011). "Endosome maturation." EMBO J **30**(17): 3481-3500.
Hurley, J. H. and P. I. Hanson (2010). "Membrane budding and scission by the ESCRT machinery: it's all in the neck." Nat Rev Mol Cell Biol **11**(8): 556-566.
Huxley, H. E. (1963). "ELECTRON MICROSCOPE STUDIES ON THE STRUCTURE OF NATURAL AND SYNTHETIC PROTEIN FILAMENTS FROM STRIATED MUSCLE." J Mol Biol **7**: 281-308.
Huynh, K. K. and S. Grinstein (2007). "Regulation of vacuolar pH and its modulation by some microbial species." Microbiol Mol Biol Rev **71**(3): 452-462.
Idrissi, F. Z., A. Blasco, A. Espinal and M. I. Geli (2012). "Ultrastructural dynamics of proteins involved in endocytic budding." Proc Natl Acad Sci U S A **109**(39): E2587-2594.
Idrissi, F. Z. and M. I. Geli (2014). "Zooming in on the molecular mechanisms of endocytic budding by time-resolved electron microscopy." Cell Mol Life Sci **71**(4): 641-657.
Itoh, T. and P. De Camilli (2006). "BAR, F-BAR (EFC) and ENTH/ANTH domains in the regulation of membrane-cytosol interfaces and membrane curvature." Biochim Biophys Acta **1761**(8): 897-912.
Jean, S. and A. A. Kiger (2012). "Coordination between RAB GTPase and phosphoinositide regulation and functions." Nat Rev Mol Cell Biol **13**(7): 463-470.
Jeng, R. L., E. D. Goley, J. A. D'Alessio, O. Y. Chaga, T. M. Svitkina, G. G. Borisy, R. A. Heinzen and M. D. Welch (2004). "A Rickettsia WASP-like protein activates the Arp2/3 complex and mediates actin-based motility." Cell Microbiol **6**(8): 761-769.
Jentsch, T. J. (2007). "Chloride and the endosomal-lysosomal pathway: emerging roles of CLC chloride transporters." J Physiol **578**(Pt 3): 633-640.
Jia, D., T. S. Gomez, D. D. Billadeau and M. K. Rosen (2012). "Multiple repeat elements within the FAM21 tail link the WASH actin regulatory complex to the retromer." Mol Biol Cell **23**(12): 2352-2361.
Jia, D., T. S. Gomez, Z. Metlagel, J. Umetani, Z. Otwinowski, M. K. Rosen and D. D. Billadeau (2010). "WASH and WAVE actin regulators of the Wiskott-Aldrich syndrome protein (WASP) family are controlled by analogous structurally related complexes." Proc Natl Acad Sci U S A **107**(23): 10442-10447.
Jones, M. C., P. T. Caswell and J. C. Norman (2006). "Endocytic recycling pathways: emerging regulators of cell migration." Curr Opin Cell Biol **18**(5): 549-557.

Jongsma, M. L., I. Berlin, R. H. Wijdeven, L. Janssen, G. M. Janssen, M. A. Garstka, H. Janssen, M. Mensink, P. A. van Veelen, R. M. Spaapen and J. Neefjes (2016). "An ER-Associated Pathway Defines Endosomal Architecture for Controlled Cargo Transport." Cell **166**(1): 152-166.
Jung, G., K. Remmert, X. Wu, J. M. Volosky and J. A. Hammer, 3rd (2001). "The Dictyostelium CARMIL protein links capping protein and the Arp2/3 complex to type I myosins through their SH3 domains." J Cell Biol **153**(7): 1479-1497.
Kahr, W. H., F. G. Pluthero, A. Elkadri, N. Warner, M. Drobac, C. H. Chen, R. W. Lo, L. Li, R. Li, Q. Li, C. Thoeni, J. Pan, G. Leung, I. Lara-Corrales, R. Murchie, E. Cutz, R. M. Laxer, J. Upton, C. M. Roifman, R. S. Yeung, J. H. Brumell and A. M. Muise (2017). "Loss of the Arp2/3 complex component ARPC1B causes platelet abnormalities and predisposes to inflammatory disease." Nat Commun **8**: 14816.
Kaksonen, M., H. B. Peng and H. Rauvala (2000). "Association of cortactin with dynamic actin in lamellipodia and on endosomal vesicles." J Cell Sci **113 Pt 24**: 4421-4426.
Kaksonen, M. and A. Roux (2018). "Mechanisms of clathrin-mediated endocytosis." Nat Rev Mol Cell Biol.
Kaksonen, M., Y. Sun and D. G. Drubin (2003). "A pathway for association of receptors, adaptors, and actin during endocytic internalization." Cell **115**(4): 475-487.
Kaksonen, M., C. P. Toret and D. G. Drubin (2005). "A modular design for the clathrin- and actin-mediated endocytosis machinery." Cell **123**(2): 305-320.
Katzmann, D. J., M. Babst and S. D. Emr (2001). "Ubiquitin-dependent sorting into the multivesicular body pathway requires the function of a conserved endosomal protein sorting complex, ESCRT-I." Cell **106**(2): 145-155.
Katzmann, D. J., C. J. Stefan, M. Babst and S. D. Emr (2003). "Vps27 recruits ESCRT machinery to endosomes during MVB sorting." J Cell Biol **162**(3): 413-423.
Kerkhoff, E., J. C. Simpson, C. B. Leberfinger, I. M. Otto, T. Doerks, P. Bork, U. R. Rapp, T. Raabe and R. Pepperkok (2001). "The Spir actin organizers are involved in vesicle transport processes." Current Biology **11**(24): 1963-1968.
Kessels, M. M. and B. Qualmann (2004). "The syndapin protein family: linking membrane trafficking with the cytoskeleton." J Cell Sci **117**(Pt 15): 3077-3086.
Ketel, K., M. Krauss, A. S. Nicot, D. Puchkov, M. Wieffer, R. Muller, D. Subramanian, C. Schultz, J. Laporte and V. Haucke (2016). "A phosphoinositide conversion mechanism for exit from endosomes." Nature **529**(7586): 408-412.
Kirchhausen, T. (2000). "Clathrin." Annu Rev Biochem **69**: 699-727.
Kirchhausen, T. (2000). "Three ways to make a vesicle." Nat Rev Mol Cell Biol **1**(3): 187-198.
Kirchhausen, T., D. Owen and S. C. Harrison (2014). "Molecular structure, function, and dynamics of clathrin-mediated membrane traffic." Cold Spring Harb Perspect Biol **6**(5): a016725.
kleine Balderhaar, H. J. and C. Ungermann (2013). "CORVET and HOPS tethering complexes–coordinators of endosome and lysosome fusion." J Cell Sci **126**(6): 1307-1316.
Knauth, P., T. Schluter, M. Czubayko, C. Kirsch, V. Florian, S. Schreckenberger, H. Hahn and R. Bohnensack (2005). "Functions of sorting nexin 17 domains and recognition motif for P-selectin trafficking." J Mol Biol **347**(4): 813-825.
Knight, M. J., C. Leettola, M. Gingery, H. Li and J. U. Bowie (2011). "A human sterile alpha motif domain polymerizome." Protein Sci **20**(10): 1697-1706.
Korolchuk, V. and G. Banting (2003). "Kinases in clathrin-mediated endocytosis." Biochem Soc Trans **31**(Pt 4): 857-860.
Kouranti, I., M. Sachse, N. Arouche, B. Goud and A. Echard (2006). "Rab35 regulates an endocytic recycling pathway essential for the terminal steps of cytokinesis." Curr Biol **16**(17): 1719-1725.
Krendel, M., E. K. Osterweil and M. S. Mooseker (2007). "Myosin 1E interacts with synaptojanin-1 and dynamin and is involved in endocytosis." FEBS Lett **581**(4): 644-650.
Kubo, K., M. Kobayashi, S. Nozaki, C. Yagi, K. Hatsuzawa, Y. Katoh, H. W. Shin, S. Takahashi and K. Nakayama (2015). "SNAP23/25 and VAMP2 mediate exocytic event of transferrin receptor-containing recycling vesicles." Biol Open **4**(7): 910-920.
Kukulski, W., M. Schorb, M. Kaksonen and J. A. Briggs (2012). "Plasma membrane reshaping during endocytosis is revealed by time-resolved electron tomography." Cell **150**(3): 508-520.

Kumari, S., S. Mg and S. Mayor (2010). "Endocytosis unplugged: multiple ways to enter the cell." Cell Res **20**(3): 256-275.
Kummel, D. and C. Ungermann (2014). "Principles of membrane tethering and fusion in endosome and lysosome biogenesis." Curr Opin Cell Biol **29**: 61-66.
Laemmli, U. (1970). "Glycine-SDS-PAGE for separation of proteins." Nature **227**(5).
Lampe, M., S. Vassilopoulos and C. Merrifield (2016). "Clathrin coated pits, plaques and adhesion." J Struct Biol **196**(1): 48-56.
Lane, R. F., S. M. Raines, J. W. Steele, M. E. Ehrlich, J. A. Lah, S. A. Small, R. E. Tanzi, A. D. Attie and S. Gandy (2010). "Diabetes-associated SorCS1 regulates Alzheimer's amyloid-beta metabolism: evidence for involvement of SorL1 and the retromer complex." J Neurosci **30**(39): 13110-13115.
Lapierre, L. A., R. Kumar, C. M. Hales, J. Navarre, S. G. Bhartur, J. O. Burnette, D. W. Provance, Jr., J. A. Mercer, M. Bahler and J. R. Goldenring (2001). "Myosin vb is associated with plasma membrane recycling systems." Mol Biol Cell **12**(6): 1843-1857.
Lata, S., G. Schoehn, A. Jain, R. Pires, J. Piehler, H. G. Gottlinger and W. Weissenhorn (2008). "Helical structures of ESCRT-III are disassembled by VPS4." Science **321**(5894): 1354-1357.
Le Clainche, C., D. Didry, M. F. Carlier and D. Pantaloni (2001). "Activation of Arp2/3 complex by Wiskott-Aldrich Syndrome protein is linked to enhanced binding of ATP to Arp2." J Biol Chem **276**(50): 46689-46692.
Le Clainche, C., B. S. Pauly, C. X. Zhang, A. E. Engqvist-Goldstein, K. Cunningham and D. G. Drubin (2007). "A Hip1R-cortactin complex negatively regulates actin assembly associated with endocytosis." Embo j **26**(5): 1199-1210.
Lechler, T., G. A. Jonsdottir, S. K. Klee, D. Pellman and R. Li (2001). "A two-tiered mechanism by which Cdc42 controls the localization and activation of an Arp2/3-activating motor complex in yeast." J Cell Biol **155**(2): 261-270.
LeClaire, L. L., 3rd, M. Baumgartner, J. H. Iwasa, R. D. Mullins and D. L. Barber (2008). "Phosphorylation of the Arp2/3 complex is necessary to nucleate actin filaments." J Cell Biol **182**(4): 647-654.
Lecuit, T. and F. Pilot (2003). "Developmental control of cell morphogenesis: a focus on membrane growth." Nat Cell Biol **5**(2): 103-108.
Lee, D. W., X. Wu, E. Eisenberg and L. E. Greene (2006). "Recruitment dynamics of GAK and auxilin to clathrin-coated pits during endocytosis." J Cell Sci **119**(Pt 17): 3502-3512.
Lee, J., C. Retamal, L. Cuitino, A. Caruano-Yzermans, J. E. Shin, P. van Kerkhof, M. P. Marzolo and G. Bu (2008). "Adaptor protein sorting nexin 17 regulates amyloid precursor protein trafficking and processing in the early endosomes." J Biol Chem **283**(17): 11501-11508.
Lee, W. L., M. Bezanilla and T. D. Pollard (2000). "Fission yeast myosin-I, Myo1p, stimulates actin assembly by Arp2/3 complex and shares functions with WASp." J Cell Biol **151**(4): 789-800.
Lees-Miller, J. P., G. Henry and D. M. Helfman (1992). "Identification of act2, an essential gene in the fission yeast Schizosaccharomyces pombe that encodes a protein related to actin." Proc Natl Acad Sci U S A **89**(1): 80-83.
Lemmon, M. A. (2008). "Membrane recognition by phospholipid-binding domains." Nat Rev Mol Cell Biol **9**(2): 99-111.
Lev, S. (2010). "Non-vesicular lipid transport by lipid-transfer proteins and beyond." Nature Reviews Molecular Cell Biology **11**: 739.
Leyton-Puig, D., T. Isogai, E. Argenzio, B. van den Broek, J. Klarenbeek, H. Janssen, K. Jalink and M. Innocenti (2017). "Flat clathrin lattices are dynamic actin-controlled hubs for clathrin-mediated endocytosis and signalling of specific receptors." Nat Commun **8**: 16068.
Li, J., P. J. Peters, M. Bai, J. Dai, E. Bos, T. Kirchhausen, K. V. Kandror and V. W. Hsu (2007). "An ACAP1-containing clathrin coat complex for endocytic recycling." J Cell Biol **178**(3): 453-464.
Li, X. and M. Donowitz (2008). "Fractionation of subcellular membrane vesicles of epithelial and nonepithelial cells by OptiPrep density gradient ultracentrifugation." Methods Mol Biol **440**: 97-110.
Lin, S. X., B. Grant, D. Hirsh and F. R. Maxfield (2001). "Rme-1 regulates the distribution and function of the endocytic recycling compartment in mammalian cells." Nature cell biology **3**(6): 567-572.

Lin, S. X., G. G. Gundersen and F. R. Maxfield (2002). "Export from pericentriolar endocytic recycling compartment to cell surface depends on stable, detyrosinated (glu) microtubules and kinesin." Molecular biology of the cell **13**(1): 96-109.
Lindmo, K. and H. Stenmark (2006). "Regulation of membrane traffic by phosphoinositide 3-kinases." Journal of Cell Science **119**(4): 605-614.
Liu, C., J. Wang, Y. Hu, H. Xie, M. Liu and H. Tang (2017). "Upregulation of kazrin F by miR-186 suppresses apoptosis but promotes epithelial-mesenchymal transition to contribute to malignancy in human cervical cancer cells." Chin J Cancer Res **29**(1): 45-56.
Llado, A., P. Timpson, S. Vila de Muga, J. Moreto, A. Pol, T. Grewal, R. J. Daly, C. Enrich and F. Tebar (2008). "Protein kinase Cdelta and calmodulin regulate epidermal growth factor receptor recycling from early endosomes through Arp2/3 complex and cortactin." Mol Biol Cell **19**(1): 17-29.
Lu, L. and W. Hong (2014). From endosomes to the trans-Golgi network. Seminars in cell & developmental biology, Elsevier.
Lucas, M., D. C. Gershlick, A. Vidaurrazaga, A. L. Rojas, J. S. Bonifacino and A. Hierro (2016). "Structural Mechanism for Cargo Recognition by the Retromer Complex." Cell **167**(6): 1623-1635.e1614.
Luzio, J. P., M. D. Parkinson, S. R. Gray and N. A. Bright (2009). "The delivery of endocytosed cargo to lysosomes." Biochem Soc Trans **37**(Pt 5): 1019-1021.
Luzio, J. P., P. R. Pryor and N. A. Bright (2007). "Lysosomes: fusion and function." Nat Rev Mol Cell Biol **8**(8): 622-632.
Lv, S. Q., Y. H. Kim, F. Giulio, T. Shalaby, S. Nobusawa, H. Yang, Z. Zhou, M. Grotzer and H. Ohgaki (2012). "Genetic alterations in microRNAs in medulloblastomas." Brain Pathol **22**(2): 230-239.
Ma, M., C. G. Burd and R. J. Chi (2017). "Distinct complexes of yeast Snx4 family SNX-BARs mediate retrograde trafficking of Snc1 and Atg27." Traffic **18**(2): 134-144.
Machesky, L. M. and K. L. Gould (1999). "The Arp2/3 complex: a multifunctional actin organizer." Curr Opin Cell Biol **11**(1): 117-121.
Majeed, S. R., L. Vasudevan, C. Y. Chen, Y. Luo, J. A. Torres, T. M. Evans, A. Sharkey, A. B. Foraker, N. M. Wong, C. Esk, T. A. Freeman, A. Moffett, J. H. Keen and F. M. Brodsky (2014). "Clathrin light chains are required for the gyrating-clathrin recycling pathway and thereby promote cell migration." Nat Commun **5**: 3891.
Maldonado-Baez, L. and B. Wendland (2006). "Endocytic adaptors: recruiters, coordinators and regulators." Trends Cell Biol **16**(10): 505-513.
Mallam, A. L. and E. M. Marcotte (2017). "Systems-wide Studies Uncover Commander, a Multiprotein Complex Essential to Human Development." Cell Systems **4**(5): 483-494.
Malsam, J., S. Kreye and T. H. Sollner (2008). "Membrane fusion: SNAREs and regulation." Cell Mol Life Sci **65**(18): 2814-2832.
Marchand, J. B., D. A. Kaiser, T. D. Pollard and H. N. Higgs (2001). "Interaction of WASP/Scar proteins with actin and vertebrate Arp2/3 complex." Nat Cell Biol **3**(1): 76-82.
Maritzen, T. and V. Haucke (2010). "Gadkin: A novel link between endosomal vesicles and microtubule tracks." Commun Integr Biol **3**(4): 299-302.
Maritzen, T., T. Zech, M. R. Schmidt, E. Krause, L. M. Machesky and V. Haucke (2012). "Gadkin negatively regulates cell spreading and motility via sequestration of the actin-nucleating ARP2/3 complex." Proc Natl Acad Sci U S A **109**(26): 10382-10387.
Marlin, M. C. and G. Li (2015). "Biogenesis and Function of the NGF/TrkA Signaling Endosome." International review of cell and molecular biology **314**: 239-257.
Marshansky, V. and M. Futai (2008). "The V-type H+-ATPase in vesicular trafficking: targeting, regulation and function." Curr Opin Cell Biol **20**(4): 415-426.
Martin, A. C., X. P. Xu, I. Rouiller, M. Kaksonen, Y. Sun, L. Belmont, N. Volkmann, D. Hanein, M. Welch and D. G. Drubin (2005). "Effects of Arp2 and Arp3 nucleotide-binding pocket mutations on Arp2/3 complex function." J Cell Biol **168**(2): 315-328.
Martin, T. F. (2001). "PI (4, 5) P2 regulation of surface membrane traffic." Current opinion in cell biology **13**(4): 493-499.

Martinez-Quiles, N., H. Y. Ho, M. W. Kirschner, N. Ramesh and R. S. Geha (2004). "Erk/Src phosphorylation of cortactin acts as a switch on-switch off mechanism that controls its ability to activate N-WASP." Mol Cell Biol **24**(12): 5269-5280.
Matsui, Y., A. Kikuchi, S. Araki, Y. Hata, J. Kondo, Y. Teranishi and Y. Takai (1990). "Molecular cloning and characterization of a novel type of regulatory protein (GDI) for smg p25A, a ras p21-like GTP-binding protein." Mol Cell Biol **10**(8): 4116-4122.
Maxfield, F. R. and T. E. McGraw (2004). "Endocytic recycling." Nat Rev Mol Cell Biol **5**(2): 121-132.
Mayers, J. R., I. Fyfe, A. L. Schuh, E. R. Chapman, J. M. Edwardson and A. Audhya (2011). "ESCRT-0 assembles as a heterotetrameric complex on membranes and binds multiple ubiquitinylated cargoes simultaneously." J Biol Chem **286**(11): 9636-9645.
Mayers, J. R., L. Wang, J. Pramanik, A. Johnson, A. Sarkeshik, Y. Wang, W. Saengsawang, J. R. Yates, 3rd and A. Audhya (2013). "Regulation of ubiquitin-dependent cargo sorting by multiple endocytic adaptors at the plasma membrane." Proc Natl Acad Sci U S A **110**(29): 11857-11862.
McBride, H. M., V. Rybin, C. Murphy, A. Giner, R. Teasdale and M. Zerial (1999). "Oligomeric complexes link Rab5 effectors with NSF and drive membrane fusion via interactions between EEA1 and syntaxin 13." Cell **98**(3): 377-386.
McGough, A., B. Pope, W. Chiu and A. Weeds (1997). "Cofilin changes the twist of F-actin: implications for actin filament dynamics and cellular function." J Cell Biol **138**(4): 771-781.
McGough, I. J. and P. J. Cullen (2013). "Clathrin is not required for SNX-BAR-retromer-mediated carrier formation." J Cell Sci **126**(Pt 1): 45-52.
McGough, I. J., F. Steinberg, D. Jia, P. A. Barbuti, K. J. McMillan, K. J. Heesom, A. L. Whone, M. A. Caldwell, D. D. Billadeau, M. K. Rosen and P. J. Cullen (2014). "Retromer binding to FAM21 and the WASH complex is perturbed by the Parkinson disease-linked VPS35(D620N) mutation." Curr Biol **24**(14): 1670-1676.
McGraw, T. E., K. W. Dunn and F. R. Maxfield (1993). "Isolation of a temperature-sensitive variant Chinese hamster ovary cell line with a morphologically altered endocytic recycling compartment." J Cell Physiol **155**(3): 579-594.
McNally, K. E., R. Faulkner, F. Steinberg, M. Gallon, R. Ghai, D. Pim, P. Langton, N. Pearson, C. M. Danson, H. Nagele, L. L. Morris, A. Singla, B. L. Overlee, K. J. Heesom, R. Sessions, L. Banks, B. M. Collins, I. Berger, D. D. Billadeau, E. Burstein and P. J. Cullen (2017). "Retriever is a multiprotein complex for retromer-independent endosomal cargo recycling." Nat Cell Biol **19**(10): 1214-1225.
Merrifield, C. J., S. E. Moss, C. Ballestrem, B. A. Imhof, G. Giese, I. Wunderlich and W. Almers (1999). "Endocytic vesicles move at the tips of actin tails in cultured mast cells." Nat Cell Biol **1**(1): 72-74.
Merrifield, C. J., D. Perrais and D. Zenisek (2005). "Coupling between clathrin-coated-pit invagination, cortactin recruitment, and membrane scission observed in live cells." Cell **121**(4): 593-606.
Merz, A. J. and W. T. Wickner (2004). "Trans-SNARE interactions elicit Ca2+ efflux from the yeast vacuole lumen." J Cell Biol **164**(2): 195-206.
Meyer, C., D. Zizioli, S. Lausmann, E. L. Eskelinen, J. Hamann, P. Saftig, K. von Figura and P. Schu (2000). "mu1A-adaptin-deficient mice: lethality, loss of AP-1 binding and rerouting of mannose 6-phosphate receptors." Embo j **19**(10): 2193-2203.
Miki, H., T. Sasaki, Y. Takai and T. Takenawa (1998). "Induction of filopodium formation by a WASP-related actin-depolymerizing protein N-WASP." Nature **391**(6662): 93-96.
Mills, I. G., G. J. Praefcke, Y. Vallis, B. J. Peter, L. E. Olesen, J. L. Gallop, P. J. Butler, P. R. Evans and H. T. McMahon (2003). "EpsinR: an AP1/clathrin interacting protein involved in vesicle trafficking." J Cell Biol **160**(2): 213-222.
Morel, E., R. G. Parton and J. Gruenberg (2009). "Annexin A2-dependent polymerization of actin mediates endosome biogenesis." Dev Cell **16**(3): 445-457.
Moreno-Ruiz, E., M. Galan-Diez, W. Zhu, E. Fernandez-Ruiz, C. d'Enfert, S. G. Filler, P. Cossart and E. Veiga (2009). "Candida albicans internalization by host cells is mediated by a clathrin-dependent mechanism." Cell Microbiol **11**(8): 1179-1189.
Morrell, J. L., M. Morphew and K. L. Gould (1999). "A mutant of Arp2p causes partial disassembly of the Arp2/3 complex and loss of cortical actin function in fission yeast." Mol Biol Cell **10**(12): 4201-4215.

Morrison, H. A., H. Dionne, T. E. Rusten, A. Brech, W. W. Fisher, B. D. Pfeiffer, S. E. Celniker, H. Stenmark and D. Bilder (2008). "Regulation of early endosomal entry by the Drosophila tumor suppressors Rabenosyn and Vps45." Mol Biol Cell **19**(10): 4167-4176.
Muhammad, A., I. Flores, H. Zhang, R. Yu, A. Staniszewski, E. Planel, M. Herman, L. Ho, R. Kreber, L. S. Honig, B. Ganetzky, K. Duff, O. Arancio and S. A. Small (2008). "Retromer deficiency observed in Alzheimer's disease causes hippocampal dysfunction, neurodegeneration, and Abeta accumulation." Proc Natl Acad Sci U S A **105**(20): 7327-7332.
Mukherjee, S., R. N. Ghosh and F. R. Maxfield (1997). "Endocytosis." Physiol Rev **77**(3): 759-803.
Mullins, R. D., J. F. Kelleher, J. Xu and T. D. Pollard (1998). "Arp2/3 complex from Acanthamoeba binds profilin and cross-links actin filaments." Mol Biol Cell **9**(4): 841-852.
Muriel, O., A. Tomas, C. C. Scott and J. Gruenberg (2016). "Moesin and cortactin control actin-dependent multivesicular endosome biogenesis." Mol Biol Cell **27**(21): 3305-3316.
Murray, J. T., C. Panaretou, H. Stenmark, M. Miaczynska and J. M. Backer (2002). "Role of Rab5 in the recruitment of hVps34/p150 to the early endosome." Traffic **3**(6): 416-427.
Myatt, S. S., J. Wang, L. J. Monteiro, M. Christian, K. K. Ho, L. Fusi, R. E. Dina, J. J. Brosens, S. Ghaem-Maghami and E. W. Lam (2010). "Definition of microRNAs that repress expression of the tumor suppressor gene FOXO1 in endometrial cancer." Cancer Res **70**(1): 367-377.
Nakatsu, F., K. Hase and H. Ohno (2014). "The Role of the Clathrin Adaptor AP-1: Polarized Sorting and Beyond." Membranes (Basel) **4**(4): 747-763.
Naslavsky, N., J. Rahajeng, M. Sharma, M. Jovic and S. Caplan (2006). "Interactions between EHD proteins and Rab11-FIP2: a role for EHD3 in early endosomal transport." Mol Biol Cell **17**(1): 163-177.
Naslavsky, N., R. Weigert and J. G. Donaldson (2003). "Convergence of non-clathrin- and clathrin-derived endosomes involves Arf6 inactivation and changes in phosphoinositides." Mol Biol Cell **14**(2): 417-431.
Naslavsky, N., R. Weigert and J. G. Donaldson (2004). "Characterization of a nonclathrin endocytic pathway: membrane cargo and lipid requirements." Mol Biol Cell **15**(8): 3542-3552.
Neefjes, J., M. M. Jongsma and I. Berlin (2017). "Stop or Go? Endosome Positioning in the Establishment of Compartment Architecture, Dynamics, and Function." Trends Cell Biol.
Neubrand, V. E., R. D. Will, W. Mobius, A. Poustka, S. Wiemann, P. Schu, C. G. Dotti, R. Pepperkok and J. C. Simpson (2005). "Gamma-BAR, a novel AP-1-interacting protein involved in post-Golgi trafficking." Embo j **24**(6): 1122-1133.
Nordmann, M., M. Cabrera, A. Perz, C. Brocker, C. Ostrowicz, S. Engelbrecht-Vandre and C. Ungermann (2010). "The Mon1-Ccz1 complex is the GEF of the late endosomal Rab7 homolog Ypt7." Curr Biol **20**(18): 1654-1659.
Norris, A., P. Tammineni, S. Wang, J. Gerdes, A. Murr, K. Y. Kwan, Q. Cai and B. D. Grant (2017). "SNX-1 and RME-8 oppose the assembly of HGRS-1/ESCRT-0 degradative microdomains on endosomes." Proc Natl Acad Sci U S A **114**(3): E307-e316.
Nossal, R. (2001). "Energetics of clathrin basket assembly." Traffic **2**(2): 138-147.
Ohashi, E., K. Tanabe, Y. Henmi, K. Mesaki, Y. Kobayashi and K. Takei (2011). "Receptor Sorting within Endosomal Trafficking Pathway Is Facilitated by Dynamic Actin Filaments." PLoS ONE **6**(5): e19942.
Oka, T. and M. Krieger (2005). "Multi-component protein complexes and Golgi membrane trafficking." J Biochem **137**(2): 109-114.
Owen, D. J., Y. Vallis, B. M. F. Pearse, H. T. McMahon and P. R. Evans (2000). "The structure and function of the β2-adaptin appendage domain." The EMBO Journal **19**(16): 4216-4227.
Paczkowski, J. E., B. C. Richardson and J. C. Fromme (2015). "Cargo adaptors: structures illuminate mechanisms regulating vesicle biogenesis." Trends Cell Biol **25**(7): 408-416.
Padrick, S. B., L. K. Doolittle, C. A. Brautigam, D. S. King and M. K. Rosen (2011). "Arp2/3 complex is bound and activated by two WASP proteins." Proceedings of the National Academy of Sciences **108**(33): E472-E479.
Pagano, A. and M. Spiess (2005). "Reconstitution of Rab4-dependent vesicle formation in vitro." Methods Enzymol **403**: 81-92.
Palfy, M., A. Remenyi and T. Korcsmaros (2012). "Endosomal crosstalk: meeting points for signaling pathways." Trends Cell Biol **22**(9): 447-456.

Pan, C. L., P. D. Baum, M. Gu, E. M. Jorgensen, S. G. Clark and G. Garriga (2008). "C. elegans AP-2 and retromer control Wnt signaling by regulating mig-14/Wntless." Dev Cell **14**(1): 132-139.
Parachoniak, C. A., Y. Luo, J. V. Abella, J. H. Keen and M. Park (2011). "GGA3 functions as a switch to promote Met receptor recycling, essential for sustained ERK and cell migration." Dev Cell **20**(6): 751-763.
Parisis, N., L. Krasinska, B. Harker, S. Urbach, M. Rossignol, A. Camasses, J. Dewar, N. Morin and D. Fisher (2017). "Initiation of DNA replication requires actin dynamics and formin activity." Embo j **36**(21): 3212-3231.
Park, S. Y. and X. Guo (2014). "Adaptor protein complexes and intracellular transport." Bioscience reports **34**(4): e00123.
Park, S. Y. and X. Guo (2014). "Adaptor protein complexes and intracellular transport." Biosci Rep **34**(4).
Patino-Lopez, G., X. Dong, K. Ben-Aissa, K. M. Bernot, T. Itoh, M. Fukuda, M. J. Kruhlak, L. E. Samelson and S. Shaw (2008). "Rab35 and its GAP EPI64C in T cells regulate receptor recycling and immunological synapse formation." J Biol Chem **283**(26): 18323-18330.
Pavlos, N. J. and P. A. Friedman (2017). "GPCR Signaling and Trafficking: The Long and Short of It." Trends Endocrinol Metab **28**(3): 213-226.
Pechlivanis, M., A. Samol and E. Kerkhoff (2009). "Identification of a short Spir interaction sequence at the C-terminal end of formin subgroup proteins." J Biol Chem **284**(37): 25324-25333.
Perrin, L., S. Lacas-Gervais, J. Gilleron, F. Ceppo, F. Prodon, A. Benmerah, J. F. Tanti and M. Cormont (2013). "Rab4b controls an early endosome sorting event by interacting with the gamma-subunit of the clathrin adaptor complex 1." J Cell Sci **126**(Pt 21): 4950-4962.
Phillips-Krawczak, C. A., A. Singla, P. Starokadomskyy, Z. Deng, D. G. Osborne, H. Li, C. J. Dick, T. S. Gomez, M. Koenecke, J. S. Zhang, H. Dai, L. F. Sifuentes-Dominguez, L. N. Geng, S. H. Kaufmann, M. Y. Hein, M. Wallis, J. McGaughran, J. Gecz, B. Sluis, D. D. Billadeau and E. Burstein (2015). "COMMD1 is linked to the WASH complex and regulates endosomal trafficking of the copper transporter ATP7A." Mol Biol Cell **26**(1): 91-103.
Pincetic, A. and J. Leis (2009). "The mechanism of budding of retroviruses from cell membranes." Advances in virology **2009**.
Piotrowski, J. T., T. S. Gomez, R. A. Schoon, A. K. Mangalam and D. D. Billadeau (2013). "WASH knockout T cells demonstrate defective receptor trafficking, proliferation, and effector function." Mol Cell Biol **33**(5): 958-973.
Pollard, T. D. and G. G. Borisy (2003). "Cellular motility driven by assembly and disassembly of actin filaments." Cell **112**(4): 453-465.
Pons, M., I. Izquierdo, M. Andreu-Carbo, G. Garrido, J. Planaguma, O. Muriel, M. A. Del Pozo, M. I. Geli and A. M. Aragay (2017). "Phosphorylation of filamin A regulates chemokine receptor CCR2 recycling." J Cell Sci **130**(2): 490-501.
Popa, I., M. Deneka and P. van der Sluijs (2005). "Expression and Properties of the Rab4, Rabaptin-5α, AP-1 Complex in Endosomal Recycling." **403**: 526-540.
Popoff, V., G. A. Mardones, S. K. Bai, V. Chambon, D. Tenza, P. V. Burgos, A. Shi, P. Benaroch, S. Urbe, C. Lamaze, B. D. Grant, G. Raposo and L. Johannes (2009). "Analysis of articulation between clathrin and retromer in retrograde sorting on early endosomes." Traffic **10**(12): 1868-1880.
Poteryaev, D., S. Datta, K. Ackema, M. Zerial and A. Spang (2010). "Identification of the switch in early-to-late endosome transition." Cell **141**(3): 497-508.
Praefcke, G. J. and H. T. McMahon (2004). "The dynamin superfamily: universal membrane tubulation and fission molecules?" Nat Rev Mol Cell Biol **5**(2): 133-147.
Pruyne, D., M. Evangelista, C. Yang, E. Bi, S. Zigmond, A. Bretscher and C. Boone (2002). "Role of formins in actin assembly: nucleation and barbed-end association." Science **297**(5581): 612-615.
Quinlan, M. E., J. E. Heuser, E. Kerkhoff and R. D. Mullins (2005). "Drosophila Spire is an actin nucleation factor." Nature **433**(7024): 382-388.
Rabouille, C. (2017). "Retriever fetches integrins from endosomes." Nat Cell Biol **19**(10): 1144-1146.

Raiborg, C., K. G. Bache, D. J. Gillooly, I. H. Madshus, E. Stang and H. Stenmark (2002). "Hrs sorts ubiquitinated proteins into clathrin-coated microdomains of early endosomes." Nat Cell Biol **4**(5): 394-398.
Raiborg, C., K. G. Bache, A. Mehlum, E. Stang and H. Stenmark (2001). "Hrs recruits clathrin to early endosomes." EMBO J **20**(17): 5008-5021.
Raiborg, C. and H. Stenmark (2009). "The ESCRT machinery in endosomal sorting of ubiquitylated membrane proteins." Nature **458**(7237): 445-452.
Ramachandran, R. (2011). "Vesicle scission: dynamin." Semin Cell Dev Biol **22**(1): 10-17.
Rapoport, I., W. Boll, A. Yu, T. Bocking and T. Kirchhausen (2008). "A motif in the clathrin heavy chain required for the Hsc70/auxilin uncoating reaction." Mol Biol Cell **19**(1): 405-413.
Renard, H. F., L. Johannes and P. Morsomme (2018). "Increasing Diversity of Biological Membrane Fission Mechanisms." Trends Cell Biol.
Riedl, J., A. H. Crevenna, K. Kessenbrock, J. H. Yu, D. Neukirchen, M. Bista, F. Bradke, D. Jenne, T. A. Holak, Z. Werb, M. Sixt and R. Wedlich-Soldner (2008). "Lifeact: a versatile marker to visualize F-actin." Nat Methods **5**(7): 605-607.
Rink, J., E. Ghigo, Y. Kalaidzidis and M. Zerial (2005). "Rab conversion as a mechanism of progression from early to late endosomes." Cell **122**(5): 735-749.
Robinson, M. S. (2004). "Adaptable adaptors for coated vesicles." Trends in Cell Biology **14**(4): 167-174.
Robinson, M. S. and J. S. Bonifacino (2001). "Adaptor-related proteins." Curr Opin Cell Biol **13**(4): 444-453.
Robinson, M. S. and J. S. Bonifacino (2001). "Adaptor-related proteins." Curr Opin Cell Biol **13**(4): 444-453.
Robinson, R. C., K. Turbedsky, D. A. Kaiser, J. B. Marchand, H. N. Higgs, S. Choe and T. D. Pollard (2001). "Crystal structure of Arp2/3 complex." Science **294**(5547): 1679-1684.
Rodal, A. A., O. Sokolova, D. B. Robins, K. M. Daugherty, S. Hippenmeyer, H. Riezman, N. Grigorieff and B. L. Goode (2005). "Conformational changes in the Arp2/3 complex leading to actin nucleation." Nat Struct Mol Biol **12**(1): 26-31.
Rogaeva, E., Y. Meng, J. H. Lee, Y. Gu, T. Kawarai, F. Zou, T. Katayama, C. T. Baldwin, R. Cheng, H. Hasegawa, F. Chen, N. Shibata, K. L. Lunetta, R. Pardossi-Piquard, C. Bohm, Y. Wakutani, L. A. Cupples, K. T. Cuenco, R. C. Green, L. Pinessi, I. Rainero, S. Sorbi, A. Bruni, R. Duara, R. P. Friedland, R. Inzelberg, W. Hampe, H. Bujo, Y. Q. Song, O. M. Andersen, T. E. Willnow, N. Graff-Radford, R. C. Petersen, D. Dickson, S. D. Der, P. E. Fraser, G. Schmitt-Ulms, S. Younkin, R. Mayeux, L. A. Farrer and P. St George-Hyslop (2007). "The neuronal sortilin-related receptor SORL1 is genetically associated with Alzheimer disease." Nat Genet **39**(2): 168-177.
Rohatgi, R., L. Ma, H. Miki, M. Lopez, T. Kirchhausen, T. Takenawa and M. W. Kirschner (1999). "The interaction between N-WASP and the Arp2/3 complex links Cdc42-dependent signals to actin assembly." Cell **97**(2): 221-231.
Rojas, R., T. van Vlijmen, G. A. Mardones, Y. Prabhu, A. L. Rojas, S. Mohammed, A. J. Heck, G. Raposo, P. van der Sluijs and J. S. Bonifacino (2008). "Regulation of retromer recruitment to endosomes by sequential action of Rab5 and Rab7." J Cell Biol **183**(3): 513-526.
Ropers, F., E. Derivery, H. Hu, M. Garshasbi, M. Karbasiyan, M. Herold, G. Nurnberg, R. Ullmann, A. Gautreau, K. Sperling, R. Varon and A. Rajab (2011). "Identification of a novel candidate gene for non-syndromic autosomal recessive intellectual disability: the WASH complex member SWIP." Hum Mol Genet **20**(13): 2585-2590.
Rottner, K., J. Hanisch and K. G. Campellone (2010). "WASH, WHAMM and JMY: regulation of Arp2/3 complex and beyond." Trends Cell Biol **20**(11): 650-661.
Rouiller, I., X. P. Xu, K. J. Amann, C. Egile, S. Nickell, D. Nicastro, R. Li, T. D. Pollard, N. Volkmann and D. Hanein (2008). "The structural basis of actin filament branching by the Arp2/3 complex." J Cell Biol **180**(5): 887-895.
Royle, S. J. (2012). "The role of clathrin in mitotic spindle organisation." J Cell Sci **125**(Pt 1): 19-28.
Rust, M. J., M. Lakadamyali, F. Zhang and X. Zhuang (2004). "Assembly of endocytic machinery around individual influenza viruses during viral entry." Nat Struct Mol Biol **11**(6): 567-573.

Sachse, M., S. Urbe, V. Oorschot, G. J. Strous and J. Klumperman (2002). "Bilayered clathrin coats on endosomal vacuoles are involved in protein sorting toward lysosomes." Mol Biol Cell **13**(4): 1313-1328.
Saffarian, S., E. Cocucci and T. Kirchhausen (2009). "Distinct Dynamics of Endocytic Clathrin-Coated Pits and Coated Plaques." PLOS Biology **7**(9): e1000191.
Sagot, I., A. A. Rodal, J. Moseley, B. L. Goode and D. Pellman (2002). "An actin nucleation mechanism mediated by Bni1 and profilin." Nat Cell Biol **4**(8): 626-631.
Saheki, Y. and P. De Camilli (2017). "Endoplasmic Reticulum-Plasma Membrane Contact Sites." Annu Rev Biochem **86**: 659-684.
Saksena, S., J. Wahlman, D. Teis, A. E. Johnson and S. D. Emr (2009). "Functional reconstitution of ESCRT-III assembly and disassembly." Cell **136**(1): 97-109.
Sambrook, J. and D. W. Russell (2001). Molecular Cloning: A Laboratory Manual, Cold Spring Harbor Laboratory Press.
Sato, M., K. Sato, W. Liou, S. Pant, A. Harada and B. D. Grant (2008). "Regulation of endocytic recycling by C. elegans Rab35 and its regulator RME-4, a coated-pit protein." Embo j **27**(8): 1183-1196.
Sawa, M., S. Suetsugu, A. Sugimoto, H. Miki, M. Yamamoto and T. Takenawa (2003). "Essential role of the C. elegans Arp2/3 complex in cell migration during ventral enclosure." J Cell Sci **116**(Pt 8): 1505-1518.
Schafer, D. A. (2002). "Coupling actin dynamics and membrane dynamics during endocytosis." Curr Opin Cell Biol **14**(1): 76-81.
Schenck, A., L. Goto-Silva, C. Collinet, M. Rhinn, A. Giner, B. Habermann, M. Brand and M. Zerial (2008). "The endosomal protein Appl1 mediates Akt substrate specificity and cell survival in vertebrate development." Cell **133**(3): 486-497.
Schmelzl, B. and M. I. Geli (2002). "An efficient genetic screen in mammalian cultured cells." EMBO Rep **3**(7): 682-687.
Schmid, S. L. (1992). "The mechanism of receptor-mediated endocytosis: more questions than answers." Bioessays **14**(9): 589-596.
Schmidt, M. R., T. Maritzen, V. Kukhtina, V. A. Higman, L. Doglio, N. N. Barak, H. Strauss, H. Oschkinat, C. G. Dotti and V. Haucke (2009). "Regulation of endosomal membrane traffic by a Gadkin/AP-1/kinesin KIF5 complex." Proc Natl Acad Sci U S A **106**(36): 15344-15349.
Schnoor, M., T. E. Stradal and K. Rottner (2018). "Cortactin: Cell Functions of A Multifaceted Actin-Binding Protein." Trends Cell Biol **28**(2): 79-98.
Schu, P., K. Takegawa, M. Fry, J. Stack, M. Waterfield and S. Emr (1993). "Phosphatidylinositol 3-kinase encoded by yeast VPS34 gene essential for protein sorting." Science **260**(5104): 88-91.
Schwob, E. and R. P. Martin (1992). "New yeast actin-like gene required late in the cell cycle." Nature **355**(6356): 179-182.
Scita, G. and P. P. Di Fiore (2010). "The endocytic matrix." Nature **463**(7280): 464-473.
Scott, C. C., F. Vacca and J. Gruenberg (2014). "Endosome maturation, transport and functions." Semin Cell Dev Biol **31**: 2-10.
Scourfield, E. J. and J. Martin-Serrano (2017). "Growing functions of the ESCRT machinery in cell biology and viral replication." Biochem Soc Trans **45**(3): 613-634.
Seaman, M. N. (2005). "Recycle your receptors with retromer." Trends Cell Biol **15**(2): 68-75.
Seaman, M. N., A. Gautreau and D. D. Billadeau (2013). "Retromer-mediated endosomal protein sorting: all WASHed up!" Trends Cell Biol **23**(11): 522-528.
Seaman, M. N., J. M. McCaffery and S. D. Emr (1998). "A membrane coat complex essential for endosome-to-Golgi retrograde transport in yeast." J Cell Biol **142**(3): 665-681.
Semerdjieva, S., B. Shortt, E. Maxwell, S. Singh, P. Fonarev, J. Hansen, G. Schiavo, B. D. Grant and E. Smythe (2008). "Coordinated regulation of AP2 uncoating from clathrin-coated vesicles by rab5 and hRME-6." J Cell Biol **183**(3): 499-511.
Senetar, M. A., S. J. Foster and R. O. McCann (2004). "Intrasteric inhibition mediates the interaction of the I/LWEQ module proteins Talin1, Talin2, Hip1, and Hip12 with actin." Biochemistry **43**(49): 15418-15428.

Sevilla, L. M., R. Nachat, K. R. Groot and F. M. Watt (2008). "Kazrin regulates keratinocyte cytoskeletal networks, intercellular junctions and differentiation." J Cell Sci **121**(Pt 21): 3561-3569.
Sevilla, L. M., A. A. Rana, F. M. Watt and J. C. Smith (2008). "KazrinA is required for axial elongation and epidermal integrity in Xenopus tropicalis." Dev Dyn **237**(6): 1718-1725.
Shi, A., L. Sun, R. Banerjee, M. Tobin, Y. Zhang and B. D. Grant (2009). "Regulation of endosomal clathrin and retromer-mediated endosome to Golgi retrograde transport by the J-domain protein RME-8." EMBO J **28**(21): 3290-3302.
Shi, H., R. Rojas, J. S. Bonifacino and J. H. Hurley (2006). "The retromer subunit Vps26 has an arrestin fold and binds Vps35 through its C-terminal domain." Nat Struct Mol Biol **13**(6): 540-548.
Shiba, Y., H. Takatsu, H. W. Shin and K. Nakayama (2002). "Gamma-adaptin interacts directly with Rabaptin-5 through its ear domain." J Biochem **131**(3): 327-336.
Simonsen, A., J. M. Gaullier, A. D'Arrigo and H. Stenmark (1999). "The Rab5 effector EEA1 interacts directly with syntaxin-6." J Biol Chem **274**(41): 28857-28860.
Simonsen, A., R. Lippe, S. Christoforidis, J. M. Gaullier, A. Brech, J. Callaghan, B. H. Toh, C. Murphy, M. Zerial and H. Stenmark (1998). "EEA1 links PI(3)K function to Rab5 regulation of endosome fusion." Nature **394**(6692): 494-498.
Simpson, F., N. K. Hussain, B. Qualmann, R. B. Kelly, B. K. Kay, P. S. McPherson and S. L. Schmid (1999). "SH3-domain-containing proteins function at distinct steps in clathrin-coated vesicle formation." Nat Cell Biol **1**(2): 119-124.
Simunovic, M., P. Bassereau and G. A. Voth (2018). "Organizing membrane-curving proteins: the emerging dynamical picture." Curr Opin Struct Biol **51**: 99-105.
Skruzny, M., T. Brach, R. Ciuffa, S. Rybina, M. Wachsmuth and M. Kaksonen (2012). "Molecular basis for coupling the plasma membrane to the actin cytoskeleton during clathrin-mediated endocytosis." Proc Natl Acad Sci U S A **109**(38): E2533-2542.
Skruzny, M., A. Desfosses, S. Prinz, S. O. Dodonova, A. Gieras, C. Uetrecht, A. J. Jakobi, M. Abella, W. J. Hagen, J. Schulz, R. Meijers, V. Rybin, J. A. Briggs, C. Sachse and M. Kaksonen (2015). "An organized co-assembly of clathrin adaptors is essential for endocytosis." Dev Cell **33**(2): 150-162.
Small, S. A., K. Kent, A. Pierce, C. Leung, M. S. Kang, H. Okada, L. Honig, J. P. Vonsattel and T. W. Kim (2005). "Model-guided microarray implicates the retromer complex in Alzheimer's disease." Ann Neurol **58**(6): 909-919.
Soldati, T., A. D. Shapiro, A. B. Svejstrup and S. R. Pfeffer (1994). "Membrane targeting of the small GTPase Rab9 is accompanied by nucleotide exchange." Nature **369**(6475): 76-78.
Solinger, J. A. and A. Spang (2013). "Tethering complexes in the endocytic pathway: CORVET and HOPS." The FEBS journal **280**(12): 2743-2757.
Spence, E. F., D. J. Kanak, B. R. Carlson and S. H. Soderling (2016). "The Arp2/3 Complex Is Essential for Distinct Stages of Spine Synapse Maturation, Including Synapse Unsilencing." J Neurosci **36**(37): 9696-9709.
Stachowiak, J. C., E. M. Schmid, C. J. Ryan, H. S. Ann, D. Y. Sasaki, M. B. Sherman, P. L. Geissler, D. A. Fletcher and C. C. Hayden (2012). "Membrane bending by protein–protein crowding." Nature cell biology **14**(9): 944.
Stehbens, S. and T. Wittmann (2012). "Targeting and transport: how microtubules control focal adhesion dynamics." J Cell Biol **198**(4): 481-489.
Stein, M. P., Y. Feng, K. L. Cooper, A. M. Welford and A. Wandinger-Ness (2003). "Human VPS34 and p150 are Rab7 interacting partners." Traffic **4**(11): 754-771.
Steinberg, F., M. Gallon, M. Winfield, E. C. Thomas, A. J. Bell, K. J. Heesom, J. M. Tavare and P. J. Cullen (2013). "A global analysis of SNX27-retromer assembly and cargo specificity reveals a function in glucose and metal ion transport." Nat Cell Biol **15**(5): 461-471.
Steinberg, F., K. J. Heesom, M. D. Bass and P. J. Cullen (2012). "SNX17 protects integrins from degradation by sorting between lysosomal and recycling pathways." J Cell Biol **197**(2): 219-230.
Stenmark, H. (2009). "Rab GTPases as coordinators of vesicle traffic." Nat Rev Mol Cell Biol **10**(8): 513-525.
Stenmark, H., G. Vitale, O. Ullrich and M. Zerial (1995). "Rabaptin-5 is a direct effector of the small GTPase Rab5 in endocytic membrane fusion." Cell **83**(3): 423-432.

Stockinger, W., B. Sailler, V. Strasser, B. Recheis, D. Fasching, L. Kahr, W. J. Schneider and J. Nimpf (2002). "The PX-domain protein SNX17 interacts with members of the LDL receptor family and modulates endocytosis of the LDL receptor." Embo j **21**(16): 4259-4267.
Stoddart, A., M. L. Dykstra, B. K. Brown, W. Song, S. K. Pierce and F. M. Brodsky (2002). "Lipid rafts unite signaling cascades with clathrin to regulate BCR internalization." Immunity **17**(4): 451-462.
Stoorvogel, W., V. Oorschot and H. J. Geuze (1996). "A novel class of clathrin-coated vesicles budding from endosomes." J Cell Biol **132**(1-2): 21-33.
Stuffers, S., A. Brech and H. Stenmark (2009). "ESCRT proteins in physiology and disease." Experimental cell research **315**(9): 1619-1626.
Suetsugu, S., M. Hattori, H. Miki, T. Tezuka, T. Yamamoto, K. Mikoshiba and T. Takenawa (2002). "Sustained Activation of N-WASP through Phosphorylation Is Essential for Neurite Extension." Developmental Cell **3**(5): 645-658.
Sugino, H. and S. Hatano (1982). "Effect of fragmin on actin polymerization: evidence for enhancement of nucleation and capping of the barbed end." Cell Motil **2**(5): 457-470.
Sullivan, C. S., J. L. Scheib, Z. Ma, R. P. Dang, J. M. Schafer, F. E. Hickman, F. M. Brodsky, K. S. Ravichandran and B. D. Carter (2014). "The adaptor protein GULP promotes Jedi-1-mediated phagocytosis through a clathrin-dependent mechanism." Mol Biol Cell **25**(12): 1925-1936.
Sun, Y., N. T. Leong, T. Jiang, A. Tangara, X. Darzacq and D. G. Drubin (2017). "Switch-like Arp2/3 activation upon WASP and WIP recruitment to an apparent threshold level by multivalent linker proteins in vivo." Elife **6**.
Sun, Y., A. C. Martin and D. G. Drubin (2006). "Endocytic internalization in budding yeast requires coordinated actin nucleation and myosin motor activity." Dev Cell **11**(1): 33-46.
Suraneni, P., B. Rubinstein, J. R. Unruh, M. Durnin, D. Hanein and R. Li (2012). "The Arp2/3 complex is required for lamellipodia extension and directional fibroblast cell migration." J Cell Biol **197**(2): 239-251.
Svitkina, T. M. and G. G. Borisy (1999). "Arp2/3 complex and actin depolymerizing factor/cofilin in dendritic organization and treadmilling of actin filament array in lamellipodia." J Cell Biol **145**(5): 1009-1026.
Swarbrick, J. D., D. J. Shaw, S. Chhabra, R. Ghai, E. Valkov, S. J. Norwood, M. N. Seaman and B. M. Collins (2011). "VPS29 is not an active metallo-phosphatase but is a rigid scaffold required for retromer interaction with accessory proteins." PLoS One **6**(5): e20420.
Symons, M., J. M. Derry, B. Karlak, S. Jiang, V. Lemahieu, F. McCormick, U. Francke and A. Abo (1996). "Wiskott-Aldrich syndrome protein, a novel effector for the GTPase CDC42Hs, is implicated in actin polymerization." Cell **84**(5): 723-734.
Symons, M. H. and T. J. Mitchison (1991). "Control of actin polymerization in live and permeabilized fibroblasts." J Cell Biol **114**(3): 503-513.
Tabuchi, M., I. Yanatori, Y. Kawai and F. Kishi (2010). "Retromer-mediated direct sorting is required for proper endosomal recycling of the mammalian iron transporter DMT1." J Cell Sci **123**(Pt 5): 756-766.
Takahashi, H., J. R. Mayers, L. Wang, J. M. Edwardson and A. Audhya (2015). "Hrs and STAM function synergistically to bind ubiquitin-modified cargoes in vitro." Biophys J **108**(1): 76-84.
Takenawa, T. and S. Suetsugu (2007). "The WASP-WAVE protein network: connecting the membrane to the cytoskeleton." Nat Rev Mol Cell Biol **8**(1): 37-48.
Taylor, M. J., D. Perrais and C. J. Merrifield (2011). "A high precision survey of the molecular dynamics of mammalian clathrin-mediated endocytosis." PLoS Biol **9**(3): e1000604.
Teasdale, R. D. and B. M. Collins (2012). "Insights into the PX (phox-homology) domain and SNX (sorting nexin) protein families: structures, functions and roles in disease." Biochem J **441**(1): 39-59.
Teckchandani, A., E. E. Mulkearns, T. W. Randolph, N. Toida and J. A. Cooper (2012). "The clathrin adaptor Dab2 recruits EH domain scaffold proteins to regulate integrin beta1 endocytosis." Mol Biol Cell **23**(15): 2905-2916.
Teis, D., S. Saksena and S. D. Emr (2008). "Ordered assembly of the ESCRT-III complex on endosomes is required to sequester cargo during MVB formation." Dev Cell **15**(4): 578-589.

Teis, D., S. Saksena and S. D. Emr (2009). "SnapShot: the ESCRT machinery." Cell **137**(1): 182-182 e181.
Temkin, P., B. Lauffer, S. Jager, P. Cimermancic, N. J. Krogan and M. von Zastrow (2011). "SNX27 mediates retromer tubule entry and endosome-to-plasma membrane trafficking of signalling receptors." Nat Cell Biol **13**(6): 715-721.
Teo, H., D. J. Gill, J. Sun, O. Perisic, D. B. Veprintsev, Y. Vallis, S. D. Emr and R. L. Williams (2006). "ESCRT-I core and ESCRT-II GLUE domain structures reveal role for GLUE in linking to ESCRT-I and membranes." Cell **125**(1): 99-111.
Traub, L. M. (2009). "Clathrin Couture: Fashioning Distinctive Membrane Coats at the Cell Surface." PLOS Biology **7**(9): e1000192.
Trombetta, E. S. and I. Mellman (2005). "Cell biology of antigen processing in vitro and in vivo." Annu Rev Immunol **23**: 975-1028.
Ullrich, O., H. Horiuchi, C. Bucci and M. Zerial (1994). "Membrane association of Rab5 mediated by GDP-dissociation inhibitor and accompanied by GDP/GTP exchange." Nature **368**(6467): 157-160.
Ullrich, O., H. Stenmark, K. Alexandrov, L. A. Huber, K. Kaibuchi, T. Sasaki, Y. Takai and M. Zerial (1993). "Rab GDP dissociation inhibitor as a general regulator for the membrane association of rab proteins." J Biol Chem **268**(24): 18143-18150.
Ungewickell, E. J. and L. Hinrichsen (2007). "Endocytosis: clathrin-mediated membrane budding." Current opinion in cell biology **19**(4): 417-425.
Unsworth, K. E., P. Mazurkiewicz, F. Senf, M. Zettl, M. McNiven, M. Way and D. W. Holden (2007). "Dynamin is required for F-actin assembly and pedestal formation by enteropathogenic Escherichia coli (EPEC)." Cellular microbiology **9**(2): 438-449.
Uruno, T., J. Liu, P. Zhang, Y. Fan, C. Egile, R. Li, S. C. Mueller and X. Zhan (2001). "Activation of Arp2/3 complex-mediated actin polymerization by cortactin." Nat Cell Biol **3**(3): 259-266.
Valdmanis, P. N., I. A. Meijer, A. Reynolds, A. Lei, P. MacLeod, D. Schlesinger, M. Zatz, E. Reid, P. A. Dion, P. Drapeau and G. A. Rouleau (2007). "Mutations in the KIAA0196 gene at the SPG8 locus cause hereditary spastic paraplegia." Am J Hum Genet **80**(1): 152-161.
van Bergen En Henegouwen, P. M. (2009). "Eps15: a multifunctional adaptor protein regulating intracellular trafficking." Cell Commun Signal **7**: 24.
van Dam, E. M. and W. Stoorvogel (2002). "Dynamin-dependent transferrin receptor recycling by endosome-derived clathrin-coated vesicles." Mol Biol Cell **13**(1): 169-182.
van der Sluijs, P., M. Hull, P. Webster, P. Male, B. Goud and I. Mellman (1992). "The small GTP-binding protein rab4 controls an early sorting event on the endocytic pathway." Cell **70**(5): 729-740.
van Kerkhof, P., J. Lee, L. McCormick, E. Tetrault, W. Lu, M. Schoenfish, V. Oorschot, G. J. Strous, J. Klumperman and G. Bu (2005). "Sorting nexin 17 facilitates LRP recycling in the early endosome." Embo j **24**(16): 2851-2861.
van Weering, J. R., R. B. Sessions, C. J. Traer, D. P. Kloer, V. K. Bhatia, D. Stamou, S. R. Carlsson, J. H. Hurley and P. J. Cullen (2012). "Molecular basis for SNX-BAR-mediated assembly of distinct endosomal sorting tubules." EMBO J **31**(23): 4466-4480.
van Weering, J. R., P. Verkade and P. J. Cullen (2010). "SNX-BAR proteins in phosphoinositide-mediated, tubular-based endosomal sorting." Semin Cell Dev Biol **21**(4): 371-380.
Varandas, K. C., R. Irannejad and M. von Zastrow (2016). "Retromer Endosome Exit Domains Serve Multiple Trafficking Destinations and Regulate Local G Protein Activation by GPCRs." Curr Biol.
Vardarajan, B. N., S. Y. Bruesegem, M. E. Harbour, R. Inzelberg, R. Friedland, P. St George-Hyslop, M. N. Seaman and L. A. Farrer (2012). "Identification of Alzheimer disease-associated variants in genes that regulate retromer function." Neurobiol Aging **33**(9): 2231.e2215-2231.e2230.
Varsano, T., V. Taupin, L. Guo, O. Y. Baterina and M. G. Farquhar (2012). "The PDZ Protein GIPC Regulates Trafficking of the LPA(1) Receptor from APPL Signaling Endosomes and Attenuates the Cell's Response to LPA." PLoS ONE **7**(11): e49227.
Vassilopoulos, S., C. Esk, S. Hoshino, B. H. Funke, C. Y. Chen, A. M. Plocik, W. E. Wright, R. Kucherlapati and F. M. Brodsky (2009). "A role for the CHC22 clathrin heavy-chain isoform in human glucose metabolism." Science **324**(5931): 1192-1196.

Veiga, E. and P. Cossart (2006). "The role of clathrin-dependent endocytosis in bacterial internalization." Trends Cell Biol **16**(10): 499-504.
Veltman, D. (2014). "Actin dynamics: cell migration takes a new turn with arpin." Curr Biol **24**(1): R31-33.
Viaud, J., R. Mansour, A. Antkowiak, A. Mujalli, C. Valet, G. Chicanne, J.-M. Xuereb, A.-D. Terrisse, S. Séverin and M.-P. Gratacap (2016). "Phosphoinositides: important lipids in the coordination of cell dynamics." Biochimie **125**: 250-258.
Vonderheit, A. and A. Helenius (2005). "Rab7 associates with early endosomes to mediate sorting and transport of Semliki forest virus to late endosomes." PLoS Biol **3**(7): e233.
Votteler, J. and W. I. Sundquist (2013). "Virus budding and the ESCRT pathway." Cell Host Microbe **14**(3): 232-241.
Wakeham, D. E., L. Abi-Rached, M. C. Towler, J. D. Wilbur, P. Parham and F. M. Brodsky (2005). "Clathrin heavy and light chain isoforms originated by independent mechanisms of gene duplication during chordate evolution." Proc Natl Acad Sci U S A **102**(20): 7209-7214.
Wallroth, A. and V. Haucke (2018). "Phosphoinositide conversion in endocytosis and the endolysosomal system." J Biol Chem **293**(5): 1526-1535.
Wang, C. W., P. E. Stromhaug, E. J. Kauffman, L. S. Weisman and D. J. Klionsky (2003). "Yeast homotypic vacuole fusion requires the Ccz1-Mon1 complex during the tethering/docking stage." J Cell Biol **163**(5): 973-985.
Wang, C. W., P. E. Stromhaug, J. Shima and D. J. Klionsky (2002). "The Ccz1-Mon1 protein complex is required for the late step of multiple vacuole delivery pathways." J Biol Chem **277**(49): 47917-47927.
Wang, D., M. Guo, Z. Liang, J. Fan, Z. Zhu, J. Zang, Z. Zhu, X. Li, M. Teng, L. Niu, Y. Dong and P. Liu (2005). "Crystal structure of human vacuolar protein sorting protein 29 reveals a phosphodiesterase/nuclease-like fold and two protein-protein interaction sites." J Biol Chem **280**(24): 22962-22967.
Wang, E., P. S. Brown, B. Aroeti, S. J. Chapin, K. E. Mostov and K. W. Dunn (2000). "Apical and basolateral endocytic pathways of MDCK cells meet in acidic common endosomes distinct from a nearly-neutral apical recycling endosome." Traffic **1**(6): 480-493.
Wang, Y. and V. Riechmann (2008). "Microtubule anchoring by cortical actin bundles prevents streaming of the oocyte cytoplasm." Mech Dev **125**(1-2): 142-152.
Wang, Y. J., J. Wang, H. Q. Sun, M. Martinez, Y. X. Sun, E. Macia, T. Kirchhausen, J. P. Albanesi, M. G. Roth and H. L. Yin (2003). "Phosphatidylinositol 4 phosphate regulates targeting of clathrin adaptor AP-1 complexes to the Golgi." Cell **114**(3): 299-310.
Watanabe, S. and E. Boucrot (2017). "Fast and ultrafast endocytosis." Curr Opin Cell Biol **47**: 64-71.
Watts, C. (2012). "The endosome-lysosome pathway and information generation in the immune system." Biochim Biophys Acta **1824**(1): 14-21.
Weaver, A. M., J. E. Heuser, A. V. Karginov, W. L. Lee, J. T. Parsons and J. A. Cooper (2002). "Interaction of cortactin and N-WASp with Arp2/3 complex." Curr Biol **12**(15): 1270-1278.
Weaver, A. M., A. V. Karginov, A. W. Kinley, S. A. Weed, Y. Li, J. T. Parsons and J. A. Cooper (2001). "Cortactin promotes and stabilizes Arp2/3-induced actin filament network formation." Curr Biol **11**(5): 370-374.
Wei, J., Z. Y. Fu, P. S. Li, H. H. Miao, B. L. Li, Y. T. Ma and B. L. Song (2014). "The clathrin adaptor proteins ARH, Dab2, and numb play distinct roles in Niemann-Pick C1-Like 1 versus low density lipoprotein receptor-mediated cholesterol uptake." J Biol Chem **289**(48): 33689-33700.
Weinberg, J. and D. G. Drubin (2012). "Clathrin-mediated endocytosis in budding yeast." Trends in Cell Biology **22**(1): 1-13.
Welch, M. D., J. Rosenblatt, J. Skoble, D. A. Portnoy and T. J. Mitchison (1998). "Interaction of human Arp2/3 complex and the Listeria monocytogenes ActA protein in actin filament nucleation." Science **281**(5373): 105-108.
Welz, T. and E. Kerkhoff (2017). "Exploring the iceberg: Prospects of coordinated myosin V and actin assembly functions in transport processes." Small GTPases: 1-11.

Wen, L., F. L. Tang, Y. Hong, S. W. Luo, C. L. Wang, W. He, C. Shen, J. U. Jung, F. Xiong, D. H. Lee, Q. G. Zhang, D. Brann, T. W. Kim, R. Yan, L. Mei and W. C. Xiong (2011). "VPS35 haploinsufficiency increases Alzheimer's disease neuropathology." J Cell Biol **195**(5): 765-779.
Whitley, P., B. J. Reaves, M. Hashimoto, A. M. Riley, B. V. Potter and G. D. Holman (2003). "Identification of mammalian Vps24p as an effector of phosphatidylinositol 3,5-bisphosphate-dependent endosome compartmentalization." J Biol Chem **278**(40): 38786-38795.
Wickstead, B. and K. Gull (2011). "The evolution of the cytoskeleton." J Cell Biol **194**(4): 513-525.
Wieffer, M., T. Maritzen and V. Haucke (2009). "SnapShot: endocytic trafficking." Cell **137**(2): 382 e381-383.
Wilbur, J. D., C. Y. Chen, V. Manalo, P. K. Hwang, R. J. Fletterick and F. M. Brodsky (2008). "Actin binding by Hip1 (huntingtin-interacting protein 1) and Hip1R (Hip1-related protein) is regulated by clathrin light chain." J Biol Chem **283**(47): 32870-32879.
Wilcke, M., L. Johannes, T. Galli, V. Mayau, B. Goud and J. Salamero (2000). "Rab11 regulates the compartmentalization of early endosomes required for efficient transport from early endosomes to the trans-golgi network." The Journal of cell biology **151**(6): 1207-1220.
Winter, D., T. Lechler and R. Li (1999). "Activation of the yeast Arp2/3 complex by Bee1p, a WASP-family protein." Curr Biol **9**(9): 501-504.
Winter, D., A. V. Podtelejnikov, M. Mann and R. Li (1997). "The complex containing actin-related proteins Arp2 and Arp3 is required for the motility and integrity of yeast actin patches." Curr Biol **7**(7): 519-529.
Witkos, T. M. and M. Lowe (2017). "Recognition and tethering of transport vesicles at the Golgi apparatus." Curr Opin Cell Biol **47**: 16-23.
Wollert, T. and J. H. Hurley (2010). "Molecular mechanism of multivesicular body biogenesis by ESCRT complexes." Nature **464**(7290): 864-869.
Wollert, T., C. Wunder, J. Lippincott-Schwartz and J. H. Hurley (2009). "Membrane scission by the ESCRT-III complex." Nature **458**(7235): 172-177.
Xing, Y., T. Bocking, M. Wolf, N. Grigorieff, T. Kirchhausen and S. C. Harrison (2010). "Structure of clathrin coat with bound Hsc70 and auxilin: mechanism of Hsc70-facilitated disassembly." Embo j **29**(3): 655-665.
Xu, H. and D. Ren (2015). "Lysosomal physiology." Annu Rev Physiol **77**: 57-80.
Yamashiro, D. J. and F. R. Maxfield (1987). "Acidification of morphologically distinct endosomes in mutant and wild-type Chinese hamster ovary cells." J Cell Biol **105**(6 Pt 1): 2723-2733.
Yamashiro, D. J., B. Tycko, S. R. Fluss and F. R. Maxfield (1984). "Segregation of transferrin to a mildly acidic (pH 6.5) para-Golgi compartment in the recycling pathway." Cell **37**(3): 789-800.
Yarar, D., W. To, A. Abo and M. D. Welch (1999). "The Wiskott-Aldrich syndrome protein directs actin-based motility by stimulating actin nucleation with the Arp2/3 complex." Curr Biol **9**(10): 555-558.
Ybe, J. A., F. M. Brodsky, K. Hofmann, K. Lin, S. H. Liu, L. Chen, T. N. Earnest, R. J. Fletterick and P. K. Hwang (1999). "Clathrin self-assembly is mediated by a tandemly repeated superhelix." Nature **399**(6734): 371-375.
Ybe, J. A., S. Perez-Miller, Q. Niu, D. A. Coates, M. W. Drazer and M. E. Clegg (2007). "Light chain C-terminal region reinforces the stability of clathrin heavy chain trimers." Traffic **8**(8): 1101-1110.
Yim, Y. I., T. Sun, L. G. Wu, A. Raimondi, P. De Camilli, E. Eisenberg and L. E. Greene (2010). "Endocytosis and clathrin-uncoating defects at synapses of auxilin knockout mice." Proc Natl Acad Sci U S A **107**(9): 4412-4417.
Yudowski, G. A., M. A. Puthenveedu, A. G. Henry and M. von Zastrow (2009). "Cargo-mediated regulation of a rapid Rab4-dependent recycling pathway." Mol Biol Cell **20**(11): 2774-2784.
Zecca, M., K. Basler and G. Struhl (1996). "Direct and long-range action of a wingless morphogen gradient." Cell **87**(5): 833-844.
Zech, T., S. D. Calaminus, P. Caswell, H. J. Spence, M. Carnell, R. H. Insall, J. Norman and L. M. Machesky (2011). "The Arp2/3 activator WASH regulates alpha5beta1-integrin-mediated invasive migration." J Cell Sci **124**(Pt 22): 3753-3759.

Zhang, J., X. Liu, A. Datta, K. Govindarajan, W. L. Tam, J. Han, J. George, C. Wong, K. Ramnarayanan, T. Y. Phua, W. Y. Leong, Y. S. Chan, N. Palanisamy, E. T. Liu, K. M. Karuturi, B. Lim and L. D. Miller (2009). "RCP is a human breast cancer-promoting gene with Ras-activating function." J Clin Invest **119**(8): 2171-2183.
Zhou, K., K. D. Sumigray and T. Lechler (2015). "The Arp2/3 complex has essential roles in vesicle trafficking and transcytosis in the mammalian small intestine." Mol Biol Cell **26**(11): 1995-2004.
Zimmerberg, J. and S. McLaughlin (2004). "Membrane curvature: how BAR domains bend bilayers." Curr Biol **14**(6): R250-252.
Zuchero, J. B., A. S. Coutts, M. E. Quinlan, N. B. Thangue and R. D. Mullins (2009). "p53-cofactor JMY is a multifunctional actin nucleation factor." Nat Cell Biol **11**(4): 451-459.